

# THE BELL SYSTEM TECHNICAL JOURNAL

DEVOTED TO THE SCIENTIFIC AND ENGINEERING ASPECTS  
OF ELECTRICAL COMMUNICATION

Telephony by Pulse Code Modulation . . . *W. M. Goodall* 395

Some Results on Cylindrical Cavity Resonators  
*J. P. Kinzer and I. G. Wilson* 410

Precision Measurement of Impedance Mismatches in  
Waveguide . . . . . *Allen F. Pomeroy* 446

Reflex Oscillators . . . . . *J. R. Pierce and W. G. Shepherd* 460

Abstracts of Technical Articles by Bell System Authors . . 682

Contributors to This Issue . . . . . 691

AMERICAN TELEPHONE AND TELEGRAPH COMPANY  
NEW YORK

50¢ per copy

\$1.50 per Year

# THE BELL SYSTEM TECHNICAL JOURNAL

*Published quarterly by the  
American Telephone and Telegraph Company  
195 Broadway, New York, N. Y.*

---

## EDITORS

R. W. King

J. O. Perrine

## EDITORIAL BOARD

W. H. Harrison

O. E. Buckley

O. B. Blackwell

M. J. Kelly

H. S. Osborne

A. B. Clark

J. J. Pilliod

F. J. Feely

---

## SUBSCRIPTIONS

Subscriptions are accepted at \$1.50 per year. Single copies are 50 cents each.  
The foreign postage is 35 cents per year or 9 cents per copy.

---

Copyright, 1947

American Telephone and Telegraph Company

# The Bell System Technical Journal

Vol. XXVI

July, 1947

No. 3

## Telephony By Pulse Code Modulation\*

By W. M. Goodall

An experiment in transmitting speech by Pulse Code Modulation, or PCM, is described in this paper. Each sample amplitude of a pulse amplitude modulation or PAM signal is transmitted by a code group of ON-OFF pulses.  $2^n$  amplitude values can be represented by an  $n$ -digit binary number code. For a nominal 4 kc. speech band these  $n$  ON-OFF pulses are transmitted 8000 times a second. Experimental equipment for coding the PAM pulses at the transmitter and decoding the PCM pulses at the receiver is described. Experiments with this equipment indicate that a three-unit code appears to be necessary for a minimum grade of circuit, while a six- or seven-unit code will provide good quality.

### INTRODUCTION

THIS paper describes an experiment in transmitting speech by PCM, or pulse code modulation. The writer is indebted to his colleagues in the Research Department, C. E. Shannon, J. R. Pierce and B. M. Oliver, for several interesting suggestions in connection with the basic principles of PCM given in this paper. Work on a different PCM system was carried on simultaneously in the Systems Development Department of the Bell Laboratories by H. S. Black. This in turn led to the development of an 8-channel portable system for a particular application. This system is being described in a forthcoming paper by H. S. Black and J. O. Edson.<sup>1</sup> A method for pulse code modulation is proposed in a U. S. Patent issued to A. H. Reeves.<sup>2</sup>

The material now presented is composed of three parts. The first deals with basic principles, the second describes the experimental PCM system, while the last discusses the results obtained.

### BASIC PRINCIPLES

PCM involves the application of two basic concepts. These concepts are namely, the time-division principle and the amplitude quantization

\* Paper presented in part at joint meeting of International Scientific Radio Union and Inst. Radio Engineers on May 5, 1947 at Washington, D. C.

<sup>1</sup> Paper presented on June 11, 1947 at A. I. E. E. Summer General Meeting, Montreal, Canada. Accepted for publication in forthcoming issue of *A. I. E. E. Transactions*.

<sup>2</sup> A. H. Reeves, *U. S. Patent* # 2,272,070, Feb. 3, 1942, assigned to International Standard Electric Corp.; also, French patent # 852,183, October 23, 1939.

principle. The essence of the time-division principle is that any input wave can be represented by a series of regularly occurring instantaneous samples, provided that the sampling rate is at least twice the highest frequency in the input wave.<sup>3</sup> For present purposes the amplitude quantization principle states that a complex wave can be approximated by a wave having a finite number of amplitude levels, each differing by one quantum, the size of the quantum jumps being determined by the degree of approximation desired.

Although other arrangements are possible, in this paper we will consider the application of these two basic principles in the following order. First the input wave is sampled on a time-division basis. Then each of the samples so obtained is represented by a quantized amplitude or integer number. Each of these integer numbers is represented as a binary number of  $n$  digits, the binary number system being chosen because it can readily be

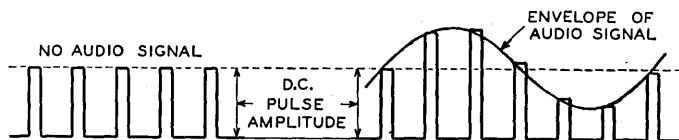


Fig. 1—Pulses in a PAM System.

represented by ON-OFF or two-position pulses.  $2^n$  discrete levels can be represented by a binary number of  $n$  digits.<sup>4</sup> Thus, PCM represents each quantized amplitude of a time-division sampling process by a group of ON-OFF pulses, where these pulses represent the quantized amplitude in a binary number system.

The discussion so far has been in general terms. The principles just discussed will now be illustrated by examples.

Multiplex transmission of speech channels by sending short pulses selected sequentially from the respective speech channels, is now well known in the telephone art and is called time-division multiplex. When the pulses consist simply of short samples of the speech waves, their varying amplitudes directly represent the speech waves and the system is called pulse amplitude modulation or PAM. In PAM the instantaneous amplitude of the speech wave is sampled at regular intervals. The amplitude so obtained is trans-

<sup>3</sup> This is because the DC, fundamental and harmonics of the wave at the left in Fig. 1 all become modulated in the wave at the right, and if the highest modulating frequency exceeds half the sampling rate, the lower sideband of the fundamental will fall in the range of the modulating frequency and will not be excluded by the low-pass filter. The result is distortion.

<sup>4</sup> In a decimal system the digits can have any one of 10 values, 0 to 9 inclusive. In a binary system, the digits can have only two values, either 0 or 1.



mitted as a pulse of corresponding amplitude. In order to transmit both positive and negative values a constant or d-c value of pulse amplitude can be added. (See Fig. 1.) When this is done positive values of the information wave correspond to pulse amplitudes greater than the constant value while negative values correspond to pulse amplitudes less than the constant value. At the receiver a reproduction of the original speech wave will be obtained at the output of a low-pass filter.

The PCM system considered in this paper starts with a PAM system and adds equipment at the terminals to enable the transmission of a group of ON-OFF pulses or binary digits to represent each instantaneous pulse amplitude of the PAM system. Representation of the amplitude of a single PAM pulse by a finite group of ON-OFF pulses or binary digits requires quantization of the audio wave. In other words, we cannot represent the actual amplitude closer than  $\frac{1}{2}$  "quantum". The number of amplitude levels required depends upon the grade of circuit desired. The disturbance which results from the quantization process has been termed quantizing noise. For this type of noise a signal-to-noise ratio of 33 db would be obtained for 32 amplitude levels and this grade of circuit was deemed sufficiently good for a preliminary study. These 32 amplitude levels can be obtained with 5 binary digits, since  $32 = 2^5$ .

Figure 2 shows how several values of PAM pulse amplitude can be represented by this binary code. The first column gives the digit pulses which are sent between the transmitter and receiver while the second column shows the same pulse pattern with each pulse weighted according to its assigned value, and the final column shows the sum of the weighted values. The sum, of course, represents the PAM pulse to the nearest lower amplitude unit. The top row where all the digits are present shows, in the middle wave form, the weighted equivalent of each digit pulse. By taking different combinations of the five digits all integer amplitudes between 31 and 0 can be represented. The examples shown are for 31, 18, 3, and 0.

Referring to Fig. 3 sampling of the audio wave (a) yields the PAM wave (b). The PAM pulses are coded to produce the code groups or PCM signal (c). The PCM pulses are the ones sent over the transmission medium. For a sampling rate of 8000 per second, there would be 8000 PAM pulses per second for a single channel. The digit pulse rate would be 40,000 pps for a five-digit code. For a time-division multiplex of N channels both of these pulse rates would be multiplied by N.

Wave form (d) shows the decoded PAM pulses where the amplitudes are shown under the pulses. The original audio wave is repeated as wave form (e). It will be noted that the received signal is delayed by one PAM pulse interval. It is also seen that the decoded pulses do not fit exactly on this curve. This is the result of quantization and the output of the low-pass

filter will contain a quantizing disturbance not shown in (e) which was not present in the input signal.

A signal that uses regularly occurring ON-OFF pulses can be "regenerated" and repeated indefinitely without degradation. A pulse can be "regenerated" by equipment which transmits an undistorted pulse provided a somewhat distorted pulse is received, and transmits nothing otherwise.

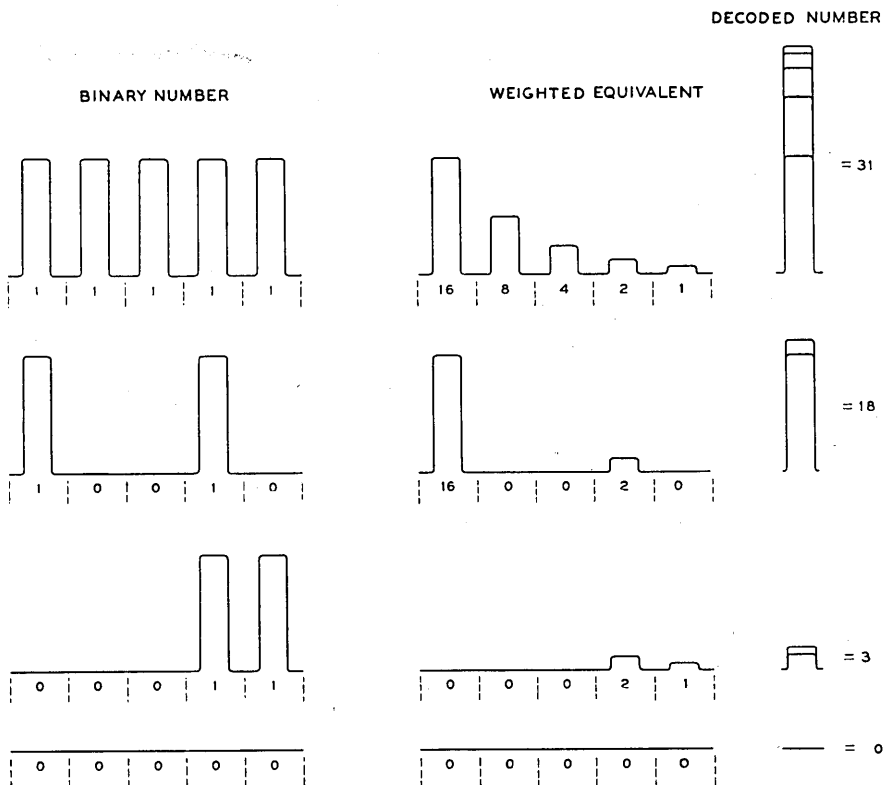


Fig. 2—Binary and decimal equivalents.

Thus, the received signal at the output of the final decoder is of the same quality as one produced by a local monitoring decoder. To accomplish this result, it is necessary, of course, to regenerate the digit pulses before they have been too badly mutilated by noise or distortion in the transmission medium.

The regenerative property of a quantized signal can be of great importance in a long repeated system. For example, with a conventional system each repeater link of a 100-link system must have a signal-to-noise ratio 20 db

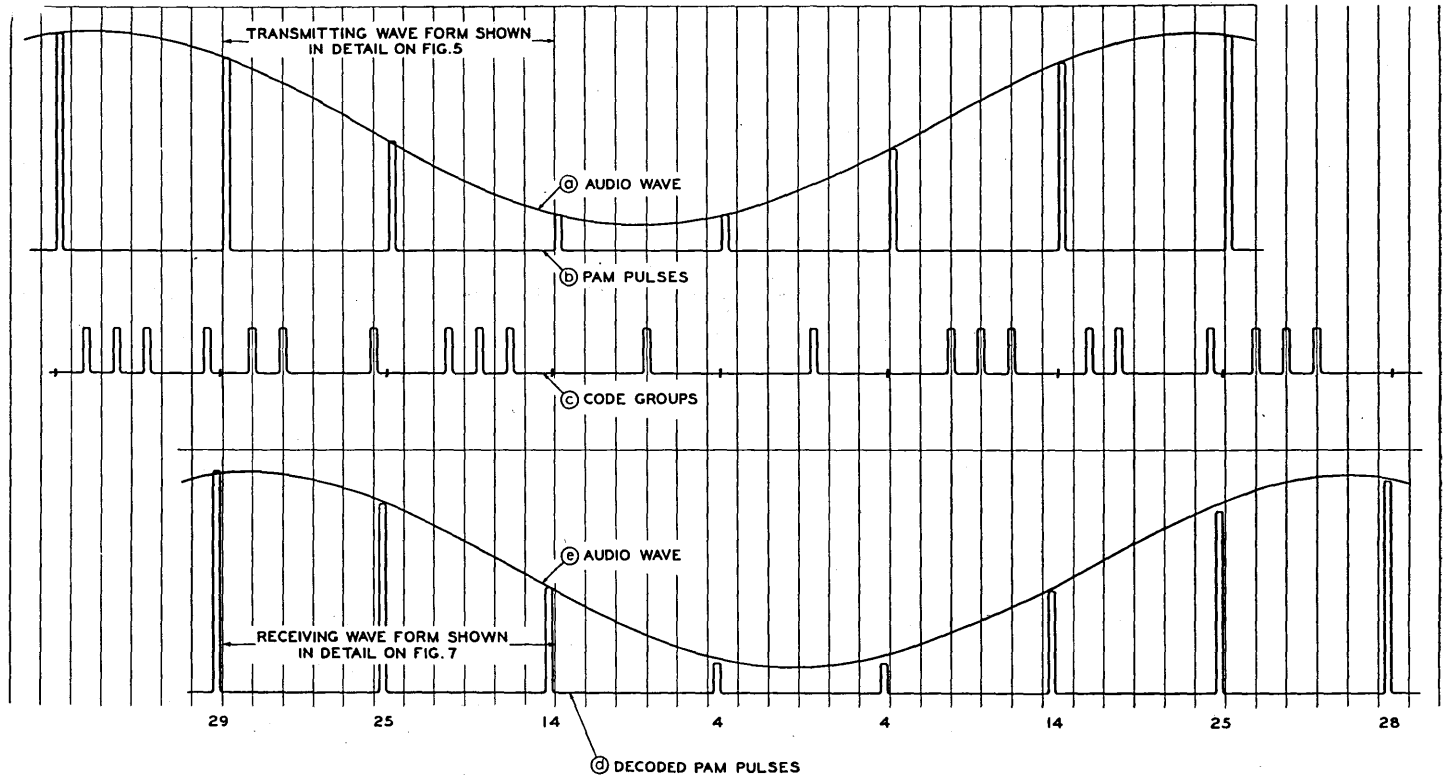


Fig. 3—PAM and PCM transmitting and receiving wave forms (amplitude vs. time).

better than the complete system. For PCM, however, with regenerative repeaters the required signal-to-noise ratio in the radio part of the system is independent of the number of links. Hence, we have a method of transmission that is ideally suited to long repeated systems.

At this point we might consider the bandwidth required to send this type of signal. For a 5-digit code the required band is somewhat less than 5 times that required for a PAM system. It is somewhat less than 5 times because in a multiplex system crosstalk becomes a serious problem. In a PAM system this crosstalk would add up on a long system in somewhat the same manner as noise. In order to reduce the crosstalk it would probably be necessary to use a wider band for the PAM repeater system than would be required for a single-link system. For PCM, on the other hand, by using regeneration the whole system requirement for crosstalk can be used for each link. In addition, a relatively greater amount of crosstalk can be tolerated since only the presence or absence of a pulse needs to be determined. Both of these factors favor PCM. This is a big subject and for the present we need only conclude that from considerations of the type just given the bandwidth penalty of PCM is not nearly as great as might first be expected.

The same two factors that were mentioned in connection with crosstalk also apply to noise, and a PCM signal can be transmitted over a circuit which has a much lower signal-to-noise ratio than would be required to transmit a PAM signal, for example.

Hence, we conclude that PCM for a long repeated system has some powerful arguments on its side because of its superior performance even though it may require somewhat greater bandwidth. There are other factors where PCM differs from more conventional systems but a discussion of these factors is beyond the scope of this paper.

The previous discussion may be summarized as follows: One begins with a pulse amplitude modulation system in which the pulse amplitude is modulated above and below a mean or d-c value as indicated in Fig. 1. It is assumed that it will be satisfactory to limit the amplitude range to be transmitted to a definite number of amplitude levels. This enables each PAM pulse to be represented by a code group of ON-OFF pulses, where the number of amplitude levels is given by  $2^n$ ,  $n$  being the number of elements in each code group. With this system the digit pulses can be "regenerated" and the quality of the overall transmission system can be made to depend upon the terminal equipment alone.

#### EXPERIMENTAL PCM EQUIPMENT

The experimental coder used in these studies might be designated as one of the "feedback subtraction type". It functions as follows: Each PAM pulse is stored as a charge on a condenser in a storage circuit. (See Fig. 4.)

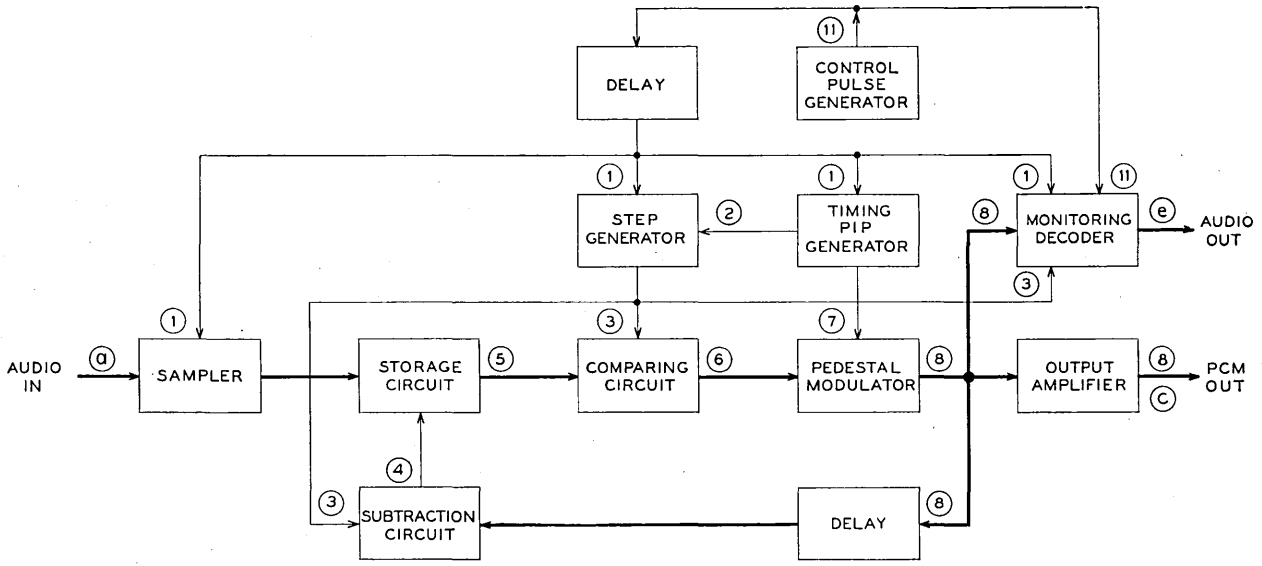


Fig. 4—PCM Transmitter block schematic.

The voltage across this condenser is compared with a reference voltage. The magnitude of this reference voltage corresponds to the d-c pulse amplitude of Fig. 1. The voltage has a magnitude of 16 units. If the magnitude of the condenser voltage exceeds the magnitude of the 16-unit voltage, a positive pedestal voltage is obtained in the output of the comparing circuit. This pedestal voltage is amplified, limited and applied to the pedestal modulator. The pedestal modulator serves as a gate for timing pulses from the timing pip generator. If the pedestal voltage and timing pulse are applied simultaneously to the pedestal modulator, a pulse is obtained in the output. In the present case this pulse corresponds to the presence of the 16-unit digit in the code group which represents this PAM pulse. This digit pulse after amplification and limiting is (1) sent out over the line (PCM out) and (2) fed back through a suitable delay circuit to a subtraction circuit. The function of the subtraction circuit is to subtract a charge from the condenser corresponding to the 16-unit digit. The charge remaining on the condenser is now compared with a new reference voltage which is  $\frac{1}{2}$  the magnitude of the first reference voltage or 8 units. If the magnitude of the voltage across the condenser exceeds this new reference voltage the above process is repeated and the second digit pulse is transmitted and another charge, this time corresponding to the 8-unit digit, is subtracted from the remaining charge upon the condenser.

If the magnitude of the voltage across the condenser is less than the reference voltage, in either case above, then no pedestal will be produced and no digit pulse be transmitted. Since no pulse is transmitted, no charge will be subtracted from the condenser. Thus the charge remaining upon the condenser after each operation represents the part of the original PAM pulse remaining to be coded. The reference voltage wave consists of a series of voltages each of which is  $\frac{1}{2}$  of the preceding one. There is one step on the reference voltage function for each digit to be coded.

A better understanding of the coding process can be had by reference to the various wave forms involved. For completeness, wave forms from audio input to the coded pulse signal are shown for the transmitter in Figs. 3 and 5 and from the coded pulse signal to audio output for the receiver in Figs. 7 and 3. In the diagram the abscissas are time and the ordinates are amplitudes. Some of these wave forms have already been discussed in connection with Fig. 3. Since the coder functions in the same manner for each PAM pulse the detailed wave forms of the coding and decoding processes are shown for only two amplitudes. The block schematic for the transmitter is given on Fig. 4, while that for the receiver is given in Fig. 6. The letters on Figs. 4 and 6 refer to the wave forms on Fig. 3, while the numbers refer to the wave forms in Figs. 5 and 7.

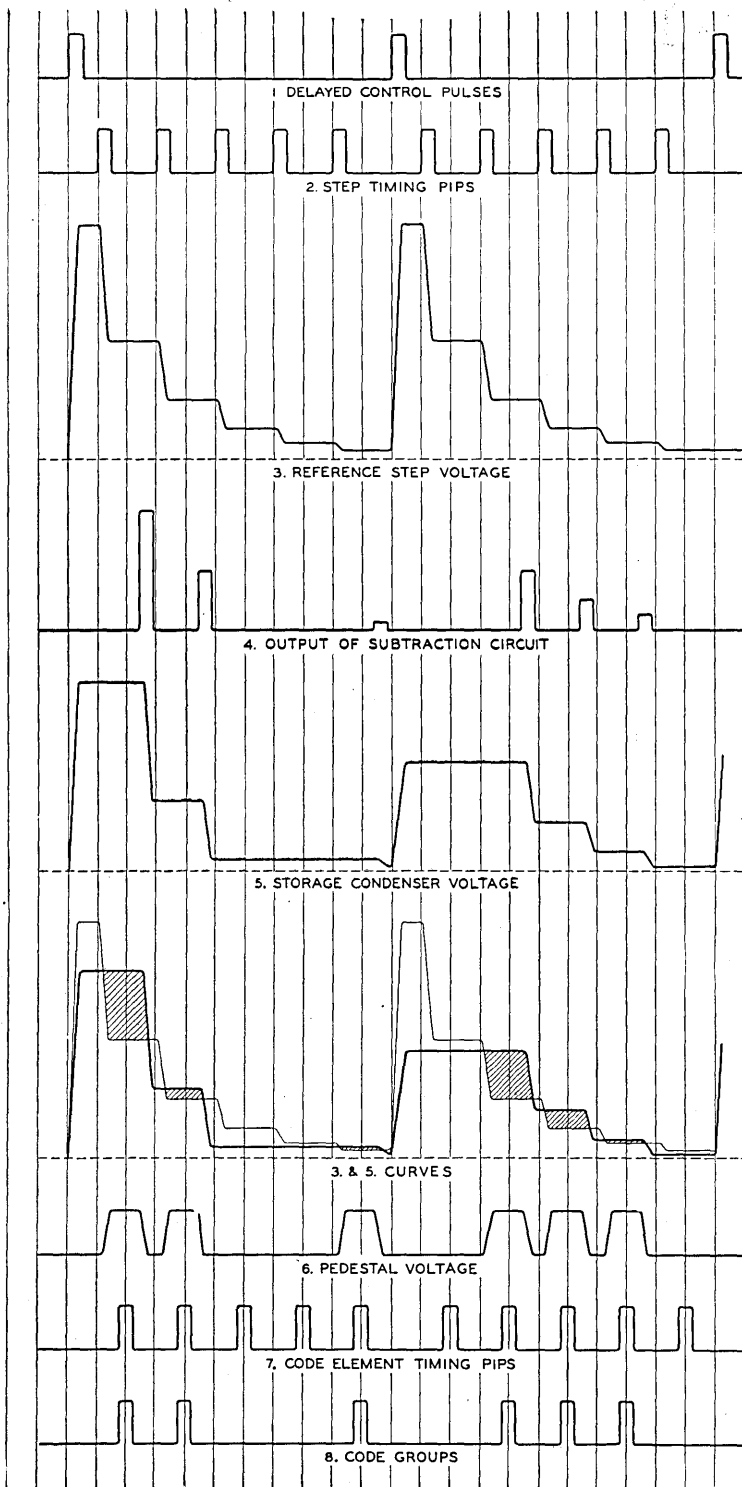


Fig. 5—Detailed wave forms for PCM Transmitter (amplitude vs. time).

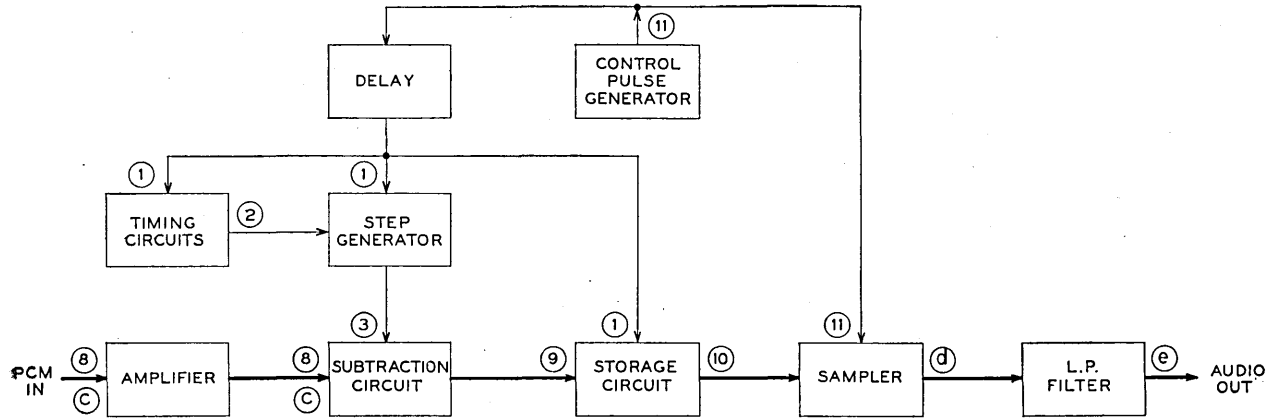


Fig. 6—PCM Receiver block schematic.



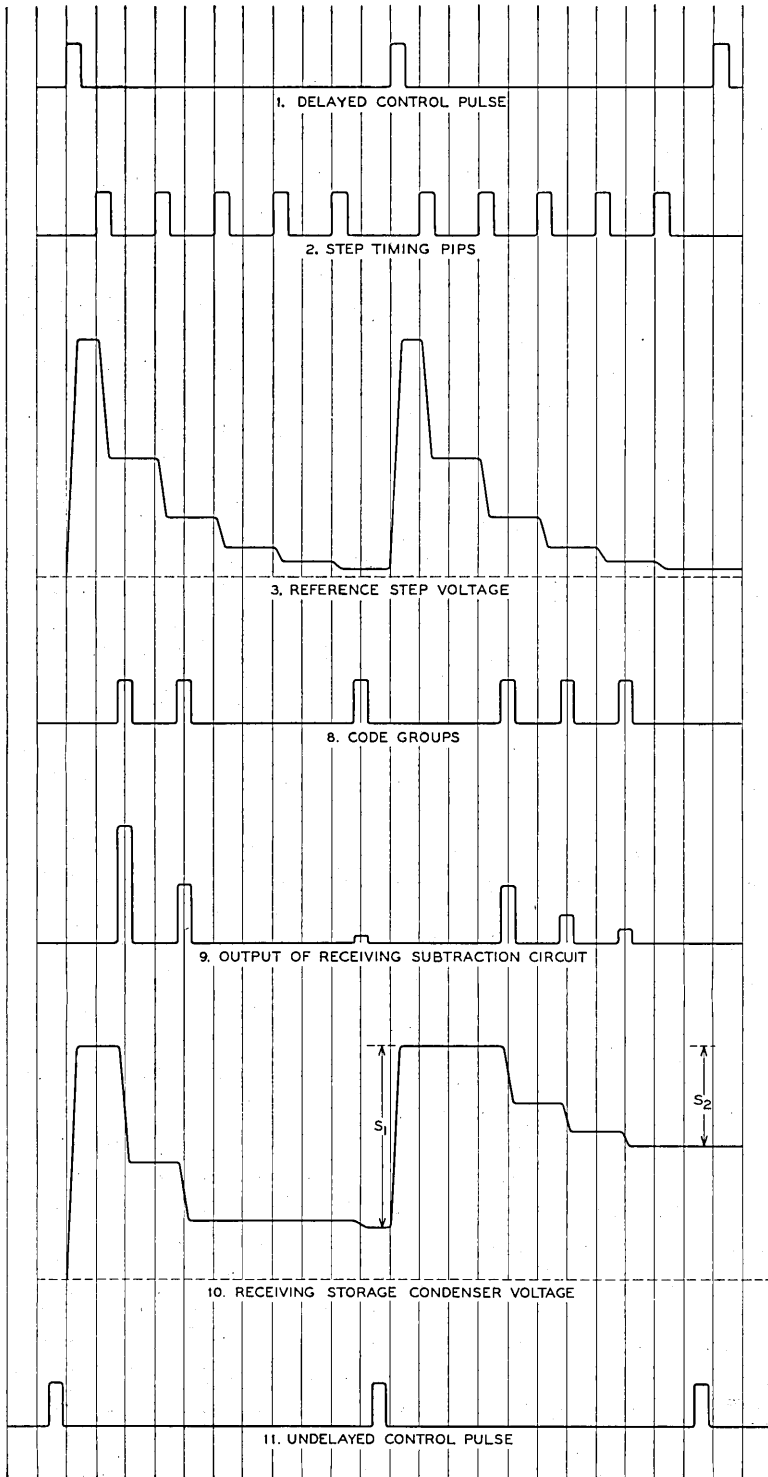


Fig. 7—Detailed wave forms for PCM Receiver (amplitude vs. time).

Referring to Figs. 4 and 5, the "delayed control pulse" Curve 1 is the principal timing pulse for the transmitting coder. It is used to sample the audio wave and to start the step and timing-pip generators. Two sets of timing-pips are produced; one, Curve 2, is used to generate the reference step voltage while the other, Curve 7, is used for timing the digit pulses. The reference step voltage, Curve 3, is used in the comparing circuit and in the subtraction circuit. Curve 4 gives the output of the subtraction circuit, while Curve 5 is the voltage on the storage condenser. The next plot gives Curves 3 and 5 superimposed; the shaded area on this plot corresponds to the time during which a pedestal voltage is generated. The pedestal voltage is given by Curve 6, and the output of the pedestal modulator is given by Curve 8. This last curve is a plot of the two code groups corresponding to the two PAM pulses being coded.

In studying these wave forms it will be noted that the delayed control pulse, the two sets of timing-pips and the reference step voltage curves are the same for each code group. On the other hand the storage condenser voltage, the pedestal voltage, the group of code pulses, and the group of pulses from the subtraction circuit are different for each code group.

It will be recalled that a pedestal voltage is produced during the time that the condenser voltage exceeds the reference step voltage. The leading edge of each pedestal pulse is generated by the falling part of the reference step voltage. The trailing edge of each pedestal pulse is produced by the falling part of the condenser voltage. This drop in condenser voltage is the result of the operation of the subtraction circuit. The output of the subtraction circuit depends upon the delayed digit pulse which has just been passed by the pedestal pulse. Its magnitude depends upon the reference voltage step that applies to the particular digit being transmitted. The function of the delay in the feedback path is to allow the outgoing digit pulse to be completed before the pedestal is terminated.

It is seen that the pedestal voltage contains the same information as the transmitted code groups. Under ideal conditions the use of auxiliary timing pulses would not be required. However, in a practical circuit the leading edge of the pedestal varies, both as to relative timing and as to rate of rise. Under these conditions the auxiliary timing-pips permit accurate timing of the outgoing PCM pulses, as well as constant pulse shape for the input to the subtraction circuit.

Summarizing the foregoing it is seen that in the coder under discussion a comparison is made for each digit between a reference voltage and the voltage across a storage condenser. Initially the voltage across this condenser represents the magnitude of the PAM pulse being coded. After each digit the voltage remaining on the condenser represents the magnitude of the original PAM pulse remaining to be coded. A pedestal voltage is

obtained in the output of the comparing circuit whenever the storage condenser voltage exceeds the reference step voltage.

This pedestal, if present, allows a timing pulse to be sent out as a digit of the code group. This digit pulse is also delayed and fed back to a subtraction circuit which reduces the charge on the condenser by a magnitude corresponding to the digit pulse just transmitted. This process is repeated step by step until the code is completed.

Synchronizing the two control pulse generators, one at the transmitter and one at the receiver, is essential to the proper operation of the equipment. This may be accomplished in a variety of ways. The best method of synchronizing to use would depend upon the application. Although the control could easily be obtained by transmitting a synchronizing pulse over the line, the equipment would have been somewhat more complicated and for these tests a separate channel was used to synchronize the control pulse generators at the terminals.

Having thus established the timing of the receiving control pulse generator shown in Fig. 6 relative to the received code groups, the receiver generates a new set of waves as shown in Fig. 7. Except for delay in the transmission medium, the first three curves are the same as those shown in Fig. 5 for the transmitter. (1) is the delayed control pulse, (2) is the step timing wave, and (3) is the reference step voltage. Curve 8 is the received code group and (9) is the output current of the subtraction circuit. (10) gives the wave form of the voltage across the receiving storage circuit, and (11) gives the curve for the undelayed control pulse.

The receiver functions as follows: The storage condenser is charged to a fixed voltage by each delayed control pulse. The charge on the condenser is reduced by the output of the subtraction circuit. The amount of charge that is subtracted depends upon which digit of the group produces the subtraction pulse. This amount is measured by the reference step voltage. At the end of the code group the voltage remaining on the condenser is sampled by the undelayed control pulse.

It is seen that the storage subtraction circuits in the transmitter and receiver function in similar ways. In the transmitter the original voltage on the condenser depends upon the audio signal, and after the coding process this voltage is substantially zero. The receiver starts with a fixed maximum voltage and after the decoding process the sample that is delivered to the output low-pass filter is given by the voltage reduction of the condenser during the decoding process. Except that the conditions at beginning and end of the coding and decoding periods are different as discussed above, the subtraction process is the same for both units.

The monitoring decoder in the transmitter operates in the same manner described above, except that it employs the various waves already generated for other uses in the transmitter (see Fig. 4).

## EXPERIMENTAL RESULTS

An experimental system was set up as shown in Fig. 8. The pulse code modulator, radio transmitter, and antenna comprised the transmitting terminal; while an antenna, radio receiver and pulse code demodulator were used for the receiving terminal. A short air-path separated the terminals. The transmitter used a pulsed magnetron oscillator and the receiver employed a broad-band superheterodyne circuit. The results obtained with this system were similar to those obtained by connecting the pulse code

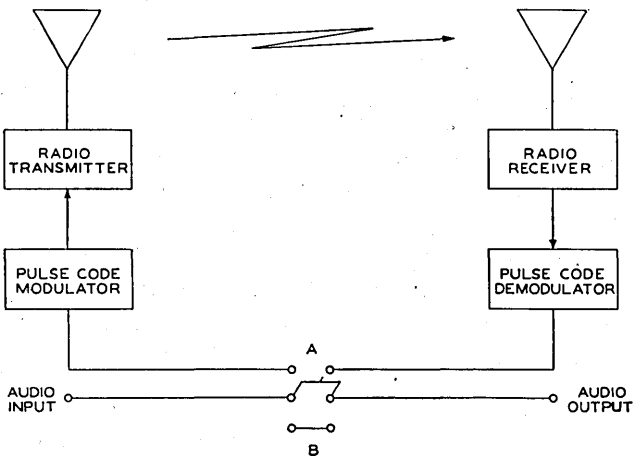


Fig. 8—Block diagram of PCM system.

modulator and demodulator together without the radio equipment. In fact, unless a large amount of attenuation was inserted in the path the presence of the radio circuit could not be detected.

It was possible to adjust the PCM transmitter so that different numbers of digits could be produced. A brief study was made of the number of digits required. It was found that, with regulated volume, a minimum of three or four digits was necessary for good intelligibility for speech though, surprisingly enough, a degree of intelligibility was obtained with a single one. With six digits both speech and music were of good quality when regulated volume was used. Even with six digits, however, it was possible to detect the difference between PCM and direct transmission in A-B tests. This could be done most easily by a comparison of the noise in the two systems. If unregulated volume were used several more digits would probably be desirable for high quality transmission.

In listening to the speech transmitted over the PCM system one obtained the impression that the particular sound patterns of a syllable or a word

could be transmitted with three or four digits. If the volume range of the talker varied it would be necessary to add more digits to allow for this variation. Over and above these effects, however, the background noise which is present to a greater or lesser extent in all communication circuits, is quantized by the PCM system. If the size of the quanta or amplitude step is too large the circuit will have a characteristic sound, which can easily be identified. Since the size of the quanta is determined by the number of digits, it is seen that the number of digits required depends not alone upon the speech but also upon the background noise present in the input signal.

Summarizing, experimental results obtained indicate that at least 3 digits are desirable for a minimum grade of circuit and that as many as 6 or more will provide for a good quality circuit. If we wish to transmit a nominal speech band of 4000 cycles, PCM requires the 8000 pulses per second needed by any time-division system, multiplied by the number of digits transmitted. The extra bandwidth required for PCM, however, buys some real advantages including freedom from noise, crosstalk and signal mutilation, and ability to extend the circuit through the use of the regenerative principle.

The writer wishes to acknowledge the assistance of Mr. A. F. Dietrich in the construction and testing of the PCM equipment discussed in this paper.

## Some Results on Cylindrical Cavity Resonators

By J. P. KINZER and I. G. WILSON

Certain hitherto unpublished theoretical results on cylindrical cavity resonators are derived. These are: an approximation formula for the total number of resonances in a circular cylinder; conditions to yield the minimum volume circular cylinder for an assigned  $Q$ ; limitation of the frequency range of a tunable circular cylinder as set by ambiguity; resonant frequencies of the elliptic cylinder; resonant frequencies and  $Q$  of a coaxial resonator in its higher modes; and a brief discussion of fins in a circular cylinder.

The essential results are condensed in a number of new tables and graphs.

### INTRODUCTION

THE subject of wave guides and the closely allied cavity resonators was of considerable interest even prior to 1942, as shown in the bibliography. It is believed that this bibliography includes virtually everything published up to the end of 1942. During the war, many applications of cavity resonators were made. Among these was the use of a tunable circular cylinder cavity in the  $TE_{01n}$  mode as a radar test set; this has been treated in previous papers.<sup>1,2</sup> During this development, a number of new theoretical results were obtained; some of these have been published.<sup>2</sup> Here we give the derivation of these results together with a number of others not previously disclosed.

In the interests of brevity, an effort has been made to eliminate all material already published. For this reason, the topics are rather disconnected, and it is also assumed that the reader has an adequate background in the subject, such as may be obtained from a study of references 3 to 7 of the bibliography, or a text such as Sarbacher and Edson.<sup>8</sup>

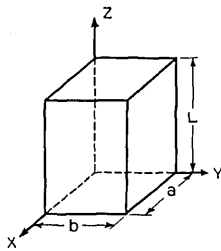
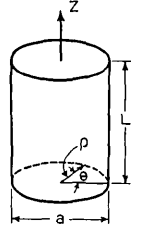
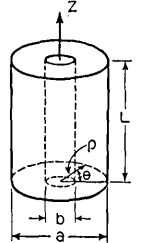
A convenient reference and starting point is afforded by Fig. 1, taken from the Wilson, Schramm, Kinzer paper.<sup>2</sup> This figure also explains most of the notation used herein.

### ACKNOWLEDGEMENT

In this work, as in any cooperative scientific development, assistance and advice were received from many individuals and appropriate appreciation therefor is herewith extended. In some cases, explicit credit for special contributions has been given.

### CONTENTS

1. Approximation formula for number of resonances in a circular cylindrical cavity resonator.
2. Conditions for minimum volume for an assigned  $Q$ .

TYPE OF CAVITY & CO-ORDINATE SYSTEM	MODE	FIELD EQUATIONS *	DEFINITIONS	RESTRICTIONS ON $l, m, n$	NORMAL WAVELENGTHS	APPROXIMATION FOR TOTAL NUMBER OF MODES (TE & TM) HAVING $\lambda > \lambda_0$	FORMULAS FOR $Q \frac{\delta}{\lambda}$	DEFINITIONS
RECTANGULAR PRISM 	TM	$E_x = \sqrt{\frac{\mu}{\epsilon}} \frac{k_1 k_3}{k^2} \cos k_1 x \sin k_2 y \sin k_3 z$ $E_y = \sqrt{\frac{\mu}{\epsilon}} \frac{k_2 k_3}{k^2} \sin k_1 x \cos k_2 y \sin k_3 z$ $E_z = -\sqrt{\frac{\mu}{\epsilon}} \frac{k_1^2 + k_2^2}{k^2} \sin k_1 x \sin k_2 y \cos k_3 z$ $H_x = -\frac{k_2}{k} \sin k_1 x \cos k_2 y \cos k_3 z$ $H_y = \frac{k_1}{k} \cos k_1 x \sin k_2 y \cos k_3 z$ $H_z = 0$	$k_1 = \frac{l\pi}{a}$ $k_2 = \frac{m\pi}{b}$ $k_3 = \frac{n\pi}{L}$ $k^2 = k_1^2 + k_2^2 + k_3^2$ $\lambda = \frac{2\pi}{k}$	$l > 0$ $m > 0$	$\lambda = \frac{2}{\sqrt{\left(\frac{l}{a}\right)^2 + \left(\frac{m}{b}\right)^2 + \left(\frac{n}{L}\right)^2}}$	$N = 8.38 \frac{V}{\lambda_0} - \frac{P}{\lambda_0}$ $V = abL$ $P = a + b + L$	$\frac{abL}{4} \frac{(p^2 + q^2)(p^2 + q^2 + r^2)^{\frac{1}{2}}}{p^2 b(a+L) + q^2 a(b+L)}$ $n > 0$ $\frac{abL}{2} \frac{(p^2 + q^2)^{\frac{3}{2}}}{p^2 b(a+2L) + q^2 a(b+2L)}$ $n = 0$	$p = \frac{l}{a}$ $q = \frac{m}{b}$ $r = \frac{n}{L}$
	TE	$E_x = -\sqrt{\frac{\mu}{\epsilon}} \frac{k_2}{k} \cos k_1 x \sin k_2 y \sin k_3 z$ $E_y = \sqrt{\frac{\mu}{\epsilon}} \frac{k_1}{k} \sin k_1 x \cos k_2 y \sin k_3 z$ $E_z = 0$ $H_x = \frac{k_1 k_3}{k^2} \sin k_1 x \cos k_2 y \cos k_3 z$ $H_y = \frac{k_2 k_3}{k^2} \cos k_1 x \sin k_2 y \cos k_3 z$ $H_z = -\frac{k_1^2 + k_2^2}{k^2} \cos k_1 x \cos k_2 y \sin k_3 z$	$l, m, n =$ INTEGRAL INDICES IDENTIFYING THE MODES. MAY ASSUME THE VALUE ZERO, SUBJECT TO RESTRICTIONS GIVEN IN ADJOINING COLUMN	$l + m > 0$ $n > 0$	SAME AS TM MODES		$\frac{abL}{4} \frac{(p^2 + q^2)(p^2 + q^2 + r^2)^{\frac{3}{2}}}{aL[p^2 r^2 + (p^2 + q^2)^2] + bL[q^2 r^2 + (p^2 + q^2)^2] + ab r^2 (p^2 + q^2)}$ $lm > 0$ $\frac{abL}{2} \frac{(q^2 + r^2)^{\frac{3}{2}}}{q^2 L(b+2a) + r^2 b(L+2a)}$ $l = 0$ $\frac{abL}{2} \frac{(p^2 + r^2)^{\frac{3}{2}}}{p^2 L(a+2b) + r^2 a(L+2b)}$ $m = 0$	
CIRCULAR CYLINDER 	TM	$E_\rho = -\sqrt{\frac{\mu}{\epsilon}} \frac{k_3}{k} J_0(k_1 \rho) \cos \ell \theta \sin k_3 z$ $E_\theta = \sqrt{\frac{\mu}{\epsilon}} \frac{k_3}{k} \frac{J_0'(k_1 \rho)}{k_1 \rho} \sin \ell \theta \sin k_3 z$ $E_z = \sqrt{\frac{\mu}{\epsilon}} \frac{k_1}{k} J_0(k_1 \rho) \cos \ell \theta \cos k_3 z$ $H_\rho = -\ell \frac{J_0'(k_1 \rho)}{k_1 \rho} \sin \ell \theta \cos k_3 z$ $H_\theta = -J_0'(k_1 \rho) \cos \ell \theta \cos k_3 z$ $H_z = 0$	$k_1 = \frac{2.4048}{a}$ $k_3 = \frac{n\pi}{L}$ $k^2 = k_1^2 + k_3^2$ $\lambda = \frac{2\pi}{k}$	$m > 0$	$\lambda = \frac{2}{\sqrt{\left(\frac{2.4048}{\pi a}\right)^2 + \left(\frac{n}{L}\right)^2}}$ $(fa)^2 = \left(\frac{c r_{lm}}{\pi}\right)^2 + \left(\frac{cn}{2}\right)^2 \left(\frac{a}{L}\right)^2$	$N = 4.38 \frac{V}{\lambda_0} + 0.09 \frac{S}{\lambda_0}$ $V = \frac{\pi a^2 L}{4}$ $S = \pi a L$	$\frac{r_{lm}}{2\pi} [1 + p^2 R^2]^{\frac{1}{2}} \cdot \frac{1}{1+R}$ $n > 0$ $\frac{r_{lm}}{\pi} \frac{1}{2+R}$ $n = 0$	$R = \frac{a}{L}$ $p = \frac{n\pi}{2r_{lm}}$
	TE	$E_\rho = -\sqrt{\frac{\mu}{\epsilon}} \ell \frac{J_0(k_1 \rho)}{k_1 \rho} \sin \ell \theta \sin k_3 z$ $E_\theta = -\sqrt{\frac{\mu}{\epsilon}} J_0'(k_1 \rho) \cos \ell \theta \sin k_3 z$ $E_z = 0$ $H_\rho = \frac{k_3}{k} J_0'(k_1 \rho) \cos \ell \theta \cos k_3 z$ $H_\theta = -\ell \frac{k_3}{k} \frac{J_0'(k_1 \rho)}{k_1 \rho} \sin \ell \theta \cos k_3 z$ $H_z = \frac{k_1}{k} J_0(k_1 \rho) \cos \ell \theta \sin k_3 z$	$r_{lm} =$ mth ZERO OF $J_0(x)$ FOR TM MODES $r_{lm} =$ mth ZERO OF $J_0'(x)$ FOR TE MODES	$m > 0$ $n > 0$		$f =$ FREQUENCY $C = \sqrt{\mu\epsilon} =$ VELOCITY OF ELECTROMAGNETIC WAVES IN DIELECTRIC		$\frac{r_{lm}}{2\pi} [1 + p^2 R^2]^{\frac{3}{2}} \frac{1 - (r_{lm}/a)^2}{1 + p^2 R^3 + p^2 (1-R) R^2 (r_{lm}/a)^2}$
FULL COAXIAL 	TM	SAME AS FOR CIRCULAR CYLINDER, BUT SUBSTITUTE: $Z_\ell(k_1 \rho)$ FOR $J_0(k_1 \rho)$ $Z'_\ell(k_1 \rho)$ FOR $J'_0(k_1 \rho)$	SAME AS CIRCULAR CYLINDER, EXCEPT: $r_{lm} =$ mth ZERO OF $[J_0(\eta x) Y_0(x) - J_0(x) Y_0(\eta x)]$ $A = \frac{J_0(r_{lm})}{Y_0(r_{lm})}$ FOR TM MODES $r_{lm} =$ mth ZERO OF $[J'_0(\eta x) Y_0(x) - J'_0(x) Y_0(\eta x)]$ $A = \frac{J'_0(r_{lm})}{Y'_0(r_{lm})}$ FOR TE MODES	$m > 0$ SPECIAL CASE OF TM 0,0,n MODE, WITH $r_{lm} = 0$	SAME FORM AS FOR CYLINDER $r_{lm}$ HAS DIFFERENT VALUES	$N \approx 4.4 \frac{V}{\lambda_0}$ WITH SOME DOUBT AS TO VALUE OF THE COEFFICIENT	$\frac{r_{lm}}{2\pi} [1 + p^2 R^2]^{\frac{1}{2}} \frac{(1 - \eta^2 H')}{(1 + \eta H') + R(1 - \eta^2 H')}$ $n > 0$ $\frac{r_{lm}}{\pi} \frac{(1 - \eta^2 H')}{2(1 + \eta H') + R(1 - \eta^2 H')}$ $n = 0$ THESE EXPRESSIONS ARE NOT VALID FOR SMALL $\eta$ WHEN $l = 0$	$R = \frac{a}{L}$ $p = \frac{n\pi}{2r_{lm}}$
TE	WHERE $Z_\ell(k_1 \rho) = J_\ell(k_1 \rho) - A Y_\ell(k_1 \rho)$ $Z'_\ell(k_1 \rho) = J'_\ell(k_1 \rho) - A Y'_\ell(k_1 \rho)$		$m > 0$ $n > 0$			$\frac{r_{lm}}{2\pi} \frac{[1 + p^2 R^2]^{\frac{3}{2}} M}{(1 + \eta H) + p^2 R^2 \frac{e^2}{r_{lm}^2} (1 + \frac{H}{\eta}) + p^2 R^3 M}$ WHERE $M = \left(1 - \frac{\ell^2}{r_{lm}^2}\right) - \eta^2 H \left(1 - \frac{\ell^2}{\eta^2 r_{lm}^2}\right)$	$H' = \left[\frac{Z'_\ell(\eta r_{lm})}{Z_\ell(r_{lm})}\right]^2$ $H = \left[\frac{Z_\ell(\eta r_{lm})}{Z_\ell(r_{lm})}\right]^2$	

SOURCES: HANSEN, JNL. APP. PHYS., 9, P. 654  
 BORGNIS, ANN. D. PHYS., 35, P. 359

BORGNIS, HOCHF. TECH. U. ELEK. AKUS., 56, P. 47  
 BARROW & MIEHER, PROC. I.R.E., 28, P. 184

\* THE TIME FACTOR HAS BEEN OMITTED;  
 THE E-FIELD IS IN TIME QUADRATURE  
 WITH THE H-FIELD, WITH  $\omega = ck$

Fig. 1—Formulas for cavity resonators—fields, resonant frequencies and mode shape factors for rectangular prism, circular cylinder and full coaxial.

3. Limitation of frequency range of a tunable cavity in the  $TE\ 01n$  mode as set by ambiguity.
4. Resonant frequencies of an elliptic cylinder.
5. Resonant frequencies and  $Q$  of higher order modes of a coaxial resonator.
6. Fins in a circular cylinder.

APPROXIMATION FORMULA FOR NUMBER OF RESONANCES IN A CIRCULAR CYLINDER

From Fig. 1, the resonant frequencies of the cylindrical cavity are obtained from the equation:

$$(fa)^2 = \left(\frac{cr}{\pi}\right)^2 + \left(\frac{\pi na}{2L}\right)^2 \tag{1}$$

in which  $r$  is written in place of  $r_{lm}$ , to simplify the equations. The distribution of the resonant frequencies, starting with the lowest, can be approximated by a continuous function

$$N \approx F(f_0) \approx G(\lambda_0)$$

where  $N$  represents the total number of resonances up to a frequency  $f_0$  or a wavelength  $\lambda_0$ . This is bound to be an approximation, since the true function  $F$  is discontinuous (or stepped) by virtue of the resonances being a series of discrete values. For practical purposes, if  $F$  fits the stepped curve so that the steps fluctuate above and below  $F$ , it will be a useful approximation.

Derivation of such a formula as applied to the acoustic resonances of a rectangular box has recently been a subject of investigation by Bolt<sup>9</sup> and Maa.<sup>10</sup> Only slight modifications of their method need be made to apply to the present situation.

Multiply (1) thru by  $\left(\frac{\pi}{c}\right)^2$ :

$$\left(\frac{\pi af}{c}\right)^2 = r^2 + \left(\frac{\pi an}{2L}\right)^2$$

Hence, if a point  $\left(r, \frac{\pi an}{2L}\right)$  is plotted on the  $XY$  plane the distance from the origin to this point will be  $\frac{\pi af}{c}$  and hence a measure of the resonant frequency. If all such points are plotted, they will form a lattice representing all the possible modes of resonance. The problem, then, is to find the number of lattice points in a quadrant of a circle with radius,  $R = \frac{\pi af_0}{c}$ .



The values of the Bessel zero,  $r$ , are not evenly spaced along the  $X$  axis; indeed the density, or number per unit distance, increases as  $r$  increases. Let the density be  $p(x)$ . Then the problem becomes one of finding the weight of a quadrant of material whose density varies as  $p(x)$ .

Suppose the expression for  $M$ , the number of zeros  $r$ , less than some value  $x$ , is of the form

$$M = Ax^2 + Bx$$

whence, by differentiation,

$$p(x) = 2Ax + B.$$

The weight,  $W$ , of the quadrant of a circle of radius  $R$  is then, by integration,

$$W = \frac{2}{3}AR^3 + \frac{\pi}{4}BR^2.$$

Since there are  $\frac{2L}{\pi a}$  lattice points per unit distance along the  $Y$  axis,  $\frac{2LW}{\pi a}$  is apparently the total number of points in the quadrant. However, there are two small corrections to consider. First is that in this procedure a lattice point is represented by an area and for the points along the  $X$  axis half the area, i.e., a strip  $\frac{\pi a}{4L}$  wide lying in the adjacent quadrant, has been omitted. Second is that the restriction  $n > 0$  for  $TE$  modes eliminates half the points along the  $X$  axis. As it happens, these corrections just cancel each other. Thus we have

$$N = \frac{16\pi A}{3} \frac{V}{\lambda_0^3} + \frac{\pi B}{2} \frac{S}{\lambda_0^2}$$

in which

$$V = \frac{\pi a^2 L}{4} \quad S = \pi a L \quad \lambda_0 = \frac{c}{f_0}.$$

From a tabulation<sup>11</sup> of the first 180 values of  $r$ , the empirical values  $A = 0.262$ ,  $B = 0$  were obtained. This gives

$$N = 4.39 \frac{V}{\lambda_0^3}.$$

Subsequently, from an analysis of over a thousand modes in a "square cylinder" ( $a = L$ ), Dr. Alfredo Baños, formerly of M.I.T. Radiation Laboratory, has calculated the empirical formula

$$N = 4.38 \frac{V}{\lambda_0^3} + 0.089 \frac{S}{\lambda_0^2} \quad (2)$$

from which  $A = 0.262$ ,  $B = 0.057$ . These values give better agreement with the 180 tabulated values of  $r$ .

There is a two-fold degeneracy in a circular cylinder for modes with  $\ell > 0$ , which is removed, for example, when the cylinder is made elliptical. The total number of modes, then, counting degeneracies twice, is about  $2N$ , which brings (2) in line with the general result that, in any cavity resonator, the total number of modes is of the order  $\frac{8\pi}{3} \frac{V}{\lambda_0^3}$ .

#### MINIMUM VOLUME OF CIRCULAR CYLINDER FOR ASSIGNED $Q$

In practical applications of resonant cavities, the conditions of operation may require high values of  $Q$  which can be attained only by the use of high order modes. The total number of modes, most of which are undesired, can then be reduced only by making the cavity volume as small as possible, consistent with meeting the requirement on  $Q$ .

It will be shown that, for a cylinder, operation in the  $TE_{01n}$  mode very probably gives the smallest volume for an assigned  $Q$ .

#### *Statement of Problem*

When the relative proportions (the shape) of a cavity and the mode of oscillation are fixed, both the  $Q$  and the volume,  $V$ , of the cavity are functions of the operating wavelength,  $\lambda$ . Since we are primarily interested in the relationship between  $Q$  and  $V$ , with  $\lambda$  fixed, some simplification can be made by eliminating  $\lambda$  as a parameter. This may be done by a change of variables to  $Q \frac{\delta}{\lambda}$  and  $\frac{V}{\lambda^3}$ , respectively; to simplify the typography, these quantities will be denoted by single symbols:

$$P \equiv Q \frac{\delta}{\lambda}$$

$$W \equiv \frac{V}{\lambda^3}.$$

We are, consequently, interested in the following specific problem:

In a circular cylindrical resonator, which is the optimum mode family and what is the corresponding shape to obtain the smallest value of  $W$  for a preassigned value of  $P$ ?

A rigorous solution cannot be obtained by the methods of elementary calculus, since  $P$  is not a continuous function of the mode of oscillation. However, a possible procedure is to assume continuity, and examine the relation between  $P$  and  $W$  under this assumption. If sufficiently positive results are obtained, the conclusions may then be carried over to the discontinuous (i.e., the physical) case with reasonable assurance that, except

perhaps for special values, the correct answer is obtained. We proceed on this basis.

### Solution

To permit a more coherent presentation of the arguments, only their general outline follows. More mathematical details are given later.

We start with the formulas for  $Q \frac{\delta}{\lambda}$  ( $= P$ ) as given in Fig. 1.

The first operation is to show that, under comparable conditions, i.e.,  $\lambda$ ,  $r$ ,  $n$  fixed, the  $TE_{0mn}$  modes give the highest values of  $P$ . That this is plausible can be seen in a general manner from the equations as they stand. For the  $TE$  modes, if  $\ell = 0$ , the numerator of the fraction is largest. Also,  $P$  simplifies, and the denominator roughly reduces the expression in square brackets to the  $1/2$  power. Now compare this expression with those for the  $TM$  modes. That for the  $TM$  modes ( $n > 0$ ) is smaller because of the factor  $(1 + R)$  in the denominator. Finally, that for the  $TM$  modes ( $n = 0$ ) is still smaller, because  $1 < (1 + p^2 R^2)^{1/2}$ .

This leaves only the  $TE_{0mn}$  modes to be considered, and the next step is to show that  $m = 1$  is the most favorable value. Since the relation between  $P$  and  $W$  is complicated, a parameter  $\varphi$  is introduced, with  $\varphi$  defined by

$$\tan \varphi = pR. \quad (3)$$

The resulting parametric equations are:

$$P = \frac{r}{2\pi} \frac{1}{\cos^3 \varphi + \frac{1}{p} \sin^3 \varphi} \quad (4)$$

$$W = \frac{pr^3}{4\pi^2} \frac{1}{\cos^2 \varphi \sin \varphi}. \quad (5)$$

For each of the discrete values of  $r$  and  $n$  ( $n$  is related to  $p$ ) then, plots of  $P$  vs  $W$  can be prepared as shown in Fig. 2 for the  $TE_{01n}$  modes.

Inspection of Fig. 2 shows that the best value of  $Q$  does not correspond to a minimum of  $W$  or a maximum of  $P$  for a given value of  $n$ , but rather to a point on the "envelope" of the curves. To get the envelope, we assume  $p$  to be continuous and proceed in the standard manner. It turns out that, by solving (4) for  $p$  in terms of  $P$ ,  $r$  and  $\varphi$ , substituting the resulting expression in  $W$ , and setting  $\frac{\partial W}{\partial \varphi} = 0$  an equation is obtained which, when solved for  $\varphi$ , gives the values of  $\varphi$  which lie on the envelope.

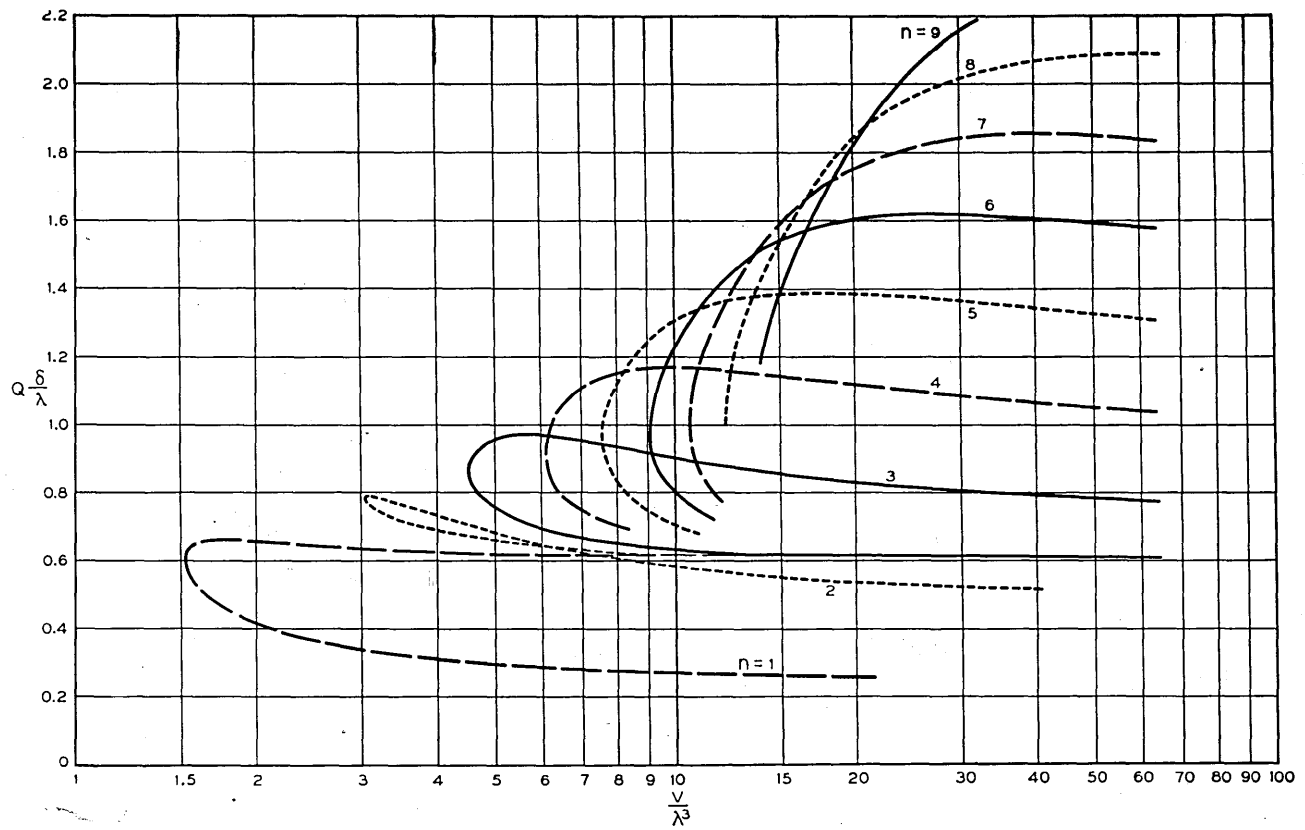


Fig. 2—Relation between  $Q \frac{\delta}{\lambda}$  ( $= P$ ) and  $\frac{V}{\lambda^3}$  ( $= W$ ) in cylindrical cavity resonator operating in  $TE 01n$  mode.

We next substitute this expression for  $\varphi$  in  $W$  and calculate  $\frac{\partial W}{\partial r}$  assuming now that  $r$  is continuous, and find that  $W$  has no minimum. Practically, this means that the smallest value of  $r$  should be used, i.e., the  $TE_{01n}$  mode.

Finally, since from Fig. 2 it is seen that the envelope is reasonably smooth for values of  $Q \frac{\delta}{\lambda} > 1$ , the expression for  $\varphi$  derived on the assumption of continuous  $p$  is used to obtain a simple relation of great utility in practical cavity design.

#### *Details of solution*

In (3), since  $R$  must be finite for a physical cylinder,  $0 < \tan \varphi < \infty$ ,  $0 < \sin \varphi < 1$ , and  $0 < \cos \varphi < 1$ . Hence we may always divide by  $\sin \varphi$  or  $\cos \varphi$ . Note that  $\varphi$  ranges between  $0^\circ$  and  $90^\circ$ .

From Fig. 1,

$$k = \frac{2r(1 + p^2 R^2)^{1/2}}{a}$$

whence

$$k \sin \varphi = \frac{2prR}{a} \quad (6)$$

$$k \cos \varphi = \frac{2r}{a}. \quad (7)$$

We define  $W$  by:

$$W \equiv \frac{V}{\lambda^3} = \frac{\pi a^3}{4R} \frac{k^3}{8\pi^3}. \quad (8)$$

Substituting (6) and (7) in (8),

$$W = \frac{pr^3}{4\pi^2} \frac{1}{\cos^2 \varphi \sin \varphi}. \quad (5')$$

Substitution of (3) into the expression for  $Q \frac{\delta}{\lambda}$  ( $= P$ ) for the  $TE$  modes as given in Fig. 1 yields, after some manipulation

$$P = \frac{r}{2\pi} \cdot \frac{1 - (\ell/r)^2}{\cos^3 \varphi + \frac{1}{p} \sin^3 \varphi + \left( \cos \varphi - \frac{1}{p} \sin \varphi \right) (\ell/r)^2 \sin^2 \varphi}$$

To show that any value of  $\ell > 0$  reduces  $P$  below its value when  $\ell = 0$ , let

$$\begin{aligned}
 a &= \cos^3 \varphi + \frac{1}{p} \sin^3 \varphi \\
 b &= \left( \cos \varphi - \frac{1}{p} \sin \varphi \right) \sin^2 \varphi \\
 c &= (\ell/r)^2.
 \end{aligned}$$

It suffices to show that

$$\frac{1}{a} > \frac{1-c}{a+bc}$$

where the question is in doubt because  $b$  may take on negative values. If the inequality is to be valid, it is necessary only that  $(b+a) > 0$ , that is,  $\cos \varphi > 0$ . Hence, for the  $TE$  modes, only  $\ell = 0$  needs be considered. For this case, the expression for  $P$  simplifies to

$$P = \frac{r}{2\pi} \frac{1}{\cos^3 \varphi + \frac{1}{p} \sin^3 \varphi} \tag{4'}$$

For the  $TM$  modes, there is similarly obtained

$$P = \frac{r}{2\pi} \frac{1}{\cos \varphi + \frac{1}{p} \sin \varphi} \quad n > 0 \tag{9}$$

$$P = \frac{r}{2\pi} \frac{\cos \varphi}{\cos \varphi + \frac{1}{2p} \sin \varphi} \quad n = 0. \tag{10}$$

It is easy to show, since  $\cos \varphi < 1$  and  $\sin \varphi < 1$ , that both (9) and (10) are less than (4').

Hence we have shown that, under comparable conditions, i.e.,  $r$  and  $p$  constant, the  $TE\ 0mn$  modes have higher values of  $P$  than any others. There is one flaw in the argument, viz.,  $r$  takes on discrete values and cannot be made the same for all modes. It is conceivable, therefore, that for some specific values of  $P$ , a mode other than the  $TE\ 0mn$  can be found which gives a smaller  $W$  than either of the two "adjacent"  $TE\ 0mn$  modes, one having a value of  $r$  higher, the other lower, than the supposed high- $P$  mode. This situation requires further refinement, and hence complication, in the analysis; we pass over this point.

Having so far indicated that the  $TE\ 0mn$  modes are the best, our next objective is find the best value of  $m$ , if possible.

By use of the parametric equations (4) and (5), Fig. 2 has been plotted for  $r = 3.83$  ( $TE_{01n}$  modes) and values of  $n$  from 1 to 9. This drawing shows that, for each discrete value of  $r$ , minimum  $W/P$  is given by points on the "envelope" of the family of curves.

The standard method of obtaining the envelope is to express  $W$  as a function of  $P$  with  $n$  as parameter ( $r$  is assumed fixed, for the moment), i.e.,  $W = F(P, n)$ , and then set  $\frac{\partial F}{\partial n} = 0$ . However, in this case it is easier to express  $W = G(P, \varphi)$  and  $\varphi = H(n)$ , whence

$$\frac{\partial F}{\partial n} = \frac{\partial G}{\partial \varphi} \cdot \frac{\partial \varphi}{\partial n}$$

and the envelope is obtained by setting  $\frac{\partial G}{\partial \varphi} = 0$  provided  $\frac{\partial \varphi}{\partial n} \neq 0$ . We proceed, therefore, as follows.

Assume  $p$  is continuous, and solve (4) for  $p$ , obtaining:

$$p = \frac{\sin^3 \varphi}{\frac{r}{2\pi P} - \cos^3 \varphi}. \quad (11)$$

Now substitute (11) in (5). This gives  $W$  as a function of  $P$  and  $\varphi$ :

$$W = \frac{r^3}{4\pi^2} \left[ \frac{\sin^2 \varphi}{\cos^2 \varphi \left( \frac{r}{2\pi P} - \cos^3 \varphi \right)} \right]. \quad (12)$$

To solve  $\frac{\partial W}{\partial \varphi} = 0$ , we differentiate and simplify. This yields

$$5 \cos^3 \varphi - 3 \cos^5 \varphi = \frac{r}{\pi P}. \quad (13)$$

Substituting (13) back into (11) yields

$$p = \frac{2 \sin \varphi}{3 \cos^3 \varphi} \quad (14)$$

The situation so far is that, with  $P$  and  $r$  assigned,  $W$  lies on the envelope and is a minimum when  $\varphi$  satisfies (13);  $p$  is then given by (14). Obviously, for (13) to hold, it is necessary that

$$\frac{r}{2\pi P} < 1.$$

To obtain the best value of  $r$ , the procedure is to differentiate  $W_{\min}$  with respect to  $r$ , assuming now that  $r$  is continuous, and examine for a mini-

num. We can, however, first differentiate (12) by setting

$$\frac{dW}{dr} = \frac{\partial W}{\partial r} + \frac{\partial W}{\partial \varphi} \cdot \frac{\partial \varphi}{\partial r}$$

and then substitute from (13). However, when (13) is satisfied,  $\frac{\partial W}{\partial \varphi} = 0$ .

This process yields

$$\frac{dW}{dr} = \frac{r^2 (2 - 3 \cos^2 \varphi)}{\pi^2 9 \sin^2 \varphi \cos^5 \varphi}.$$

This shows  $\frac{dW}{dr}$  to be positive, when  $\cos^2 \varphi < \frac{2}{3}$ . Hence  $\frac{dW}{dr} = 0$  corresponds to a maximum, rather than a minimum.\* If  $\cos^2 \varphi < \frac{2}{3}$ , that is,  $\varphi > 35^\circ 16'$ , then  $r$  should be as small as possible. The smallest  $r$  is 3.83, for the *TE* 01*n* modes. For  $r = 3.83$ , and  $\varphi > 35^\circ$ , from (13) there is obtained  $P > 0.75$ .

The analysis thus indicates that, for values of  $P = Q \frac{\delta}{\lambda}$  greater than 0.75, the *TE* 01*n* mode yields the smallest ratio  $W/P$  or  $V/Q$ .

An interesting and simple relation between  $fa$  and  $R$  for minimum  $W/P$  can easily be derived from the foregoing equations. Substitute (14) back into (6), thereby obtaining

$$k = \frac{4Rr}{3a \cos^3 \varphi}. \tag{15}$$

Now use (7) with (15) to eliminate  $\cos \varphi$ , replace  $k$  by  $2\pi/\lambda$ , and  $r$  by 3.83, its numerical value for the *TE* 01*n* modes. This gives

$$\left(\frac{a}{\lambda}\right)^2 R = 2.23$$

or by substituting  $\lambda = \frac{c}{f}$ ,  $c = 3 \times 10^{10}$ ,

$$(fa)^2 R = 20.1 \times 10^{20}.$$

This useful relation was first discovered by W. A. Edson.

Some further discussion is of interest. It is realized that a number of points have not been taken care of in a manner entirely satisfactory mathematically, but nevertheless important practical results have been obtained. As an example, since  $p$  and  $r$  can assume only discrete values, there are

\* It is for this reason that the determination of the stationary values of  $W(r, p, \varphi)$ , subject to the constraint  $P(r, p, \varphi) = \text{constant}$ , by La Grange multipliers fails to yield the desired least value of  $W/P$ .



specific situations where some mode other than the  $TE\ 01n$  gives a smaller  $W/P$ . For example, it may be shown that for  $P$  between 0.97 and 1.14 the  $TE\ 021$  mode yields a smaller  $W$  than the  $TE\ 013$  or  $TE\ 014$  modes. However, the margin is small, and for larger  $P$ , the  $TE\ 02n$  modes become progressively poorer.

LIMITATION ON FREQUENCY RANGE OF TUNABLE CAVITY AS SET  
BY AMBIGUITY

In the design of a tunable cylindrical resonant cavity intended for use in the  $TE\ 01n$  mode, the requirements on  $Q$  may dictate a diameter large enough to sustain  $TE\ 02n'$  or  $TE\ 03n'$  modes. Also, the range of variation of cavity length may be such that the  $TE\ 01(n+1)$  mode is supported. As the cavity is required to tune over a certain range of frequency, the maximum frequency range possible in the  $TE\ 01n$  mode without interference from the  $TE\ 01(n+1)$ † or any  $TE\ 02$  or  $TE\ 03$  modes is of interest. The interference from the  $TE\ 01(n+1)$  limits the useful range of the  $TE\ 01n$  by the presence of extraneous responses at more than one dial setting for a given frequency or more than one frequency for a given dial setting. In applications so far made, it has been possible to eliminate extraneous responses from the  $TE\ 02$  and  $TE\ 03$  modes, but crossings of these modes with the main  $TE\ 01n$  mode have not been permitted. No designs have had diameters sufficiently large to support  $TE\ 04$  modes.

The desired relations are easily obtained by simple algebraic manipulation of equation (1). For simplicity in presentation of the results, we introduce some symbols applicable to this section only:

$$A = \left[ \frac{cr_{\ell,m}}{\pi} \right]^2 \quad B = \left[ \frac{c}{2} \right]^2 = 2.247 \times 10^{20}$$

$$A_0 = \text{value of } A \text{ for } TE\ 01n \text{ modes} = 13.371 \times 10^{20}$$

$$t = A/A_0$$

$$x_0 = (a/L)^2 \text{ at low frequency end of useful range of } TE\ 01n \text{ mode}$$

$$F = \text{frequency range ratio} = \frac{\text{maximum } f}{\text{minimum } f}$$

The values of  $A$  and  $t$  depend upon the interfering mode under consideration. For the  $TE\ 02n$  modes,  $A = 44.822 \times 10^{20}$ ,  $t = 3.3522$ .

The two typical cases of interest are shown on Fig. 3. For case I, am-

† It is easy to show that the extraneous response from the  $TE\ 01(n-1)$  mode is not limiting. The proof depends on the inequality  $n^2 > (n+1)(n-1)$ .

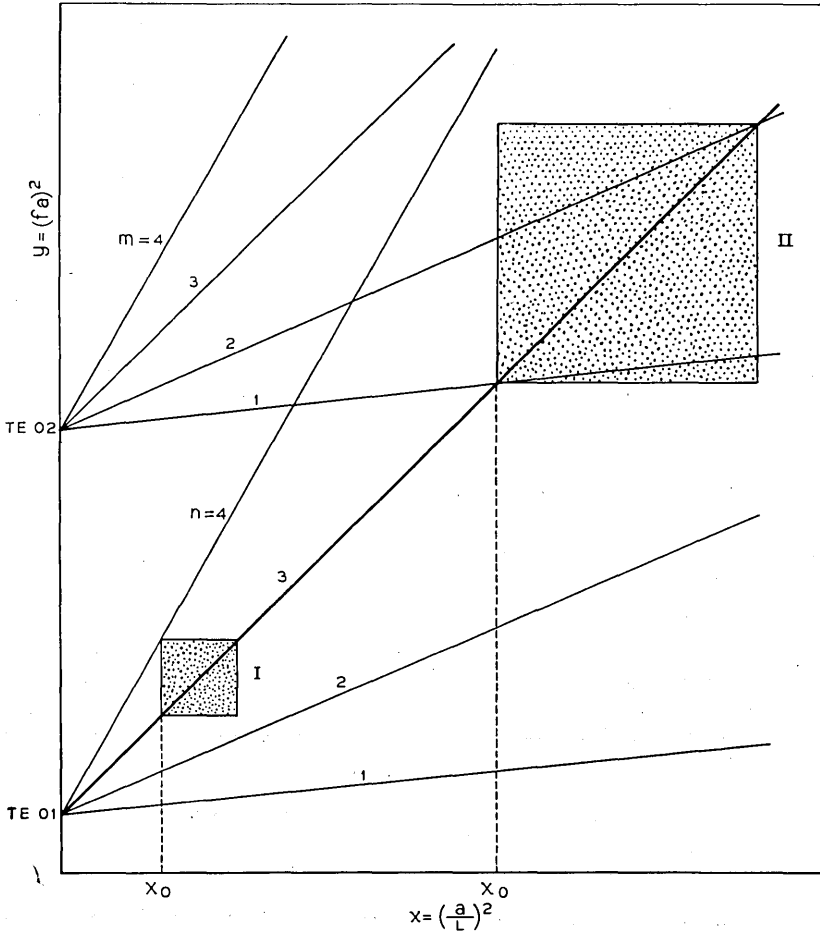


Fig. 3—Mode chart illustrating types of interference with  $TE\ 01n$  mode.

biguity from  $TE\ 01(n + 1)$  mode, it is found that

$$F^2 = \frac{A_0 + B(n + 1)^2 x_0}{A_0 + Bn^2 x_0}$$

Curves of  $F$  for this case are shown on Fig. 4.

The maximum value of  $F$  is obtained when  $x_0 = \infty$  and is

$$F_{\max} = \frac{n + 1}{n}$$

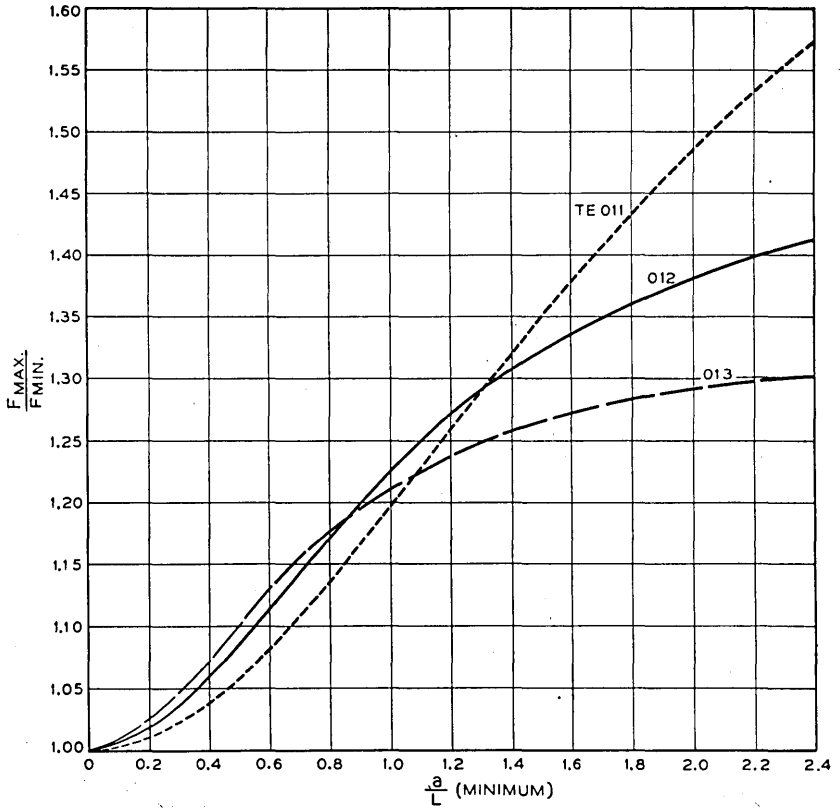


Fig. 4—Curves showing maximum value of frequency ratio without interference from  $TE\ 01(n+1)$  mode (case I of Fig. 3).

TABLE I.—Case II: Maximum Frequency Range Ratio,  $F$ , for  $TE\ 01n$  Mode when Limited by Mode Crossings with  $TE\ 02m$  and  $TE\ 02(m+1)$  Modes.

$m$	$n = 3$		$n = 4$		$n = 12$	
	$F$	$(a/L)_{min}$	$F$	$(a/L)_{min}$	$F$	$(a/L)_{min}$
1	1.198	1.323	1.086	0.966	1.008	0.313
2			1.242	1.080	1.013	0.316
3					1.019	0.322
4					1.027	0.331
5					1.037	0.343
6					1.051	0.360
7					1.071	0.384
8					1.104	0.418
9					1.168	0.471
10					1.345	0.564

For case II, range limited by mode crossings, it is found that

$$x_0 = \frac{A - A_0}{B(n^2 - n'^2)}$$

$$F^2 = \frac{(n^2 - n'^2)[n^2 t - (n' + 1)^2]}{(n^2 t - n'^2)[n^2 - (n' + 1)^2]}$$

Some values for this case are given in Table I.

The formulas above are general and may be used for any pair of mode types by using the appropriate values for  $A$  and  $t$ .

#### THE ELLIPTIC CYLINDER

In the design of high  $Q$  circular cylinder cavity resonators operating in the  $TE_{01n}$  mode, it is desirable to know how much ellipticity is tolerable, so that suitable manufacturing limits may be set. The elliptical wave guide has already been studied, notably by Brillouin<sup>12</sup> and Chu,<sup>13</sup> but the results are not in suitable form or of adequate precision for the present purposes. More recently tables<sup>14</sup> have become available which permit the calculation of some of the properties of the elliptical cylindrical resonator.

The elliptical cavity involves Mathieu functions, which are considerably more complicated than Bessel functions.<sup>16</sup> The tables give the numerical coefficients of series expansions, in terms of sines, cosines, and Bessel functions, of the Mathieu functions up to the fourth order. These tables have been used for the calculation of some quantities of interest in connection with elliptical deformations of a circular cylinder in the  $TE_{01n}$  mode.

#### *The Ellipse*

All mathematical treatments of the ellipse (including the tables mentioned above) use the eccentricity,  $e$ , as the quantity describing the amount of departure from the circular form. The eccentricity is the ratio

$$e = \frac{\text{distance between foci}}{\text{major axis}}$$

This is not a quantity subject to direct measurement, hence we here introduce and use throughout the ellipticity,  $E$ , defined as

$$E = \frac{\text{difference between major and minor diameters}}{\text{major diameter}}$$

It is clear that the ellipticity is easily obtained directly.

Again, many results are given in terms of the major diameter. Since we are interested in deformations from circular, and in such deformations the

perimeter remains constant, while the major diameter changes, we have expressed our results in terms of an average diameter, defined as

$$D = \frac{\text{perimeter}}{\pi}$$

Figure 5 shows the ellipse and various relations of interest.

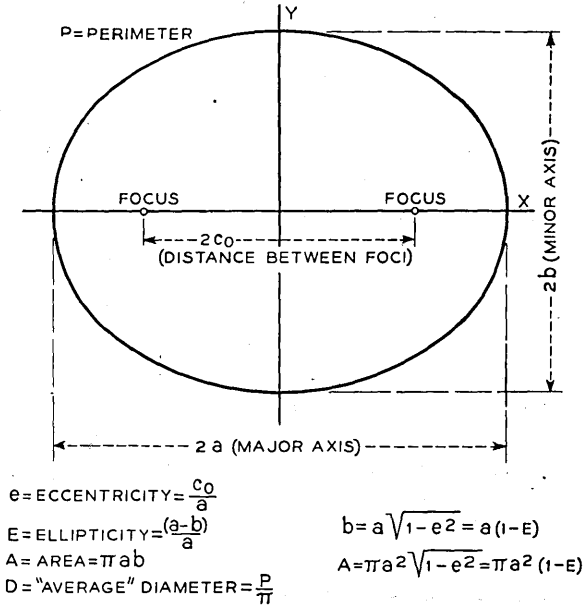


Fig. 5—The ellipse

*Elliptic Coordinates and Functions*

The elliptic coordinate system is shown on Fig. 6. Following Stratton,<sup>15</sup> we have used  $\xi$  in place of the table's  $z$ , since we wish to use  $z$  as the coordinate along the longitudinal axis. Stratton also uses  $\eta = \cos \varphi$  as the angular coordinate; this is frequently convenient.

Analogous to  $\cos \ell \theta$  and  $\sin \ell \theta$  in the circular case, there are even and odd\* angular functions, denoted by

$${}^o S_\ell(c, \cos \varphi) \text{ and } {}^e S_\ell(c, \cos \varphi)$$

which reduce to  $\cos \ell \theta$  and  $\sin \ell \theta$  respectively when  $c \rightarrow 0$ . Similarly, there are even and odd\* radial functions, denoted by

$${}^o J_\ell(c, \xi) \text{ and } {}^e J_\ell(c, \xi)$$

\* For  $\ell = 0$ , only even functions exist.

which both reduce to  $J_\ell(k_1\rho)$  when  $c \rightarrow 0$ . In the above,  $c$  is a parameter related to the ellipticity.\* The tables do not give values of the functions, but rather give numerical coefficients

$$D_n^\ell \text{ and } F_n^\ell$$

of expansions in series of cosine, sine and Bessel functions, which permit one to calculate the elliptic cylinder functions. The coefficients, of course,

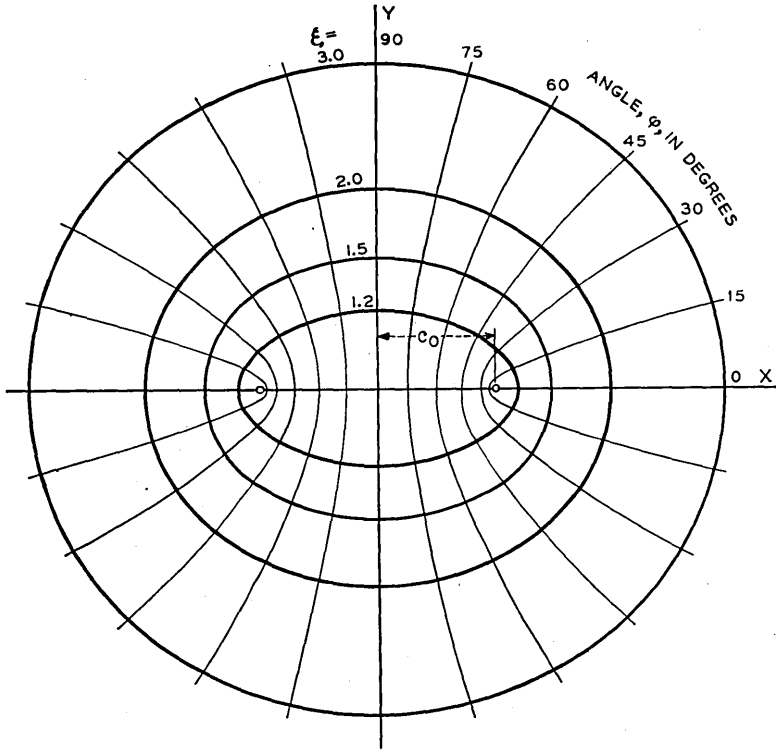


Fig. 6—Elliptic coordinate system

depend on the parameter  $c$ ; the largest value of  $c$  in the tables is 4.5, which corresponds to an ellipticity of 39% in a cylinder operating in the  $TE_{01n}$  mode.\*\* For this case, Bessel functions up to  $J_{12}(x)$  and  $J'_{12}(x)$  are needed for calculating the radial function. It is clear that calculations on elliptic cylinders have not been put on a simple basis.

\* Not to be confused with  $c$  = velocity of electromagnetic waves; the symbol  $c$  is here carried over from the published tables.

\*\* An ellipticity of 39% means that the difference between maximum and minimum diameters is 39% of the maximum diameter. For a given  $c$ , the ellipticity depends on the mode.

*Field Equations*

The equations for the fields are easily obtained from section 6.12 of Stratton's book, and are given in Table II, which is self-explanatory, except for the quantity  $c$ , which we now proceed to discuss.

*Resonant Frequencies*

The elliptic cylinder has the major diameter,  $2a$ , and the focal distance,  $2c_0$ . The equation of its surface is then expressed by  $\xi = \frac{a}{c_0} = \alpha$ . On this surface,  $E_\eta$  must vanish. This requires that  ${}^{oo}J'_\ell(c, \alpha) = 0$  for *TE* modes and that  ${}^{oo}J_\ell(c, \alpha) = 0$  for *TM* modes. The series expansions are in terms of  $c\xi$  as variable. Let  $c\alpha = r'_{\ell m}$  or  $r_{\ell m}$  be the roots of the above equations. Then  $\frac{c}{c_0} = \frac{r}{a}$  (dropping the subscripts  $\ell, m$ ). Now, in working out the solution of the differential equations, it turned out that  $c = c_0 k_1$ . Here  $k_1$  is one component of the wave number,  $k\uparrow$ . Hence  $k_1 = \frac{r}{a}$ . Furthermore, the eccentricity is  $e = \frac{c_0}{a} = \frac{c}{r}$ . The indicated procedure is: 1) choose a value of  $c$ ; 2) find the various values of  $r$  for which the radial function or its derivative is zero; 3) then calculate the corresponding eccentricity and resonant frequency. Notice that for a given value of  $c$ , the values of  $r$  will depend on the mode, and hence so will the eccentricity.

We now wish to express our results in terms of the ellipticity and the average diameter. To convert eccentricity to ellipticity, we use

$$E = 1 - \sqrt{1 - e^2}.$$

The perimeter of the ellipse is given by  $P = 4aE(e)$  where  $E(e)$  is the complete elliptic integral of the second kind.††

In terms of the average diameter we find

$$k_1 = \frac{2}{D} \left[ \frac{2rE(e)}{\pi} \right]$$

or calling the quantity in brackets  $s$ ,  $k_1 = \frac{2s}{D}$ . This is now in the same form as  $k_1$  for a circular cylinder of diameter  $D$ . The quantity  $s$  is the reciprocal of Chu's  $\frac{\lambda_c}{S}$ .

† It is recalled that

$$k = \frac{2\pi}{\lambda} = \sqrt{k_1^2 + k_3^2}; \quad k_1 = \frac{r}{a}; \quad k_3 = \frac{n\pi}{L}.$$

†† This is tabulated as  $E(\alpha)$  in Jahnke & Emde, p. 85, with  $\alpha = \sin^{-1}e$ .

We have calculated and give in Table III values of  $r$ ,  $e$ ,  $E$  and  $s$  for several values of  $c$  and for a few modes of special interest. For three cases,  ${}^eTE$  01,  ${}^eTM$  11 and  ${}^oTM$  11, we have determined an empirical formula to fit the calculated values of  $s$ . These are also given in Table III.

TABLE II. ELLIPTIC CYLINDER FIELDS

*TE* Modes

$$E_\xi = -k \sqrt{\frac{\mu}{\epsilon} \frac{\sqrt{1-\eta^2}}{q}} S'_\ell(c, \eta) J_\ell(c, \xi) \sin k_3 z \cos \omega t$$

$$E_\eta = k \sqrt{\frac{\mu}{\epsilon} \frac{\sqrt{\xi^2-1}}{q}} S_\ell(c, \eta) J'_\ell(c, \xi) \sin k_3 z \cos \omega t$$

$$H_\xi = k_3 \frac{\sqrt{\xi^2-1}}{q} S_\ell(c, \eta) J'_\ell(c, \xi) \cos k_3 z \sin \omega t$$

$$H_\eta = k_3 \frac{\sqrt{1-\eta^2}}{q} S'_\ell(c, \eta) J_\ell(c, \xi) \cos k_3 z \sin \omega t$$

$$H_z = k_1^2 S_\ell(c, \eta) J_\ell(c, \xi) \sin k_3 z \sin \omega t$$

*TM* Modes

$$E_\xi = -k_3 \frac{\sqrt{\xi^2-1}}{q} S_\ell(c, \eta) J'_\ell(c, \xi) \sin k_3 z \cos \omega t$$

$$E_\eta = -k_3 \frac{\sqrt{1-\eta^2}}{q} S'_\ell(c, \eta) J_\ell(c, \xi) \sin k_3 z \cos \omega t$$

$$E_z = k_1^2 S_\ell(c, \eta) J_\ell(c, \xi) \cos k_3 z \cos \omega t$$

$$H_\xi = -k \sqrt{\frac{\epsilon}{\mu} \frac{\sqrt{1-\eta^2}}{q}} S'_\ell(c, \eta) J_\ell(c, \xi) \cos k_3 z \sin \omega t$$

$$H_\eta = k \sqrt{\frac{\epsilon}{\mu} \frac{\sqrt{\xi^2-1}}{q}} S_\ell(c, \eta) J'_\ell(c, \xi) \cos k_3 z \sin \omega t$$

Notes:

Derivatives are with respect to  $\xi$  and  $\eta$ .

$S_\ell$  and  $J_\ell$  carry prefixed superscripts,  $e$  or  $o$ , since they may be either even or odd.

$$q = c_0 \sqrt{\xi^2 - \eta^2} \quad c = c_0 k_1$$

$$k_1 = \frac{r_{\ell,m}}{a} \quad k_3 = \frac{n\pi}{L} \quad k^2 = k_1^2 + k_3^2$$

$2c_0$  is distance between foci of ellipse.

$a$  is the semi major diameter of the ellipse.

$r_{\ell,m}$  is the value of  $c\xi$  that makes

$$J_\ell(c, \xi) = 0 \text{ for } TM \text{ modes}$$

$$J'_\ell(c, \xi) = 0 \text{ for } TE \text{ modes.}$$



TABLE III ROOT VALUES OF RADIAL ELLIPTIC CYLINDER FUNCTIONS

Mode	$c$	$r$	$e$	$E$	$s$	
${}^{\circ}TE\ 01$	0	3.8317	0	0	3.8317	
	0.2	3.8343	0.05216	0.001361	3.8317	
	0.4	3.8423	0.10410	0.005434	3.8318	
	0.6	3.8558	0.15561	0.012181	3.8324	
	0.8	3.8753	0.20643	0.021539	3.8337	
	1.0	3.9015	0.25631	0.033406	3.8366	
	1.2	3.9349	0.30496	0.047636	3.8417	
	1.4	3.9763	0.35209	0.064033	3.8500	
	1.6	4.0264	0.39738	0.082346	3.8624	
	2.0	4.154	0.4814	0.12351	3.902	
	3.0	4.634	0.6474	0.2378	4.101	
	4.0	5.29	0.756	0.346	4.42	
	4.5	5.66	0.795	0.393	4.62	
	$s = 3.8317 + 4.33 E^2 + 1.9E^3$					
${}^{\circ}TM\ 11$	0	3.8317	0	0	3.8317	
	0.2	3.8330	0.05218	0.001362	3.8304	
	0.4	3.8370	0.10425	0.005449	3.8265	
	0.6	3.8436	0.15610	0.012259	3.8201	
	0.8	3.8532	0.20762	0.021791	3.8113	
	1.0	3.8658	0.25868	0.034036	3.8003	
	1.2	3.8818	0.30913	0.048981	3.7874	
	1.4	3.9015	0.35884	0.066599	3.7727	
	1.6	3.9253	0.40761	0.086844	3.7568	
	4.5	5.13	0.878	0.520	3.91	
	$s = 3.8317 - 0.96E + 1.1E^2$					
	${}^{\circ}TM\ 11$	0	3.8317	0	0	3.8317
		0.2	3.8356	0.05214	0.001361	3.8330
		0.4	3.8474	0.10397	0.005419	3.8370
0.6		3.8670	0.15516	0.012111	3.8436	
0.8		3.8944	0.20542	0.021326	3.8530	
1.0		3.9298	0.25446	0.032918	3.8654	
1.2		3.9731	0.30203	0.046701	3.8809	
1.4		4.0243	0.34788	0.062462	3.8997	
$s = 3.8317 + 0.95E + 2.2E^2$						
${}^{\circ}TE\ 22$	0	6.706	0	0	6.706	
	0.4	6.712	0.0596	0.00178	6.706	
	0.8	6.729	0.1189	0.00709	6.705	
	1.2	6.756	0.1776	0.01590	6.702	
	1.6	6.788	0.2357	0.02817	6.693	
	2.0	6.826	0.2930	0.04389	6.677	
${}^{\circ}TE\ 22$	0	6.706	0	0	6.706	
	0.4	6.712	0.0596	0.00178	6.706	
	0.8	6.730	0.1189	0.00709	6.706	
	1.2	6.762	0.1775	0.01587	6.708	
	1.6	6.810	0.2350	0.02799	6.715	
	2.0	6.877	0.2908	0.04323	6.729	

Mode	$c$	$r$	$e$	$E$	$s$
*TE 32	0	8.015	0	0	8.015
	0.4	8.020	0.0499	0.00124	8.015
	0.8	8.035	0.0996	0.00497	8.015
	1.2	8.059	0.1489	0.01115	8.014
	1.6	8.093	0.1977	0.01974	8.013
	2.0	8.135	0.2459	0.03070	8.010
*TE 32	0	8.015	0	0	8.015
	0.4	8.020	0.0499	0.00124	8.015
	0.8	8.035	0.0996	0.00497	8.015
	1.2	8.060	0.1489	0.01115	8.015
	1.6	8.097	0.1976	0.01972	8.018
	2.0	8.146	0.2455	0.03061	8.022
*TM 01	0	2.4048	0		
	0.2	2.4090	0.08302		
	0.4	2.4216	0.16518		
	0.6	2.4431	0.24559		
	0.8	2.4739	0.32337		
	1.0	2.5149	0.39762		
*TE 11	0	1.8412	0		
	0.2	1.8416	0.10860		
	0.4	1.8430	0.21704		
	0.6	1.8452	0.32516		
	0.8	1.8484	0.43280		
	1.0	1.8527	0.53975		

## Notes:

Superscripts  $e$  and  $o$  on mode designation signify even and odd.

$c$  is parameter used in the Tables (Stratton, Morse, Chu, Hutner, "Elliptic Cylinder and Spheroidal Wave Functions")

$r$  is the value of the argument which, for  $TM$  modes, makes the radial function zero and, for  $TE$  modes, makes its derivative zero.

$e$  is the eccentricity of the ellipse;

$$e = \frac{\text{distance between foci}}{\text{major diameter}}$$

$E$  is the ellipticity of the ellipse;

$$E = \frac{\text{difference between major and minor diam.}}{\text{major diameter}}$$

$s$  is the root value, referred to the "average diameter"; it is related to  $r$  by:

$$s = \frac{r}{\pi} \frac{\text{perimeter}}{\text{major diameter}}$$

The quantity  $s$  is also related to the cutoff wavelength in an elliptical wave guide according to:

$$s = \frac{\text{perimeter of guide}}{\text{cutoff wavelength}}$$

Resonator  $Q$ 

Although the calculation of the root values is straightforward and not overly laborious, the same cannot be said for the integrations involved in the determination of resonator  $Q$ . The procedure is obvious: The field

equations are given; it is only necessary to integrate  $H^2 d\tau$  over the volume and  $H^2 d\sigma$  over the surface and get  $Q$  from

$$Q = \frac{2}{\delta} \frac{\int H^2 d\tau}{\int H^2 d\sigma} \quad (16)$$

with  $\delta$  = skin depth, a known constant. Unfortunately the integrations cannot at present be expressed in closed form. A numerical solution can be obtained by a combination of integration in series and of numerical integration.

The calculations have been made for the  ${}^eTE$  01 mode with  $c = 2.0$ , for which  $r = 4.154$ . This value of  $c$  corresponds in this case to an ellipticity of about 12%; in a 4" cylinder this would amount to 1/2" difference between largest and smallest diameters. Evaluation\* of the integrals yields:

$$\int_V H^2 d\tau = 12.307 k_3^2 L + 12.294 k_1^2 L$$

$$\int_S H^2 d\sigma = 49.228 k_3^2 + 0.1619 k_1 k_3^2 L + 6.6847 k_1^2 L$$

Substituting  $k_1 = \frac{7.804}{D}$  and  $k_3 = \frac{\pi n}{L}$ , one obtains, finally

$$Q\delta = 0.471 D \left( \frac{1 + 0.1622 n^2 R^2}{1 + 0.0039 n^2 R^2 + 0.1529 n^2 R^3} \right).$$

For a circular cylinder,

$$Q_c \delta = 0.5 D \left( \frac{1 + 0.1681 n^2 R^2}{1 + 0.1681 n^2 R^3} \right).$$

Comparison of these two formulas for  $Q\delta$  shows that the losses in the end plates ( $n^2 R^3$  term) are less with respect to the side wall losses in the elliptical cylinder. The net loss in  $Q\delta$ , as described by the reduction in the multiplier from 0.5 to 0.471, is thus presumably ascribable to an increase in side wall losses (stored energy assumed held constant). The additional term in  $n^2 R^2$  in the denominator is responsible for the difference in the attenuation-frequency behavior of elliptical vs circular wave guide as shown by Chu, Fig. 4. Incidentally, these results agree numerically with those of Chu.

\* Numerical integration was by Weddle's rule; intervals of  $5^\circ$  in  $\varphi$  and 0.1 in  $x$  were used. The calculations were made by Miss F. C. Larkey.

Corresponding expressions for the resonant wavelength are

$$\lambda = \frac{\pi D}{s \sqrt{1 + \left(\frac{\pi n D}{2sL}\right)^2}} = \frac{0.805 D}{\sqrt{1 + 0.1622 n^2 R^2}}$$

$$\lambda_c = \frac{0.820 D}{\sqrt{1 + 0.1681 n^2 R^2}}$$

As an example, take  $n = 1, R = 1$ , then

(Circular) $Q_c \delta = 0.500 D$	$\lambda_c = 0.759 D$
(Elliptical) $Q \delta = 0.473 D$	$\lambda = 0.747 D$
Ratio = 0.946	Ratio = 0.984.

*Conclusions*

The mathematics of the elliptic cylinder have not yet been developed to the point where the design of cavities of large ellipticity could be undertaken. On the other hand, sufficient results have been obtained to indicate that the ellipticity in a cavity intended to be circular, resulting from any reasonable manufacturing deviations, would not have a noticeable effect on the resonant frequencies or  $Q$  values, at least away from mode crossings.

FULL CYLINDRICAL COAXIAL RESONATOR

The full coaxial resonator has been of some interest because of various suggestions for the use of a central rod for moving the tuning piston in a  $TE_{01n}$  cavity.

The cylindrical coaxial resonator, with the central conductor extending the full length of the resonator, has modes similar to the cylinder. In fact, the cylinder may be considered as a special case of the coaxial. The indices  $\ell, m, n$  have much the same meaning and the resonant frequencies are determined by the same equation (1). However, now the value of  $r$  depends in addition (see Fig. 1) upon  $\eta$ , where

$$\eta = \frac{\text{diameter inner conductor}}{\text{diameter outer conductor}} = \frac{b}{a}$$

The problem now arises of how best to represent the relations between  $f, a, b$  and  $L$ . The  $r$ 's depend on  $\eta$ ; so one possibility is to determine their values for a given  $\eta$  and then construct a series of mode charts, one for each value of  $\eta$ .

A more flexible arrangement is to plot the values of  $r$  vs  $\eta$  and allow the user to construct graphs suitable for the particular purpose in hand. An equivalent scheme has been used by Borgnis.<sup>18</sup>

It turns out that as  $\eta \rightarrow 1, r(1 - \eta) \rightarrow m\pi$ , for the  $TM$  modes and the

*TE*  $0mn$  modes, and  $r(1 - \eta) \rightarrow (m - 1)\pi$  for all other *TE* modes. For the former modes,  $r$  becomes very large as  $\eta \rightarrow 1$ , that is, as the inner conductor fills the cavity more and more, the frequency gets higher and higher. For the *TE*  $\ell 1n$  modes, however, as the inner conductor grows, the frequency falls to a limiting value. This is discussed in more detail by Borgnis.<sup>18</sup>

Figure 7 shows  $r(1 - \eta)$  vs  $\eta$ , for a few of the lower modes; the scale for  $\eta$  between 0.5 and 1.0 is collapsed since this region does not appear to be of great engineering interest. A different procedure is used for the roots of the *TE*  $\ell 1n$  modes. Figure 8 is a direct plot of  $r$  vs  $\eta$  for a few of the lower modes. In this case,  $r \rightarrow \ell$  as  $\eta \rightarrow 1$ .

#### *Distribution of Normal Modes*

The calculation of the distribution of the resonant modes for the coaxial case follows along the lines of that for the cylinder, as given previously. The difference lies in the distribution of the roots  $r$ , which now depend upon the parameter  $\eta$ . The determination of this latter distribution offers difficulties. There is some evidence, however, that the normal modes will follow, at least to a first approximation, the same law as the cylinder, viz.:

$$N = 4.4 \frac{V}{\lambda_0^3}$$

with some doubt regarding the value of the coefficient.

#### $Q \frac{\delta}{\lambda}$ in Coaxial Resonator

The integrations needed to obtain this factor are relatively straightforward, but a little complicated. The final results are given in Fig. 1.

The defining equation is (16); the components of  $H$  are given in Fig. 1. The integrations can be done with the aid of integrals given by McLachlan<sup>17</sup> and the following indefinite integral:

$$\int \left[ \ell \frac{2Z_\ell^2(x)}{x^2} + Z_\ell'^2(x) \right] x dx \\ = \frac{x^2}{2} \left[ Z_\ell'^2(x) + \frac{2Z_\ell(x)Z_\ell'(x)}{x} + Z_\ell^2(x) \left( 1 - \frac{\ell^2}{x^2} \right) \right]$$

which can be verified by differentiation, remembering that  $y = Z_\ell(x)$  is a solution of  $y'' + \frac{1}{x} y' + \left( 1 - \frac{\ell^2}{x^2} \right) y = 0$ .

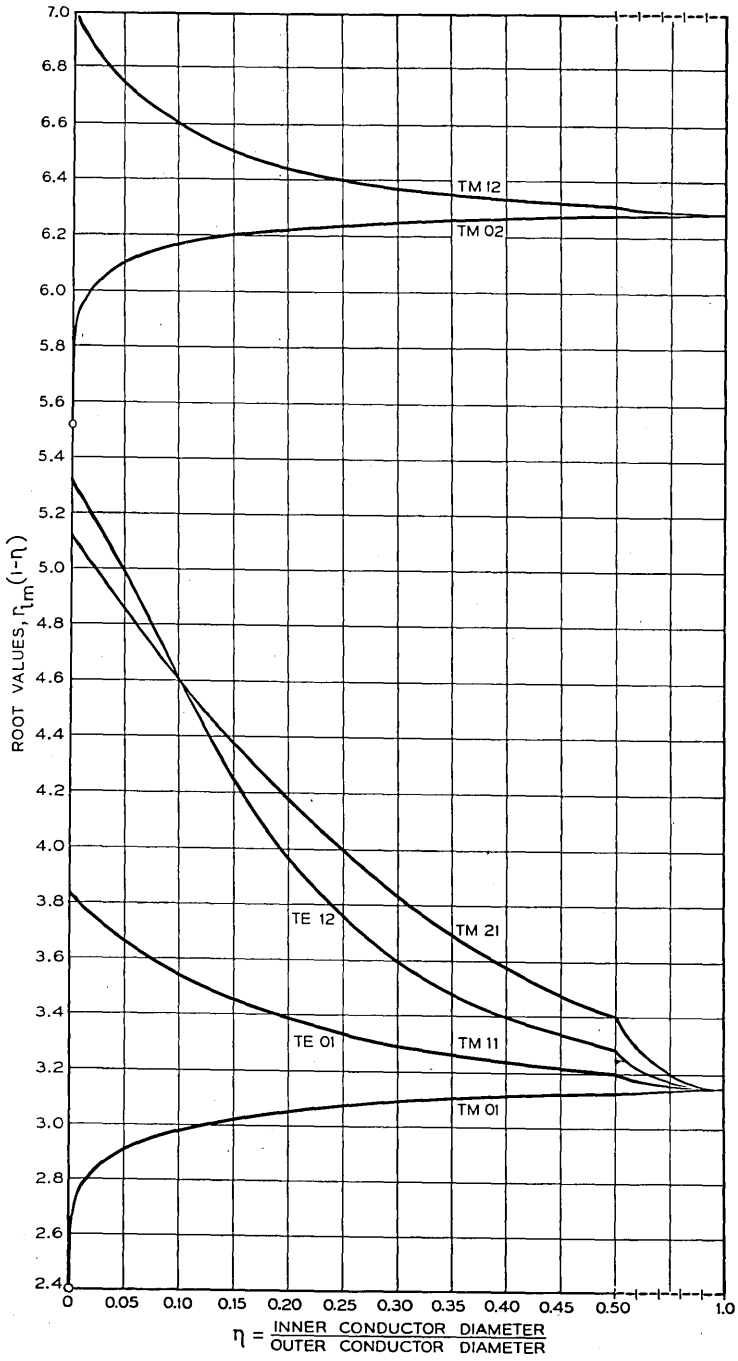


Fig. 7—Full coaxial resonator root values  $r_{tm}(1-\eta)$

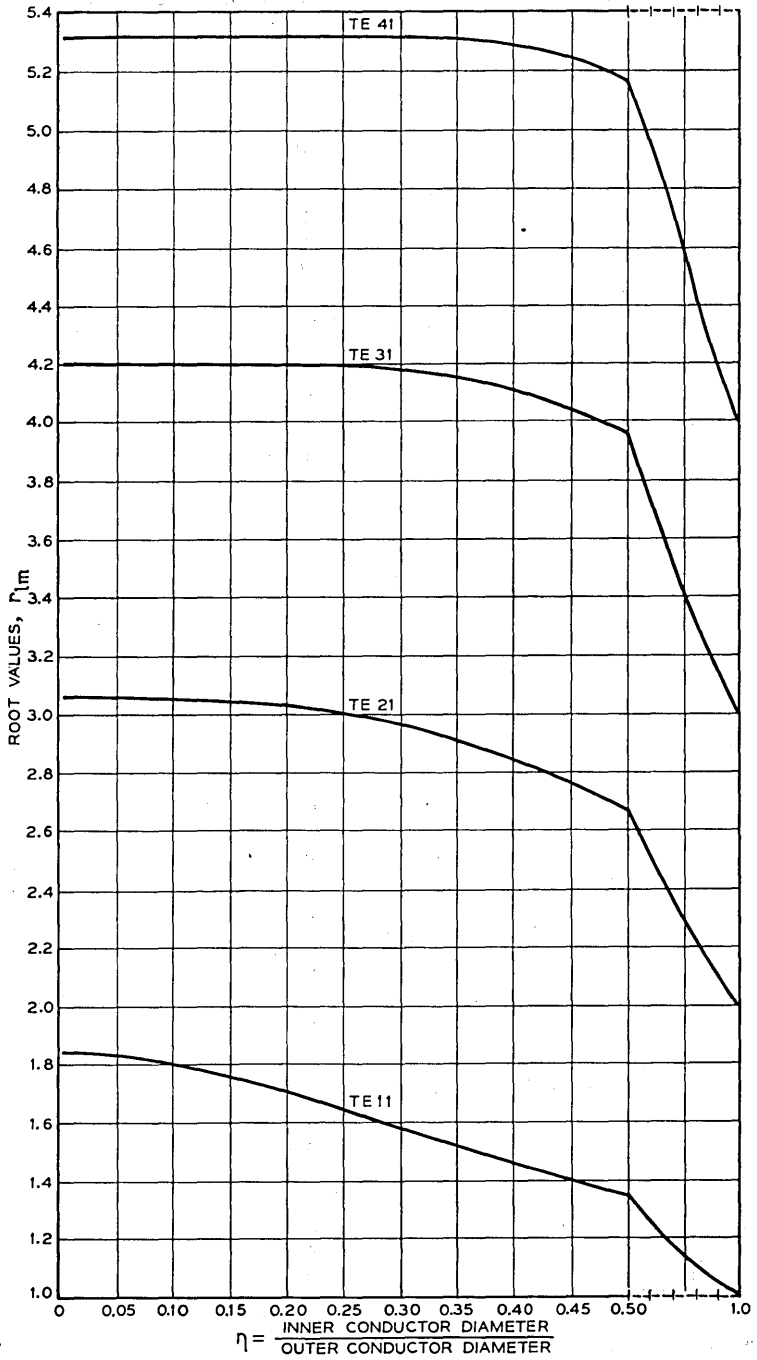


Fig. 8—Full coaxial resonator root values  $r_{lm}$

An investigation needs to be made of the behavior of the formulas as  $\eta \rightarrow 0$  before any conclusion may be drawn regarding their blending into those for the cylinder. For *TE* modes with  $\ell = 0$ , the term involving  $\frac{H}{\eta}$  disappears, hence no question arises. Consider then  $\ell > 0$ , and let  $x = \eta r$  for the discussion following. From expansions given in McLachlan, it is easy to show that, for small  $x$

$$Y_\ell(x) \approx -\frac{(\ell - 1)!}{\pi} \left(\frac{2}{x}\right)^\ell \quad Y'_\ell(x) \approx \frac{\ell!}{\pi} \left(\frac{2}{x}\right)^\ell \frac{1}{x}$$

$$J_\ell(x) \approx \frac{x^\ell}{2^\ell \ell!} \quad J'_\ell(x) \approx \frac{x^{\ell-1}}{2^\ell (\ell - 1)!}$$

Since, from Fig. 1,

$$A = \frac{J'_\ell(r)}{Y'_\ell(r)} = \frac{J'_\ell(\eta r)}{Y'_\ell(\eta r)} = \frac{J'_\ell(x)}{Y'_\ell(x)}$$

it is found, upon substitution of the approximations given above:

$$Z_\ell(x) \approx \frac{2x^\ell}{2^\ell \ell!}$$

That is,  $Z_\ell(x) \sim x^\ell$  and hence  $\rightarrow 0$  as  $x \rightarrow 0$ . Furthermore  $Z_\ell(r)$  remains finite as  $\eta \rightarrow 0$ . Hence  $H \sim x^{2\ell}$  and  $\frac{H}{\eta} \sim x^{2\ell-1}$ . Therefore, for  $\ell > 0$ ,  $\frac{H}{\eta} \rightarrow 0$  as  $\eta \rightarrow 0$ .

Hence, the expression for  $Q \frac{\delta}{\lambda}$  for the coaxial structure reduces to that for the cylinder, for any value of  $\ell$ , in the *TE* modes.

For the *TM* modes, and for  $\ell > 0$ , an entirely similar argument shows that  $H'$  remains finite as  $\eta \rightarrow 0$ . Hence, the expression for  $Q \frac{\delta}{\lambda}$  for these modes also reduces to that for the cylinder.

For the *TM* modes, and with  $\ell = 0$ , we have

$$Z'_0(x) = -J_1(x) + J_0(x) \frac{Y_1(x)}{Y_0(x)}$$

For  $x \rightarrow 0$ ,  $J_1(x) \rightarrow 0$  and  $J_0(x) \rightarrow 1$ , hence for small  $x$ ,

$$Z'_0(x) \sim \frac{Y_1(x)}{Y_0(x)}$$



Now substitute the approximate values of the  $Y$  for small  $x$ . The result is

$$Z'_0(x) \sim \frac{1}{x \log \frac{x}{2}}$$

Since  $Z'_0(r)$  is finite, it follows that

$$\eta H' \sim \frac{1}{x \left( \log \frac{x}{2} \right)^2}$$

and it is easily shown that  $\eta H' \rightarrow \infty$  as  $\eta \rightarrow 0$ . On the other hand,  $\eta^2 H' \rightarrow 0$  as  $\eta \rightarrow 0$ . Hence,  $Q \frac{\delta}{\lambda} \rightarrow 0$  as  $\eta \rightarrow 0$ . On the other hand, for  $\eta = 0$ , a

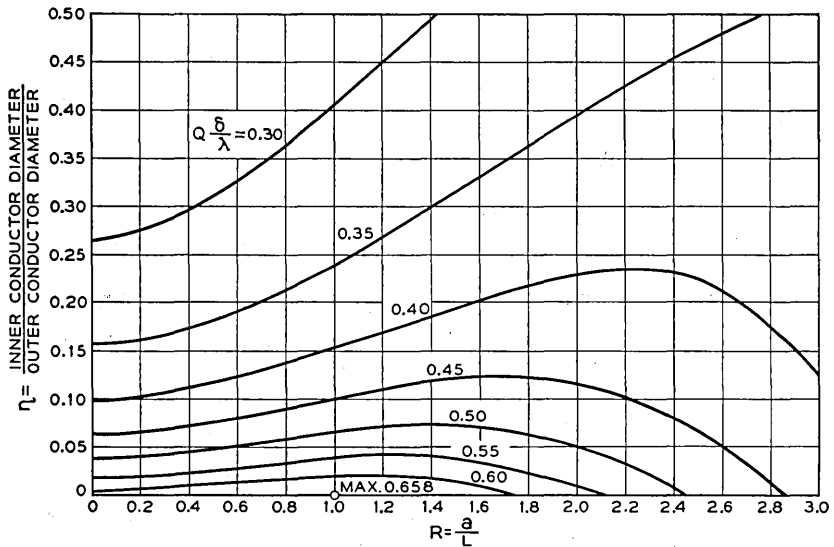


Fig. 9—Coaxial resonator.  $TE_{011}$  mode Contour lines of  $Q \frac{\delta}{\lambda}$

perfect cylinder exists whose  $Q \frac{\delta}{\lambda}$  is not zero. It is concluded that the expression for  $Q \frac{\delta}{\lambda}$  does not apply for small  $\eta$  for the  $TM$  modes with  $\ell = 0$ .

Thus it is seen that the expressions for the factor  $(Q \frac{\delta}{\lambda})$  reduce to those given for the cylinder, when  $\eta = 0$ , except for  $TM$  modes with  $\ell = 0$ . For these latter cases, the factor approaches zero as  $\eta$  approaches zero, because  $\eta H'$  increases without limit. This means that an assumption

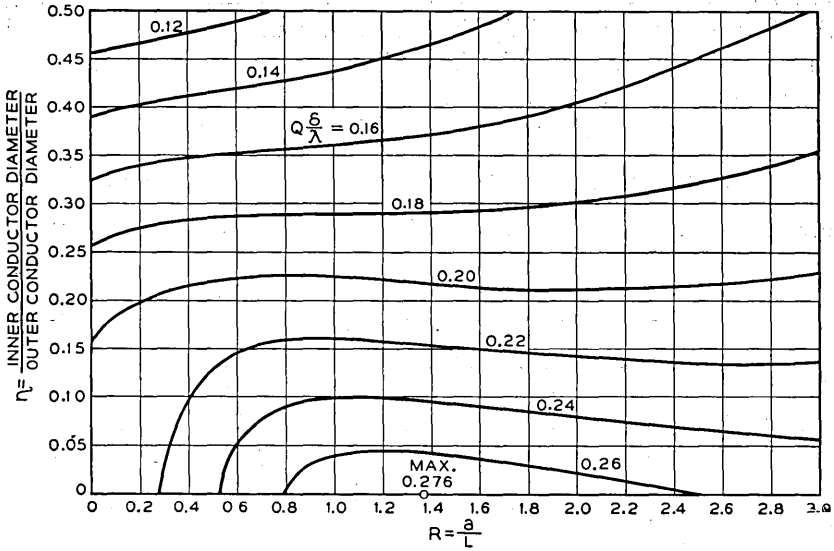


Fig. 10—Coaxial resonator.  $TE_{111}$  mode Contour lines of  $Q \frac{\delta}{\lambda}$

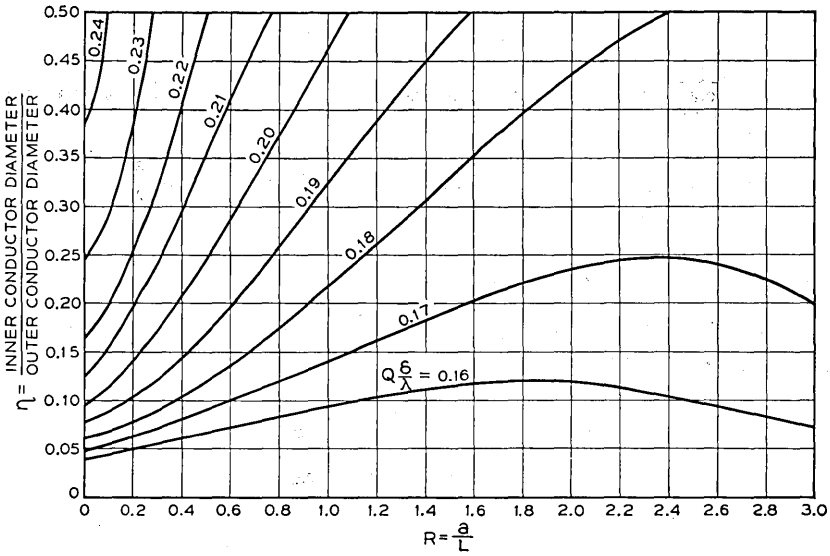


Fig. 11—Coaxial resonator.  $TM_{011}$  mode Contour lines of  $Q \frac{\delta}{\lambda}$

which was made in the derivation of the  $Q$  values is not valid for small  $\eta$ ; that is, the fields for the dissipative case are not the same as those derived on the basis of perfectly conducting walls.

The expressions for the factor are rather complicated, as it depends on several parameters. When a given mode is chosen, the number of parameters reduces to two,  $\eta$  and  $R$ . Contour diagrams of  $Q \frac{\delta}{\lambda}$  vs  $\eta$  and  $R$  are given on Figs. 9, 10, 11 and 12 for the  $TE$  011,  $TE$  111,  $TM$  011 and  $TM$  111

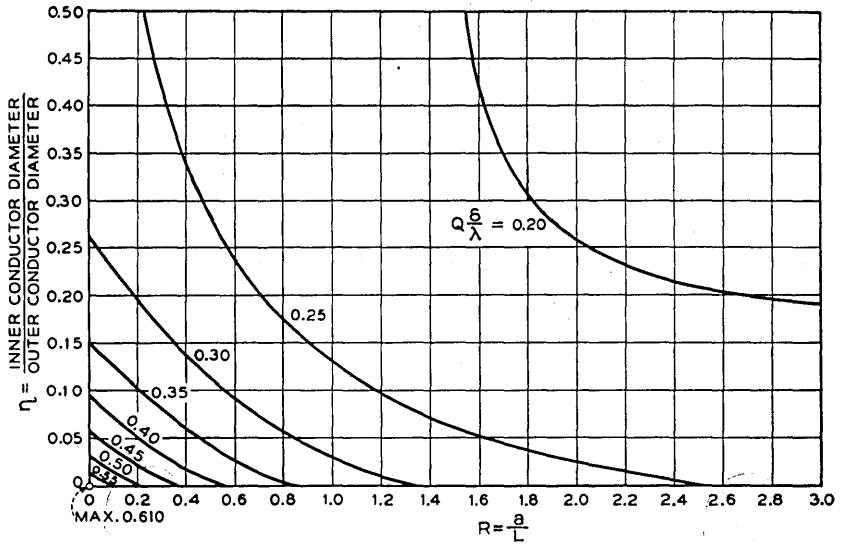


Fig. 12—Coaxial resonator.  $TM$  111 mode Contour lines of  $Q \frac{\delta}{\lambda}$

modes. As mentioned above, the true behavior of  $Q \frac{\delta}{\lambda}$  for the  $TM$  011 mode for small  $\eta$  is not given by the above formula, so this contour diagram has been left incomplete.

FINS IN A CAVITY RESONATOR

The suppression of extraneous modes is always an important problem in cavity design. Among the many ideas advanced along these lines is the use of structures internal to the cavity.

It is well known that if a thin metallic fin or septum is introduced into a cavity resonator in a manner such that it is everywhere perpendicular to the  $E$ -lines of one of the normal modes, then the field configuration and

frequency of that particular mode are undisturbed. For example, Fig. 13 shows the  $E$ -lines in a  $TE_{11n}$  mode in a circular cylinder. If the upper half of the cylinder wall is replaced by a new surface, shown dotted, the field and frequency in the resulting flattened cylinder will be the same as

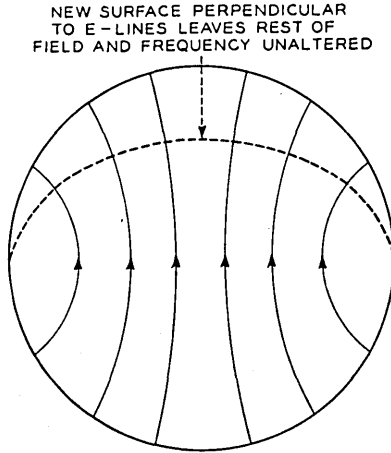


Fig. 13— $E$  Lines in  $TE_{11n}$  mode

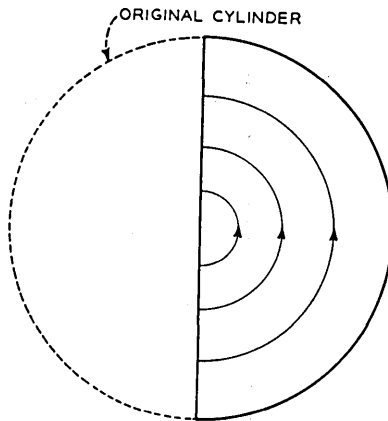


Fig. 14—"TE $01n$ " mode in half-cylinder

before. Indeed, they will also be the same in the crescent-shaped resonator indicated in the figure.

Except for isolated cases, all the other modes of the original cylinder will be perturbed in frequency since the old fields fail to satisfy the boundary conditions over the new surface. Furthermore, if the original cylinder was

circular, its inherent double degeneracy will be lost and each of the original modes (with minor exceptions) will split into two.

Although the frequency and fields of the undisturbed mode are the same, the  $Q$  is not necessarily so. For example, Fig. 14 shows a "TE  $01n$  mode" in a half cylinder.\*

It is easy to calculate  $Q \frac{\delta}{\lambda}$  for this case. The result is

$$Q \frac{\delta}{\lambda} = \frac{r}{2\pi} \cdot \frac{(1 + p^2 R^2)^{3/2}}{1 + p^2 R^3 + K_1 + K_2 p^2 R^2} \quad (17)$$

in which

$$K_1 = 1.290 \quad K_2 = 0.653.$$

Here  $K_1$  and  $K_2$  are constants which account for the resistance losses in the flat side. For the full cavity, shown dotted in Fig. 14, eq. (17) holds with  $K_1 = K_2 = 0$ . If the circular cavity has a partition extending from the center to the rim along the full length, (17) holds with the values of  $K_1$  and  $K_2$  halved. If a fin projects from the rim partway into the interior, still other values of  $K_1$  and  $K_2$  are required. It is a simple matter to compute these for various immersions; Fig. 15 shows curves of  $K_1$  and  $K_2$ . The following table gives an idea of the magnitudes involved:

MODE: TE 0,1,12  $R = 0.4$

Fin, % $a$	$Q \frac{\delta}{\lambda}$	Ratio
0%	2.573	1.0
10	2.536	.985
20	2.479	.965
50	2.04	.79
100	1.47	.57

The question now is asked, "Suppose a longitudinal fin were used, small enough to cause only a tolerable reduction in the  $Q$ . Would such a fin ameliorate the design difficulties due to extraneous modes?"

Some of the effects seem predictable. All modes with  $\ell > 0$  will be split to some extent, into two modes of different frequencies. Consider the TE  $12n$  mode, for example. There will be one mode, of the same frequency as the original whose orientation must be such that its  $E$ -lines are perpendicular to the fin. The  $Q$  of this mode would be essentially unchanged. There will be a second mode, oriented generally  $90^\circ$  from the first, whose  $E$ -lines will be badly distorted (and the frequency thereby lowered) in the vicinity

\* Solutions for a cylinder of this cross-section are known and all the resonant frequencies and  $Q$  values could be computed, if they had any application.

of the fin. It would be reasonable to expect the  $Q$  of this mode to be appreciably lowered because of the concentrated field there. If two fins at  $90^\circ$  were present, there would be no orientation of the original  $TE_{12n}$  mode which would satisfy the boundary conditions. In this case both new modes

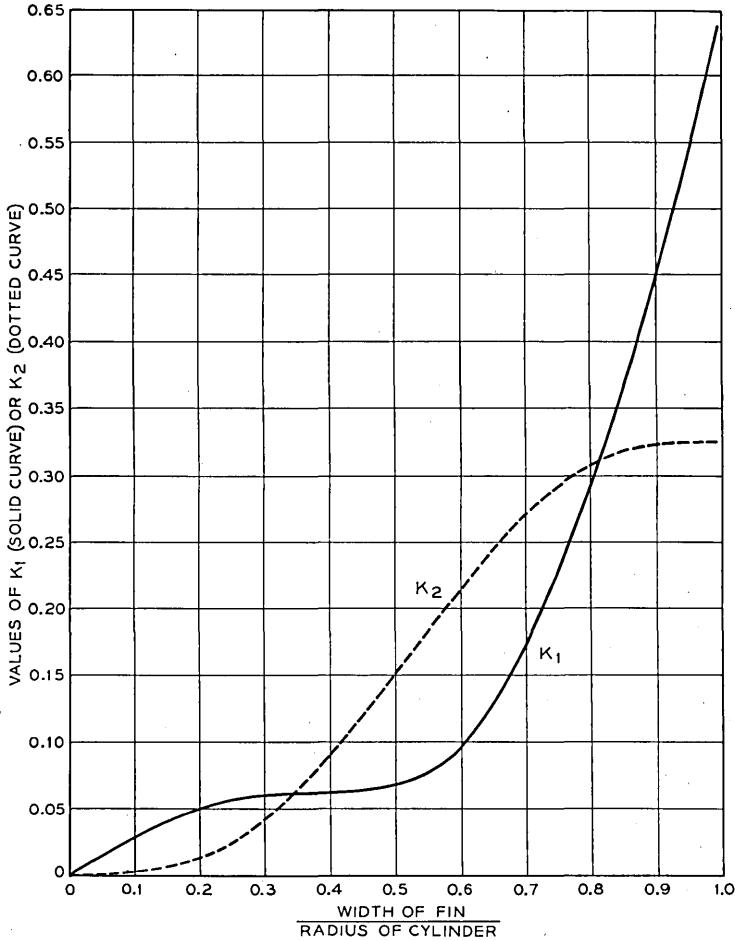


Fig. 15—Constants for calculation of  $Q$  of  $TE_{01n}$  mode in cylinder with longitudinal fin.

would be perturbed in frequency from the original value. If both fins were identical, the perturbations would be equal and a double degeneracy ensue. Similar effects would happen to the other types of modes.

The major advantage derivable from such effects would appear to be in extraneous transmissions. The fin serves to orient positively the fields in

the cavity, and the input and output coupling locations can then be appropriately chosen. On the basis that internal couplings are responsible for mode crossing difficulties, one might hazard a guess that a real fin would increase such couplings.

Another application of fins might be in a wave guide feed in which it is desired to establish only a  $TE_{0m}$  wave. In this case,  $Q$  is not so important and larger fins can be used. If these extended virtually to the center and  $x$  of them were present (with uniform angular spacing) all types of wave transmission having  $\ell$  less than  $x/2$ ,  $x$  even or  $\ell$  less than  $x$ ,  $x$  odd, would be suppressed. This use of fins is an extension of the wires that have been proposed in the past.

#### CONCLUSION

It is hoped that the foregoing, which covers some of the theoretical work done by the author during the war, will be of value to other workers in cavity resonators. There is much that needs to be done and hardly time for duplication of effort.

#### BIBLIOGRAPHY

1. E. I. Green, H. J. Fisher, J. G. Ferguson, "Techniques and Facilities for Radar Testing," *B.S.T.J.*, 25, pp. 435-482 (1946).
2. I. G. Wilson, C. W. Schramm, J. P. Kinzer, "High  $Q$  Resonant Cavities for Microwave Testing" *B.S.T.J.*, 25, pp. 408-434 (1946).
3. J. R. Carson, S. P. Mead, S. A. Schelkunoff, "Hyper-Frequency Wave Guides—Mathematical Theory," *B.S.T.J.*, 15, pp. 310-333 (1936).
4. G. C. Southworth, "Hyperfrequency Wave Guides—General Considerations and Experimental Results," *B.S.T.J.*, 15, pp. 284-309 (1936).
5. W. W. Hansen "A Type of Electrical Resonator," *Jour. App. Phys.*, 9, pp. 654-663 (1938).—A good general treatment of cavity resonators. Also deals briefly with coupling loops.
6. W. W. Hansen and R. D. Richtmyer, "On Resonators Suitable for Klystron Oscillators," *Jour. App. Phys.*, 10, pp. 189-199 (1939).—Develops mathematical methods for the treatment of certain shapes with axial symmetry, notably the "dimpled sphere," or hour glass.
7. W. L. Barrow and W. W. Micher, "Natural Oscillations of Electrical Cavity Resonators," *Proc. I.R.E.*, 28, pp. 184-191 (1940). An experimental investigation of the resonant frequencies of cylindrical, coaxial and partial coaxial (hybrid) cavities.
8. R. Sarbacher and W. Edson, "Hyper and Ultrahigh Frequency Engineering," John Wiley and Sons, (1943).
9. R. H. Bolt, "Frequency Distribution of Eigentones in a Three-Dimensional Continuum," *J.A.S.A.*, 10, pp. 228-234 (1939)—Derivation of better approximation formula than the asymptotic one; comparison with calculated exact values.
10. Dah-You Maa, "Distribution of Eigentones in a Rectangular Chamber at Low-Frequency Range," *J.A.S.A.*, 10, pp. 235-238 (1939)—Another method of deriving an approximation formula.
11. I. G. Wilson, C. W. Schramm, J. P. Kinzer, "High  $Q$  Resonant Cavities for Microwave Testing," *B.S.T.J.*, 25, page 418, Table III (1946).
12. L. Brillouin, "Theoretical Study of Dielectric Cables," *Elec. Comm.*, 16, pp. 350-372 (1938)—Solution for elliptical wave guides.
13. L. J. Chu, "Electromagnetic Waves in Elliptic Hollow Pipes of Metal," *Jour. App. Phys.*, 9, pp. 583-591 (1938).
14. Stratton, Morse, Chu, Hutner, "Elliptic Cylinder and Spheroidal Wave Functions," M.I.T. (1941).

15. J. A. Stratton, "Electromagnetic Theory," McGraw-Hill, (1941).
16. F. Jahnke and E. Emde, "Tables of Functions," pp. 288-293, Dover Publications (1943).
17. N. W. McLachlan, "Bessel Function for Engineers," Clarendon Press, Oxford (1934).
18. F. Borgnis, "Die konzentrische Leitung als Resonator," *Hochf. tech. u. Elek. Akus.*, 56, pp. 47-54, (1940).—Resonant modes and  $Q$  of the full coaxial resonator. For long abstract, see *Wireless Engineer*, 18, pp. 23-25, (1941).

## ADDITIONAL BIBLIOGRAPHY

19. J. J. Thomson, "Notes on Recent Researches in Electricity and Magnetism," Oxford, Clarendon Press, 1893,—§300 gives the resonant frequencies of the  $TE$  modes in a cylinder with  $a/L = 0$ ; §315-316 consider two concentric spheres; §317-318 treat of the  $Q$  of the spherical cavity.
20. Lord Rayleigh, "On the passage of electric waves through tubes or the vibrations of dielectric cylinders" *Phil. Mag.*; 43, pp. 125-132 (1897).—Considers rectangular and circular cross-sections.
21. A. Becker, "Interferenzröhren für elektrische Wellen," *Ann. d. Phys.*, 8, pp. 22-62 (1902)—Abstract in *Sci. Abs.*, 5, No. 1876 (1902)—Experimental work at 5 cm. and 10 cm.
22. R. H. Weber, "Elektromagnetische Schwingungen in Metallröhren," *Ann. d. Phys.*, 8, pp. 721-751 (1902)—Abstract in *Sci. Abs.*, 6A, No. 96 (1903).
23. A. Kalähne, "Elektrische Schwingungen in ringförmigen Metallröhren," *Ann. d. Phys.*, 18, pp. 92-127 (1905).—Abstract in *Sci. Abs.*, 8A, No. 2247 (1905).
24. G. Mie, "Beiträge zur Optik trüber Medien, speziell kolloidaler Metallösungen," *Ann. d. Phys.*, 25, pp. 337-445 (1908)—A part of this article deals with the solution of the equations for the sphere; also shown are the  $E$  and  $H$  lines for the lowest eight resonant modes.
25. H. W. Droste, "Ultrahochfrequenz-Übertragung längs zylindrischen Leitern und Nichtleitern," *TFT*, 27, pp. 199-205, 273-279, 310-316, 337-341 (1931)—Abstract in *Wireless Engr.*, 15, p. 617, No. 4209 (1938).
26. W. L. Barrow, "Transmission of Electromagnetic Waves in Hollow Tubes of Metal," *Proc. I.R.E.*, 24, pp. 1298-1328 (1936)—A development of the equations of propagation together with a discussion of terminal connections.
27. S. A. Schelkunoff, "Transmission Theory of Plane Electromagnetic waves," *Proc. I.R.E.*, 25, pp. 1457-1492 (1937)—Treats waves in free space and in cylindrical tubes of arbitrary cross-section; special cases; rectangle, circle, sector of circle and ring.
28. L. J. Chu, "Electromagnetic Waves in Elliptic Hollow Pipes of Metal," *Jour. App. Phys.*, 9, pp. 583-591 (1938)—A study of field configurations, critical frequencies, and attenuations.
29. G. Reber, "Electric Resonance Chambers," *Communications*, Vol. 18, No. 12, pp. 5-8 (1938).
30. F. Borgnis, "Elektromagnetische Eigenschwingungen dielektrischer Räume," *Ann. d. Phys.*, 35, pp. 359-384 (1939). Solution of Maxwell's equations for rectangular prism, circular cylinder, sphere; also derivations of stored energy and  $Q$  values.
31. W. W. Hansen, "On the Resonant Frequency of Closed Concentric Lines," *Jour. App. Phys.*, 10, pp. 38-45 (1939).—Series approximation method for  $TM_{00p}$  mode.
32. R. D. Richtmyer, "Dielectric Resonators," *Jour. App. Phys.*, 10, pp. 391-398 (1939).
33. H. R. L. Lamont, "Theory of Resonance in Microwave Transmission Lines with Discontinuous Dielectric," *Phil. Mag.*, 29, pp. 521-540 (1940).—With bibliography covering wave guides, 1937-1939.
34. E. H. Smith, "On the Resonant Frequency of a Type of Klystron Resonator," *Phys. Rev.*, 57, p. 1080 (1940).—Abstract.
35. W. C. Hahn, "A New Method for the Calculation of Cavity Resonators," *Jour. App. Phys.*, 12, pp. 62-68 (1941).—Series approximation method for certain circularly symmetric resonators.
36. E. U. Condon, "Forced Oscillations in Cavity Resonators," *Jour. App. Phys.*, 12 pp. 129-132 (1941).—Formulas for coupling loop and capacity coupling.
37. W. L. Barrow and H. Schaevitz, "Hollow Pipes of Relatively Small Dimensions," *A.I.E.E. Trans.*, 60, pp. 119-122 (1941).—Septate coaxial wave guide and cavity resonator, based on bending a flat rectangular guide into a cylinder.



38. H. König, "The Laws of Similitude of the Electromagnetic Field, and Their Application to Cavity Resonators," *Wireless Engr.*, 19, p. 216-217, No. 1304 (1942).—"The law of similitude has strict validity only if a reduction in dimensions by the factor  $1/m$  is accompanied by an increase in the conductivity of the walls by the factor  $m$ ." Original article in *Hochf; tech u. Elek:akus*, 58, pp. 174-180 (1941).
39. S. Ramo, "Electrical Concepts at Extremely High Frequencies," *Electronics*, Vol. 9, Sept. 1942, pp. 34-41, 74-82. A non-mathematical description of the physical phenomena involved in vacuum tubes, cavity resonators, transmission lines and radiators.
40. J. Kemp, "Wave Guides in Electrical Communication," *Jour. I.E.E.*, V. 90, Pt. III, pp. 90-114 (1943).—Contains an extensive listing of U. S. and British patents.
41. H. A. Wheeler, "Formulas for the Skin Effect," *Proc. I.R.E.*, 30, pp. 412-424 (1942).—Includes: a chart giving the skin depth and surface resistivity of several metals over a wide range of frequency; simple formulas for H.F. resistance of wires, transmission lines, coils and for shielding effect of sheet metal.
42. R. C. Colwell and J. K. Stewart, "The Mathematical Theory of Vibrating Membranes and Plates," *J.A.S.A.*, 3, pp. 591-595 (1932)—Chladni figures for a square plate.
43. R. C. Colwell, "Nodal Lines in A Circular Membrane" *J.A.S.A.*, 6, p. 194 (1935)—Abstract.
44. R. C. Colwell, "The Vacuum Tube Oscillator for Membranes and Plates," *J.A.S.A.*, 7, pp. 228-230 (1936)—Photographs of Chladni figures on circular plates.
45. R. C. Colwell, A. W. Friend, J. K. Stewart, "The Vibrations of Symmetrical Plates and Membranes," *J.A.S.A.*, 10, pp. 68-73 (1938).
46. J. K. Stewart and R. C. Colwell, "The Calculation of Chladni Patterns," *J.A.S.A.*, 11, pp. 147-151 (1939).
47. R. C. Colwell, J. K. Stewart, H. D. Arnett, "Symmetrical Sand Figures on Circular Plates," *J.A.S.A.*, 12, pp. 260-265 (1940).
48. V. O. Knudsen, "Resonance in Small Rooms," *J.A.S.A.*, 4, pp. 20-37 (1932)—Experimental check on the values of the eigentones.
49. H. Cremer & L. Cremer, "The Theoretical Derivations of the Laws of Reverberation," *J.A.S.A.*, 9, pp. 356-357 (1938)—Abstract of *Akustische Zeits.*, 2, pp. 225-241, 296-302 (1937)—Eigentones in a rectangular chamber.
50. H. E. Hartig and C. E. Swanson, "Transverse Acoustic Waves in Rigid Tubes," *Phys. Rev.*, 54, pp. 618-626 (1938)—Experimental verification of the presence of acoustic waves in a circular duct, corresponding to the *TE* and *TM* electromagnetic waves; shows an agreement between calculated and experimental values of the resonant frequencies, with errors of the order of  $\pm 1\%$ .
51. D. Riabouchinsky, *Comptes Rendus*, 207, pp. 695-698 (1938) and 269, pp. 664-666 (1939). Also in Science Abstracts A42, # 364 (1939) and A43, # 1236 (1940).—Treats of supersonic analogy of the electromagnetic field.
52. F. V. Hunt, "Investigation of Room Acoustics by Steady State Transmission Measurements," *J.A.S.A.*, 10, pp. 216-227 (1939).
53. R. Bolt, "Standing Waves in Small Models," *J.A.S.A.*, 10, p. 258 (1939).
54. L. Brillouin, "Acoustical Wave Propagation in Pipes," *J.A.S.A.*, 11, p. 10 (1939)—Analogy with *TE* waves.
55. P. E. Sabine, "Architectural Acoustics: Its Past and Its Possibilities," *J.A.S.A.*, 11 pp. 21-28, (1939).—Pages 26-28 give an illuminating review of the theoretical work in acoustics.
56. R. H. Bolt, "Normal Modes of Vibration in Room Acoustics: Angular Distribution Theory," *J.A.S.A.*, 11, pp. 74-79 (1939).—Eigentones in rectangular chamber.
57. R. H. Bolt, "Normal Modes of Vibration in Room Acoustics: Experimental Investigations in Non-rectangular Enclosures," *J.A.S.A.*, 11, pp. 184-197 (1939).
58. L. Brillouin, "Le Tuyau Acoustique comme Filtre Passe-Haut," *Rev. D'Acous.*, 8, pp. 1-11 (1939).—A comparison with *TM* waves; some historical notes, tracing the inception of the theory back to 1849.
59. E. Skudrzyk, "The Normal Modes of Vibration of Rooms with Non-Planar Walls," *J.A.S.A.*, 11, pp. 364-365 (1940).—Abstract of *Akustische Zeits.*, 4, p. 172 (1939).—Considers the equivalent of the *TM*  $OO_p$  mode.
60. G. M. Roe, "Frequency Distribution of Normal Modes," *J.A.S.A.*, 13, pp. 1-7 (1941).—A verification of Maa's result for a rectangular room, and an extension to the cylinder, sphere and several derived shapes, which leads to the result that the number of normal modes (acoustic) below a given frequency is the same for all shapes.

61. R. S. Bolt, H. Feshbach, A. M. Clogston, "Perturbation of Sound Waves in Irregular Rooms," *J.A.S.A.*, 14, pp. 65-73 (1942)—Experimental check of eigentones in a trapezoid vs calculated values.

ABSTRACTS OF FOREIGN LANGUAGE ARTICLES IN WIRELESS ENGINEER

62. H. Gemperlein, "Measurements on Acoustic Resonators," 16, p. 200, No. 1504 (1939).  
 63. M. Jouguet, "Natural Electromagnetic Oscillations of a Cavity," 16, p. 511, No. 3873, (1939).  
 64. M. S. Neiman, "Convex Endovibrators," 17, p. 65, No. 455, (1940).  
 65. F. Borgnis, "The Fundamental Electric Oscillations of Cylindrical Cavities," 17, p. 112, No. 905, (1940). See also *Sci. Abs.*, B43, No. 343 (1940).  
 66. H. Buchholz, "Ultra-Short Waves in Concentric Cables, and the "Hollow-Space" Resonators in the Form of a Cylinder with Perforated-Disc Ends," 17, p. 166, No. 1301 (1940).  
 67. J. Müller, "Investigation of Electromagnetic Hollow Spaces," 17, p. 172, No. 1379 (1940).—*Sci. Abs.*, B43, No. 857 (1940).  
 68. V. I. Bunimovich, "An Oscillating System with Small Losses," 17, p. 173, No. 1380 (1940).  
 69. M. S. Neiman, "Convex Endovibrators," 17, p. 218, No. 1743 (1940).  
 70. M. S. Neiman, "Toroidal Endovibrators," 17, p. 218, No. 1744 (1940).  
 71. H. Buchholz, "The Movement of Electromagnetic Waves in a Cone-Shaped Horn," 17, p. 370, No. 3009 (1940).—Cavity formed by cone closed by spherical cap.  
 72. O. Schriever, "Physics and Technique of the Hollow-Space Conductor," 18, p. 18 No. 2, (1941).—Review of history.  
 73. F. Borgnis, "Electromagnetic Hollow-Space Resonators in Short-Wave Technique," 18, p. 25, No. 61, (1941).  
 74. T. G. Owe Berg, "Elementary Theory of the Spherical Cavity Resonator," 18, p. 287, No. 1843 (1941).  
 75. F. Borgnis, "A New Method for measuring the Electric Constants and Loss Factors of Insulating Materials in the Centimetric Wave Band," 18, p. 514, No. 3435 (1941).—An application of the cylindrical cavity resonator.  
 76. V. I. Bunimovich, "The Use of Rectangular Resonators in Ultra-High-Frequency Technique," 19, p. 28, No. 65 (1942). Use in 17 cm oscillator.  
 77. V. I. Bunimovich, "A Rectangular Resonator used as a Wavemeter for Decimetric and Centimetric Waves," 19, p. 37, No. 176 (1942).  
 78. M. Watanabe, "On the Eigenschwingungen of the Electromagnetic Hohlraum," 19, p. 166, No. 927 (1942).  
 79. F. Borgnis, "The Electrical Fundamental Oscillation of the Cylindrical Two-Layer Cavity," 19, p. 370, No. 2306 (1942). Considers cylindrical resonator with two concentric internal cylinders of different dielectric constant.  
 80. W. Ludenia, "The Excitation of Cavity Resonators by Saw-Tooth Oscillations," 19, p. 422-423, No. 2641 (1942).  
 81. Ya. L. Al'pert, "On the Propagation of Electromagnetic Waves in Tubes," 19, p. 520, No. 3181 (1942).—Calculation of losses in a cylindrical wave guide.  
 82. V. I. Bunimovich, "The Propagation of Electromagnetic Waves along Parallel Conducting Planes," 19, p. 520, No. 3182 (1942).—Equations for  $Z_0$  and attenuation of rectangular wave guide, and resonant frequency and  $Q$  of rectangular cavity.  
 83. C. G. A. von Lindern & G. de Vries, "Resonators for Ultra-High Frequencies," 19, p. 524, No. 3206 (1942).—Discusses transition from solenoid to toroidal coil to "single turn" toroid, i.e., toroidal cavity resonator.

ABSTRACTS IN SCIENCE ABSTRACTS

84. L. Bouthillon, "Coordination of the Different Types of Oscillations," A39, No. 1773 (1936).—General theory of mechanical, acoustic, optical and electric oscillations.  
 85. Bürck, Kotowski, and Lichte, "Resonance Effects in Rooms, their Measurement and Stimulation," A39, No. 5226 (1936).  
 86. G. Jäger, "Resonances of Closed and Open Rooms, Streets and Squares," 40A, No. 306 (1937).  
 87. K. W. Wagner, "Propagation of Sound in Buildings," A40, No. 2199(1937).—Transmission through a small hole in a wall.  
 88. M. Jouguet, "Natural Electromagnetic Oscillations of a Spherical Cavity," 42A, No. 3822 (1939).  
 89. H. R. L. Lamont, "Use of the Wave Guide for Measurement of Micro-wave Dielectric Constants," 43A, No. 2684 (1940).

## Precision Measurement of Impedance Mismatches in Waveguide

By ALLEN F. POMEROY

A method is described for determining accurately the magnitude of the reflection coefficient caused by an impedance mismatch in waveguide by measuring the ratio between incident and reflected voltages. Reflection coefficients of any value less than 0.05 (0.86 db standing wave ratio) can be measured to an accuracy of  $\pm 2.5\%$ .

**L**ONG waveguide runs installed in microwave systems are usually composed of a number of short sections coupled together. Although the reflection at each coupling may be small, the effect of a large number in tandem may be serious. Therefore, it is desirable to measure accurately the very small reflection coefficients<sup>1</sup> due to the individual couplings.

A commonly adopted method for determining reflection coefficients in phase and magnitude in transmission lines has been to measure the standing wave ratio by means of a traveling detector. Such a system when carefully engineered, calibrated and used is capable of good results, especially for standing waves greater than about 0.3 *db*.

Traveling detectors were in use in the Bell Telephone Laboratories in 1934 to show the reactive nature of an impedance discontinuity in a waveguide. A traveling detector was pictured in a paper<sup>2</sup> in the April 1936 Bell System Technical Journal. Demonstrations and measurements using a traveling detector were included as part of a lecture on waveguides by G. C. Southworth given before the Institute of Radio Engineers in New York on February 1, 1939 and before the American Institute of Electrical Engineers in Philadelphia on March 2, 1939.

Methods for determining the magnitude only of a reflection coefficient by measuring incident and reflected power have been developed by the Bell Telephone Laboratories. A method used during World War II incorporated a directional coupler<sup>3</sup>. The method described in this paper is a refinement of this directional coupler method and is capable of greatly increased accuracy. It uses a hybrid junction<sup>4</sup> to separate the voltage reflected by the mismatch being measured from the voltage incident to the mismatch. Each is measured separately and their ratio is the reflection coefficient.

The problem to be considered is the measurement of the impedance mismatch introduced by a coupling between two pieces of waveguide due to differences in internal dimensions of the two waveguides and to imperfections in the flanges. The basic setup might be considered to be as shown in Fig. 1. The setup comprises a signal oscillator, a hybrid junction, a

calibrated detector and indicator, a termination  $Z'$ , a piece of waveguide  $EF$  (the flange  $E$  of which is to be part of the coupling  $BE$  to be measured) and a termination  $Z$  inserted into the waveguide piece  $EF$  so that the reflection coefficient of the coupling  $BE$  alone will be measured. In addition a fixed shorting plate should be available for attachment to flange  $B$ .

Four cases are considered:

- I. Termination  $Z$  and  $Z'$  perfect, only one coupling on hybrid junction.
- II. Termination  $Z$  imperfect, termination  $Z'$  perfect, only one coupling on hybrid junction.
- III. Termination  $Z$  perfect, four couplings on hybrid junction.
- IV. Termination  $Z$  imperfect, four couplings on hybrid junction.

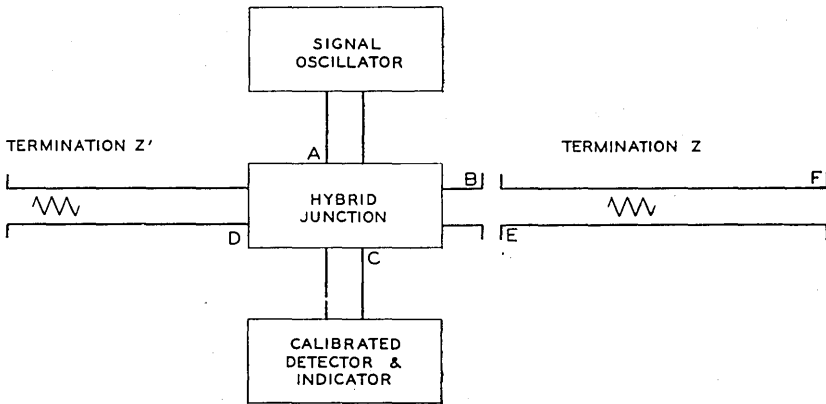


Fig. 1—Block schematic for cases I and II.

It is assumed in all cases that:

1. The hybrid junction has the properties as defined in the discussion of case I.
2. The signal oscillator absorbs all the power reflected through arm  $A$  of the hybrid junction.
3. The calibrated detector and indicator absorb all the power transmitted through arm  $C$  of the hybrid junction.
4. The oscillator output and frequency are not changed when the hybrid junction arm  $B$  is short-circuited.
5. The attenuation of waveguide may be neglected.

#### I. TERMINATION $Z$ AND $Z'$ PERFECT, ONLY ONE COUPLING ON HYBRID JUNCTION

In this case the hybrid junction, termination  $Z'$  and termination  $Z$ , as shown in Fig. 1, are all considered to be perfect. This means for the hybrid junction that its electrical properties are such that the energy from

the oscillator splits equally in paths  $AD$  and  $AB$ . The half in  $AD$  is completely absorbed in the perfect termination  $Z'$ . The half in  $AB$  is partly reflected from the impedance mismatch due to the waveguide coupling  $BE$  and the remainder is absorbed in the perfect termination  $Z$ . Again due to the properties of the perfect hybrid junction, the impedance presented by the arm  $B$  when arms  $A$  and  $C$  are perfectly terminated is also perfect, and the reflected energy from waveguide coupling  $BE$  splits equally in paths  $BA$  and  $BC$ . The part in  $BA$  is absorbed by the oscillator. The part in  $BC$  representing the voltage reflected from the coupling  $BE$  is measured by the calibrated detector and indicator. The magnitude of the incident voltage may be measured when the waveguide piece  $EF$  is replaced by the fixed shorting plate.

It is convenient to measure voltages applied to the calibrated detector and indicator in terms of attenuator settings in  $db$  for a reference output indicator reading. Then the ratio expressed in  $db$  between incident and reflected voltages (hereafter called  $W$ ) is

$$W_2 \text{ (due to the coupling } BE) = A_1 - A_2 \quad (1)$$

where  $A_1$  is attenuator setting for incident voltage and  $A_2$  is attenuator setting for reflected voltage.

Both reflection coefficient and standing wave ratio may be expressed in terms of  $W$ . For if

$$X = \text{voltage due to incident power} \quad (2)$$

and  $Y = \text{voltage due to reflected power}, \quad (3)$

then reflection coefficient =  $\frac{Y}{X}$  (4)

and voltage standing wave ratio =  $\frac{|X| + |Y|}{|X| - |Y|}$  (5)

Since  $W(db) = 20 \log_{10} \frac{|X|}{|Y|}$  (6)

then in  $db$ , standing wave ratio =  $20 \log_{10} \frac{1 + \text{antilog } \frac{W}{20}}{-1 + \text{antilog } \frac{W}{20}}$  (7)

Standing wave ratio plotted versus  $W$  is shown in Fig. 2. Reflection coefficient versus  $W$  can be found in any "voltage ratios to  $db$ " table.

## II. TERMINATION $Z$ IMPERFECT, TERMINATION $Z'$ PERFECT, ONLY ONE COUPLING ON HYBRID JUNCTION

In Fig. 1, if the termination  $Z$  is not perfect, there will be two reflected voltages from branch  $B$ . The vector diagram of the voltage at  $C$  might be

represented as in Fig. 3, where vector 0-1 represents the voltage reflected from coupling  $BE$  and vector 1-2 represents the voltage reflected from the termination  $Z$ . To make measurements, termination  $Z$  should be movable

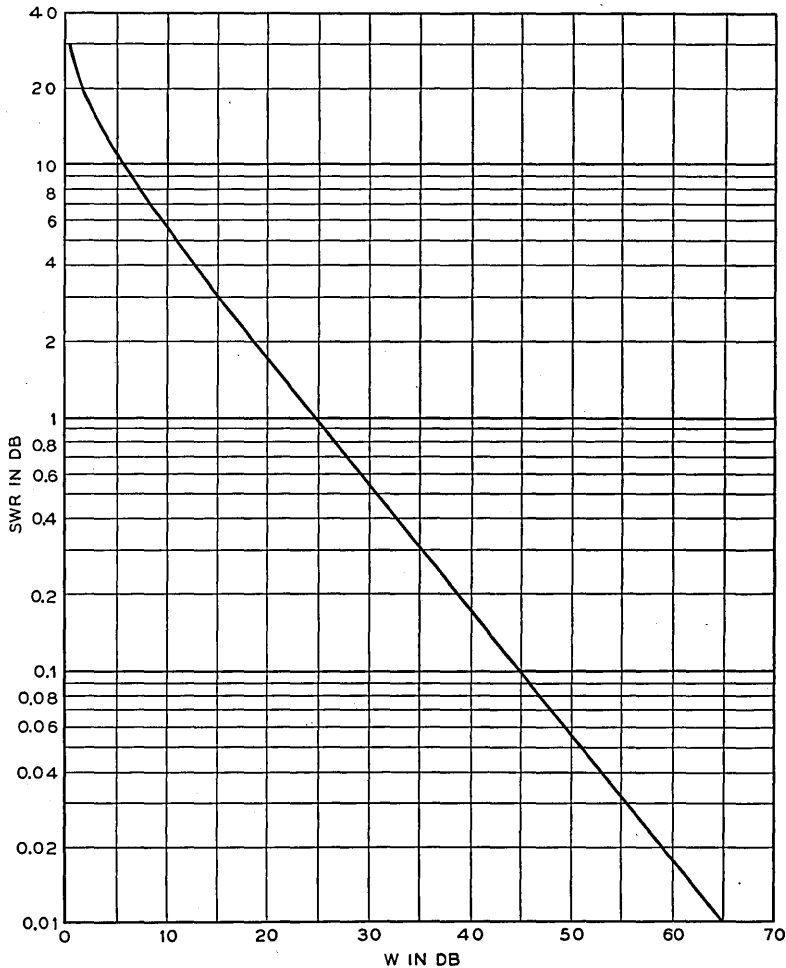


Fig. 2—Standing wave ratio (SWR) versus  $W$ .

and the magnitude of its reflection coefficient be the same at a given position of rest for either direction of approach, and be the same for positions of rest over an interval of a half a wavelength in waveguide.

The reflected voltage is measured twice, once for minimum output as the position of the termination  $Z$  is adjusted and again for maximum output. Then

$$V_{\min} = V_b - V_z \text{ and } V_{\max} = V_b + V_z \quad (8)$$

where  $V_b$  is voltage reflected from coupling  $BE$  and  $V_z$  is voltage reflected from termination  $Z$ .

Equations (8) can be solved for  $V_b$  and  $V_z$  for

$$V_b = \frac{V_{\max} + V_{\min}}{2} \quad \text{and} \quad V_z = \frac{V_{\max} - V_{\min}}{2} \quad (9)$$

The incident voltage is measured as before. Therefore, using equation (6)

$$W' = 20 \log \left| \frac{V_a}{V_b} \right| \quad \text{and} \quad W'' = 20 \log \left| \frac{V_a}{V_z} \right| \quad (10)$$

where  $W'$  is due to coupling  $BE$ ,  $W''$  is due to termination  $Z$  and  $V_a$  is incident voltage.

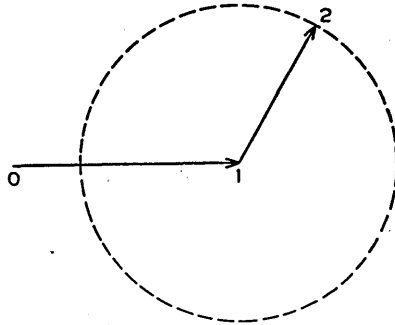


Fig. 3—Vector diagram of voltages reflected from coupling  $BE$  and termination  $Z$ .

A more practical solution involving only addition, subtraction and the use of the characteristics in Fig. 4 is now presented. The settings of the detector attenuator for incident voltage, minimum output and maximum output might be  $A_1$ ,  $A_3$  and  $A_4$ .

$$\text{Then } W_3 = A_1 - A_3 \text{ and } W_4 = A_1 - A_4 \quad (11)$$

$$\text{But } W_3 = 20 \log \left| \frac{V_a}{|V_b| - |V_z|} \right| \quad \text{and} \quad W_4 = 20 \log \left| \frac{V_a}{|V_b| + |V_z|} \right| \quad (12)$$

$$\text{and } W_3 - W_4 = 20 \log \left| \frac{|V_b| + |V_z|}{|V_b| - |V_z|} \right| = 20 \log \frac{1 + \text{antilog } \frac{T}{20}}{-1 + \text{antilog } \frac{T}{20}} \quad (13)$$

$$\text{where } 20 \log \left| \frac{V_b}{V_z} \right| = T = W'' - W' \quad (14)$$

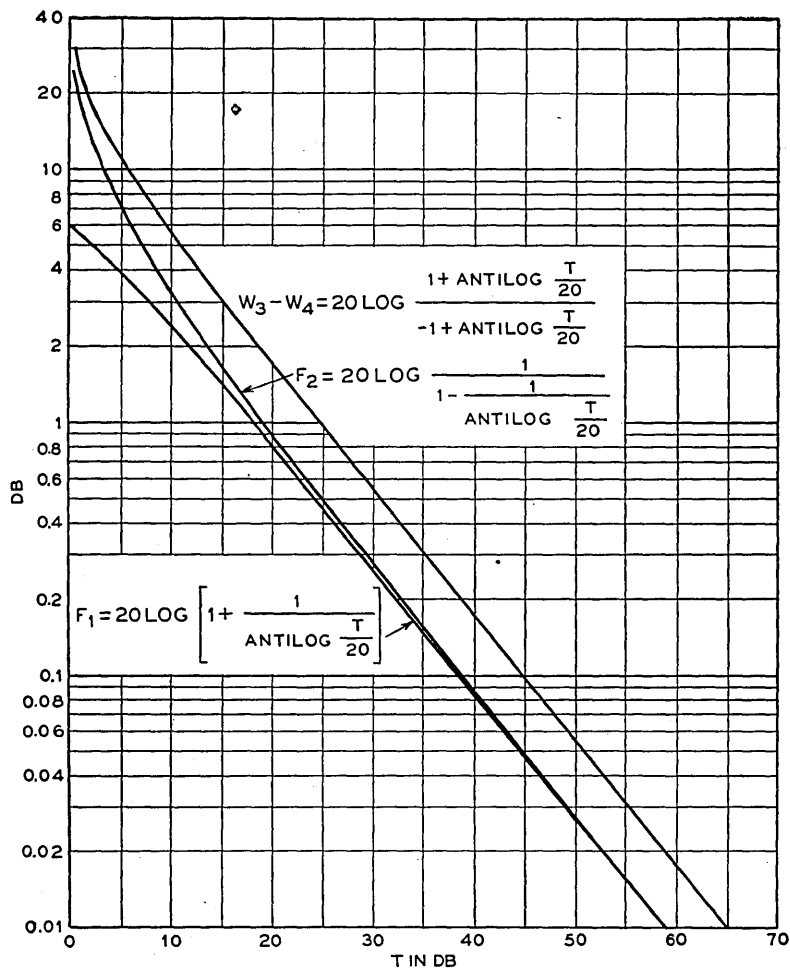


Fig. 4— $F_1$ ,  $F_2$  and  $W_3 - W_4$

There is an  $F_1(T) = 20 \log \left( 1 + \frac{1}{\text{antilog} \frac{T}{20}} \right)$

and an  $F_2(T) = 20 \log \frac{1}{1 - \frac{1}{\text{antilog} \frac{T}{20}}}$  (15)

such that  $W' = W_4 + F_1 = W_3 - F_2$

$W'' = T + W_4 + F_1 = T + W_3 - F_2$  (16)

and  $F_1 + F_2 = W_3 - W_4$



Figure 4 shows  $F_1$ ,  $F_2$  and their sum  $W_3 - W_4$  plotted versus  $T$ . It may be noted that  $W_3 - W_4$  versus  $T$  has the same values as  $SWR$  versus  $W$  in Fig. 2.

Using equations (16) and Fig. 4,  $W'$  and  $W''$  may be evaluated for the particular values of  $W_3$  and  $W_4$  in equation (11). In the evaluation, if there is uncertainty as to which reflection coefficient belongs to the waveguide coupling  $BE$  and which belongs to the termination  $Z$ , a termination with a different magnitude of reflection coefficient should be used and the technique repeated. The reflection coefficient which is the same in the two cases is of course that due to the waveguide coupling  $BE$ .

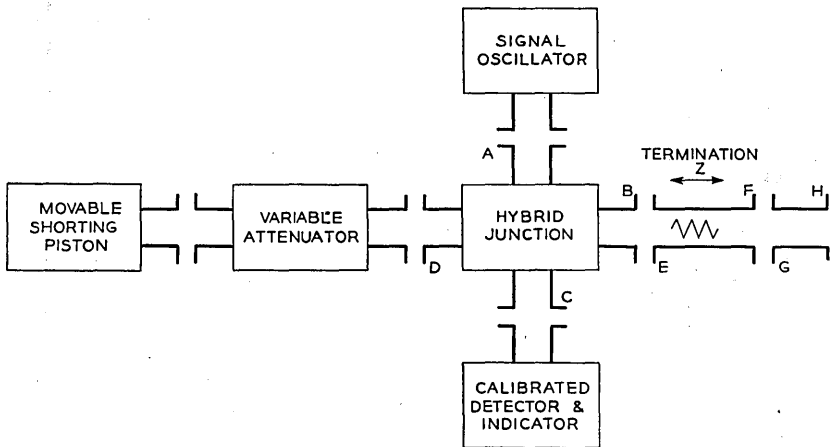


Fig. 5—Block schematic for cases III and IV.

It is assumed in the above solution that multiple reflections between the two impedance mismatches are inconsequential. Appendix A outlines a procedure for evaluating the maximum probable error due to multiple reflections.

### III. TERMINATION $Z$ PERFECT, FOUR COUPLINGS ON HYBRID JUNCTION

In this case the setup might be as shown in Fig. 5. This setup differs from that shown in Fig. 1 in that the hybrid junction has four couplings shown, termination  $Z'$  has been replaced by a variable attenuator and a movable shorting piston, and the waveguide coupling  $FG$  is to be measured instead of coupling  $BE$ . The hybrid junction and the termination  $Z$  are assumed to be perfect as defined for case I.

Since it is the object of the measuring method to measure impedance mismatches in branch  $B$ , it is desirable to make the voltage at  $C$  depend only on power reflected from branch  $B$ . This is accomplished by adjusting

branch  $D$  so that the voltages due to the flanges of the hybrid junction are cancelled.

The vector diagram of the voltage at  $C$  might be represented as in Fig. 6. Vector 0-1 represents the voltage at  $C$  when input is applied to  $A$ , due to the impedance mismatch at the coupling  $BE$ . Vector 1-2 represents that due to the mismatch at coupling  $D$ . Vector 2-3 represents that due to the mismatch at the variable attenuator, (which will usually change in magnitude and probably in phase for different settings). Vector 3-0 represents the voltage at  $C$  due to the cancelling voltage from the branch  $D$ . Its phase can be varied by changing the position of the movable shorting piston. Its magnitude can be varied by changing the setting of the variable attenuator. When the adjustment is accomplished effectively no power reaches the detector. It is necessary that the reflection coefficients of

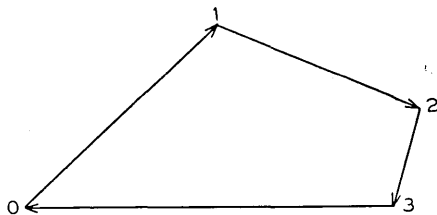


Fig. 6—Vector diagram of voltages at terminal  $C$ .

couplings  $A$ ,  $B$ , and  $C$  be small so that multiple reflections caused by them will not affect the accuracy of measurement.

The reflected power from coupling  $FG$  may be measured when waveguide  $GH$  is connected to waveguide  $EF$  as shown in Fig. 5 and termination  $Z$  is located within waveguide  $GH$ . The detector attenuator setting might be  $A_5$ . The incident power may be measured as before when termination  $Z$  is withdrawn from the waveguide  $EF$  and the piece of waveguide  $GH$  is replaced by a fixed shorting plate.

$$W_5 \text{ (due to reflection coefficient of the coupling } FG) = A_1 - A_5 \quad (17)$$

#### IV. TERMINATION $Z$ IMPERFECT, FOUR COUPLINGS ON HYBRID JUNCTION

In Fig. 5 if the movable termination  $Z$  is not perfect, there will be two reflected voltages in branch  $B$  when the adjustment is being made. The vector diagram of the voltage at  $C$  might be as in Fig. 7. This is the same as Fig. 6 except that a new vector 0-5 represents the voltage due to the mismatch of the movable termination  $Z$ . The adjustment is accomplished the same as in the last section except that the criterion is to have no change in detector output as the movable termination  $Z$  is moved axially over a

range of a half a wavelength in waveguide. As for the last case it is necessary that the reflection coefficients of the couplings  $A$ ,  $B$  and  $C$  be small if good accuracy is desired.

When measuring the coupling  $FG$  the procedure and evaluation are the same as for case II.

Part of a laboratory setup as used at about 4 kilomegacycles is shown in Fig. 8. It includes a hybrid junction, a variable attenuator, a movable shorting piston, a straight section of waveguide and a movable termination which consists of a cylinder of phenol resin and carbon with a tapered section at one end. It is mounted in a phenolic block so that it may be moved axially in the wave guide.

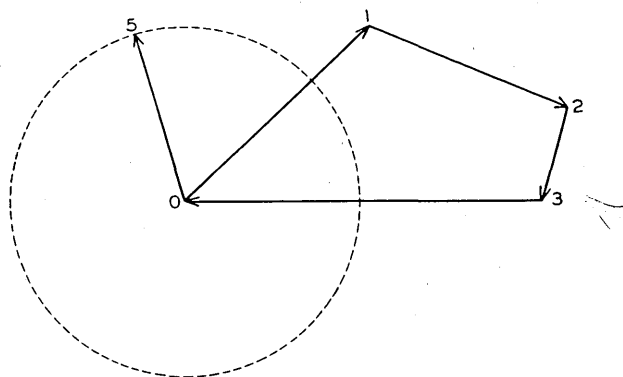


Fig. 7—Part of a laboratory setup as used at 4 kilomegacycles.

In cases III and IV if the hybrid junction has “poor balance” so that voltage appears at  $C$  when input is applied to arm  $A$  even though  $B$  and  $D$  are perfectly terminated, the adjusting procedure will cancel this voltage as well. Measuring accuracy will not be impaired provided the other assumptions are fulfilled.

#### MEASURING $W$ —A FITTING WHICH DOES NOT ADMIT OF MEASURING EACH END SEPARATELY

A piece with a configuration unsuited to the preceding technique may be measured by connecting it between two straight pieces of waveguide such as between flanges  $F$  and  $G$  in Fig. 5. The  $W$  due to the vector sum of the reflection coefficients of the coupling at one end, any irregularities and the coupling at the other end, is measured. Due to the distance between the mismatches, the vector sum will vary over the frequency band of interest.

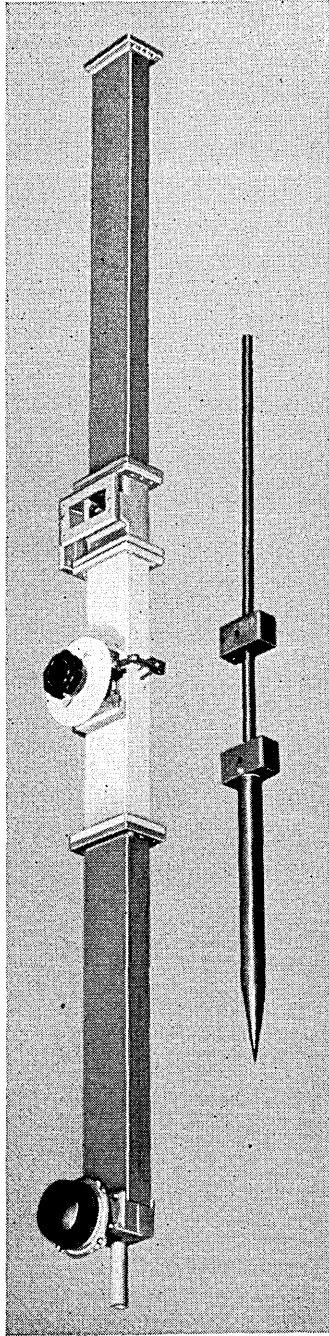


Fig. 8—Vector diagram of voltages at terminal  $C$  when termination  $Z$  is not perfect.

## ACCURACY

There are three important sources of error. The first is lack of proper adjustment. The second is that due to the detector attenuator calibration. The third is that due to multiple reflections.

Experience and care can almost eliminate the first source. The second source may have a magnitude of twice the detector attenuator calibration error. In equations (1) and (17) this is readily apparent. The evaluation of  $W$  using equations (16) introduces negligibly more error provided  $W_3 - W_4$  is made large by proper choice of the magnitude of the reflection coefficient of the termination  $Z$ . The possible errors due to multiple reflections between the waveguide impedance discontinuity being measured and an imperfect termination are discussed in Appendix A. If the impedance presented by the arm  $B$  of the hybrid junction is not perfect, energy reflected from the hybrid junction will be partly absorbed in the termination and cause an error in the measurement. If the magnitude of this reflection coefficient is known, the maximum error may be computed.

If a detector attenuator calibration error of  $\pm 0.1$  db is assumed to be the only contributing error, it is possible to measure the  $W$  due to an impedance mismatch to an accuracy of  $\pm 0.2$  db provided the  $W$  is greater than 26 db. These numbers correspond to measuring a standing wave ratio of any value less than 0.86 db to an accuracy of  $\pm 0.02$  db or reflection coefficients of any value less than 0.05 to an accuracy of  $\pm 2.5\%$ .

## APPENDIX A

MAXIMUM PROBABLE ERROR DUE TO MAGNITUDE OF REFLECTION  
COEFFICIENT BEING MEASURED WHEN MEASURING A  
WAVEGUIDE COUPLING

The purpose of this appendix is to derive equations so that the maximum probable error due to multiple reflections may be calculated. The assumptions may not be rigorous but the mathematical treatment appears to represent a reasonable approximation. It is assumed that there is no dissipation in waveguide  $EF$ , waveguide  $GH$  and in coupling  $FG$ .

The electrical relations of the coupling  $FG$  and the movable termination  $Z$  might be represented as in Fig. 9, where  $K_a$  = characteristic impedance of waveguide  $EF$  and  $K_b$  = characteristic impedance of waveguide  $GH$ . The first few multiple reflections from the two discontinuities, coupling  $FG$  and termination  $Z$ , can be illustrated as in Fig. 10.

Evaluation of the magnitudes of the reflections can be accomplished as outlined in paragraph 7.13, page 210 in the book "Electromagnetic Waves"\* by S. A. Schelkunoff.

\* Published by D. Van Nostrand, Inc., New York City, 1943.

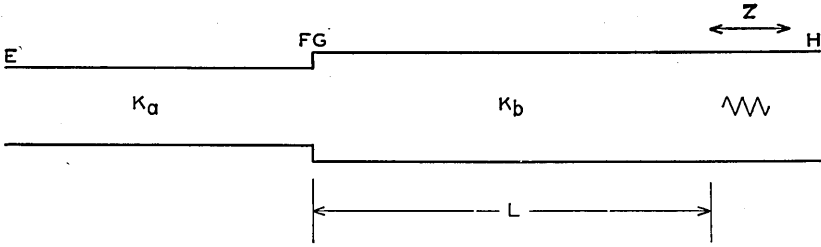


Fig. 9—Relation between coupling  $FG$  and termination  $Z$ .

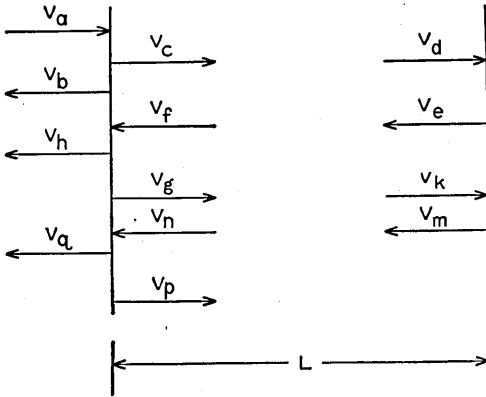


Fig. 10—Multiple reflections from two planes of discontinuity.

$$V_a = \text{Incident voltage} \tag{18}$$

$$V_b = rV_a \tag{19}$$

where  $r = \frac{K_b - K_a}{K_b + K_a}$  (20)

$$V_c = V_a + V_b = V_a(1 + r) \tag{21}$$

$$V_d = e^{-i\beta L} V_c = e^{-i\beta L} V_a(1 + r) \tag{22}$$

$$V_e = zV_d = ze^{-i\beta L} V_a(1 + r) \tag{23}$$

where  $z = \frac{Z - Z_b}{Z + Z_b}$  (24)

$$V_f = e^{-i\beta L} V_e = ze^{-i2\beta L} V_a(1 + r) \tag{25}$$

$$V_g = -rV_f = ze^{-i2\beta L} V_a(1 + r)(-r) \tag{26}$$

where  $-r = \frac{K_a - K_b}{K_a + K_b}$  (27)

$V_h = V_f + V_g = ze^{-i2\beta L} V_a(1+r)(1-r)$  (28)

$V_k = e^{-i\beta L} V_g = ze^{-i3\beta L} V_a(1+r)(-r)$  (29)

$V_m = zV_k = z^2e^{-i3\beta L} V_a(1+r)(-r)$  (30)

$V_n = e^{-i\beta L} V_m = z^2e^{-i4\beta L} V_a(1+r)(-r)$  (31)

$V_p = -rV_n = z^2e^{-i4\beta L} V_a(1+r)(-r)^2$  (32)

$V_q = V_n + V_p = z^2e^{-i4\beta L} V_a(1-r^2)(-r)$  (33)

For purposes of analysis it is now assumed that further multiple reflections are negligible.

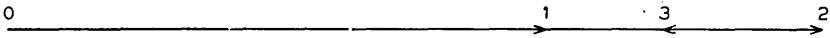


Fig. 11—Vector voltage diagram for maximum vector sum.

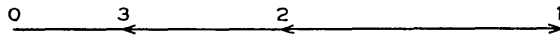


Fig. 12—Vector voltage diagram for minimum vector sum.

Equations (19), (28) and (33) are the reflected voltages that combine vectorially to be measured. If  $\beta L = 0, \pi, 2\pi, \dots, n\pi$  then the vector voltage diagram might appear as in Fig. 11. If  $BL = \frac{\pi}{2}, \frac{3\pi}{2}, \frac{5\pi}{2}, \dots, \frac{(2n-1)\pi}{2}$  then the vector voltage diagram might appear as in Fig. 12.

The following example illustrates the calculations involved in computing the errors due to the magnitude of the reflection coefficient being measured. The assumptions are such that an appreciable error is computed. If one assumes  $r = 0.316$  and  $z = 0.282$ , then from equation (6)  $W_r = 10$  db and  $W_z = 11$  db. In Figs. 11 and 12,

vector 0-1 =  $r$ , vector 1-2 =  $z(1-r^2)$ , vector 2-3 =  $rz^2(1-r^2)$  (34)

then

$W_{0-1} = 10$  db,  $W_{1-2} = 11.00 + 0.92 = 11.92$  db,  
and  $W_{2-3} = 10.00 + 22.00 + 0.92 = 32.92$  db (35)

In order to evaluate vector 0-2 in Fig. 11 (the vector sum of vectors 0-1 and 1-2), one calculates their difference  $T$ .

$T = 11.92 - 10.00 = 1.92$  db (36)

For  $T = 1.92$  db,  $F_1 = 5.10$  db (37)

therefore  $W_{0-2} = 10.00 - 5.10 = 4.90$  db (38)

In order to evaluate vector 0-3 in Fig. 11 (the vector difference of vectors 0-2 and 2-3) one calculates their difference  $T$ .

$$T = 32.92 - 4.90 = 28.02 \text{ db} \quad (39)$$

$$\text{For } T = 28.02 \text{ db, } F_2 = 0.36 \text{ db} \quad (40)$$

$$\text{therefore } W_{0-3} = 4.90 \pm 0.36 = 5.26 \text{ db} = W_4 \quad (41)$$

In order to evaluate vector 0-2 in Fig. 12 (the vector difference between vectors 0-1 and 1-2), one uses  $T$  from equation (36).

$$\text{For } T = 1.92 \text{ db, } F_2 = 14.10 \text{ db} \quad (42)$$

$$\text{therefore } W_{0-2} = 10.00 + 14.10 = 24.10 \text{ db} \quad (43)$$

In order to evaluate vector 0-3 in Fig. 12 (the vector difference between vectors 0-2 and 2-3), one calculates their difference  $T$ .

$$T = 32.92 - 24.10 = 8.82 \text{ db} \quad (44)$$

$$\text{For } T = 8.82 \text{ db, } F_2 = 3.93 \text{ db} \quad (45)$$

$$\text{therefore } W_{0-3} = 24.10 + 3.93 = 28.03 \text{ db} = W_3 \quad (46)$$

Using equation (16)

$$W_3 - W_4 = 22.77 \text{ db, } T = 1.24 \text{ db, } F_1 = 5.40 \text{ and therefore } W = 9.66 \text{ db.}$$

Since we started by assuming  $W_r = 10 \text{ db}$ , the error amounts to  $0.34 \text{ db}$ .

#### REFERENCES

1. Page 120, "Transmission Networks and Wave Filters," T. E. Shea. Published by D. Van Nostrand, Inc., New York City, 1929.
2. "Hyper-frequency Waveguides—General Considerations and Experimental Results," G. C. Southworth, *Bell System Technical Journal*, April, 1936.
3. "Directional Couplers." W. W. Mumford, *Proceedings of the Institute of Radio Engineers*, February 1947.
4. "Hybrid Circuits for Microwaves," W. A. Tyrrell. A paper accepted for publication in the *Proceedings of the Institute of Radio Engineers*.
5. "Note on a Reflection-Coefficient Meter," Nathaniel I. Korman, *Proceedings of the Institute of Radio Engineers and Waves and Electrons*, September 1946.
6. "Probe Error in Standing-Wave Detectors," William Altar, F. B. Marshall and L. P. Hunter, *Proceedings of the Institute of Radio Engineers and Waves and Electrons*, January 1946.
7. Pages 20 to 24, "Practical Analysis of UHF Transmission Lines—Resonant Sections—Resonant Cavities—Waveguides," J. R. Meagher and H. J. Markley Pamphlet published by R. C. A. Service Company, Inc., in 1943.
8. "Microwave Measurements and Test Equipments," F. J. Gaffney, *Proceedings of the Institute of Radio Engineers and Waves and Electrons*, October 1946.



# Reflex Oscillators

By J. R. PIERCE and W. G. SHEPHERD

## TABLE OF CONTENTS

I. Introduction.....	463
II. Electronic Admittance—Simple Theory.....	467
III. Power Production for Drift Angle of $(n + \frac{3}{4})$ Cycles.....	470
IV. Effect of Approximations.....	479
V. Special Drift Fields.....	480
VI. Electronic Gap Loading.....	482
VII. Electronic Tuning—Arbitrary Drift Angle.....	484
VIII. Hysteresis.....	493
IX. Effect of Load.....	512
A. Fixed Loads.....	513
B. Frequency Sensitive Loads—Long Line Effect.....	523
C. Effect of Short Mismatched Lines on Electronic Tuning.....	531
X. Variation of Power and Electronic Tuning with Frequency.....	537
XI. Noise Sidebands.....	542
XII. Build-up of Oscillation.....	545
XIII. Reflex Oscillator Development at the Bell Telephone Laboratories.....	550
A. Discussion of the Beating Oscillator Problem.....	550
B. A Reflex Oscillator with an External Resonator—The 707.....	553
C. A Reflex Oscillator with an Integral Cavity—The 723.....	558
D. A Reflex Oscillator Designed to Eliminate Hysteresis—The 2K29.....	563
E. Broad Band Oscillators—The 2K25.....	570
F. Thermally Tuned Reflex Oscillators—The 2K45.....	577
G. An Oscillator with Wave-Guide Output—The 2K50.....	597
H. A Millimeter—Range Oscillator—The 1464.....	603
I. Oscillators for Pulsed Applications—The 2K23 and 2K54.....	607
J. Scope of Development at the Bell Telephone Laboratories.....	620

## APPENDICES

I. Resonators.....	622
II. Modulation Coefficient.....	629
III. Approximate Treatment of Bunching.....	639
IV. Drift Angle as a Function of Frequency and Voltage.....	643
V. Electronic Admittance—Non-simple Theory.....	644
VI. General Potential Variation in the Drift Space.....	656
VII. Ideal Drift Field.....	660
VIII. Electronic Gap Loading.....	663
IX. Losses in Grids.....	673
X. Starting of Pulsed Reflex Oscillators.....	674
XI. Thermal Tuning.....	677

## SYMBOLS

<i>A</i>	A measure of frequency deviation (9.20).
<i>B</i>	Bandwidth (Appendix 10 only, ( <i>j</i> -3)).
<i>B</i>	Susceptance
<i>B</i> <sub>1</sub>	Reduced susceptance (9.7).
<i>B</i> <sub>e</sub>	Electronic susceptance.
<i>C</i>	Capacitance
<i>C</i>	Heat capacity ( <i>k</i> -1).
<i>D</i>	Reduced gap spacing (10.3).

$E_0$	Retarding field in drift space.
$F$	Drift effectiveness factor (5.4).
$G$	Conductance
$G_1, G_2$	Reduced conductances (9.6), (9.12).
$G_E$	Gap conductance of loaded resonator.
$G_e$	Electronic conductance.
$G_L$	Conductance at gap due to load.
$G_R$	Conductance at gap due to resonator loss.
$H$	Efficiency parameter (3.7).
$H_m$	Maximum value of $H$ for a given resonator loss.
$I$	Radio-frequency current.
$I_2$	Current induced in circuit by convection current returning across gap.
$I_0$	D-C beam current.
$K$	Resonator loss parameter (3.9).
$K$	Radiation loss in watts/(degree Kelvin) <sup>4</sup> ( $k-2$ ).
$L$	Inductance.
$M$	Characteristic admittance ( $a-8$ ).
$M_L$	Characteristic admittance of line.
$M_M$	Short line admittance parameter (9.38).
$N$	Drift time in cycles.
$N$	Length of line in wavelengths (Section IX only).
$N$	Transformer voltage ratio.
$P$	Power.
$Q$	Equation ( $a-10$ ).
$Q_E$	External $Q$ ( $a-11$ ).
$Q_0$	Unloaded $Q$ ( $a-12$ ).
$R$	Surface resistance ( $a-2$ ).
$S$	Scaling factor (9.17).
$T$	Temperature.
$V$	Radio-frequency voltage.
$V$	Potential in drift space (Appendix VI only).
$V_0$	D-C beam voltage at gap.
$V_R$	The repeller is at a potential ( $-V_R$ ) with respect to the cathode.
$W$	Work, energy (Appendix I).
$W$	Reduced radian frequency (10.5).
$X$	Bunching parameter (2.9).
$Y$	Admittance.
$Y_C$	Circuit admittance.
$Y_e$	Electronic admittance.
$Y_L$	Load admittance.
$Y_R$	Resonator admittance.
$Z$	Impedance.
$Z_L$	Load impedance.
$a$	Distance between grid wire centers.
$d$	Separation between grid planes or tubes forming gap.
$e$	Electronic charge ( $1.59 \times 10^{-19}$ Coulombs).
$f$	Frequency.
$f$	Factor relating to effective grid voltage (b-37).
$i$	Radio-frequency convection current.
$i_2$	Radio-frequency convection current returning across gap ( $c-4$ ).
$(i_2)_f$	Fundamental component of $i_2$ .
$j$	$\sqrt{-1}$
$k$	Boltzman's constant ( $1.37 \times 10^{23}$ joules/degree K).
$k$	Conduction loss watts/degree C ( $k-14$ ).
$l$	Length.
$m$	Mutual inductance.
$m$	Electronic mass ( $9.03 \times 10^{-21}$ gram sevens).
$n$	Repeller mode number. The number of cycles drift is $n + \frac{1}{2}$ for "optimum drift".
$p$	Reduced power (9.5).
$r$	Radius of grid wire, radius of tubes forming gap.
$t$	Time, seconds.
$u_0$	D-C velocity of electrons.

$v$	Total velocity (Appendix VIII only).
$v$	Instantaneous gap voltage
$w$	Real part of frequency (12.1).
$x$	Coordinate along beam.
$y$	A rectangular coordinate normal to $x$ .
$y$	Half-separation of planes forming symmetrical gap.
$y_e$	Magnitude of small signal electronic admittance.
$z$	A rectangular coordinate normal to $x$ (Appendix II).
$z$	A variable of integration (Appendix VI).
$\alpha$	Negative coefficient of the imaginary part of frequency (12.1).
$\beta$	Modulation coefficient.
$\beta_a$	Average value of modulation coefficient.
$\beta_0$	Modulation coefficient on axis.
$\beta_r$	Modulation coefficient at radius $r$ from axis.
$\beta_s$	Root mean squared value of modulation coefficient.
$\beta_y$	Modulation coefficient at distance $y$ from axis.
$\gamma$	$\gamma = \omega/u_0$ .
$\epsilon$	Dielectric constant of space ( $8.85 \times 10^{-14}$ farads/cm).
$\theta$	Drift angle in radians.
$\theta_g$	Gap transit angle in radians.
$\lambda$	Wavelength in centimeters.
$\phi$	A phase angle.
$\Phi$	Reduced potential (g-13).
$\sigma$	Voltage standing wave ratio.
$\tau$	Transit time.
$\tau$	Time constant of thermal tuner.
$\tau_H$	Cycling time on heating.
$\tau_C$	Cycling time on cooling.
$\psi$	Magnetic flux linkage.
$\omega$	Radian frequency.

THE reflex oscillator is a form of long-transit-time tube which has distinct advantages as a low power source at high frequencies. It may be light in weight, need have no magnetic focusing field, and can be made to operate at comparatively low voltages. A single closed resonator is used, so that tuning is very simple. Because the whole resonator is at the same dc voltage, high frequency by-pass difficulties are obviated.

The frequency of oscillation can be changed by several tens of megacycles by varying the repeller voltage ("electronic tuning"). This is very advantageous when the reflex oscillator is used as a beating oscillator. The electronic tuning can be used as a vernier frequency adjustment to the manual tuning adjustment or can be used to give an all-electrical automatic frequency-control. Electronic tuning also makes reflex oscillators serve well as frequency modulated sources in low power transmitters.

The single resonator tuning property makes it possible to construct oscillators whose mechanical tuning is wholly electronically controlled. Such control is achieved by making the mechanical motion which tunes the cavity subject to the thermal expansion of an element heated by electron bombardment.

The efficiency of the reflex oscillator is generally low. The wide use of the 707B, the 723A, the 726A and subsequent Western Electric tubes shows that this defect is outweighed by the advantages already mentioned.

The first part of this paper attempts to give a broad exposition of the theory of the reflex oscillator. This theoretical material provides a background for understanding particular problems arising in reflex oscillator design and operation. The second part of the paper describes a number of typical tubes designed at the Bell Telephone Laboratories and endeavors to show the relation between theory and practice.

The theoretical work is presented first because reflex oscillators vary so widely in construction that theoretical results serve better than experimental results as a basis for generalization about their properties. While the reflex oscillator is simple in the sense that some sort of theory about it can be worked out, in practice there are many phenomena which are not included in such a theory. This leaves one in some doubt as to how well any simplified theory should apply. Multiple transits of electrons, different drift times for different electron paths and space charge in the repeller region are some factors not ordinarily taken into account which, nevertheless, can be quite important. There are other effects which are difficult to evaluate, such as distribution of current density in the beam, loss of electrons on grids or on the edges of apertures and dynamic focusing. If we could provide a theory including all such known effects, we would have a tremendous number of more or less adjustable constants, and it would not be hard to fit a large body of data to such a theory, correct or incorrect.

At present it appears that the theory of reflex oscillators is important in that it gives a semi-quantitative insight into the behavior of reflex oscillators and a guide to their design. The extent to which the present theory or an extended theory will fit actual data in all respects remains to be seen.

The writers thus regard the theory presented here as a guide in evaluating the capabilities of reflex oscillators, in designing such oscillators and in understanding the properties of such tubes as are described in the second part of this paper, rather than as an accurate quantitative tool. Therefore, the exposition consists of a description of the theory of the reflex oscillator and some simple calculations concerning it, with the more complicated mathematical work relegated to a series of chapters called appendices. It is hoped that this so organizes the mathematical work as to make it assimilable and useful, and at the same time enables the casual reader to obtain a clear idea of the scope of the theory.

## I. INTRODUCTION

An idealized reflex oscillator is shown schematically in Fig. 1. It has, of course, a resonant circuit or "resonator."<sup>1</sup> This may consist of a pair of grids forming the "capacitance" of the circuit and a single turn toroidal

<sup>1</sup> For a discussion of resonators, see Appendix I. It is suggested that the reader consult this before continuing with the main work in order to obtain an understanding of the circuit philosophy used and a knowledge of the symbols employed.

coil forming the "inductance" of the circuit. Such a resonator behaves just as do other resonant circuits. Power may be derived from it by means of a coupling loop linking the magnetic field of the single turn coil. An electron stream of uniform current density leaves the cathode and is shot across the "gap" between the two grids, traversing the radio-frequency field in this gap in a fraction of a cycle. In crossing the gap the electron stream is velocity modulated; that is, electrons crossing at different times gain

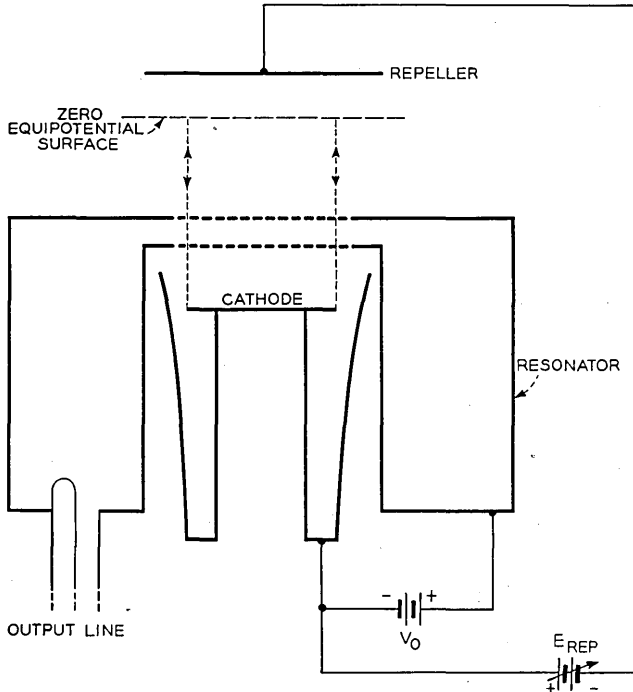


Fig. 1.—An idealized reflex oscillator with grids, shown in cross-section.

different amounts of kinetic energy from the radio-frequency voltage across the gap.<sup>2</sup> The velocity modulated electron stream is shot toward a negative repeller electrode which sends it back across the gap. In the "drift space" between the gap and the repeller the electron stream becomes "bunched" and the bunches of electrons passing through the radio frequency field in the gap on the return transit can give up power to the circuit if they are returned in the proper phase.

<sup>2</sup> The most energy any electron gains is  $\beta V$  electron volts, where  $V$  is the peak radio frequency voltage across the gap and  $\beta$  is the "modulation coefficient" or "gap factor", and is always less than unity.  $\beta$  depends on gap configuration and transit angle across the gap, and is discussed in Appendix II.

The vital features of the reflex oscillator are the bunching which takes place in the velocity modulated electron stream in the retarding field between the gap and the repeller and the control of the returning phase of the bunches provided by the adjustment of the repeller voltage. The analogy of Fig. 2 explains the cause of the bunching. The retarding drift field may

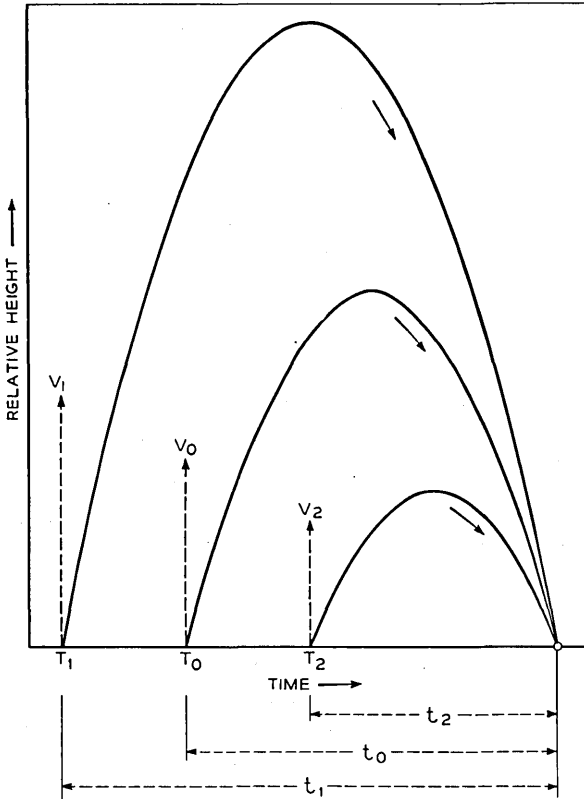


Fig. 2.—The motion of electrons in the repeller space of a reflex oscillator may be likened to that of balls thrown upward at different times. In this figure, height is plotted vs time. If a ball is thrown upward with a large velocity of  $V_1$  at a time  $T_1$ , another with a smaller velocity at a later time  $T_0$  and a third with a still smaller velocity at a still later time  $T_2$  the three balls can be made to fall back to the initial level at the same time.

be likened to the gravitational field of the earth. The drift time is analogous to the time a ball thrown upwards takes to return. If the ball is thrown upward with some medium speed  $v_0$ , it will return in some time  $t_0$ . If it is thrown upward with a low speed  $v_1$  smaller than  $v_0$ , the ball will return in some time  $t_1$  smaller than  $t_0$ . If the ball is thrown up with a speed  $v_2$  greater than  $v_0$ , it returns in some time  $t_2$  greater than  $t_0$ . Now imagine three balls thrown upward in succession, evenly spaced but with large,

medium, and small velocities, respectively.<sup>3</sup> As the ball first thrown up takes a longer time to return than the second, and the third takes a shorter time to return than the second, when the balls return the time intervals between arrivals will be less than between their departures. Thus time-position "bunching" occurs when the projection velocity with which a uniform stream of particles enters a retarding field is progressively decreased.

Figure 3 demonstrates such bunching as it actually takes place in the retarding field of a reflex oscillator. An electron crossing the gap at phase *A*

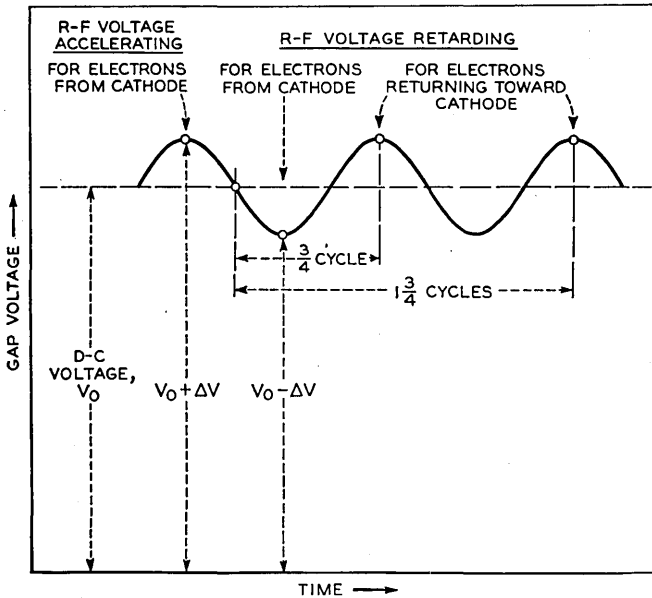


Fig. 3.—The drift time for transfer of energy from the bunched electron stream to the resonator can be deduced from a plot of gap voltage vs time.

is equivalent to the first ball since its velocity suffers a maximum increase, an electron crossing at phase *B* corresponds to the ball of velocity  $v_0$  where for the electron  $V_0$  corresponds to the d.c. injection velocity, and finally an electron crossing at phase *C* corresponds to the third ball since it has suffered a maximum decrease in its velocity. The electrons tend to bunch about the electron crossing at phase *B*. To a first order in this process no energy is taken from the cavity since as many electrons give up energy as absorb it.

The next step in the process is to bring back the grouped electrons in such a phase that they give the maximum energy to the r.f. field. Now,  $\frac{3}{4}$  of a cycle after the gap voltage in a reflex oscillator such as that shown in Fig. 1 is changing most rapidly from accelerating to retarding for electrons

<sup>3</sup> The reader is not advised to try this experimentally unless he has juggling experience.

going from the cathode, it has a maximum retarding value for electrons returning through the gap. This is true also for  $1\frac{3}{4}$  cycles,  $2\frac{3}{4}$  cycles,  $n + \frac{3}{4}$  cycles. Hence as Fig. 3 shows if the time electrons spend in the drift space is  $n + \frac{3}{4}$  cycles, the electron bunches will return at such time as to give up energy to the resonator most effectively.

## II. ELECTRONIC ADMITTANCE—SIMPLE THEORY

In Appendix III an approximate calculation is made of the fundamental component of the current in the electron stream returning through the gap of a reflex oscillator when the current is caused by velocity modulation and drift action in a uniform retarding field. The restrictive assumptions are as follows:

(1) The radio-frequency voltage across the gap is a small fraction of the d-c accelerating voltage.

(2) Space charge is neglected. Amongst other things this assumes no interaction between incoming and outgoing streams and is probably the most serious departure from the actual state of affairs.

(3) Variations of modulation coefficient for various electron paths are neglected.

(4) All sidewise deflections are neglected.

(5) Thermal velocities are neglected.

(6) The electron flow is treated as a uniform distribution of charge.

(7) Only two gap transits are allowed.

An expression for the current induced in the circuit ( $\beta$  times the electron convection current) is

$$i = 2I_0 \beta J_1 \left( \frac{\beta V \theta}{2V_0} \right) e^{j(\omega t - \theta)}. \quad (2.1)$$

Here the current is taken as positive if the beam in its second transit across the gap absorbs energy from the resonator. The voltage across the gap at the time the stream returns referred to the same phase reference as the current is  $v = V e^{-j(\omega t - \pi/2)}$ . Hence the admittance appearing in shunt with the gaps will be

$$Y_e = \frac{2I_0 \beta}{V} J_1 \left( \frac{\beta V \theta}{2V_0} \right) e^{j((\pi/2) - \theta)}. \quad (2.2)$$

For small values of  $V$  approaching zero this becomes

$$Y_{es} = \frac{I_0 \beta^2 \theta}{2V_0} e^{j((\pi/2) - \theta)} = y_e e^{j((\pi/2) - \theta)}. \quad (2.3)$$

$$y_e = \frac{I_0 \beta^2 \theta}{2V_0}. \quad (2.4)$$



Here we define  $Y_{es}$  as the small signal value of the admittance, and  $y_e$  as the magnitude of this quantity. If we plot the function  $Y_{es}$  in a complex admittance plane it takes the form of a geometric spiral as shown in Fig. 4.

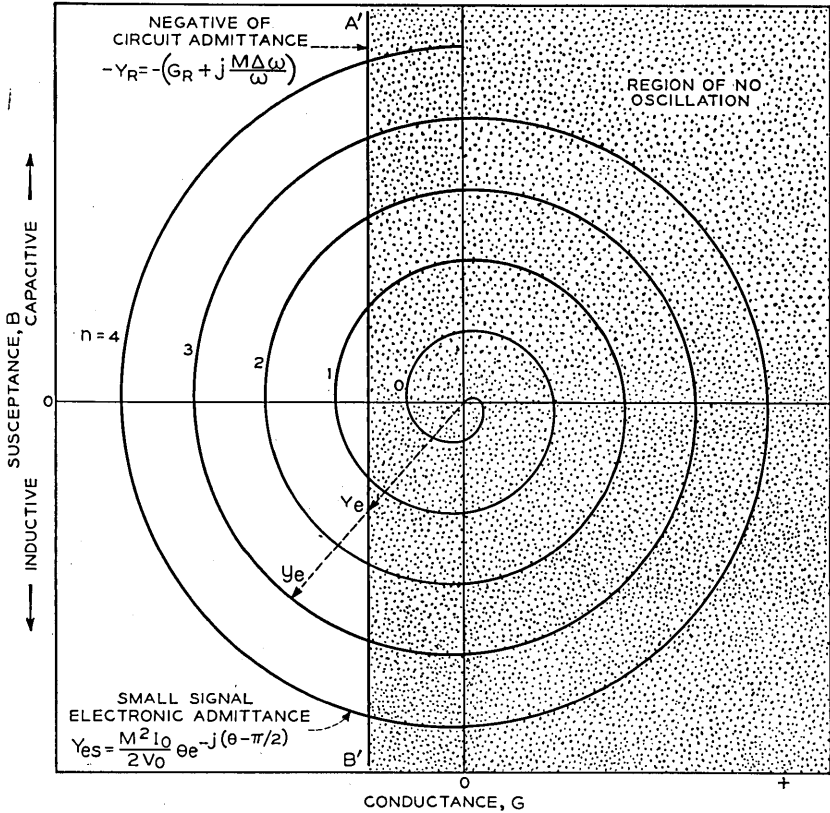


Fig. 4.—The negative of the circuit admittance (the heavy vertical line) and the small signal electronic admittance (the spiral) are shown in a plot of susceptance vs conductance. Each position along the circuit admittance line corresponds to a certain frequency. Each position along the spiral corresponds to a certain drift angle.

Such a presentation is very helpful in acquiring a qualitative understanding of the operation of a reflex oscillator.

In Appendix I it is shown that the admittance of the resonant circuit in the neighborhood of resonance is very nearly

$$Y_R = G_R + j2M\Delta\omega/\omega \tag{2.5}$$

where  $G_R$  is a constant. The negative of such an admittance has been plotted in Fig. 4 as the vertical line  $A'B'$ . Vertical position on this line is

proportional to the frequency at which the resonator is driven. The condition for stable oscillation is

$$Y_R + Y_e = 0. \quad (2.6)$$

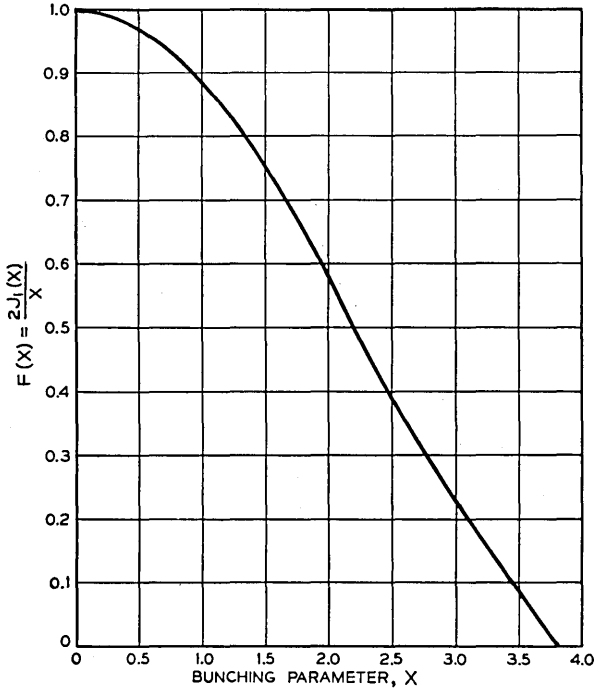


Fig. 5.—Relative amplitude of electronic admittance vs the bunching parameter  $X$ . The bunching parameter increases linearly with radio frequency gap voltage so that this curve shows the reduction in magnitude of electronic admittance with increasing voltage.

We may rewrite (2.2) for any given value of  $\theta$  as

$$Y_e = y_e F(V) e^{j((\pi/2)-\theta)} \quad (2.7)$$

where

$$F(V) = \frac{2J_1\left(\frac{\beta V \theta}{2V_0}\right)}{\frac{\beta V \theta}{2V_0}} = \frac{2J_1(X)}{X}. \quad (2.8)$$

The quantity

$$X = \frac{\beta V \theta}{2V_0} \quad (2.9)$$

is called the bunching parameter. A plot of the function  $F(V)$  vs  $X$  is shown in Fig. 5. For any given value of  $\theta$  and for fixed operating conditions

it is a function of  $V$  only and its action is clearly to reduce the small signal value of the admittance until condition (2.6) is satisfied. It will be observed that this function affects the magnitude only and not the phase of the admittance.

Thus, as indicated in Fig. 4, when oscillation starts the admittance is given by the radius vector of magnitude  $y_e$ , terminating on the spiral, and as the oscillation builds up this vector shrinks until in accordance with (12.6) it terminates on the circuit-admittance line  $A'B'$ , which is the locus of vectors  $(-Y_R)$ . The electronic admittance vector may be rotated by a change in the repeller voltage which changes the value of  $\theta$ . This changes the vertical intercept on line  $A'B'$ , and since the imaginary component of the circuit admittance, that is the height along  $A'B'$ , is proportional to frequency, this means that the frequency of oscillation changes. It is this property which is known as electronic tuning.

Oscillation will cease when the admittance vector has rotated to an angle such that it terminates on the intersection of the spiral and the circuit-admittance line  $A'B'$ . It will be observed that the greater is the number of cycles of drift the greater is the electronic tuning to extinction. While it is not as apparent from this diagram, it is also true that the greater the number of cycles of drift the greater the electronic tuning to intermediate power points. Vertical lines farther to the left correspond to heavier loads, and from this it is apparent that the electronic tuning to extinction decreases with the loading. By sufficient loading it is possible to prevent some repeller modes (i.e. oscillations of some  $n$  values) from occurring. Since losses in the resonant cavity of the oscillator represent some loading, some modes of low  $n$  value will not occur even in the absence of external loading.

### III. POWER PRODUCTION FOR DRIFT ANGLE OF $(n + \frac{3}{4})$ CYCLES

Now, from equation (2.2) it may be seen that  $Y_e$  will be real and negative for  $\theta = \theta_n = (n + \frac{3}{4})2\pi$ . Because  $\theta$  also appears in the argument of the Bessel function this value of  $\theta$  is not exactly the value to make the real component of  $Y_e$  a maximum. However, for the reasonably large values of  $n$  encountered in practical oscillators this is a justifiable approximation. Suppose, then, we consider the case of  $n + \frac{3}{4}$  cycles drift, calling this an optimum drift time. Using the value of  $n$  as a parameter we plot the magnitude of the radio-frequency electron current in the electron stream returning across the gap given by equation (2.1) as a function of the radio-frequency voltage across the gap. This variation is shown in Fig. 6. As might be expected, the greater the number of cycles the electrons drift in the drift space, the lower is the radio-frequency gap voltage required to produce a given amount of bunching and hence a given radio frequency electron current. It may be seen from Fig. 6 that as the radio-frequency gap voltage

is increased, the radio-frequency electron current gradually increases until a maximum value is reached, representing as complete bunching as is possible, after which the current decreases with increasing gap voltage. The maximum value of the current is approximately the same for various drift times, but occurs at smaller gap voltages for longer drift times.

The radio-frequency power produced is the voltage times the current. As the given maximum current occurs at higher voltages for shorter drift

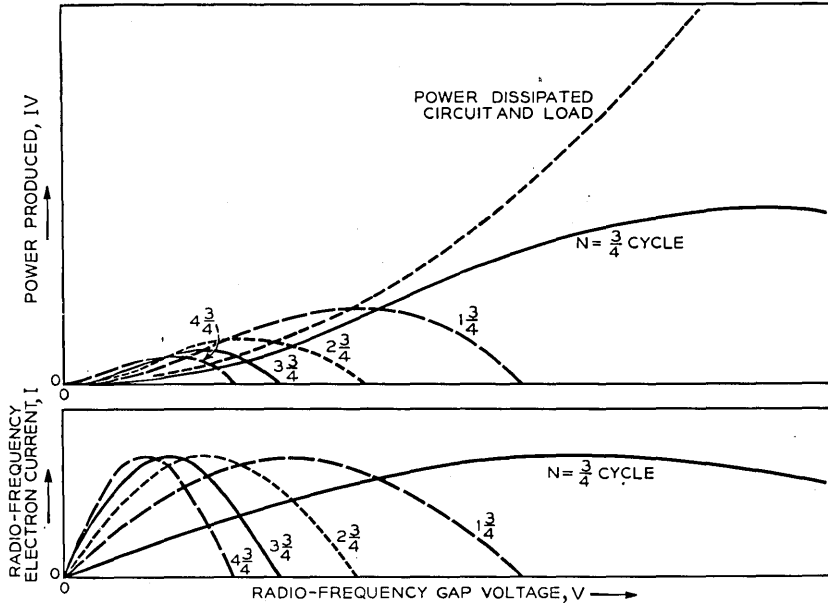


Fig. 6.—Radio frequency electron convection current  $I$  and the radio frequency power given up by the electron stream can be plotted vs the radio frequency gap voltage  $V$  for various drift times measured in cycles. Maximum current occurs at higher voltage for shorter drift times. For a given number of cycles drift, maximum power occurs at a higher gap voltage than that for maximum current. If the power produced for a given drift time is higher at low voltages than the power dissipated in the circuit and load (dashed curve), the tube will oscillate and the amplitude will adjust itself to the point at which the power dissipation and the power production curves cross.

times, the maximum power produced will be greater for shorter drift times. This is clearly brought out in the plots of power vs. voltage shown in Fig. 6.

The power dissipated in the circuits and load will vary as the square of the radio-frequency voltage. Part of this power will go into the load coupled with the circuit and part into unavoidable circuit losses. A typical curve of power into the circuit and load vs. radio-frequency voltage is shown in Fig. 6. Steady oscillation will take place at the voltage for which the power production curve crosses the power dissipation curve. For instance, in Fig. 6 the power dissipation curve crosses the power production curve for

$1\frac{3}{4}$  cycles drift at the maximum or hump of the curve. This means that the circuit impedance for the dissipation curve shown is such as to result in maximum production of power for  $1\frac{3}{4}$  cycles drift. For  $2\frac{3}{4}$  cycles drift and for longer drifts, the power dissipation curve crosses the power production curves to the right of the maximum and hence the particular circuit loading shown does not result in maximum power production for these longer drift times. This is an example of operation with lighter than optimum load. The power dissipation curve might cross the power production curve to the left of the maximum, representing a condition of too heavy loading for production of maximum power output. The power dissipation curve in Fig. 6 lies always above the power production curve for a drift of  $\frac{3}{4}$  cycles. This means that the oscillator for which the curves are drawn, if loaded to give the power dissipation curve shown, would not oscillate with the short drift time of  $\frac{3}{4}$  cycles, corresponding to a very negative repeller voltage.

In general, the conclusions reached by examining Fig. 6 are borne out in practice. The longer the drift time, that is, the less negative the repeller, the lower is the power output. For very negative repeller voltages, however, corresponding to very short drift times, the power either falls off, which means that most of the available power is dissipated in circuit losses, or the oscillator fails to operate at all because, for all gap voltages, the power dissipated in circuit losses is greater than the power produced by the electron stream.

Having examined the situation qualitatively, we want to make a somewhat more quantitative investigation, and to take some account of circuit losses. In the course of this we will find two parameters are very important. One is the parameter  $X$  previously defined by equation (2.9), which expresses the amount of bunching the beam has undergone. In considering a given tube with a given drift time, the important thing to remember about  $X$  is that it is proportional to the  $r$ - $f$  gap voltage  $V$ . For  $\theta = \theta_n$  expression (2.2) is a pure conductance and we can express the power produced by the electron stream as one half the square of the peak  $r$ - $f$  voltage times the circuit conductance which for stable oscillation is equal to the negative of the electronic conductance given by (2.2). This may be written with the aid of (2.9) as

$$P = 2(I_0 V_0 / \theta_n) X J_1(X). \quad (3.1)$$

Suppose we take into account the resonator losses but not the power lost in the output circuit, which in a well designed oscillator should be small. If the resonator has a shunt resonant conductance (including electronic loading) of  $G_R$ , the power dissipated in the resonator is

$$P_R = V^2 G_R / 2. \quad (3.2)$$

Then the power output for  $\theta_n$  is

$$P = 2(I_0 V_0 / \theta_n) X J_1(X) - V^2 G_R / 2. \quad (3.3)$$

The efficiency,  $\eta$ , is given by

$$\eta = \frac{P}{P_{DC}} = \frac{2}{\theta} \left[ X J_1(X) - \frac{G_R \theta_n V^2}{4 I_0 V_0} \right]. \quad (3.4)$$

From (2.4) and (2.9)

$$\frac{\theta_n V^2}{2 I_0 V_0} = \frac{1}{y_e} X^2. \quad (3.5)$$

Hence we may write

$$\eta = \frac{1}{(n + 3/4)} \frac{1}{\pi} \left[ X J_1(X) - \frac{G_R X^2}{y_e} \frac{1}{2} \right]. \quad (3.6)$$

Let us write  $\eta = \frac{H}{N}$  where  $N = (n + \frac{3}{4})$ . We may now make a generalized examination of the effect of losses on the efficiency by examining the function

$$H = (1/\pi) [X J_1(X) - (G_R/y_e) X^2/2]. \quad (3.7)$$

Thus, the efficiency for  $\theta = \theta_n$  is inversely proportional to the number of cycles drift and is proportional to a factor  $H$  which is a function of  $X$  and of the ratio  $G_R/y_e$ , that is, the ratio of resonator loss conductance to small signal electronic conductance.<sup>4</sup> For  $n + \frac{3}{4}$  cycles drift, the small signal electronic conductance is equal to the small signal electronic admittance.

For a given value of  $G_R/y_e$  there is an optimum value of  $X$  for which  $H$  has a maximum  $H_m$ . We can obtain this by differentiating (3.7) with respect to  $X$  and setting the derivative equal to zero, giving

$$\begin{aligned} X J_0(X) - (G_R/y_e) X &= 0 \\ J_0(X) &= (G_R/y_e). \end{aligned} \quad (3.8)$$

If we put values from this into (3.7) we can obtain  $H_m$  as a function of  $G_R/y_e$ . This is plotted in Fig. 7. The considerable loss of efficiency for values of  $G_R/y_e$  as low as .1 or .2 is noteworthy. It is also interesting to note that for  $G_R/y_e$  equal to  $\frac{1}{3}$ , the fractional change in power is equal to the fractional change in resonator resistance, and for  $G_R/y_e$  greater than  $\frac{1}{3}$ , the fractional power change is greater than the fractional change in resonator resistance. This helps to explain the fall in power after turn-on in some tubes, for an increase in temperature can increase resonator resistance considerably.

<sup>4</sup> An electronic damping term discussed in Appendix VIII should be included in resonator losses. The electrical loss in grids is discussed briefly in Appendix IX.

In the expression for the admittance, the drift angle,  $\theta$ , appears as a factor. This factor plays a double role in that it determines the phase of the admittance but also in a completely independent manner it determines, in part, the magnitude of the admittance.  $\theta$  as it has appeared in the foregoing analysis, which was developed on the basis of a linear retarding field, is the actual drift angle in radians. As will be shown in a later section, certain special repeller fields may give effective drift action for a given angle greater than the same angle in a linear field. Such values of effective drift angle may have fractional optimum values although the phase must still be such as to give within the approximations we have been using a pure conductance at optimum. In order to generalize the following work we will speak of an effective drift time in cycles,  $N_E = FN$ , where  $N$  is the actual drift time in cycles,  $n + \frac{3}{4}$ , and  $F$  is the number of times this drift is more effective than the drift in a linear field.

Suppose we have a tube of given  $\beta^2$ ,  $I_0$ ,  $V_0$  and resonator loss  $G_R$  and wish to find the optimum effective drift time,  $FN$ , and determine the effect on the efficiency of varying  $FN$ . It will be recalled that for very low losses we may expect more power output the fewer the number of cycles drift. However the resonator losses may cut heavily into the generated power, for short drift angles. With short drift angles the optimum load conductance becomes small compared to the loss conductance so that although the generated power is high only a small fraction goes to the useful load. There is, therefore, an optimum value which can be obtained using the data of Fig. 7. We define a parameter

$$K = \frac{2V_0}{\beta^2 I_0} G_R \quad (3.9)$$

which compares the resonator loss conductance with the small signal electronic admittance per radian of drift angle. Then in terms of  $K$ ,  $\frac{G_R}{y_e} = \frac{K}{\theta}$ . Hence, for a fixed value of  $K$ , various values of  $\theta = 2\pi FN$  define values of  $\frac{G_R}{y_e}$ . When one uses these values in connection with Fig. 7 he determines the corresponding values of  $H_m$  and hence the efficiency,  $\eta = \frac{H_m}{FN}$ . These values of  $\eta$  are plotted against  $FN$  as in Fig. 8 with values of  $K$  as a parameter. In this plot  $K$  is a measure of the lossiness of the tube. The optimum drift angle for any degree of lossiness is evident as the maximum of one of these curves.

The maximum power outputs in various repeller modes,  $n = 0, 1$  etc. and the repeller voltages for these various power outputs correspond to discrete values of  $n$  and  $FN$  lying along a curve for a particular value of  $K$ .

Thus, the curves illustrate the variation of power from mode to mode as the repeller voltage is changed over a wide range.

Changes in resonator loss or differences in loss between individual tubes of the same type correspond to passing from a curve for one value of  $K$  to a curve for another value of  $K$ .

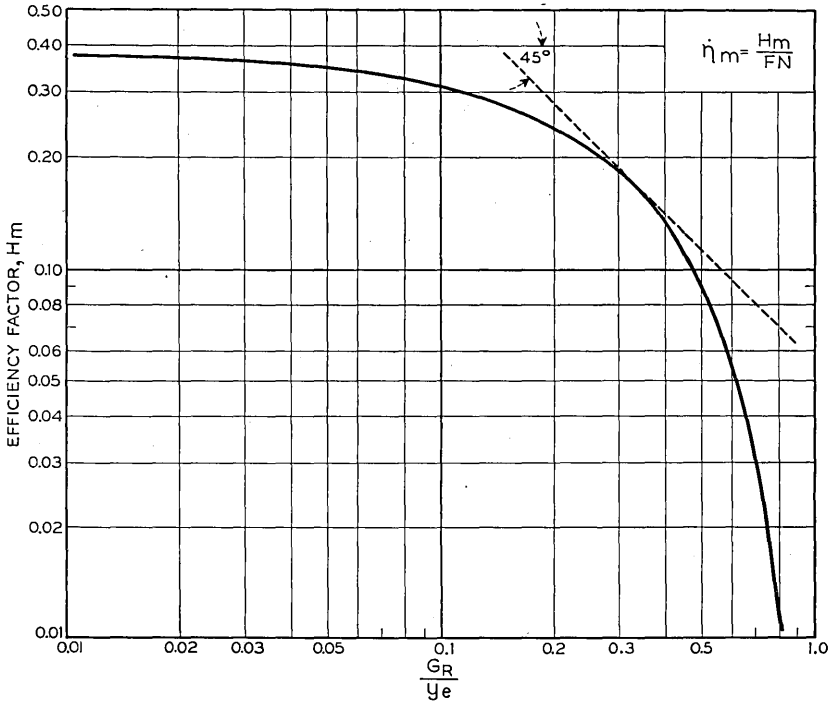


Fig. 7.—Efficiency factor  $H_m$  vs the ratio of resonator loss conductance to the small signal electronic admittance. Efficiency changes rapidly with load as the loss conductance approaches in magnitude the small signal electronic admittance. The efficiency is inversely proportional to the number of cycles drift.

It will be observed from this that although, from an efficiency standpoint, it is desirable to work at low values of drift time such low drift times lead to an output strongly sensitive to changes in resonator losses.

Perhaps the most important question which the user of the oscillator may ask with regard to power production for optimum drift is; what effect does the external load have upon the performance? If we couple lightly to the oscillator the  $r$ - $f$  voltage generated will be high but the power will not be extracted. If we couple too heavily the voltage will be low, the beam will not be efficiently modulated and the power output will be low. There is



apparently an optimum loading. Best output is not obtained when the external load matches the generator impedance as in the case of an amplifier.

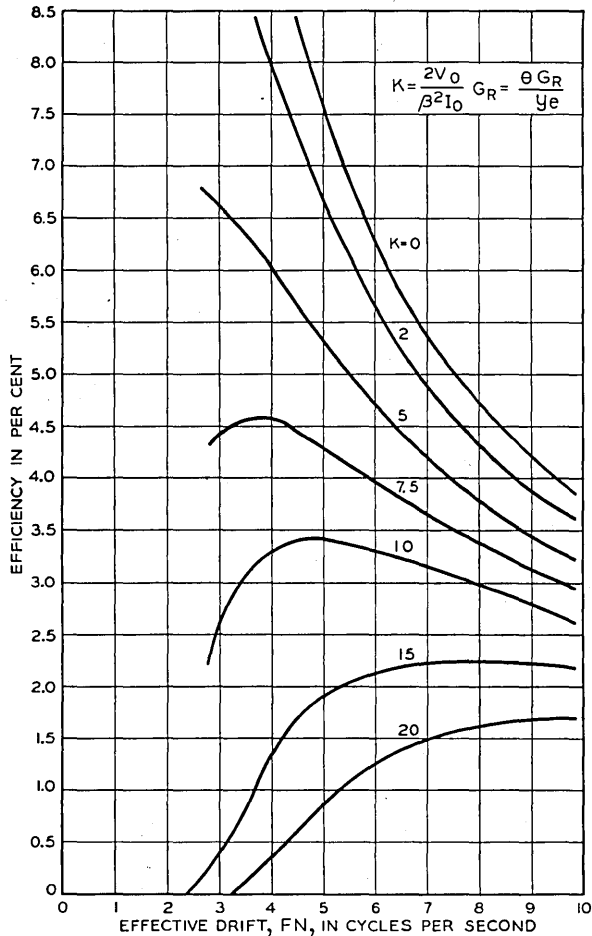


Fig. 8.—Efficiency in per cent vs the effective cycles drift for various values of a parameter  $K$  which is proportional to resonator loss. These curves indicate how the power output differs for various repeller modes for a given loss. Optimum power operating points will be represented by points along one of these curves. For a very low loss resonator, the power is highest for short drift times and decreases rapidly for higher repeller modes. Where there is more loss, the power varies less rapidly from mode to mode.

We return to equation (3.7) for  $H$  and assume that we are given various values of  $\frac{G_R}{y_e}$ . With these values as parameters we ask what variation in efficiency may be expected as we vary the ratio of the load conductance,  $G_L$ , to the small signal admittance,  $y_e$ . When  $\frac{G_L}{y_e} + \frac{G_R}{y_e} = 1$  oscillation

will just start and no power output will be obtained. We can state the general condition for stable operation as  $Y_e + Y_c = 0$ , where  $Y_c$  is the vector sum of the load and circuit admittances. For the optimum drift time this becomes

$$\frac{G_c}{y_e} = \frac{2J_1(X)}{X} \quad (3.10)$$

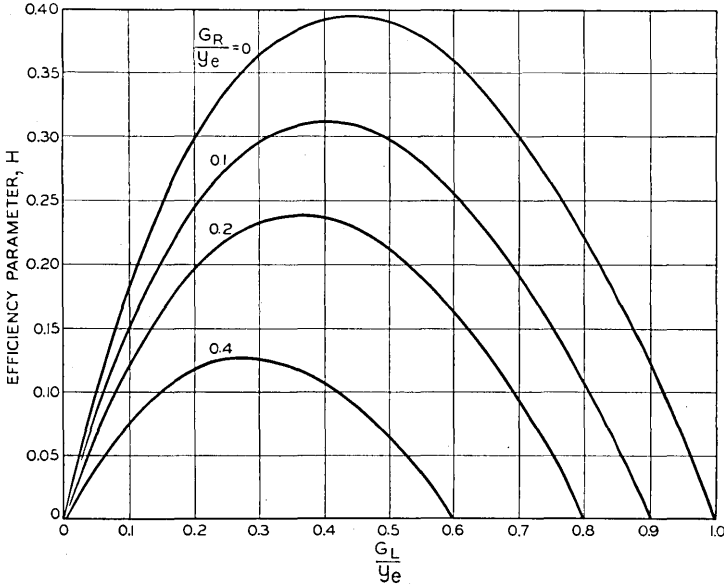


Fig. 9.—Efficiency parameter  $H$  vs the ratio of load conductance to the magnitude of the small signal electronic admittance. Curves are for various ratios of resonator loss conductance to small signal electronic admittance. The curves are of similar shapes and indicate that the tube will cease oscillating ( $H = 0$ ) when loaded by a conductance about  $\frac{1}{2}$  as large as that for optimum power.

where

$$\frac{G_c}{y_e} = \frac{G_L + G_R}{y_e} \quad (3.11)$$

Hence for a given value of  $\frac{G_R}{y_e}$  we may assume values for  $\frac{G_L}{y_e}$  between zero and  $1 - \frac{G_R}{y_e}$  and these in (3.11) will define values of  $X$ . These values of  $X$  substituted in (3.7) will define values of  $H$  which we then plot against the assumed values for  $\frac{G_L}{y_e}$ , as in Fig. 9. Thus we have the desired function of the variation of efficiency factor against load.

From the curves of Fig. 9 it can be seen that the maximum efficiency is obtained when the external conductance is made equal to approximately half the available small signal conductance; i.e.  $\frac{1}{2}(y_e - G_R)$ . This can be seen more clearly in the plot of Fig. 10. Equation (3.8) gives the condition for maximum efficiency as

$$\frac{G_R}{y_e} = J_0(X).$$

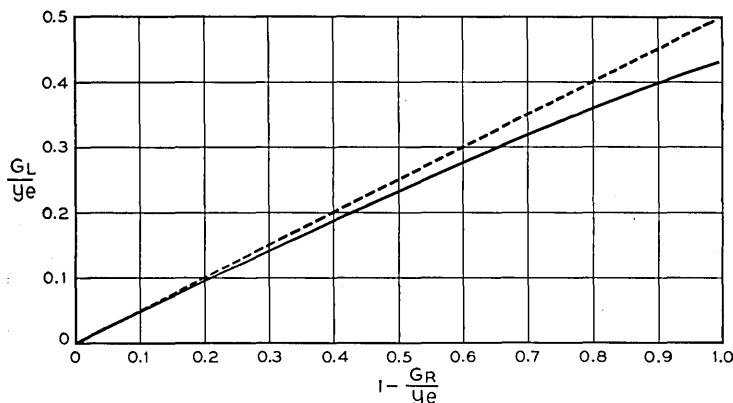


Fig. 10.—The abscissa measures the fractional excess of electronic negative conductance over resonator loss conductance. The ordinate is the load conductance as a fraction of electronic negative conductance. The tube will go out of oscillation for a load conductance such that the ordinate is equal to the abscissa. The load conductance for optimum power output is given by the solid line. The dashed line represents a load conductance half as great as that required to stop oscillation.

If we assume various values for  $\frac{G_R}{y_e}$  these define values of  $X_0$  which when substituted in

$$\frac{G_L}{y_e} = \frac{G_C}{y_e} - \frac{G_R}{y_e} = \frac{2J_1(X_0)}{X_0} - J_0(X_0) \quad (3.12)$$

give the value of the external load for optimum power. We plot these data against the available conductance

$$\left(1 - \frac{G_R}{y_e}\right) = 1 - J_0(X) \quad (3.13)$$

as shown in Fig. 10.

In Fig. 10 there is also shown a line through the origin of slope 1/2. It can thus be seen that the optimum load conductance is slightly less than half the available small signal or starting conductance. This relation is independent of the repeller mode, i.e. of the value  $FN$ . This does not mean

that the load conductance is independent of the mode, since we have expressed all our conductances in terms of  $y_e$ , the small signal conductance, and this of course depends on the mode. What it does say is that, regardless of the mode, if the generator is coupled to the load conductance for maximum output, then, if that conductance is slightly more than doubled oscillation will stop. It is this fact which should be borne in mind by the circuit designer. If greater margin of safety against "pull out" is desired it can be obtained only at the sacrifice of efficiency.

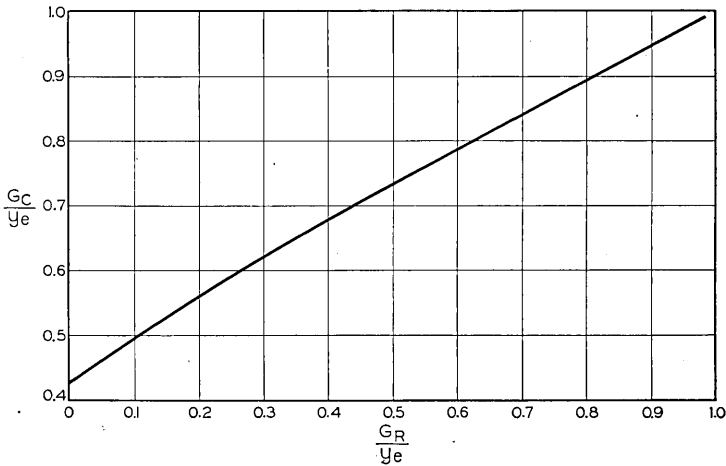


Fig. 11.—The ratio of total circuit conductance for optimum power to small signal electronic admittance, vs the ratio of resonator loss conductance to small signal electronic admittance.

An equivalent plot for the data of Fig. 10, which will be of later use, is shown in Fig. 11. This gives the value of  $\frac{G_C}{y_e}$  for best output for various values of  $\frac{G_R}{y_e}$ .

#### IV. EFFECT OF APPROXIMATIONS

The analysis presented in Section II is misleading in some respects. For instance, for a lossless resonator and  $N = \frac{3}{4}$  cycles, the predicted efficiency is 53%. However, our simple theory tells us that to get this efficiency, the radio-frequency gap voltage  $V$  multiplied by the modulation coefficient  $\beta$  (that is, the energy change an electron suffers in passing the gap) is  $1.018V_0$ . This means that (a) some electrons would be stopped and would not pass the gap (b) many other electrons would not be able to pass the gap against a retarding field after returning from drift region (c) some electrons would

cross the gap so slowly that for them  $\beta$  would be very small and their effect on the circuit would also be small (d) there might be considerable loading of the resonator due to transit time effects in the gap. Of course, it is not justifiable to apply the small signal theory in any event, since it was derived on the assumption that  $\beta V$  is small compared with  $V_0$ .

In Appendix IV there is presented a treatment by R. M. Ryder of these Laboratories in which it is not assumed that  $\beta V \ll V_0$ . This work does not, however, take into account variation of  $\beta$  with electron speed or the possibility of electrons being turned back at the gap.

For drift angles of  $1\frac{3}{4}$  cycles and greater, the results of Ryder's analysis are almost indistinguishable from those given by the simple theory, as may be seen by examining Figs. 128-135 of the Appendix. His curves approach the curves given by the simple theory for large values of  $n$ .

For small values of  $n$ , and particularly for  $\frac{3}{4}$  cycles drift, Ryder's work shows that optimum power is obtained with a drift angle somewhat different from  $n + \frac{3}{4}$  cycles. Also, Fig. 131 shows that the phase of the electronic admittance actually varies somewhat with amplitude, and Fig. 130 shows that its magnitude does not actually pass through zero as the amplitude is increased.

The reader is also referred to a paper by A. E. Harrison.<sup>5</sup>

The reader may feel at this point somewhat uneasy about application of the theory to practice. In most practical reflex oscillators, however, the value of  $n$  is 2 or greater, so that the theory should apply fairly well. There are, however, so many accidental variables in practical tubes that it is well to reiterate that the theory serves primarily as a guide, and one should not expect quantitative agreement between experiment and theory. This will be apparent in later sections, where in a few instances the writers have made quantitative calculations.

## V. SPECIAL DRIFT FIELDS

In the foregoing sections a theory for a reflex oscillator has been developed on the assumption that the repeller field is a uniform retarding electrostatic field. Such a situation rarely occurs in practice, partly because of the difficulty of achieving such a field and partly because such a field may not return the electron stream in the manner desired. In an effort to get some information concerning actual drift fields, we may extend the simple theory already presented to include such fields by redefining  $X$  as

$$X = \beta VF\theta/2V_0. \quad (5.1)$$

Here the factor  $F$  is included. As defined in Section III this is the factor which relates the effectiveness of a given drift field in bunching a velocity

<sup>5</sup> A. E. Harrison, "Graphical Methods for Analysis of Velocity Modulation Bunching," *Proc. I.R.E.*, 33.1, pp. 20-32, June 1945.

modulated electron stream with the bunching effectiveness of a field with the same drift angle  $\theta$  but with a linear variation of potential with distance. Suppose, for instance, that the variation of transit time,  $\tau$ , with energy gained in crossing the gap  $V$  is for a given field

$$\partial\tau/\partial V \quad (5.2)$$

and for a linear potential variation and the same drift angle

$$(\partial\tau/\partial V)_1. \quad (5.3)$$

Then the factor  $F$  is defined as

$$F = (\partial\tau/\partial V)/(\partial\tau/\partial V)_1. \quad (5.4)$$

In appendix *V*,  $F$  is evaluated in terms of the variation of potential with distance.

The efficiency is dependent on the effectiveness of the drift action rather than on the total number of cycles drift except of course for the phase requirements. Thus, for a nonlinear potential variation in the drift space we should have instead of (3.7)

$$\eta = H/FN. \quad (5.5)$$

In the investigation of drift action, one procedure is to assume a given drift field and try to evaluate the drift action. Another is to try to find a field which will produce some desirable kind of drift action. As a matter of fact, it is easy to find the best possible drift field (from the point of view of efficiency) under certain assumptions.

The derivation of the optimum drift field, which is given in appendix VII, hinges on the fact that the time an electron takes to return depends only on the speed with which it is injected into the drift field. Further, the variation in modulation coefficient for electrons returning with different speeds is neglected. With these provisos, the optimum drift field is found to be one in which electrons passing the gap when the gap voltage is decelerating take  $\pi$  radians to return, and electrons which pass the gap when the voltage is accelerating take  $2\pi$  radians to return, as illustrated graphically in Fig. 136, Appendix VII. A graph of potential vs. distance from gap to achieve such an ideal drift action is shown in Fig. 137 and the general appearance of electrodes which would achieve such a potential distribution approximately is shown in Fig. 138.

With such an ideal drift field, the efficiency of an oscillator with a lossless resonator is

$$\eta_i = (2/\pi)(\beta V/V_0). \quad (5.6)$$

For a linear potential variation in the drift space, at the optimum  $r$ - $f$  gap voltage, according to the approximate theory presented in Section III the efficiency for a lossless resonator is

$$\eta = (.520)(\beta V/V_0). \quad (5.7)$$

Comparing, we find an improvement in efficiency for the ideal drift field in the ratio

$$\eta_i/\eta = 1.23, \quad (5.8)$$

or only about 20%. Thus, the linear drift field is quite effective. The ideal drift field does have one advantage; the bunching is optimum for all gap voltages or, for a given gap voltage, for all modulation coefficients since ideally an infinitesimal  $a$ - $c$  voltage will change the transit time from  $\pi$  to  $2\pi$  and completely bunch the beam. This should tend to make the efficiency high despite variations in  $\beta$  over various parts of the electron flow. The limitation imposed by the fact that electrons cannot return across the gap against a high voltage if they have been slowed up in their first transit across the gap remains.

This last mentioned limitation is subject to amelioration. In one type of reflex oscillator which has been brought to our attention the electrons cross the gap the first time in a region in which the modulation coefficient is small. If the gap has mesh grids, a hole may be punched in the grids and a beam of smaller diameter than the hole focussed through it. Then the beam may be allowed to expand and recross a narrow portion of the gap, where the modulation coefficient is large. Thus, in the first crossing no electrons lose much energy (because  $\beta$  is small) and in the second crossing all can cross the gap where  $\beta V$  is large and hence can give up a large portion of their energy.

## VI. ELECTRONIC GAP LOADING

So far, attention has been concentrated largely on electronic phenomena in the drift or repeller region. To the long transit time across the gap there has been ascribed merely a reduction in the effect of the voltage on the electron stream by the modulation coefficient  $\beta$ . Actually, the long transit across the gap can give rise to other effects.

One of the most obvious of these other effects is the production of an electronic conductance across the gap. If it is positive, such a conductance acts just as does the resonator loss conductance in reducing the power output. Petrie, Strachey and Wallis of Standard Telephones and Cables have treated this matter in an interesting and rather general way. Their work, in a slightly modified form, appears in Appendix VIII, to which the reader is referred for details.

The work tells us that, considering longitudinal fields only, the electron flow produces a small signal conductance component across the gap

$$G_{eL} = \frac{I_0}{4V_0} \frac{\partial \beta^2}{\partial \gamma} \quad (6.1)$$

$$\gamma = \frac{\omega}{u_0} \quad (6.2)$$

Here  $\beta$  is the modulation coefficient and  $u_0$  is the electron speed.  $I_0$  and  $V_0$  are beam current and beam voltage. If the gap has a length  $d$ , the transit angle across it is  $\theta_g = \gamma d$  and (6.1) may be rewritten

$$G_{eL} = -\frac{I_0 \theta_g}{4V_0} \frac{\partial \beta^2}{\partial \theta_g} \quad (6.3)$$

It is interesting to compare this conductance with the magnitude of the small-signal electronic admittance,  $y_e$ . In doing so, we should note that the current crosses the gap twice, and on each crossing produces an electronic conductance. Thus, the appropriate comparison between loss conductance and electronic admittance is  $2G_{eL}/y_e$ . Using (6.3) we obtain

$$2G_{eL}/y_e = -\frac{\theta_g}{\theta} \frac{1}{\beta^2} \frac{\partial \beta^2}{\partial \theta_g} \quad (6.4)$$

Usually, the drift angle  $\theta$  is much larger than the gap transit angle  $\theta_g$ . Further, if we examine the curves for modulation coefficient  $\beta$  which are given in Appendix II, we find that  $(\partial \beta^2 / \partial \theta_g) / \beta^2$  will not be very large. Thus, we conclude that in general the total loss conductance for longitudinal fields will be small compared with the electronic admittance. An example in Appendix VIII gives  $(2G_{eL}/y_e)$  as about 1/10. It seems that this effect will probably be less important than various errors in the theory of the reflex oscillator.

Even though this electronic gap loading is not very large, it may be interesting to consider it further. We note, for instance, that the conductance  $G_{eL}$  is positive when  $\beta^2$  decreases as gap transit angle increases. For parallel fine grids this is so from  $\theta_g = 0$  to  $\theta_g = 2\pi$  (see Fig. 119 of Appendix II). At  $\theta_g = 2\pi$ , where  $\beta = 0$ ,  $\partial \beta^2 / \partial \theta_g = 0$ , and the gap loading is zero. In a region beyond  $\theta_g = 2\pi$ ,  $\partial \beta^2 / \partial \theta_g$  becomes positive and the gap conductance is negative. Thus, for some transit angles a single gap can act to produce oscillations. For still larger values of  $\theta_g$ ,  $G_{eL}$  alternates between positive and negative. Gap transit angles of greater than  $2\pi$  are of course of little interest in connection with reflex oscillators, as for such transit angles  $\beta$  is very small.

For narrow gaps with large apertures rather than fine grids,  $\partial \beta^2 / \partial \theta_g$



never becomes very negative and may remain positive and the gap loading conductance due to longitudinal fields be always positive. In such gaps, however, transverse fields can have important effects, and (6.3) no longer gives the total gap conductance. Transverse fields act to throw electrons approaching the gap outward or inward, into stronger or weaker longitudinal fields, and in this manner the transverse fields can either cause the electrons to give up part of their forward velocity, transferring energy to the resonator, or to pick up forward velocity, taking energy from the resonator. An analysis of the effect of transverse fields is given in Appendix VIII, and this is applied in calculating the total conductance, due both to longitudinal and to transverse fields, of a short gap between cylinders with a uniform current density over the aperture. It is found that the transverse fields contribute a minor part of the total conductance, and that this contribution may be either positive or negative, but that the total gap conductance is always positive (see Appendix VIII, Fig. 140).

The electron flow across the gap produces a susceptive component of admittance. This susceptive component is in general more difficult to calculate than the conductive component. It is not very important; it serves to affect the frequency of oscillation slightly but not nearly so much as a small change in repeller voltage.

Besides such direct gap loading, the velocity modulation and drift action within a gap of fine grids actually produce a small bunching of the electron stream. In other words, the electron stream leaving such a gap is not only velocity modulated but it has a small density modulation as well. This convection current will persist (if space-charge debunching is not serious) and, as the electrons return across the gap, it will constitute a source of electronic admittance. We find however, that in typical cases (see Appendix VIII, (h59)–(h63)), this effect is small and is almost entirely absent in gaps with coarse grids or large apertures.

Secondary electrons produced when beam electrons strike grid wires and grid frames or gap edges constitute another source of gap loading. It has been alleged that if the frames supporting the grids or the tubes forming a gap have opposed parallel surfaces of width comparable to or larger than the gap spacing, large electron currents can be produced through secondary emission, the  $r$ - $f$  field driving electrons back and forth between the opposed surfaces. It would seem that this phenomenon could take place only at quite high  $r$ - $f$  levels, for an electron would probably require of the order of 100 volts energy to produce more than one secondary in striking materials of which gaps are usually constructed.

## VII. ELECTRONIC TUNING—ARBITRARY DRIFT ANGLE

So far, the "on tune" oscillation of reflex oscillators has been considered except for a brief discussion in Section II, and we have had to deal only with

real admittances (conductances). In this section the steady state operation in the case of complex circuit and electronic admittances will be discussed. The general condition for oscillation states that, breaking the circuit at any point the sum of the admittances looking in the two directions is zero. Particularly, the electronic admittance  $Y_e$  looking from the circuit to the electron stream, must be minus the circuit admittance  $Y_c$ , looking from the electron stream to the circuit. Here electronic admittance is used in the sense of an admittance averaged over a cycle of oscillation and fulfilling the above condition.

It is particularly useful to consider the junction of the electron stream and the circuit because the electronic admittance  $Y_e$  and the circuit admittance  $Y_c$  have very different properties, and if conditions are considered elsewhere these properties are somewhat mixed and full advantage cannot be taken of their difference.

The average electronic admittance with which we are concerned is a function chiefly of the amplitude of oscillation. Usually its magnitude decreases with increasing amplitude of oscillation, and its phase may vary as well, although this is a large signal effect not shown by the simple theory. In reflex oscillators the phase may be controlled by changing the repeller voltage. The phase and magnitude of the electronic admittance also vary with frequency. Usually, however, the rate of change with frequency is slow compared with that of the circuit admittance in the vicinity of any one resonant mode. By neglecting this change of electronic admittance with frequency in the following work, and concentrating our attention on the variation with amplitude and repeller voltage, we will emphasize the important aspects without serious error. However, the variation of electronic admittance with frequency should be kept in mind in considering behavior over frequency ranges of several per cent.<sup>6</sup>

The circuit admittance is, of course, independent of amplitude and is a rapidly varying function of frequency. It is partly dependent on what is commonly thought of as the resonator or resonant circuit of the oscillator, but is also profoundly affected by the load, which of course forms a part of the circuit seen from the electron stream. The behavior of the oscillator is determined, then, by the electronic admittance, the resonant circuit and the load. The behavior due to circuit and load effects applies generally to all oscillators, and the simplicity of behavior of the electronic admittance is such that similarities of behavior are far more striking than differences.

We have seen from Appendix I that at a frequency  $\Delta\omega$  away from the resonant frequency  $\omega_0$  where  $\Delta\omega \ll \omega_0$ , the admittance at the gap may be expressed as:

$$Y_c = G_c + j2M\Delta\omega/\omega_0. \quad (7.1)$$

<sup>6</sup> Appendix IV discusses the variation of phase with frequency and repeller voltage. The variation of phase of electronic admittance with frequency is included in Section IX A.

Here the quantity  $M$  is the characteristic admittance of the resonator, which depends on resonator shape and is unaffected by scaling from one frequency to another.  $G_c$  is the shunt conductance due to circuit and to load.  $Y_c$  as given by (7.1) represents to the degree of approximation required the admittance of any resonant circuit and load with only one resonance near the frequency of oscillation.

It is profitable to consider again in more detail a complex admittance plot similar to Fig. 4. In Fig. 12 the straight vertical line is a plot of (7.1).

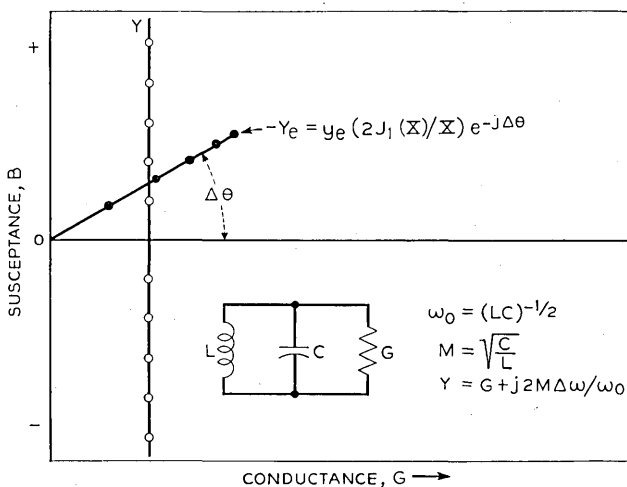


Fig. 12.—The resonator and its load can be represented as a shunt resonant circuit with a shunt conductance  $G$ . For frequencies near resonance, the conductance is nearly constant and the susceptance  $B$  is proportional to frequency, so that when susceptance is plotted vs conductance, the admittance  $Y$  is a vertical straight line. The circles mark off equal increments of frequency. The electronic admittance is little affected by frequency but much affected by amplitude. The negative of an electronic admittance  $Y_e$  having a constant phase angle  $\Delta\theta$  is shown in the figure. The dots mark off equal amplitude steps. Oscillation will occur at a frequency and amplitude specified by the intersection of the curves  $Y$  and  $-Y_e$ .

The circles mark equal frequency increments. Now if we neglect the variation of the electronic admittance with phase, then the negative of the small signal electronic admittance on this same plot will be a vector, the locus of whose termination will be a circle. The vector is shown in Fig. 12. The dots mark off admittance values corresponding to equal amplitude increments as determined by the data of Fig. 5.

Steady oscillation will take place at the frequency and amplitude represented by the intersection of the two curves. If the phase angle  $\Delta\theta$  of the  $-Y_e$  curve is varied by varying the repeller voltage, the point of intersection will shift on both the  $Y_c$  curve and the  $-Y_e$  curve. The shift along the

$Y_c$  curve represents a change in frequency of oscillation; the shift along the  $-Y_e$  curve represents a change in the amplitude of oscillation. If we know the variation of amplitude with position along the  $-Y_e$  curve, and the variation of frequency with position along the  $Y_c$  curve, we can obtain both the amplitude and frequency of oscillation as a function of the phase of  $-Y_e$ , which is in turn a function of repeller voltage.

From (2.3) and (2.7) we can write  $-Y_e$  in terms of the deviation of drift angle  $\Delta\theta$  from  $n + \frac{3}{4}$  cycles.

$$-Y_e = y_e(2J_1(X)/X)e^{j\Delta\theta}. \quad (7.2)$$

The equation relating frequency and  $\Delta\theta$  can be written immediately from inspection of Fig. 12.

$$\begin{aligned} 2M\Delta\omega/\omega_0 &= -G_c \tan \Delta\theta \\ \Delta\omega/\omega_0 &= -(G_c/2M) \tan \Delta\theta \\ \Delta\omega/\omega_0 &= -(1/2Q) \tan \Delta\theta. \end{aligned} \quad (7.3)$$

Here  $Q$  is the loaded  $Q$  of the circuit.

The maximum value of  $\Delta\theta$  for which oscillation can occur (at zero amplitude) is an important quantity. From Fig. 12 this value, called  $\Delta\theta_0$ , is obviously given by

$$\begin{aligned} \cos \Delta\theta_0 &= G_c/y_e = (G_c/M)(M/y_e) \\ &= (M/y_e)/Q. \end{aligned} \quad (7.4)$$

From this we obtain

$$\tan \Delta\theta_0 = \pm (Q^2(y_e/M)^2 - 1)^{\frac{1}{2}}. \quad (7.5)$$

By using (7.3) we obtain

$$(\Delta\omega/\omega_0)_0 = \pm (\frac{1}{2}) (y_e/M) (1 - (M/y_e Q)^2)^{\frac{1}{2}} \quad (7.6)$$

or

$$(\Delta\omega/\omega_0)_0 = \pm (\frac{1}{2}) (y_e/M) (1 - (G_c/y_e)^2)^{\frac{1}{2}}. \quad (7.7)$$

These equations give the electronic tuning from maximum amplitude of oscillation to zero amplitude of oscillation (extinction).

The equation relating amplitudes may be as easily derived from Fig. 12.

$$G_c^2 + (2M\Delta\omega/\omega)^2 = y_e^2 (2J_1(X)/X)^2 \quad (7.8)$$

at

$$\begin{aligned} \Delta\omega &= 0 \text{ let } X = X_0. \text{ Then} \\ \Delta\omega/\omega_0 &= (y_e/2M) ((2J_1(X)/X)^2 - (2J_1(X_0)/X_0)^2)^{\frac{1}{2}}. \end{aligned} \quad (7.9)$$

It is of interest to have the value of  $\Delta\omega/\omega_0$  at half the power for  $\Delta\omega = 0$ . At half power,  $X = X_0/\sqrt{2}$ , so

$$(\Delta\omega/\omega_0)_{\frac{1}{2}} = (y_e/2M)((2J_1(X_0/\sqrt{2})/(X_0/\sqrt{2}))^2 - (2J_1(X_0)/X_0)^2)^{\frac{1}{2}}. \quad (7.10)$$

For given values of modulation coefficient and  $V_0$ ,  $X$  is a function of the  $r$ - $f$  gap voltage  $V$  and also of drift angle and hence of  $\Delta\theta$ , or repeller voltage (see Appendix IV). For the fairly large values of  $\theta$  typical of most reflex oscillators, we can neglect the change in  $X$  due directly to changes in  $\Delta\theta$ , and consider  $X$  as a direct measure of the  $r$ - $f$  gap voltage  $V$ . Likewise  $y_e$  is a function of drift time whose variation with  $\Delta\theta$  can and will be disregarded. Hence from (7.9) we can plot  $(X/X_0)^2$  vs.  $\Delta\omega/\omega_0$  and regard this as a representation of normalized power vs. frequency.

Let us consider now what (7.3) and (7.9) mean in connection with a given reflex oscillator. Suppose we change the load. This will change  $Q$  in (7.3) and  $X_0$  in (7.9). From the relationship previously obtained for the condition for maximum power output,  $G_R/y_e = J_0(X_0)$ , we can find the value of  $X_0$  that is,  $X$  at  $\Delta\omega = 0$ , for various ratios of  $G_R/y_e$ . For  $G_R = 0$  (zero resonator loss) the optimum power value of  $X_0$  is 2.4. When there is some resonator loss, the optimum total conductance for best power output is greater and hence the optimum value of  $X_0$  is lower.

In Fig. 13 use is made of (7.3)  $\Delta\omega/\omega_0$  in plotted vs.  $\Delta\theta$  (which decreases as the repeller is made more negative) for several values of  $Q$ , and in Fig. 14, (7.9), is used to plot  $(X/X_0)^2$  vs.  $(2M/y_e)\Delta\omega/\omega_0$ , which is a generalized electronic tuning variable, for several values of  $X_0$ . These curves illustrate typical behavior of frequency vs. drift angle or repeller voltage and power vs. frequency for a given reflex oscillator for various loads. In practice, the  $S$  shape of the frequency vs. repeller voltage curves for light loads (high  $Q$ ) is particularly noticeable. The sharpening of the amplitude vs. frequency curves for light loads is also noticeable, though of course the cusp-like appearance for zero load and resonator loss cannot be reproduced experimentally. It is important to notice that while the plot of output vs. frequency for zero load is sharp topped, the plot of output vs. repeller voltage for zero load is not.

Having considered the general shape of frequency vs. repeller voltage curves and power vs. frequency curves, it is interesting to consider curves of electronic tuning to extinction  $((\Delta\omega/\omega_0)_0)$  and electronic tuning to half power  $((\Delta\omega/\omega_0)_{\frac{1}{2}})$  vs. the loading parameter,  $(M/y_eQ) = G_c/y_e$ . Such curves are shown in Fig. 15. These curves can be obtained using (7.7) and (7.10). In using (7.10)  $X$  can be related to  $G_c/y_e$  by the relation previously derived from  $2J_1(X)/X = G_c/y_e$  and given in Fig. 5 as a function of  $X$ . It is to be noted that the tuning to the half power point,  $(\Delta\omega/\omega_0)_{\frac{1}{2}}$ , and the tuning to the extinction point,  $(\Delta\omega/\omega_0)_0$ , vary quite differently with loading.

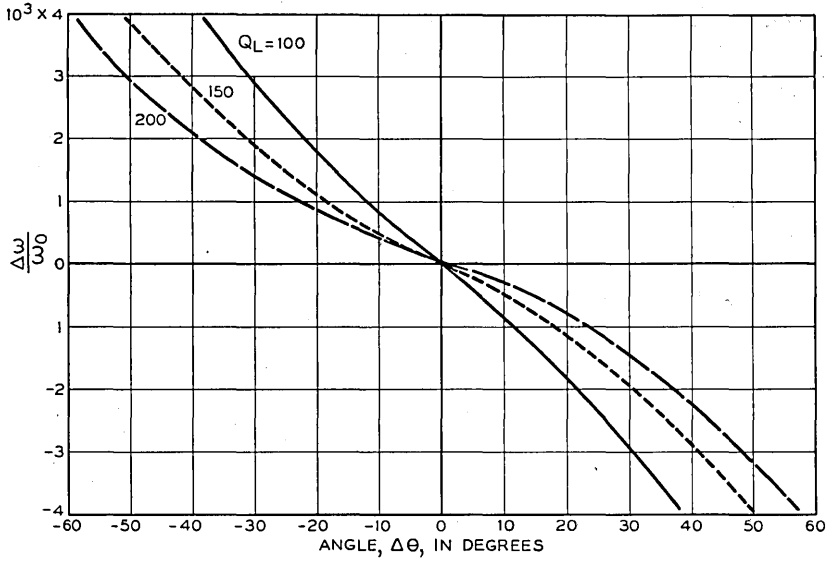


Fig. 13.—A parameter proportional to electronic tuning plotted vs deviation from optimum drift angle  $\Delta\theta$  for various values of loaded  $Q$ . For lower values of  $Q$ , the frequency varies rapidly and almost linearly with  $\Delta\theta$ . For high values of  $Q$ , the frequency curve is S shaped and frequency varies slowly with  $\Delta\theta$  for small values of  $\Delta\theta$ .

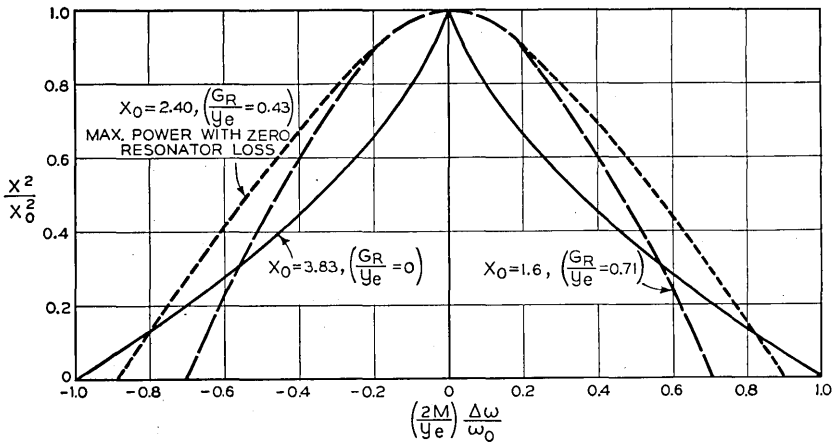


Fig. 14.—The relative power output vs a parameter proportional to the frequency deviation caused by electronic tuning, for various values of load. For zero loss and zero load, the curve is peaked. For zero loss and optimum load, the curve has its greatest width between half power points. For zero loss and greater than optimum load, the curve is narrow.

The quantity

$$(\Delta\omega/\omega_0)_{\frac{1}{2}}$$

has a maximum value at  $G_c/y_e = .433(X = 2.40)$ , which is the condition for maximum power output when the resonator loss is zero.

In Fig. 11 we have a plot of  $G_c/y_e$  vs.  $G_R/y_e$  for optimum loading (that is loading to give maximum power for  $\Delta\theta = 0$ ). This, combined with the

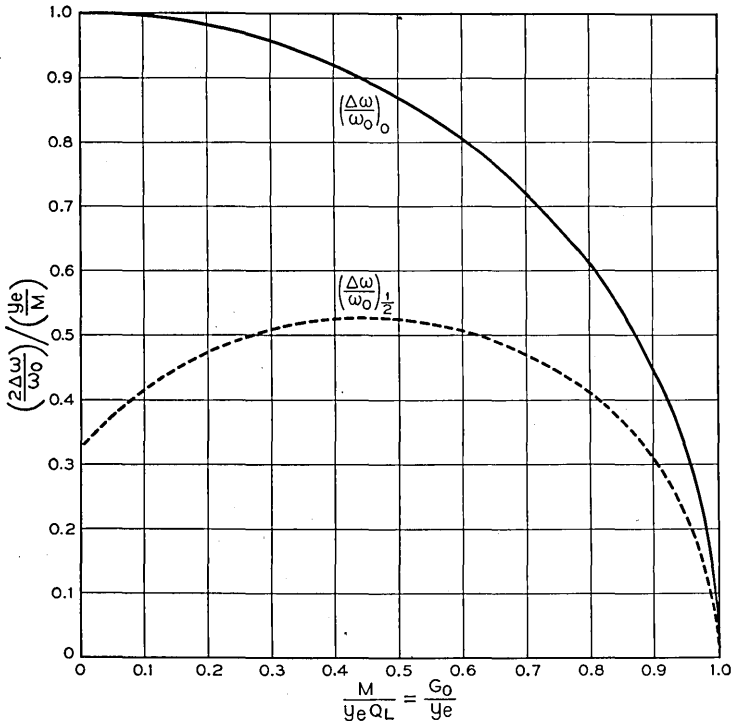


Fig. 15.—A parameter proportional to electronic tuning range vs the ratio of total circuit conductance and small signal electronic admittance. The electronic tuning to extinction  $(\Delta\omega/\omega_0)_0$  is more affected by loading than the electronic tuning to half power points  $(\Delta\omega/\omega_0)_{\frac{1}{2}}$ .

curves of Fig. 15, enables us to draw curves in the case of optimum loading for electronic tuning as a function of the resonator loss. Such curves are shown in Fig. 16.

From Fig. 16 we see that with optimum loading it takes very large resonator losses to affect the electronic tuning range to half power very much, and that the electronic tuning range to extinction is considerably more affected by resonator losses. Turning back to Fig. 7, we see that power is affected even more profoundly by resonator losses. It is interesting to

compare the effect of going from zero loss to a case in which the loss conductance is  $\frac{1}{2}$  of the small signal electronic conductance ( $G_R = y_e/2$ ). The table below shows the fraction to which the power or efficiency, the elec-

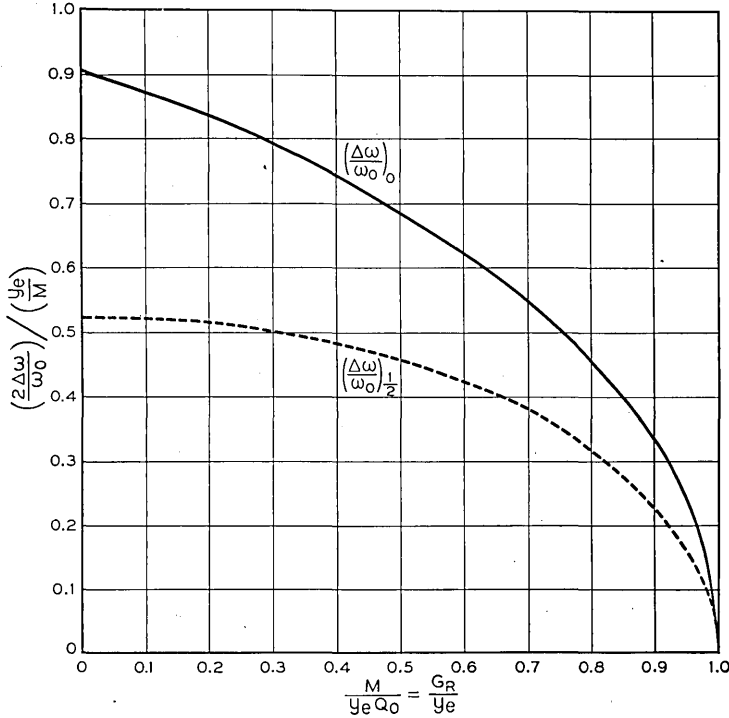


Fig. 16.—The effect of resonator loss on electronic tuning in an oscillator adjusted for optimum power output at the center of the electronic tuning range. A parameter proportional to electronic tuning is plotted vs the ratio of the resonator loss to small signal electronic admittance. The electronic tuning to extinction is more affected than the electronic tuning to half power as the loss is changed.

tronic tuning range to extinction, and the electronic tuning range to half power are reduced by this change.

Power, Efficiency ( $\eta$ )	Electronic Tuning to Extinction $(\Delta\omega/\omega_0)_0$	Electronic Tuning To Half Power $(\Delta\omega/\omega_0)_{\frac{1}{2}}$
.24	.76	.88

From this table it is obvious that efforts to control the electronic tuning by varying the ratio  $\frac{G_R}{y_e}$  are of dubious merit.



One other quantity may be of some interest; that is the phase angle of electronic tuning at half power and at extinction. We already have an expression involving  $\Delta\theta_0$  (the value at extinction) in (7.4). By taking advantage of (3.10) and (3.8) (Figs. 5 and 11), we can obtain  $\Delta\theta_0$  vs.  $G_c/y_e$

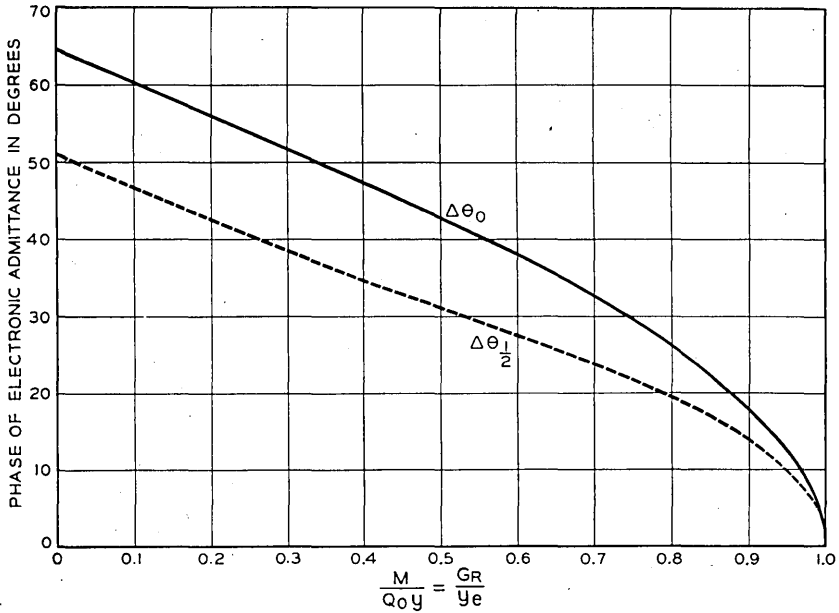


Fig. 17.—The phase of the drift angle for extinction and half power vs the ratio of resonator loss to small signal electronic admittance.

( $=M/Qy_e$ ) for optimum loading. By referring to Fig. 12 we can obtain the relation for  $\Delta\theta_{1/2}$  (the value at half power)

$$G_c = y_e [2J_1(X_0/\sqrt{2})/(X_0/\sqrt{2})] \cos \Delta\theta_{1/2}. \quad (7.11)$$

However, we have at  $\Delta\theta = 0$

$$G_c = y_e [2J_1(X_0)/X_0]. \quad (7.12)$$

Hence

$$\cos \Delta\theta_{1/2} = \frac{J_1(X_0)}{\sqrt{2}J_1(X_0/\sqrt{2})}. \quad (7.13)$$

Again, from (3.10) and (3.8) we can express  $X_0$  for optimum power at  $\Delta\theta = 0$  in terms of  $G_c/y_e$ . In Fig. 17,  $\Delta\theta_0$  and  $\Delta\theta_{1/2}$  are plotted vs.  $G_c/y_e$  for optimum loading.

## VIII. HYSTERESIS

All the analysis presented thus far would indicate that if a reflex oscillator is properly coupled to a resistive load the power output and frequency will be single-valued functions of the drift time or of the repeller voltage, as illustrated in Fig. 18. During the course of the development in these laboratories of a reflex oscillator known as the 1349XQ, it was found that even if

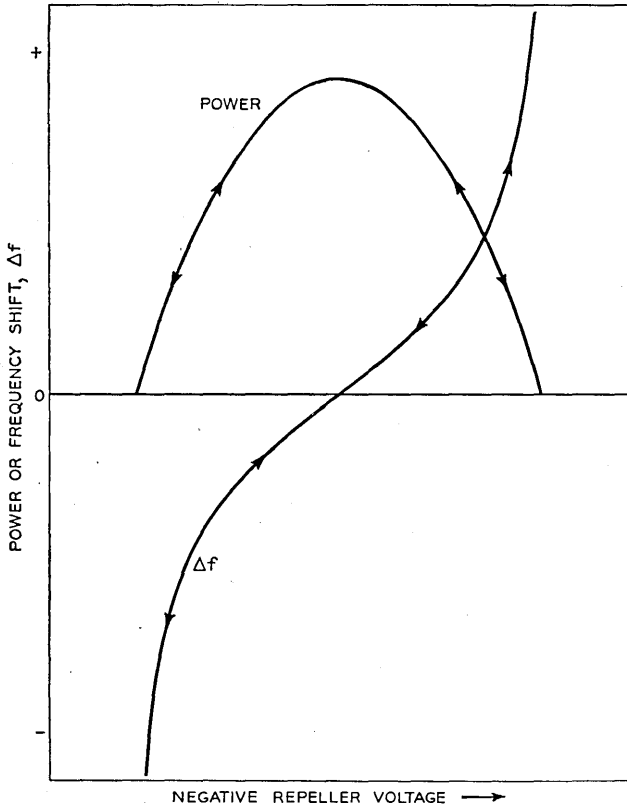


Fig. 18.—Ideal variation of power and frequency with repeller voltage, arbitrary units.

the oscillator were correctly terminated the characteristics departed violently from the ideal, as illustrated in Fig. 19. Further investigation disclosed that this departure was, to a greater or less degree, a general characteristic of all reflex oscillators in which no special steps had been taken to prevent it.

The nature of this departure from expected behavior is that the output is not a single valued function of the repeller voltage, but rather that at a given repeller voltage the output depends upon the direction from which the repel-

ler voltage is made to approach the given voltage. Consider the case illustrated in Fig. 19. The arrows indicate the direction of repeller voltage variation. If we start from the middle of the characteristic and move toward more negative values of repeller voltage, the amplitude of oscillation varies continuously until a critical value is reached, at which a sudden decrease in

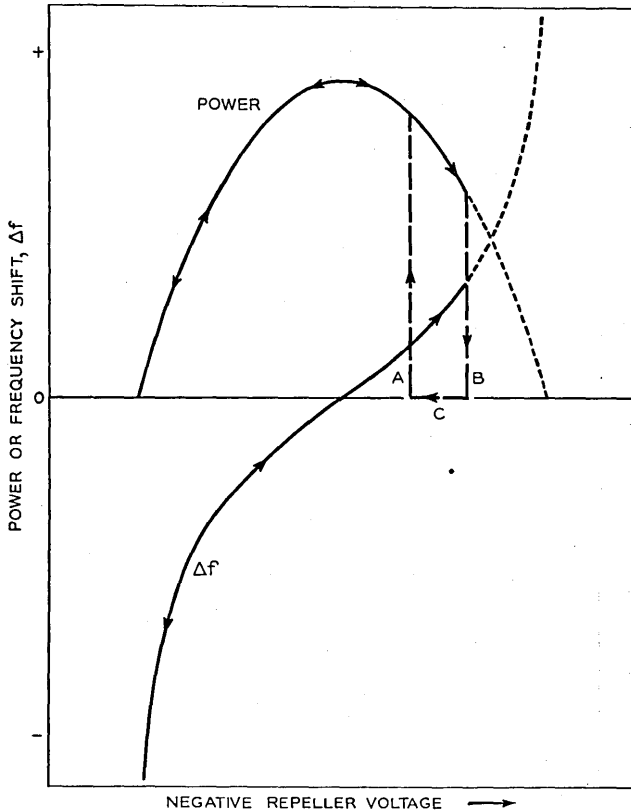


Fig. 19.—A possible variation of power and frequency with repeller voltage when there is electronic hysteresis. The arrows indicate the direction of variation of repeller voltage.

amplitude is observed. This drop may be to zero amplitude as shown or to a finite amplitude. In the latter case the amplitude may again decrease continuously as the repeller voltage is continuously varied to a new critical value, where a second drop occurs, etc. until finally the output falls to zero. In every observed case, even for more than one drop, the oscillation always dropped to zero discontinuously. Upon retracing the repeller voltage variation, oscillation does not restart at the repeller voltage at which it stopped but remains zero until a less negative value is reached, at which point the

oscillation jumps to a large amplitude on the normal curve and then varies uniformly. The discontinuities occur sometimes at one end of the characteristic and sometimes at the other, and infrequently at both. It was first thought that this behavior was caused by an improper load,<sup>7</sup> but further investigation proved that the dependence on the load was secondary and the conclusion was drawn and later verified that the effect had its origin in the electron stream. For this reason the discontinuous behavior was called electronic hysteresis.

In any self-excited oscillator having a simple resonant circuit, the oscillating circuit may be represented schematically as shown in Fig. 20. Here  $L$  and  $C$  represent the inductance and capacitance of the oscillator.  $G_R$  is a shunt conductance, representing the losses of the circuit, and  $G_L$  is the conductance of the load. Henceforth for the sake of convenience we

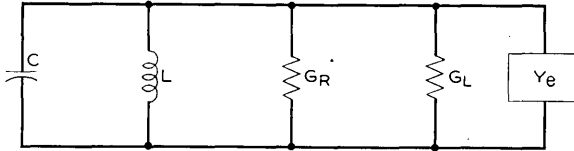


Fig. 20.—Equivalent circuit of reflex oscillator consisting of the capacitance  $C$ , inductance  $L$ , the resonator loss conductance  $G_R$ , the load conductance  $G_L$  and the electronic admittance  $Y_e$ .

will lump these and call the total  $G_L$ .  $Y_e$  represents the admittance of the electron stream. Such a circuit has a characteristic transient of the form

$$V = V_0 e^{-\alpha t} e^{j\omega t} \quad (8.1)$$

where

$$\alpha = \frac{G_e + G_L}{2C} \quad \text{and} \quad \omega \doteq \frac{1}{\sqrt{LC}}.$$

Oscillations will build up spontaneously if

$$G_{e0} + G_L < 0. \quad (8.2)$$

For stable oscillation at amplitude  $V$  we require

$$G_e[V] + G_L = 0 \quad (8.3)$$

(8.2) and (8.3) state that the amplitude of oscillation will build up until non-linearities in the electronic characteristics reduce the electronic conductance to a value equal and opposite to the total load plus circuit conductance. Thus, in general

$$Y_e = G_{e0}F_1(V) + jB_{e0}F_2(V) \quad (8.4)$$

<sup>7</sup> See Section IX.

where

$$Y_e = G_{e0} + jB_{e0} \quad (8.5)$$

is the admittance for vanishing amplitude, which is taken as a reference value. The foregoing facts are familiar to any one who has worked with oscillators.

Now, condition (8.3) may be satisfied although (8.2) is not. Then an oscillator will not be self-starting, although once started at a sufficiently large amplitude its operation will become stable. An example in common experience is a triode Class C oscillator with fixed grid bias. In such a case

$$F(V_1) > F(0) \quad (8.6)$$

holds for some  $V_1$ .

As an example of normal behavior, let us assume that  $F(V)$  is a continuous monotonically decreasing function of increasing  $V$ , with the reference value of  $V$  taken as zero. Then the conductance,  $G_e = G_{e0}F(V)$  will vary with  $V$  as shown in Fig. 21. Stable oscillation will occur when the amplitude  $V_1$  has built up to a value such that the electronic conductance curve intersects the horizontal line representing the load conductance,  $G_L$ .  $G_{e0}$  is a function of one or more of the operating parameters such as the electron current in the vacuum tube. If we vary any one of these parameters indicated as  $X_n$  the principal effect will be to shrink the vertical ordinates as shown in Fig. 21 and the amplitude of oscillation will assume a series of stable values corresponding to the intercepts of the electronic conductance curves with the load conductance. If, as we have assumed,  $F(V)$  is a monotonically decreasing function of  $V$ , the amplitude will decrease continuously to zero as we uniformly vary the parameter in such a direction as to decrease  $G_{e0}$ . Zero amplitude will, of course, occur when the curve has shrunk to the case where  $G_{e0} = G_L$ . Under these conditions the power output,  $\frac{1}{2}G_L V^2$ , will be a single value function of the parameter as shown in Fig. 22 and no hysteresis will occur.

Suppose, however, that  $F(V)$  is not a monotonically decreasing function of  $V$  but instead has a maximum so that  $G_{e0}F(V)$  appears as shown in Fig. 23. In this case, if we start with the condition indicated by the solid line and vary our parameter  $X$  in such a direction as to shrink the curve, the amplitude will decrease smoothly until the parameter arrives at a value of  $X_5$  corresponding to amplitude  $V_5$  at which the load line is tangent to the maximum of the conductance curve. Further variation of  $X$  in the same direction will cause the amplitude to jump to zero. Upon reversing the direction of the variation of the parameter, oscillation cannot restart until  $X$  arrives at a value  $X_4$  such that the zero amplitude conductance is equal to the load conductance. When this occurs the amplitude will suddenly jump to the

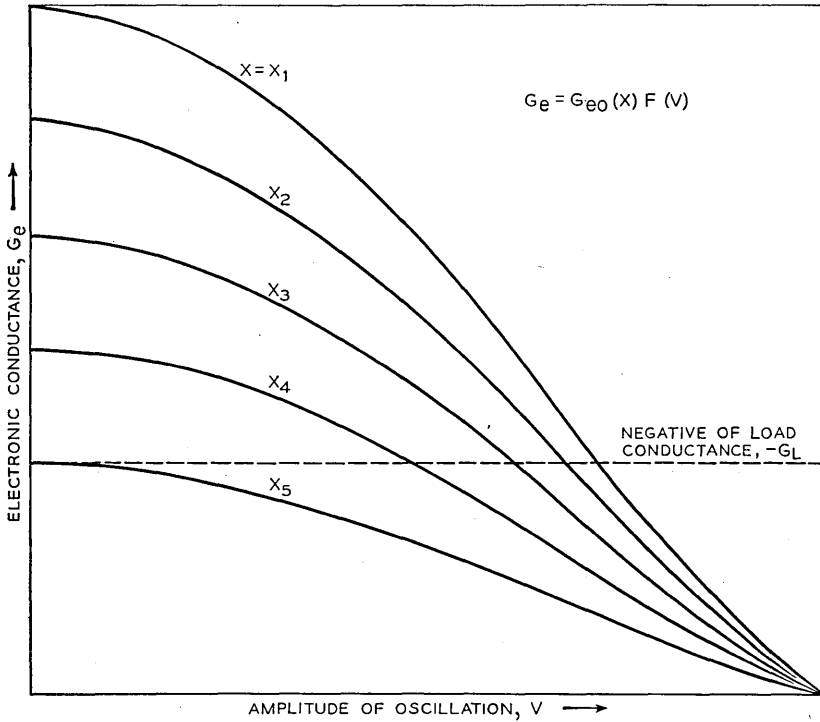


Fig. 21.—A possible variation of electronic conductance with amplitude of oscillation for the general case of an oscillator. Arbitrary units are employed. Different curves correspond to several values of a parameter  $X$  which determines the small signal values of the conductance. The load conductance is indicated by the horizontal line. Stable oscillation for any given value of the parameter  $X$  occurs at the intersection of the electronic conductance curve with the load line  $G_L$ .

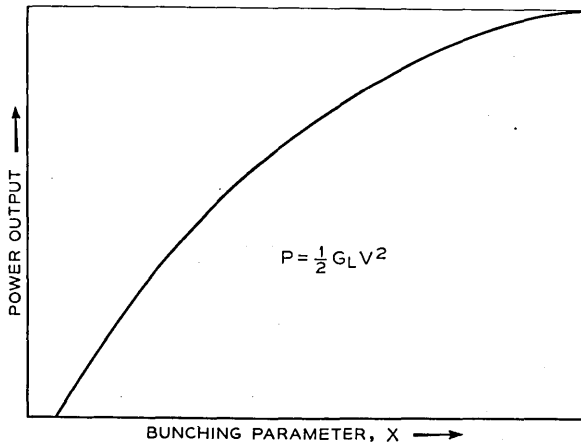


Fig. 22.—Variation of power output with the parameter  $X$  when the conditions of Fig. 21 apply.

value  $V_4$ . Under these conditions the power output will appear as shown in Fig. 24, in which the hysteresis is apparent.

Let us now consider the conditions obtaining in a reflex oscillator. Fig. 1 shows a schematic diagram of a reflex oscillator. This shows an electron gun which projects a rectilinear electron stream across the gap of a resonator.

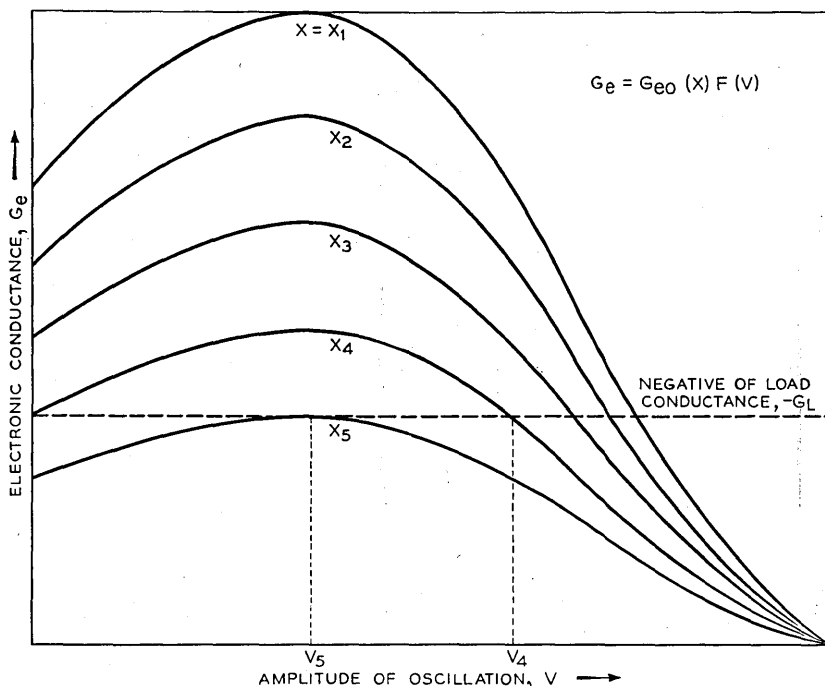


Fig. 23.—Variation of electronic conductance with amplitude of oscillation of a form which will result in hysteresis. The parameter  $X$  determines the small signal value of the conductance. The horizontal line indicates the load conductance.

After the beam passes through this gap it is retarded and returned by a uniform electrostatic field. If we carry out an analysis to determine the electronic admittance which will appear across the gap if the electrons make one round trip, we arrive at expression 2.2 which may be written

$$Y_e = \frac{I_0 \beta^2 \theta}{V_0} \frac{J_1(X)}{X} [\sin \theta + j \cos \theta] \quad (8.7)$$

where

$$X = \frac{\theta \beta V}{2V_0}$$

This admittance will be a pure conductance if  $\theta = \theta_0 = (n + \frac{3}{4}) 2\pi$ . As we have seen, in an oscillator designed specifically for electronic tuning,  $n$  usually has a value of 3 or greater and the variations  $\Delta\theta$  from  $\theta$  arising from

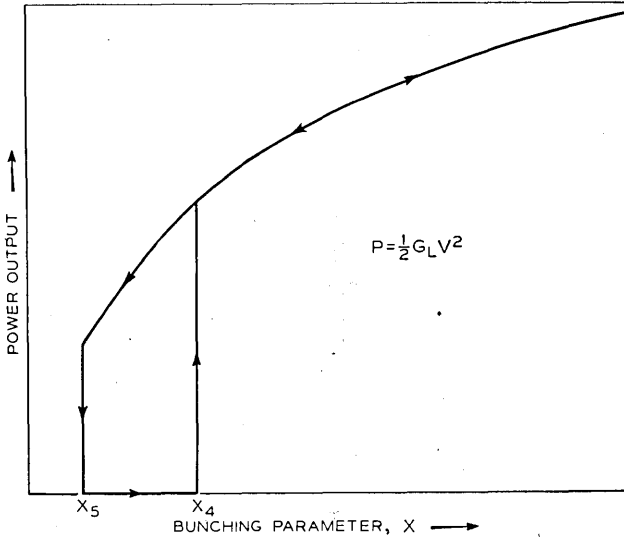


Fig. 24.—A curve of power output vs parameter  $X$  resulting from the conductance curves shown in Fig. 23 and illustrating hysteresis.

repeller voltage variation are sufficiently small so that the effect of  $\Delta\theta$  in varying  $X$  may be neglected. In this case we may write

$$G_e = -y_e \frac{2J_1(CV)}{CV} \cos \Delta\theta$$

$$y_e = \frac{i_0 \beta^2 \theta_0}{2V_0} \quad (8.8)$$

$$C = \frac{\theta_0 \beta}{2V_0}$$

The parameter which we vary in obtaining the repeller characteristic of the tube is  $\Delta\theta$ . The variation of this parameter is produced by shifting the repeller voltage  $V_R$  from the value  $V_{R0}$  corresponding to the transit angle  $\theta_0$ . Since as is shown, Fig. 25a,  $\frac{J_1(CV)}{CV}$  decreases monotonically as  $V$  increases, no explanation of hysteresis is to be found in this expression. Fig. 25b shows the smooth symmetrical variation of output with repeller voltage about the value for which  $\Delta\theta = 0$  which is to be expected.



Now suppose a second source of conductance  $G_{e2}$  exists whose amplitude function is of the form illustrated in Fig. 26a. Let us suppose that for the

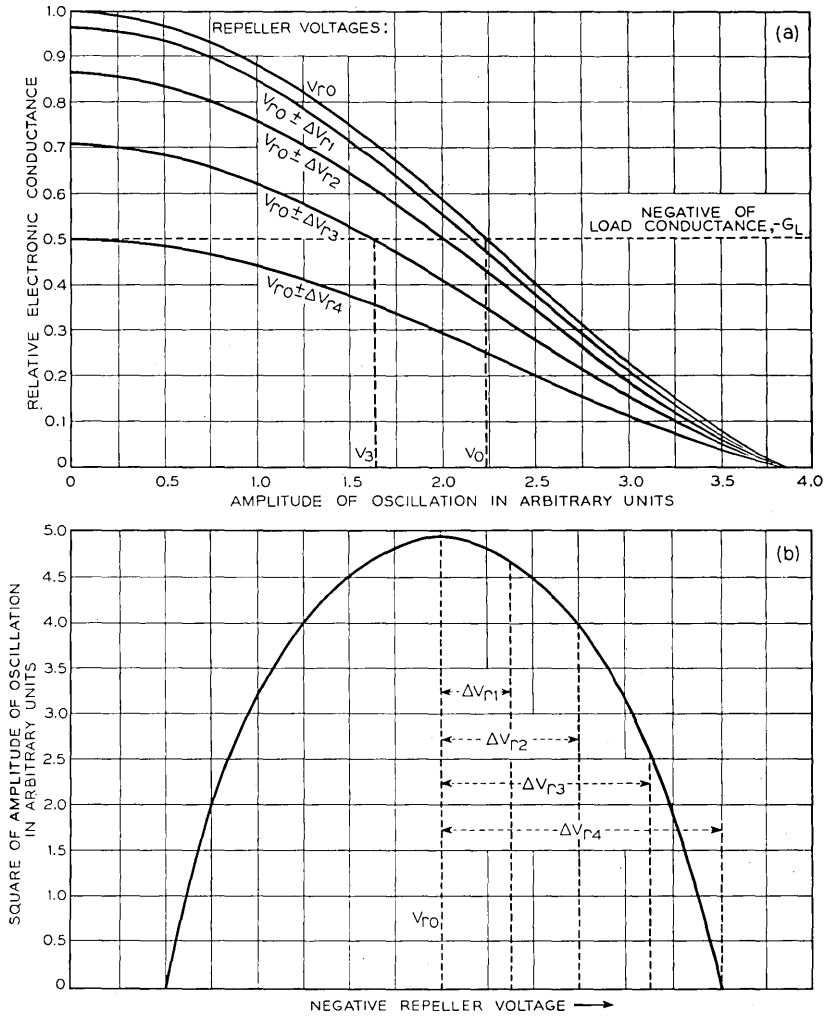


Fig. 25.—*a*. Variation of electronic conductance with amplitude of oscillation for an ideal oscillator. The parameter controlling the small signal electronic conductance is the repeller voltage which determines the transit angle in the repeller region. The horizontal line indicates the load conductance.

*b*. The variation of power output with the repeller voltage which results from the characteristics of Fig. 25*a*.

value of  $\theta_0$  assumed the phase of this conductance is such as to oppose  $G_{e1}$ ,  $G_{e2}$  may or may not be a function of  $\Delta\theta$ . For the sake of simplicity let us assume that  $G_{e2}$  varies with  $\Delta\theta$  in the same way as  $G_{e1}$ . The total conduc-

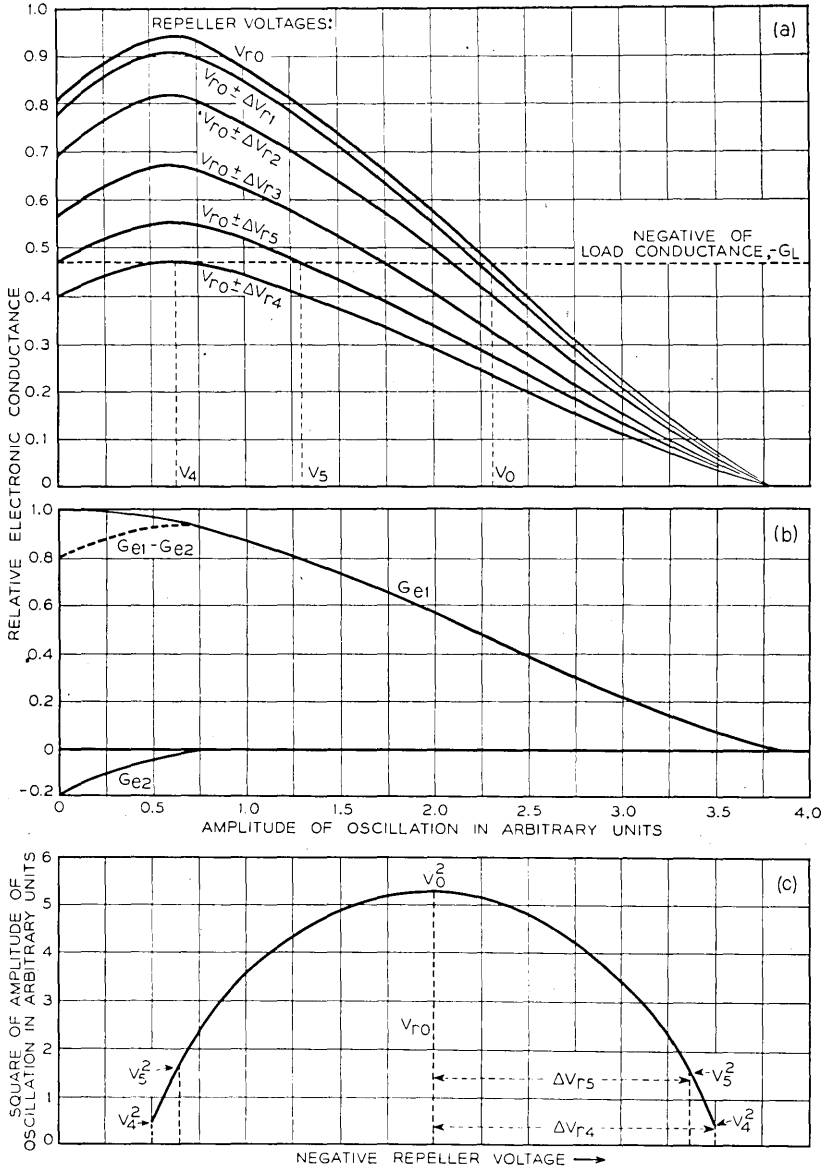


Fig. 26.—*a.* Curve  $G_{e1}$  shows the variation of electronic conductance with amplitude of oscillation for an ideal reflex oscillator. Curve  $G_{e2}$  represents the variation of a second source of electronic conductance with amplitude. The difference of these two curves indicated  $G_{e1} - G_{e2}$  shows the variation of the sum of these two conductance terms with amplitude.

*b.* Electronic conductance vs amplitude of oscillation when two conductance terms exist whose variation with repeller voltage is the same.

*c.* Power output vs repeller voltage for a reflex oscillator in which two sources of conductance occur varying with amplitude as shown in Fig. 26*b*.

tance  $G_e = G_{e1} - G_{e2}$  will appear as shown. As the repeller voltage is varied from the optimum value the conductance curve will shrink in proportion to  $\cos \Delta\theta$ , and the amplitude of oscillation for each value of  $\Delta\theta$  will adjust itself to the value corresponding to the intersection of the load line and the conductance plot as shown in Fig. 26b. When the load line becomes tangent, as for amplitude  $V_4$ , further variation of the repeller voltage in the same direction will cause oscillation to jump from  $V_4$  to zero amplitude. Correspondingly, on starting oscillation will restart with a jump to  $V_3$ . Hence, two sources of conductance varying in this way will produce conditions previously described, which would cause hysteresis as shown in Fig. 26c. The above assumptions lead to hysteresis symmetrically disposed about the optimum repeller voltage. Actually, this is rarely the case, but the explanation for this will be deferred.

Fig. 27 shows repeller characteristics for an early model of a reflex oscillator designed at the Bell Telephone Laboratories. The construction of this oscillator was essentially that of the idealized oscillator of Fig. 1 upon which the simple theory is based. However, the repeller characteristics of this oscillator depart drastically from the ideal. It will be observed that a double jump occurs in the amplitude of oscillation. The arrows indicate the direction of variation of the repeller voltage. The variation in the frequency of oscillation is shown, and it will be observed that this also is discontinuous and presents a striking feature in that the rate of change of frequency with voltage actually reverses its sign for a portion of the range. A third curve is shown which gives the calculated phase  $\Delta\theta$  of the admittance arising from drift in the repeller field. This lends very strong support to the hypothesis of the existence of a second source of conductance, since this phase varies by more than  $180^\circ$ , so that for some part of the range the repeller conductance must actually oppose oscillation. The zero value phase is arbitrary, since there is no way of determining when the total angle is  $(n + \frac{3}{4})2\pi$ .

Having recognized the circumstances which can lead to hysteresis in the reflex oscillator, the problem resolves itself into locating the second source of conductance and eliminating it.

A number of possible sources of a second conductance term were investigated in the particular case of the 1349 oscillator, and most were found to be of negligible importance. It was found that at least one important second source of conductance arose from multiple transits of the gap made by electrons returning to the cathode region. In the case of the 1349 a design of the electron optical system which insured that the electron stream made only one outgoing and one return transit of the gap eliminated the hysteresis in accordance with the hypothesis.

Inasmuch as multiple transits appear to be the most common cause for hysteresis in reflex oscillator design, it seems worthwhile to obtain a more detailed understanding of the mechanism in this case. Other possible

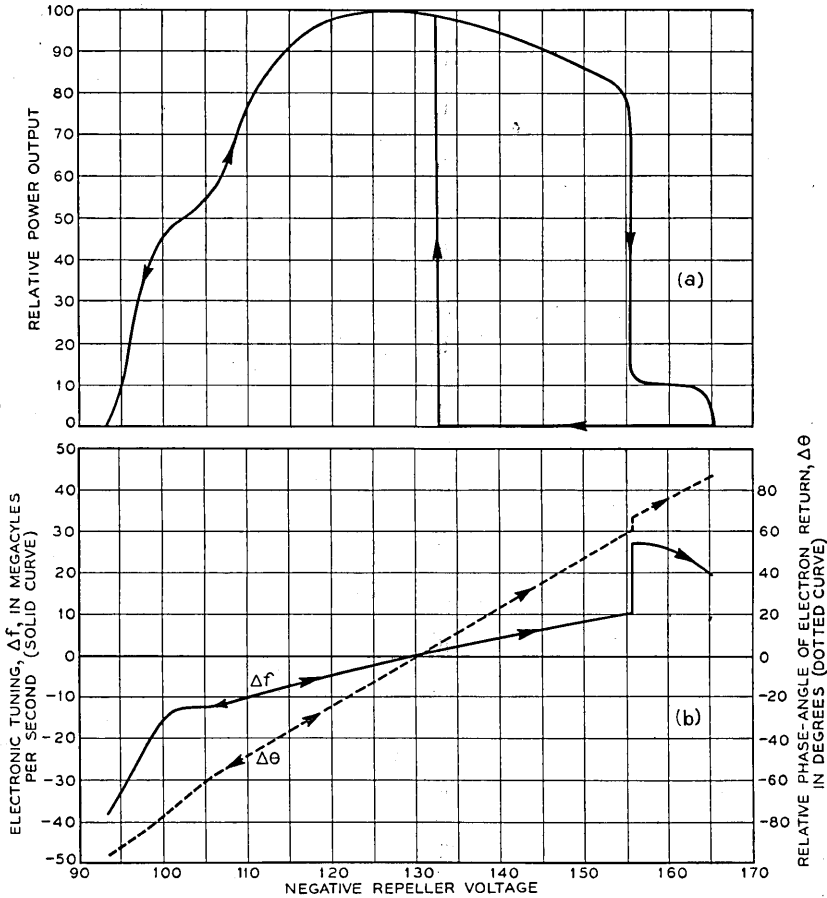


Fig. 27.—Amplitude, frequency and transit phase variation with the repeller voltage obtained experimentally for a reflex oscillator exhibiting electronic hysteresis. The arrows indicate the direction of variation of the repeller voltage.

mechanisms such as velocity sorting on the repeller will give rise to similar effects and can be understood from what follows.

In the first order theory, the electrons which have retraversed the gap are conveniently assumed to vanish. Actually, of course, the returning stream is remodulated and enters the cathode space. Unfortunately, the

conditions in the cathode region are very complex, and an exact analysis would entail an unwarranted amount of effort. However, from an approximate analysis one can obtain a very simple and adequate understanding of the processes involved.

Let us examine the conditions existing after the electrons have returned through the gap of the idealized reflex oscillator. In the absence of oscillation, with an ideal rectilinear stream and ideally fine grids all the electrons which leave the cathode will return to it. When oscillation exists all electrons which experience a net gain of energy on the two transits will be captured by the cathode, while those experiencing a net loss will not reach it, but instead will return through the gap for a third transit, etc. In a practical oscillator even in the absence of oscillation only a fraction of the electrons which leave the cathode will be able to return to the cathode, because of losses in axial velocity produced by deflections by the grid wires and various other causes. As a result, it will not be until an appreciable amplitude of oscillation has been reached that a major proportion of the electrons which have gained energy will be captured by the cathode. On the other hand, there will be an amplitude of oscillation above which no appreciable change in the number captured will occur.

The sorting action which occurs on the cathode will produce a source of electronic admittance. Another contribution may arise from space charge interaction of the returning bunched beam with the outgoing stream. A third component arises from the continued bunching resulting from the first transit of the gap. From the standpoint of this third component the reflex oscillator with multiple transits suggests the action of a cascade amplifier. The situation is greatly complicated by the nature of the drift field in the cathode space. All three mechanisms suggested above may combine to give a resultant second source. Here we will consider only the third component. Consider qualitatively what happens in the bunching action of a reflex oscillator. Over one cycle of the r.f. field, the electrons tend to bunch about the electron which on its first transit crosses the gap when the field is changing from an accelerating to a decelerating value. The group recrosses the gap in such a phase that the field extracts at least as much energy from every electron as it gave up to any electron in the group. When we consider in addition various radial deflections, we see that very few of the electrons constituting this bunch can be lost on the cathode.

Although it is an oversimplification, let us assume that we have a linear retarding field in the cathode region and also that none of the electrons are intercepted on the cathode. To this order of approximation a modified cascade bunching theory would hardly be warranted and we will consider only that the initial bunching action is continued. Under these conditions,

we can show that the admittance arising on the third transit of the gap will have the form

$$Y'_e = +I'_0 \frac{\beta^2 \theta_t}{V_0} \frac{J_1 \left( \frac{\theta_t \beta V}{2V_0} \right)}{\frac{\theta_t \beta V}{2V_0}} [\sin \theta_t + j \cos \theta_t] \quad (8.9)$$

where  $I'_0$  is the effective d.c. contributing to the third transit.  $\theta_t = \theta + \theta_c$  is the total transit angle made up of the drift angle in the repeller space,  $\theta$ , and the drift angle in the cathode space  $\theta_c$ . As before, assume that the small changes in  $\theta_t$  caused by the changing repeller voltage over the electronic tuning range exercise an appreciable effect only in changing the sine and cosine terms. Then we may write

$$Y'_e = G'_e + jB'_e = y'_e \frac{2J_1(C_2V)}{C_2V} [\sin \theta_t + j \cos \theta_t] \quad (8.10)$$

where

$$C_2 = \frac{\theta_{t0} \beta V}{2V_0}, \quad \text{and} \quad y'_e = \frac{\beta^2 I'_0 \theta_{t0}}{2V_0}.$$

If  $\Delta\theta = \theta_t - \theta_{t0}$

$$G'_e = y'_e \frac{2J_1(C_2V)}{C_2V} [\sin \theta_{t0} \cos \Delta\theta_t + \cos \theta_{t0} \sin \Delta\theta_t]. \quad (8.11)$$

Now

$$\begin{aligned} \Delta\theta &= \omega_0 \tau \frac{\Delta V_R}{V_R + V_0} + \Delta\omega \tau_0 \\ \Delta\theta_c &= \Delta\omega \tau_c \\ \Delta\theta_t &= \omega_0 \tau \frac{\Delta V_R}{V_R + V_0} + \Delta\omega \tau_0 + \Delta\omega \tau_c. \end{aligned} \quad (8.12)$$

We observe that the phase angle of the admittance arising on the third transit varies more rapidly with repeller voltage (i.e., frequency) than the phase angle of the second transit admittance. This is of considerable importance in understanding some of the features of hysteresis.

Let us consider (8.11) for some particular values of  $\theta_c$  or  $\theta_t$ . We remember that  $\theta_t$  is greater than  $\theta$  and hence  $C_2 > C_1$ . Since this is so, the limiting function  $\frac{2J_2(C_2V)}{C_2V}$  will become zero at a lower value of  $V$  than  $\frac{2J_1(C_1V)}{C_1V}$ .

We will consider two cases  $\theta_t = (n + \frac{1}{4})2\pi$  and  $\theta_t = (n + \frac{3}{4})2\pi$ . These

correspond respectively to a conductance aiding and bucking the conductance arising on the first return. In case 1 we have

$$G'_e = -y'_e \frac{2J_1(C_2 V)}{C_2 V} \cos \Delta\theta_t \quad (8.13)$$

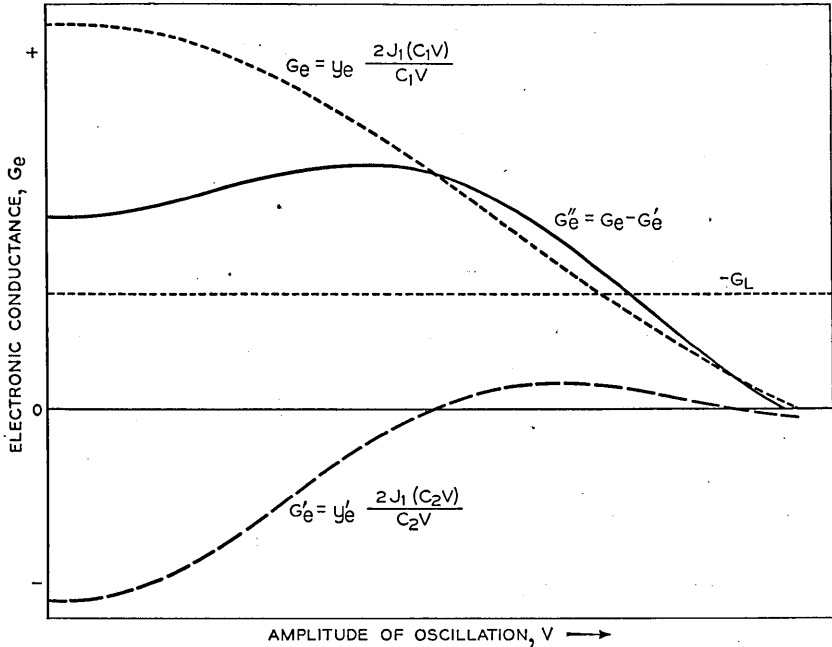


Fig. 28.—Theoretically derived variation of electronic conductance with amplitude of oscillation. Curve  $G_e$  represents conductance arising from drift action in the repeller space. Curve  $G'_e$  represents the conductance arising from continuing drift in the cathode region.  $G''_e$  represents the conductance variation with amplitude which will result if  $G_e$  and  $G'_e$  are in phase opposition.

and case 2

$$G'_e = +y'_e \frac{2J_1(C_2 V)}{C_2 V} \cos \Delta\theta_t \quad (8.14)$$

Figure 28 illustrates case (2) and Fig. 29 case (1). If  $\cos \Delta\theta_t$  and  $\cos \Delta\theta$  varied in the same way with repeller voltage, the resultant limiting function would shrink without change in form as the repeller voltage was varied, and it is apparent that Fig. 28 would then yield the conditions for hysteresis and Fig. 29 would result in conditions for a continuous characteristic. If Fig. 28 applied we should expect hysteresis symmetrical about the optimum repeller voltage. We recall, however, that in Fig. 27 hysteresis

occurred only on one end of the repeller characteristic and was absent on the other. The key to this situation lies in the fact that  $\Delta\theta_i$  and  $\Delta\theta$  do not vary in the same way when the repeller voltage is changed and the frequency shifts as shown in (8.12). As a result, the resulting limiting function does not shrink uniformly with repeller voltage, since the contribution  $G_e'$  changes more rapidly than  $G_e$ . Hence we should need a continuous series of pictures of the limiting function in order to understand the situation completely.

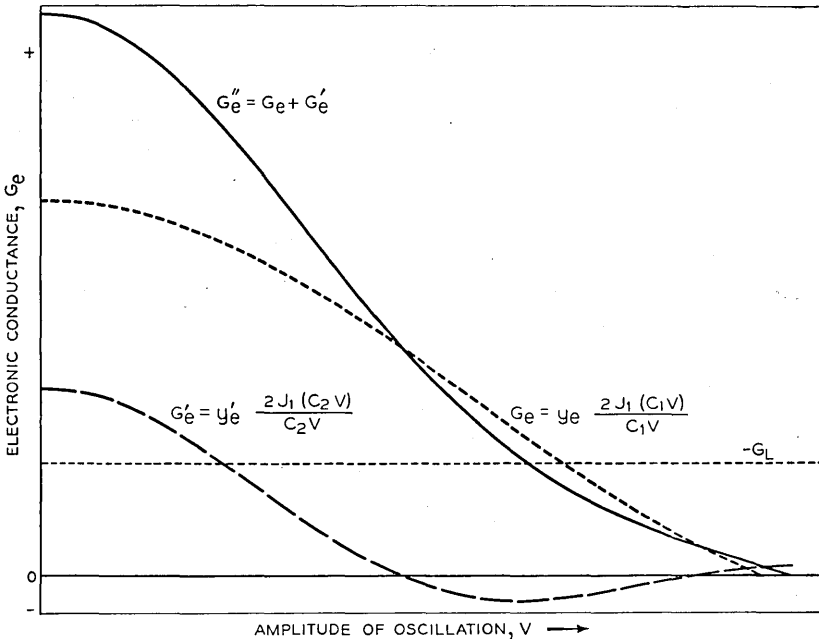


Fig. 29.—Theoretically derived curves of electronic conductance vs amplitude of oscillation. Curve  $G_e''$  shows the variation of the resultant electronic conductance when the repeller space contribution and the cathode space contribution are in phase addition.

Suppose we consider Fig. 29 and again assume in the interests of simplicity that  $\Delta\theta_i$  and  $\Delta\theta$  vary at the same rate. In this case we observe that in the region  $aa'$  the conductance varies very rapidly with amplitude. This would imply that in this region the output would tend to be independent of the repeller voltage. If we refer again to Fig. 27 we observe that the output is indeed nearly independent of the repeller voltage over a range.

We see that these facts all fit into a picture in which, because of the more rapid phase variation of  $\theta_i$  than  $\theta$  with repeller voltage, the limiting function at one end of the repeller voltage characteristic has the form of Fig. 28, accounting for the hysteresis, and at the other end has the form of Fig. 29,



accounting for the relative independence of the output on the repeller voltage.

In what has been given so far we have arrived qualitatively at an explanation for the variation of the amplitude. There remains the explanation for the behavior of the frequency. In this case we plot susceptance as a function of amplitude and, as in the case of the conductance, there will be several contributions. The primary electronic susceptance will be given by

$$B_e = y_e \frac{2J_1(CV)}{CV} \sin \theta. \quad (8.15)$$

Hence, as we vary the parameter  $\Delta\theta$  by changing the repeller voltage the susceptance curve swells as the conductance curve shrinks. The circuit condition for stable oscillation is that

$$B_e + 2j\Delta\omega C = 0. \quad (8.16)$$

A second source of susceptance will arise from the continuing drift in the cathode space. Referring to equation (8.10) we see that this will have the form

$$B'_e = y'_e \frac{2J_1(C_2 V)}{C_2 V} \cos \theta_t \quad (8.17)$$

and corresponding to equation (8.11) we write

$$B'_e = y'_e \frac{2J_1(C_2 V)}{C_2 V} [\cos \theta_{t0} \cos \Delta\theta_t - \sin \theta_{t0} \sin \Delta\theta_t]. \quad (8.18)$$

Consider the functions given by (8.18) for values of  $\theta_t = (n + \frac{1}{4})2\pi$  and  $(n + \frac{3}{4})2\pi$  as functions of  $V$ . These are the extreme values which we considered in the case of the conductance. The ordinates of these curves give the frequency shift as a function of the amplitude.

In case 1 we have

$$B'_e = -y'_e \frac{2J_1(C_2 V)}{C_2 V} \sin \Delta\theta_t \quad (8.19)$$

and case 2

$$B'_e = y'_e \frac{2J_1(C_2 V)}{C_2 V} \sin \Delta\theta_t. \quad (8.20)$$

The total susceptance will be the sum of the susceptance appearing across the gap as a result of the drift in the repeller space and the susceptance which appears across the gap as a result of the cascaded drift action in the repeller region and the cathode region. If  $\sin \Delta\theta_t$  and  $\sin \Delta\theta$  varied in the same way with the repeller voltage, the total susceptance would expand

or contract without change in form as the repeller voltage was varied. In Figs. 30 and 31 a family of susceptance curves are shown corresponding respectively to cases 1 and 2 above for various values of  $\Delta\theta_t$ , assuming that  $\Delta\theta_t$  and  $\Delta\theta$  vary in the same way with the repeller voltage. As the

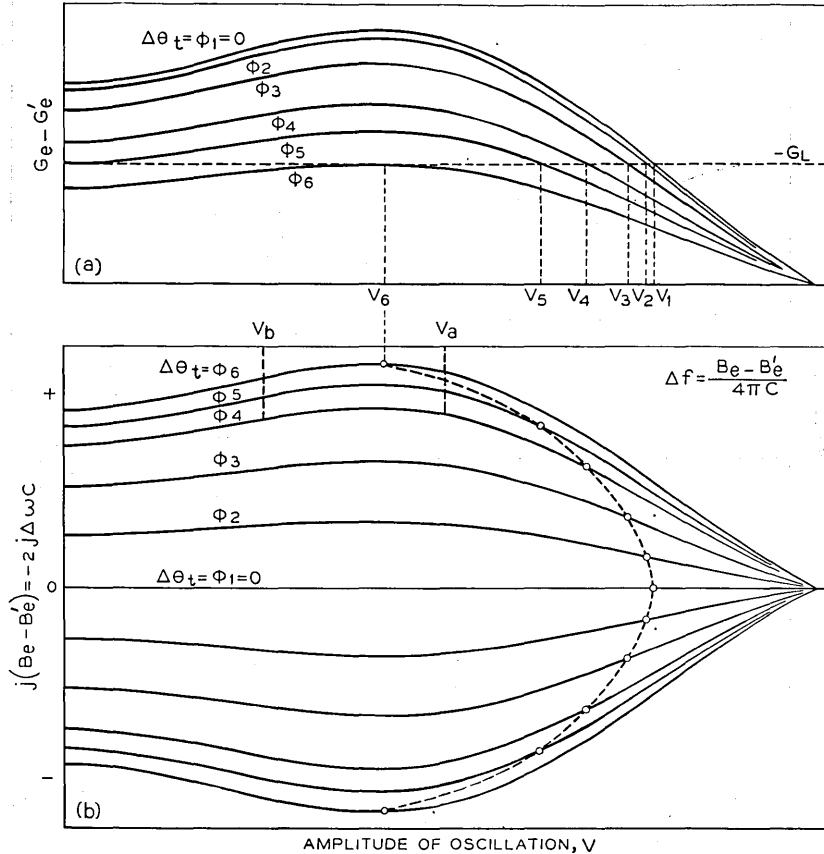


Fig. 30.—*a*. Theoretical variation of electronic conductance vs amplitude of oscillation in the case in which two components are in phase opposition. The parameter is the repeller transit phase. It is assumed that the two contributions have the same variation with this phase.

*b*. Susceptance component of electronic admittance as a function of amplitude for the case of phase opposition given in Fig. 30*a*. The parameter is the repeller phase. The dashed line shows the variation of amplitude with the susceptance shift.

repeller voltage is varied the amplitude of oscillation will be determined by the conductance limiting function. In the case of the susceptance we cannot determine the frequency from the intersection of the curve with a load line. The frequency of oscillation will be determined by the drift angle and the amplitude of oscillation. The amplitude variation with

angle may be obtained from Fig. 30a, which gives the conductance family. This gives the frequency variation with angle indicated by the curve con-

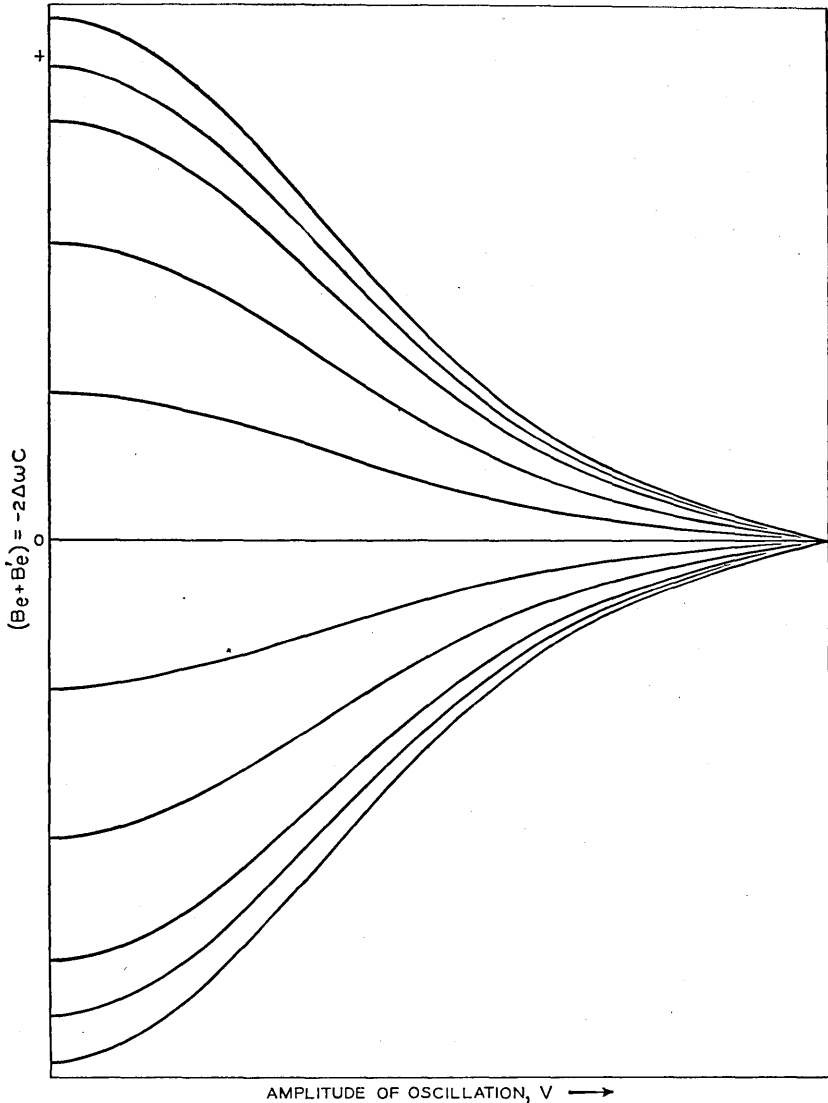


Fig. 31.—Theoretical variation of the susceptance components of electronic admittance vs amplitude of oscillation for the case in which two components of electronic susceptance are in phase addition.

necting the dots of Fig. 30b. On the assumption that  $\Delta\theta_i$  and  $\Delta\theta$  vary at the same rate with repeller voltage a symmetrical variation about  $\Delta\theta = 0$  will occur as shown in Fig. 30b. However, from the arguments used con-

cerning the conductance the actual case would involve a transition from the situation of Fig. 30b to that of Fig. 31. If a discontinuity in amplitude occurs in which the amplitude does not go to zero, it will be accompanied by a discontinuity in frequency, since the discontinuity in amplitude in general will cause a discontinuity in the susceptance. If this discontinuity in susceptance occurs between values of the amplitude such as  $V_a$  and  $V_b$  of Fig. 30, we observe that the direction of the frequency jump may be opposite to the previous variation. We also observe that if the rate of change of susceptance with amplitude is greater than the rate of change of susceptance with  $\Delta\theta$ , then in regions such as that lying between zero amplitude of  $V_b$  the rate of change of frequency with  $\Delta\theta$  may reverse its direction.

One can see that because of the longer drift time contributing to the third transit the conductance arising on the third transit may be of the same order as that arising on the second transit. In oscillators in which several repeller modes, i.e., various numbers of drift angles, may be displayed, one finds that the hysteresis is most serious for the modes with the fewest cycles of drift in the repeller space. One might expect this, since for these modes the contribution from the cathode space is relatively more important.

Some final general remarks will be made concerning hysteresis. One thing is obvious from what has been said. With the admittance conditions as depicted, if all the electronic operating conditions are fixed and the load is varied hysteresis with load can exist. This was found to be true experimentally, and in the case of oscillators working into terminated long lines it can produce disastrous effects. Where hysteresis is severe enough, it will be found that what we have chosen to call the sink margin will be much less than the theoretically expected value. An illustration of this is given in Fig. 109.

The explanation which we have given for the hysteresis in the reflex oscillator depends upon the existence of two sources of conductance. This was apparently a correct assumption in the case studied, since the elimination of the second source also eliminated the hysteresis. It is possible, however, to obtain hysteresis in a reflex oscillator with only a single source. This can occur if the phase of the electronic admittance is not independent of the amplitude. Normally, in adjusting the repeller voltage the value is chosen for the condition of maximum output. This means that the drift angle is set to a value to give maximum conductance for large amplitude. If the drift angle is then a function of the amplitude, this will mean that for small amplitude it will no longer be optimum. Thus, although the limiting function  $\frac{J_1(CV)}{CV}$  tends to increase the electronic conductance as the amplitude declines, the phase factor will oppose this increase. If the phase factor depended sufficiently strongly on the amplitude, the decrease in  $G_e$  caused by

the phase might outweigh the increase due to the function  $\frac{J_1(C_1V)}{C_1V}$ . As a result the conductance might have a maximum value for an amplitude greater than zero, leading to the conditions shown in Fig. 23, under which hysteresis can exist.

The first order theory for the reflex oscillator does not predict such an effect, since the phase is independent of amplitude. The second order theory gives the admittance as

$$Y_e = \frac{\beta_2 I_0 \theta}{2V_0} \cdot \frac{2J_1(X)}{X} e^{-j(\theta - (\pi/2))} \left( 1 - \frac{1}{4\theta^2} \left[ \frac{1}{2} X^2 (X^2 + 1) - X^3 \frac{J_0(X)}{X} - \frac{j}{2\theta} (2 - X^2) - X \frac{J_0(X)}{J_1(X)} \right] \right) \quad (8.21)$$

The quantity appearing outside the brackets is the admittance given by the first order theory. The second order correction contains real and imaginary parts which are functions of  $X$  and hence of the amplitude of oscillation. Thus, for fixed d-c conditions the admittance phase depends upon the amplitude of oscillation and hence hysteresis might occur. It should be observed that the correction terms are important only for small values of the transit angle  $\theta$ . In particular, this explanation would not suffice for the case described earlier since the design employed which eliminated the hysteresis left the variables of equation (8.21) unchanged.

#### IX. EFFECT OF LOAD

So far we have considered the reflex oscillator chiefly from the point of view of optimum performance; that is, we have attempted chiefly to evaluate its performance when it is used most advantageously. There has been some discussion of non-optimum loading, but this has been incidental to the general purpose of the work. Oscillators frequently are worked into other than optimum loads, sometimes as a result of incorrect adjustment, sometimes through mistakes in design of equipment and quite frequently by intention in order to take advantage of particular properties of the reflex oscillator when worked into specific non-optimum loads.

In this section we will consider the effects of other than optimum loads on the performance of the reflex oscillator. We may divide this discussion into two major subdivisions classified according to the type of load. The first type we call fixed element loads, and the second variable element loads. The first type is constructed of arbitrary passive elements whose constants are independent of frequency. The second category includes loads constructed of the same type of elements but connected to the oscillator by lines of sufficient length so that the frequency variation of the load admittance is appreciably modified by the line.

## A. Fixed Element Loads

In this discussion it will be assumed initially that  $\Delta\theta$ , the phase angle of  $-Y_e$ , is not affected by frequency. The results will be extended later to account for the variation of  $\Delta\theta$  with frequency. A further simplification is the use of the equivalent circuit of Fig. 118, Appendix I. Initially, the output circuit loss,  $R$ , will be taken as zero, so the admittance at the gap will be

$$Y_c = G_R + 2jM\Delta\omega/\omega + Y_L/N^2. \quad (9.1)^8$$

Here,  $G_R$  is the resonator loss conductance,  $M$  is the resonator characteristic admittance, and  $Y_L$  is the load admittance.

We will now simplify this further by letting  $G_R = 0$

$$Y_c = 2jM\Delta\omega/\omega + Y_L/N^2. \quad (9.2)$$

From Fig. 12 we see

$$G_L/N^2 = y_e[2J_1(X)/X] \cos \Delta\theta \quad (9.3)$$

$$\frac{B_L}{N^2} + \frac{2M\Delta\omega}{\omega} = -y_e[2J_1(X)/X] \sin \Delta\theta. \quad (9.4)$$

Now it is convenient to define quantities expressing power, conductance and susceptance in dimensionless form.

$$p = X^2 G_L / 2.5 N^2 y_e \quad (9.5)$$

$$G_1 = G_L / N^2 y_e \quad (9.6)$$

$$B_1 = B_L / N^2 y_e. \quad (9.7)$$

The power  $P$  produced by the electron stream and dissipated in  $G_L$  is related to  $p$

$$P = \left( \frac{2.5 I_0 V_0}{\theta} \right) p. \quad (9.8)$$

In terms of  $p$  and  $G_1$ , (9.3) can be written

$$p = (1/1.25)(2.5p/G_1)^{-\frac{1}{2}} J_1[(2.5p/G_1)^{\frac{1}{2}}] \cos \Delta\theta. \quad (9.9)$$

By dividing (9.4) by (9.3), we obtain

$$\Delta\omega/\omega_0 = (-G_L/2N^2M) \tan \Delta\theta - B_L/2N^2M \quad (9.10)$$

$$-(2M/y_e)\Delta\omega/\omega_0 = G_1 \tan \Delta\theta + B_1. \quad (9.11)$$

<sup>8</sup> To avoid confusion on the reader's part, it is perhaps well to note that we are, for the sake of generality, changing nomenclature. Hitherto we have used  $Y_L$  to denote the load at the oscillator. Actually our load as the appendix shows is usually coupled by some transformer whose equivalent transformation ratio is  $1/N^2$ , so that the admittance at the gap will be  $Y_L/N^2$ .

Equations (9.9) and (9.11) give the behavior of a reflex oscillator with zero output circuit loss as the load is changed. It is interesting to plot this behavior on a Smith chart.<sup>9</sup> Such a plot is known as a Rieke diagram or an impedance performance chart. Suppose we first make a plot for  $\Delta\theta = 0$ . This is shown in Fig. 32. Constant  $p$  contours are solid and, as

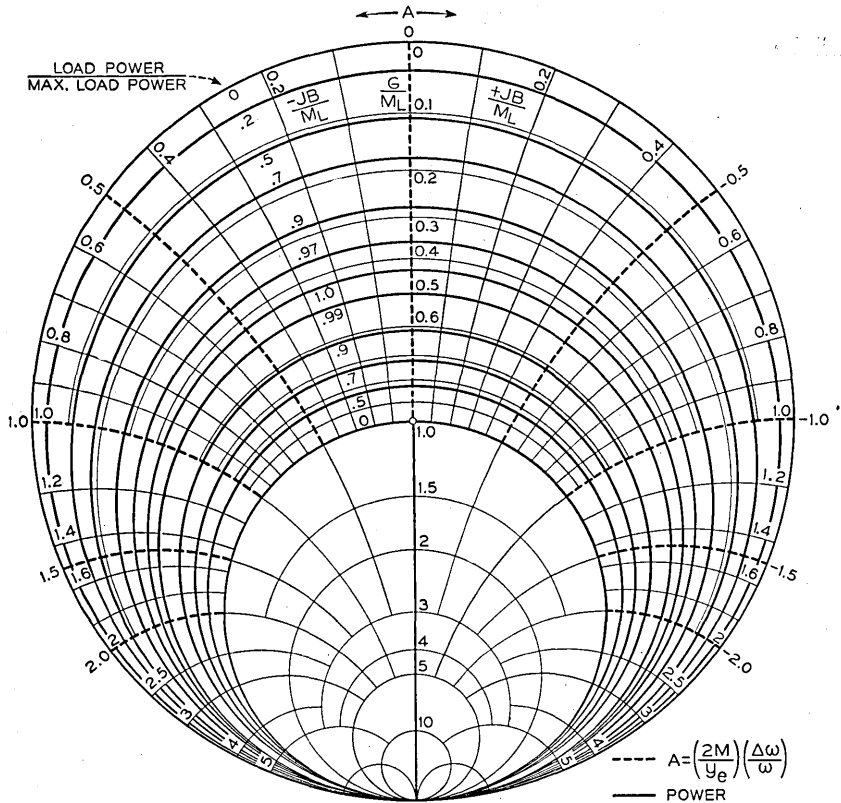


Fig. 32.—Theoretical Rieke diagram for a reflex oscillator operating with optimum drift angle. The resonator is assumed lossless. Admittances are normalized in terms of the small signal electronic admittance of the oscillator so that oscillation will stop for unity standing wave.

can be seen from the above, they will coincide with the constant conductance lines of the chart. Constant frequency curves are dashed and, for  $\Delta\theta = 0$ , they coincide with the locii of constant susceptance. The numbers on the frequency contours give values of  $(2M/y_e)(\Delta\omega/\omega_0)$ . The choice of units is such that  $G_1 = 1$  means that the load conductance is just equal to small signal electronic conductance which, it will be recalled, is the starting condition for oscillation. Hence, the  $G_1 = 1$  contour is a zero power contour. Any larger values of  $G_1$  will not permit oscillation to start, so the  $G_1$  contour

<sup>9</sup> P. H. Smith, "Transmission Line Calculator," *Electronics*, Jan. 1939, pp. 29-31.

bounds a region of zero power commonly called the "sink," since all the frequency contours converge into it. The other zero power boundary is the outer boundary of the chart,  $G_1 = 0$ , which, of course, is an open circuit load. The power contours on this chart occur in pairs, except the maximum power contour which is single. These correspond to coupling greater than and less than the optimum.

The value of  $G_1$  for any given power contour for  $\Delta\theta = 0$  may be determined by referring to Fig. 9. We are assuming no resonator loss so we use the curve for which  $G_R/y_e = 0$ . From (9.5), if  $p = 1$  we have  $G_L/N^2y_e = 2.5/X^2$  which, substituted in (9.3), gives  $XJ_1(X) = 1.25$ . This is just the condition for maximum power output with no resonator loss. From this it can be seen that we have chosen a set of normalized coordinates. Hence, in using Fig. 9, we have  $p = H/H_m$ , where  $H_m = .394$  is the maximum generalized efficiency. Thus, for any given value of  $p$  we let  $H$  in Fig. 9 have the value  $.394p$  and determine the two values of  $G_1$  corresponding to that contour.

From Fig. 32 we can construct several other charts describing the performance of reflex oscillators under other conditions. For instance, suppose we make  $\Delta\theta$  other than zero. Such a condition commonly occurs in use either through erroneous adjustment of the repeller or through intentional use of the electronic tuning of the oscillator. We can construct a new chart for this condition using Fig. 32. Consider first the constant power contours. Suppose we consider the old contour of value  $p_n$  lying along a conductance line  $G_{1n}$ . To get a new contour, we can change the label from  $p_n$  to  $p_m = p_n \cos \Delta\theta$ , and we move the contour to a conductance line  $G_n = G_m \cos \Delta\theta$ . That this is correct can be seen by substituting these values in (9.9). Consider a given frequency contour lying along  $B_1$ . We shift each point of this contour along a constant conductance line  $G_{1n}$  an amount  $B_m = G_{1n} \tan \Delta\theta$ . It will be observed that this is satisfied (9.11). In Fig. 33 this has been done for  $\tan \Delta\theta = 1$ ,  $\cos \Delta\theta = \sqrt{2}/2$ .

Now let us consider the effect of resonator loss. Suppose we have a shunt resonator conductance  $G_R$ . Let

$$G_2 = G_R/y_e. \quad (9.12)$$

Then, if the total conductance is  $G_n$ , the fraction of the power produced which goes to the load is

$$f = (G_n - G_2)/G_n = G_1/(G_1 + G_2) \quad (9.13)$$

accordingly, we multiply each power contour label by the fraction  $f$ . Then we move all contour points along constant susceptance lines to new values

$$G_m = G_n - G_2 \quad (9.14)$$

In Fig. 34, this has been done to the contours of Fig. 32, for  $G_2 = .3$ .



The diagrams so far obtained have been based on the assumption that  $\Delta\theta$  has been held constant. To obtain such a diagram experimentally would be extremely difficult. It would require that, as the frequency changed through load pulling, and hence the total transit angle  $\theta = 2\pi f\tau$  changed, an adjustment of the repeller voltage be made to correct the change. In actual practice, Rieke diagrams for a reflex oscillator are usually made holding the

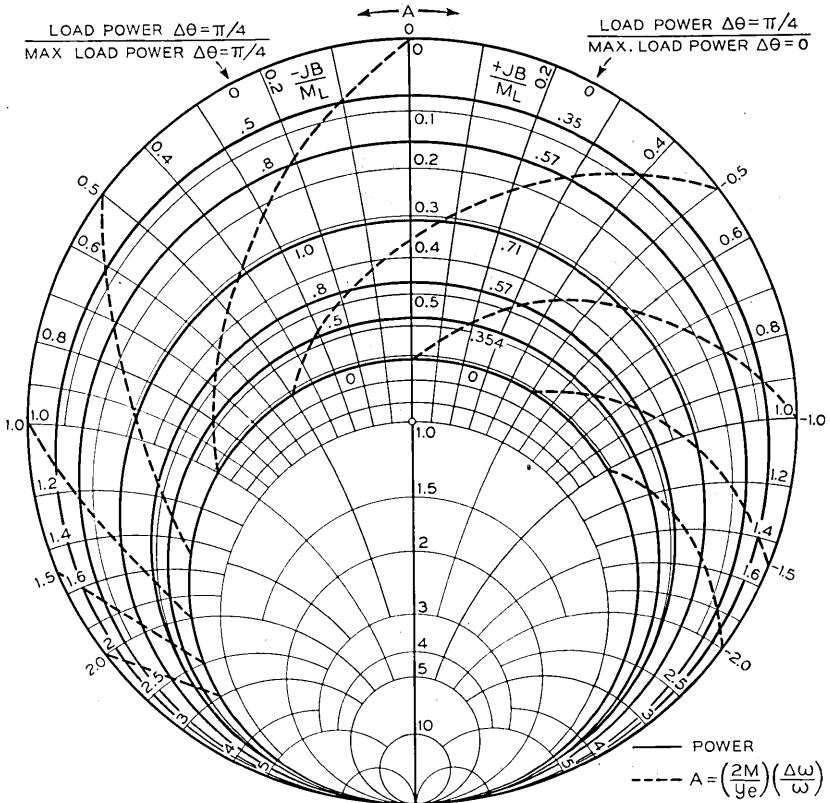


Fig. 33.—A transformation of the Rieke diagram of Fig. 32 showing the effect of shifting the drift angle away from the optimum by  $45^\circ$ .

transit time  $\tau$  constant or in other words, with fixed operating voltages. What this does to the basic diagram of Fig. 32 is not difficult to discover, provided that  $\delta\theta$  is sufficiently small so that we may ignore the variations of the Bessels functions with  $\delta\theta$ . We will first investigate the effect of fixed repeller voltage on the constant frequency contours. To do this we will rewrite (9.11), replacing  $\Delta\theta$  by  $\Delta\theta + \delta\theta$  and expand.

$$\delta\theta = \Delta\omega\tau = \frac{\Delta\omega}{\omega_0} \omega_0\tau \tag{9.15}$$

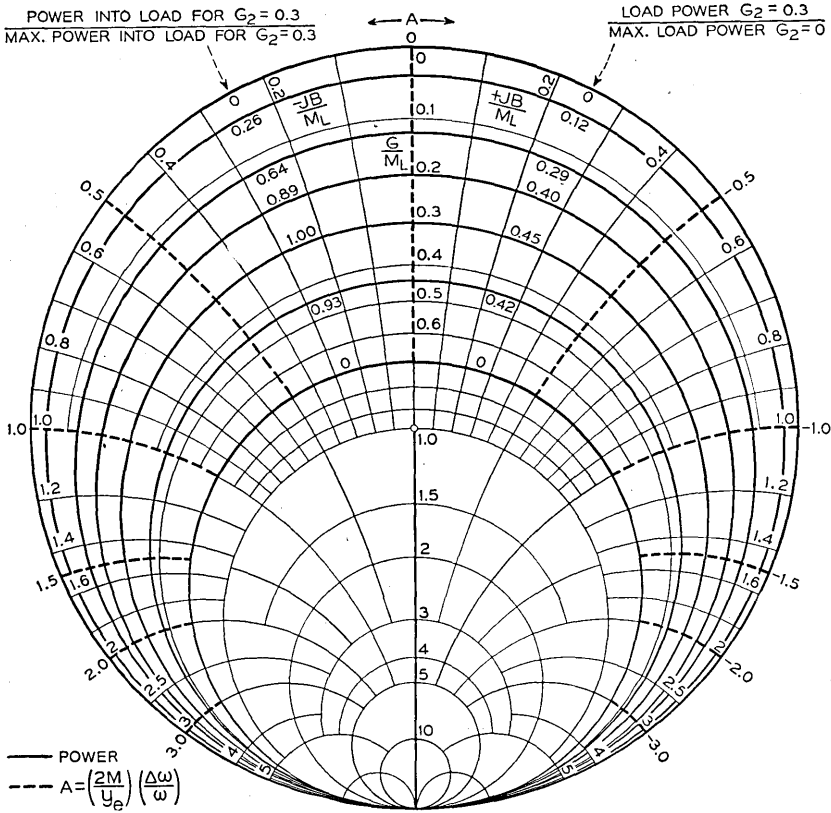


Fig. 34.—A transformation of the Rieke diagram of Fig. 32 to show the effect of the resonator loss if the phase angle is assumed to be optimum.

In rewriting (9.11) we will also replace  $G_1$  by  $G_1 + G_2$ , to take resonator loss into account. We obtain for very small values of  $\delta\theta$

$$-(2M/y_e)(\Delta\omega/\omega_0) = ((G_1 + G_2) \tan \Delta\theta + B_1)S \tag{9.16}$$

$$S = 1/(1 + (G_1 + G_2)\omega_0\tau/(2M/y_e) \cos^2 \Delta\theta)$$

$$S = 1/(1 + \omega_0\tau/2Q \cos^2 \Delta\theta). \tag{9.17}$$

$Q$  is the loaded  $Q$  of the oscillator.

To obtain the new constant frequency contours in the case of  $\Delta\theta = 0$  we shift each point of the old contour from its original position at a susceptance  $B_n$  along a constant conductance line  $G_n$  to a new susceptance line  $B_m = B_n/S$ . This neglects a second order correction. It will be observed that for small values of the conductance  $G_1$  near the outer boundary, the frequency shifts will be practically unchanged, but near the sink where the

conductance  $G_1$  is large the effect is to shift the constant frequency contours along the sink boundary away from the zero susceptance line to larger susceptance values. Hence, the constant frequency contours no longer coincide with the constant susceptance contours, not even for  $\Delta\theta = 0$ .

The change in the power contours is considerably more marked. As the frequency of the oscillator changes the transit angle is shifted from the optimum value by an amount  $\delta\theta = (\Delta\omega/\omega_0)\omega_0\tau$ . Thus the electronic conductance is reduced in magnitude by a factor  $\cos \frac{\Delta\omega}{\omega_0}\omega_0\tau$ . In particular, for the sink contour where the load conductance is just equal to the electronic conductance we see that when the repeller voltage is held constant the 0 power contour lies not on the  $G_1 = 1 - G_2$  contour but on the locus of values  $G_1 = \cos \frac{\Delta\omega}{\omega_0}\omega_0\tau - G_2$ .

In order to determine the power contours when the transit time rather than the transit angle is held constant we make use of (9.3) with addition of resonator loss. In normalized coordinates ((9.6) and (9.12)) and for a phase angle of electronic admittance  $\delta\theta$  we have

$$G_1 + G_2 = \frac{2J_1(X)}{X} \cos \delta\theta. \quad (9.18)$$

From (9.5) and (9.13) we have for the power output

$$p = \frac{G_1}{G_1 + G_2} \frac{2XJ_1(X)}{2.5} \cos \delta\theta. \quad (9.19)$$

Along any constant frequency contour  $\delta\theta$  is constant and has the value given by (9.15) in terms of  $\omega_0$  and  $\omega_0\tau$ . Hence, it will be convenient to plot  $(G_1 + G_2)$  vs  $X$  for various values of  $\delta\theta$  as a parameter. This has been done in Fig. 35. The angle  $\delta\theta$  has been specified in terms of a parameter  $A$  which appears in the Rieke diagrams as a measure of frequency deviation.

$$A = \frac{2M}{y_e} \frac{\Delta\omega}{\omega_0} \quad (9.20)$$

In terms of the parameter  $A$

$$\delta\theta = (y_e/2M)(\omega_0\tau)A. \quad (9.21)$$

Once we have the curves of Fig. 35 we can find the power for any point on the impedance performance chart. We may, for instance, choose to find the power along the constant frequency contours, for each of which  $A$  (or  $\delta\theta$ ) has certain constant values. We assume some constant resonator loss  $G_2$ . Choosing a point along the contour is merely taking a particular value of  $G_1$ . Having  $\delta\theta$ ,  $G_2$  and  $G_1$  we can obtain  $X$  from Fig. 35. Then, knowing  $X$ , we can calculate the power from (9.19).

In constructing an impedance performance chart we want constant power contours. In obtaining these it is convenient to assume a given value of  $G_2$ . We will use  $G_2 = .3$  as an example. Then we can use Fig. 35 and

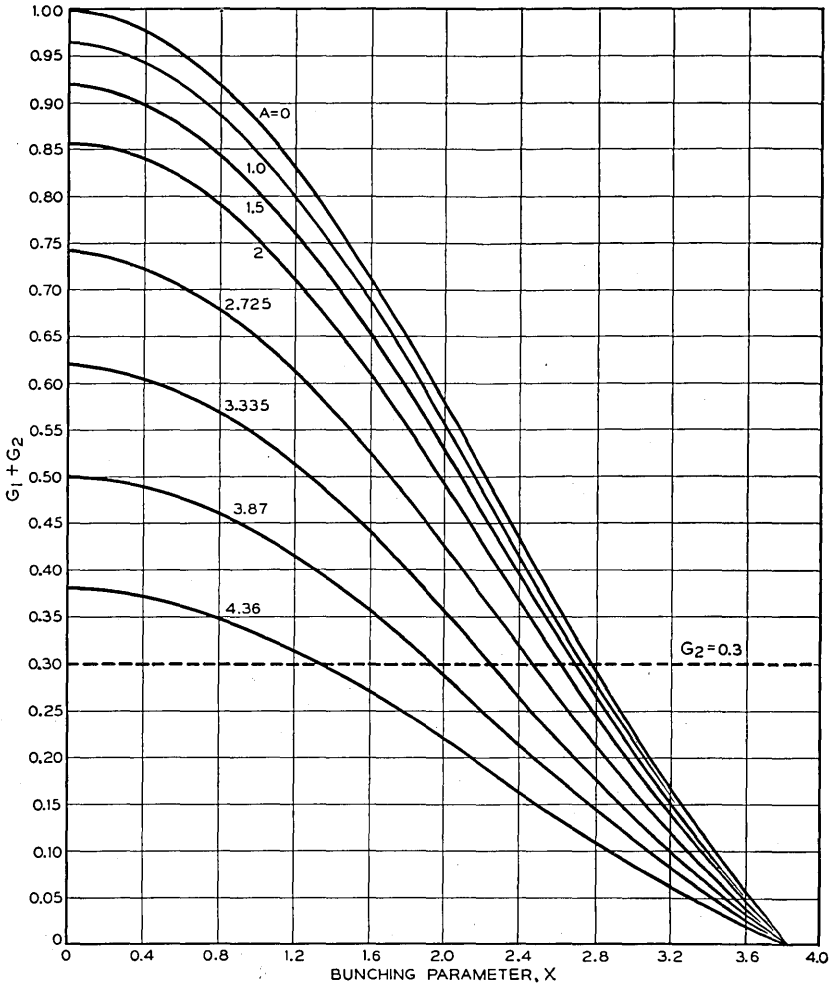


Fig. 35.—Curve of load plus loss conductance vs bunching parameter  $X$  for various values of a parameter  $A$  which gives the deviation in the drift time from the optimum time. The load and loss conductance are normalized in terms of the small signal electronic admittance. The horizontal line represents a loss conductance of  $G_2 = .3$ .

(9.19) to construct a family of curves giving  $p$  vs  $G_1$  with  $A$  (or  $\delta\theta$ ) as a parameter. In a particular case it was assumed that

$$M/y_e = 90$$

$$\omega_0\tau = 2\pi(7 + \frac{3}{4}).$$

These values are roughly those for the 2K25 reflex oscillator. Figure 36 shows  $p$  vs  $G_1$  for the particular parameters assumed above. The curves were obtained by assuming values of  $G_1$  for an appropriate  $A$  and so obtaining values of  $X$  from Fig. 35. Then the power was calculated using (9.19) and so a curve of power vs  $G_1$  for a particular value of  $A$  was constructed.

Figure 37 shows an impedance performance chart obtained from (9.16) and Fig. 36. In using Fig. 36 to obtain constant power contours, we need merely note the values of  $G_1$  at which a horizontal line on Fig. 36 intersects the curves for various values of  $A$ . Each curve either intersects such a horizontal (constant power) line at two points, or it is tangent or it does not intersect. The point of tangency represents the largest value of  $A$  at which the power can be obtained, and corresponds to the points of the crescent shaped power contours of the impedance performance chart. The maximum power contour contracts to a point.

Along the boundary of the sink, for which  $p = 0$ ,  $X = 0$  and we have from (9.18)

$$G_1 = \cos \delta\theta - G_2. \quad (9.22)$$

The results which we have obtained can be extended to include the case in which  $\Delta\theta \neq 0$ . Further, as we know from Appendix I, we can take into account losses in the output circuit by assuming a resistance in series with the load. In a well-designed reflex oscillator the output circuit has little loss. The chief effect of this small loss is to round off the points of the constant power contours.

In actually measuring the performance of an oscillator, output and frequency are plotted vs load impedance as referred to the characteristic impedance of the output line. Also, frequently the coupling is adjusted so that for a match (the center of the Smith chart) optimum power is obtained. We can transform our impedance performance chart to correspond to such a plot by shifting each point  $G$ ,  $B$  on a contour to a new point

$$G_1 = G/G_{\max}$$

$$B_1 = B/G_{\max}$$

where  $G_{\max}$  is the conductance for which maximum power is obtained. Such a transformation of Fig. 37 is shown in Fig. 38.

It will be noted in Fig. 38 that the standing wave ratio for 0 power, the sink margin, is about 2.3. This sink margin is nearly independent of the resonator loss for oscillators loaded to give maximum power at unity standing wave ratio, as has been discussed and illustrated in Fig. 10. If the sink margin must be increased or the pulling figure must be decreased<sup>10</sup> the coup-

<sup>10</sup> The pulling figure is arbitrarily defined as the maximum frequency excursion produced when a voltage standing wave ratio of  $\sqrt{2}$  is presented to the oscillator and the phase is varied through  $180^\circ$ .

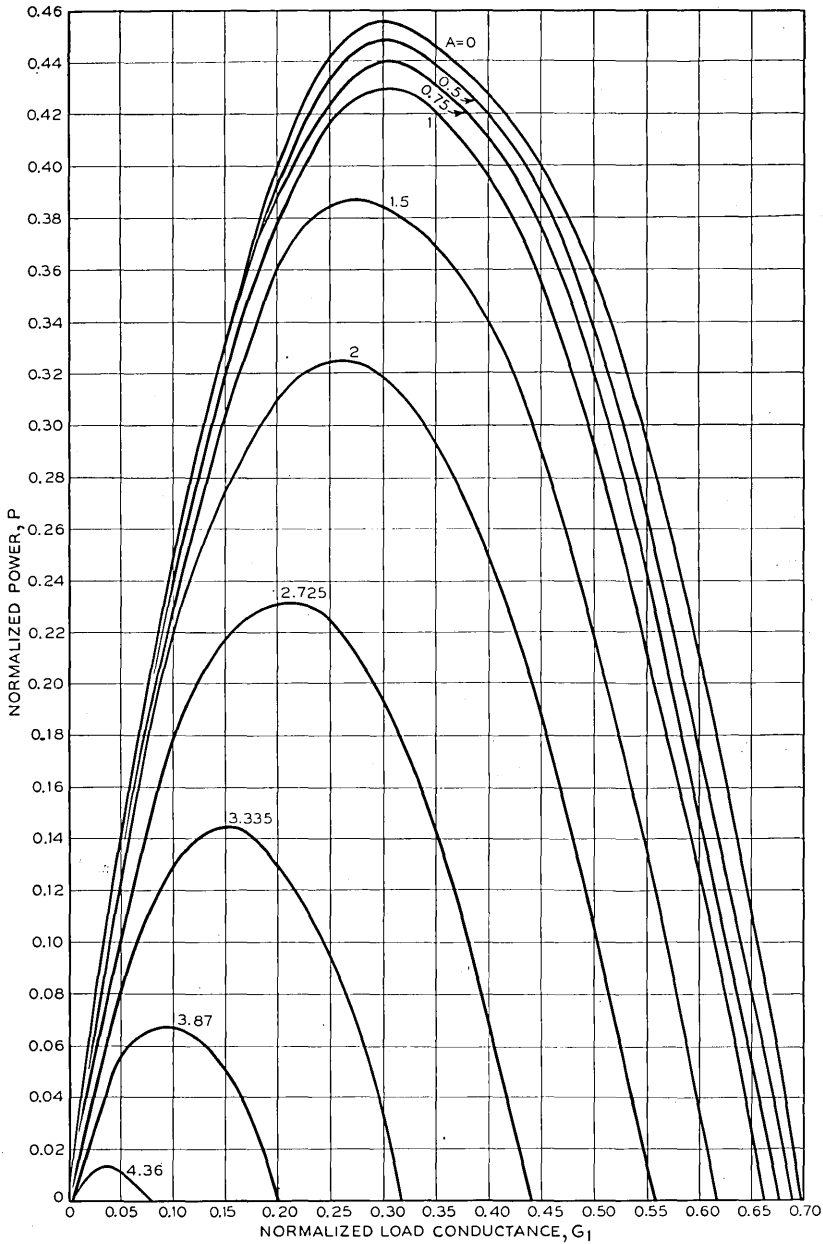


Fig. 36.—Normalized power vs normalized load conductance for various values of the parameter  $A$  which gives the deviation in drift time from the optimum drift time. These curves are computed for the case  $G_2 = .3$ . Optimum drift angle equal to  $15.5 \pi$  radians and a ratio of characteristics resonator admittance to small signal electronic admittance of 90 is assumed.

ling can be reduced so that for unity standing wave ratio the load conductance appearing at the gap is less than that for optimum power.

Finally, in making measurements the load impedance is usually evaluated at a point several wavelengths away from the resonator. If performance is plotted in terms of impedances so specified, the points on the contours of

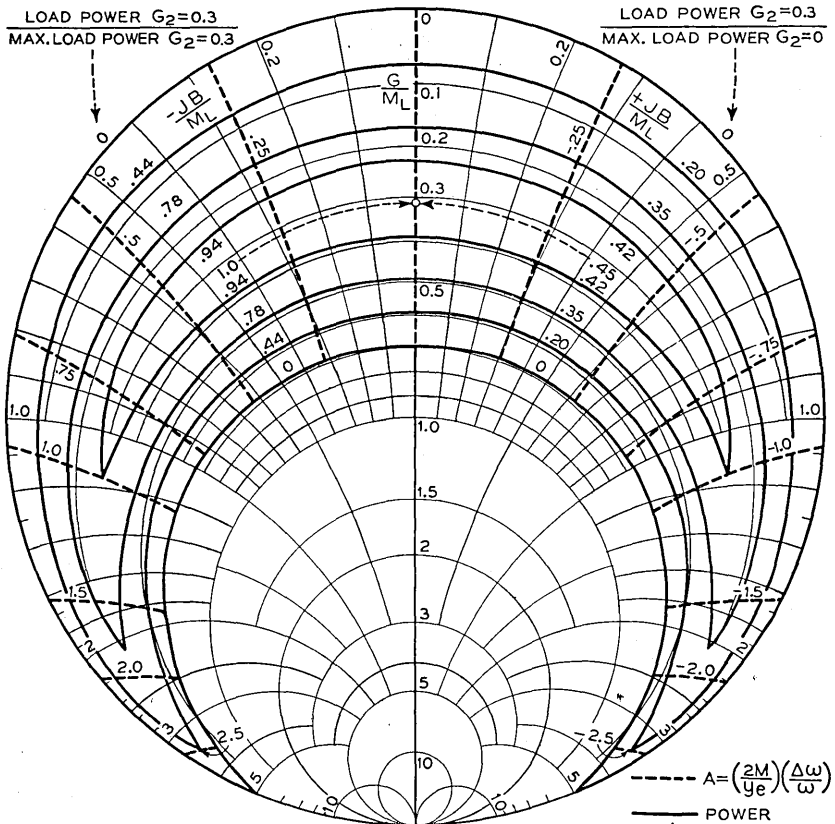


Fig. 37.—A Rieke diagram for a reflex oscillator having a lossy resonator, taking into account the variation of drift angle with frequency pulling. This results in closed power contours.

Fig. 38 appear rotated about the center. As the line length in wavelengths will be different for different frequencies, points on different frequency contours will be rotated by different amounts. This can cause the contours to overlap in the region corresponding to the zero admittance region of Fig. 38. With very long lines, the contours may overlap over a considerable region. The multiple modes of oscillation which then occur are discussed in somewhat different terms in the following section.

Figure 39 shows the performance chart of Fig. 38 as it would appear with the impedances evaluated at a point 5 wavelengths away from the resonator. Figure 71 of Section XIII shows an impedance performance chart for 2K25 reflex oscillator.

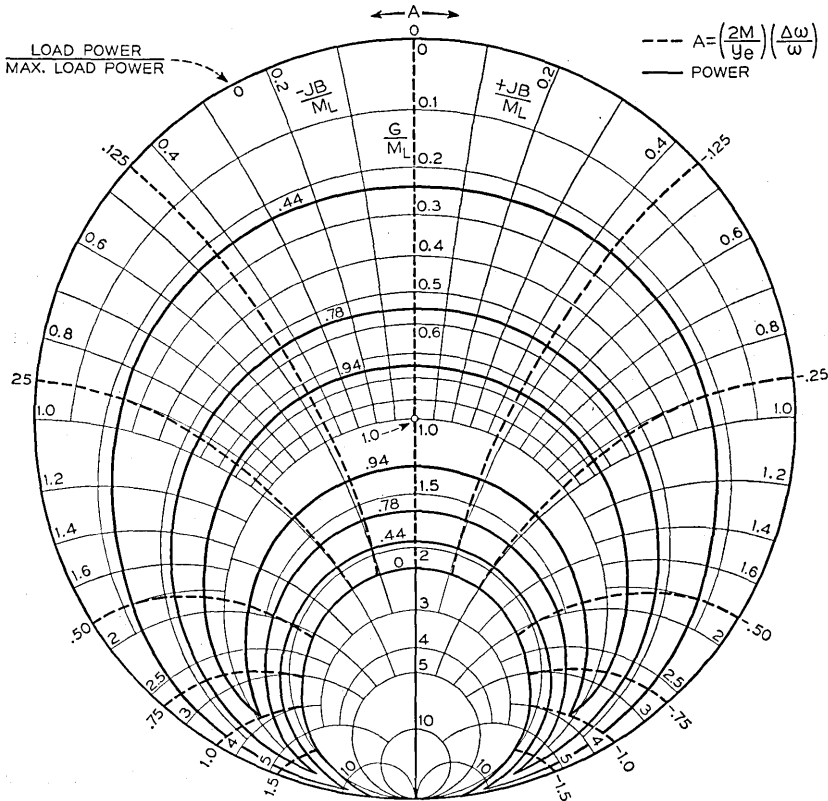


Fig. 38.—The Rieke diagram of Fig. 37 transformed to apply to the oscillator loaded for optimum power at unity standing wave.

### B. Frequency—Sensitive Loads—Long Line Effect

When the load presented to a reflex oscillator consists of a long line mismatched at the far end, or contains a resonant element, the operation of a reflex oscillator, and especially its electronic tuning, may be very seriously affected.

For instance, consider the simple circuit shown in Fig. 40. Here  $M_R$  is the characteristic admittance of the reflex oscillator resonator as seen from the output line or wave guide and  $M_L$  is the characteristic impedance of a line load  $\ell$  long, so terminated as to give a standing wave ratio,  $\sigma$ .



In the simple circuit assumed there are essentially three variables; (1) the ratio of the characteristic admittance of the resonant circuit,  $M_R$  to

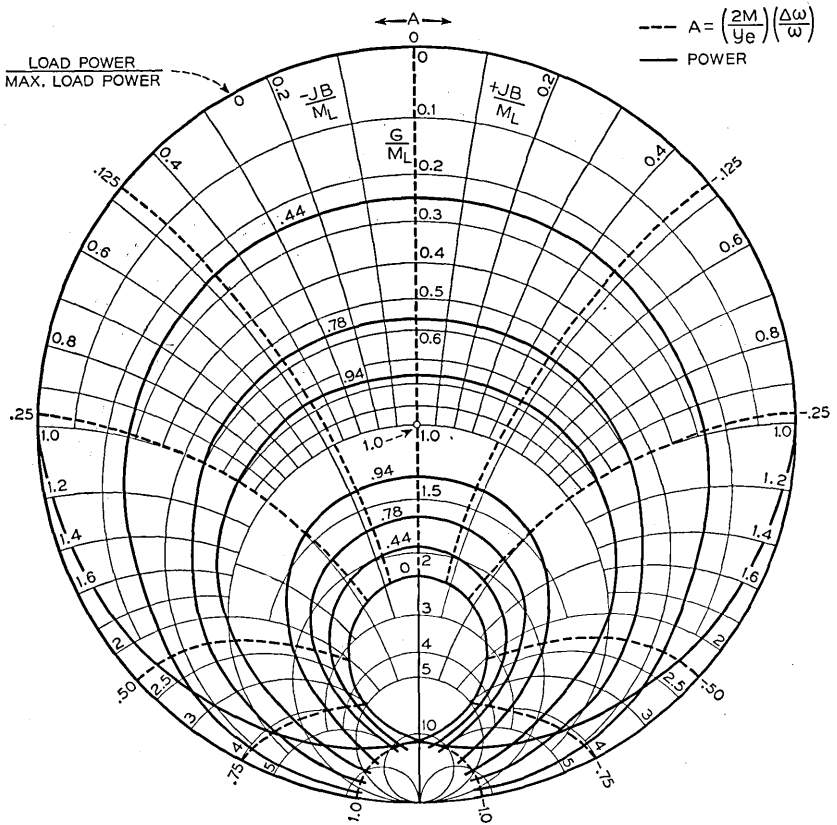


Fig. 39.—The Rieke diagram of Fig. 38 transformed to include the effect of a line five wave lengths long between the load and the oscillator.

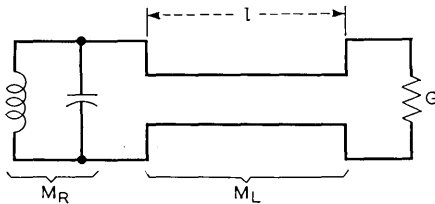


Fig. 40.—Equivalent circuit of a lossless resonator, a line and a mismatched load. that of the line,  $M_L$ . This ratio will be called the external  $Q$  and signified by  $Q_E$

$$Q_E = M_R / M_L. \tag{9.23}$$

For a lossless resonator and unity standing wave ratio, the loaded  $Q$  is equal to  $Q_E$ . For a resonator of unloaded  $Q$ ,  $Q_0$ , and for unity standing wave ratio, the loaded  $Q$ , obeys the relation

$$1/Q = 1/Q_E + 1/Q_0 \quad (9.24)$$

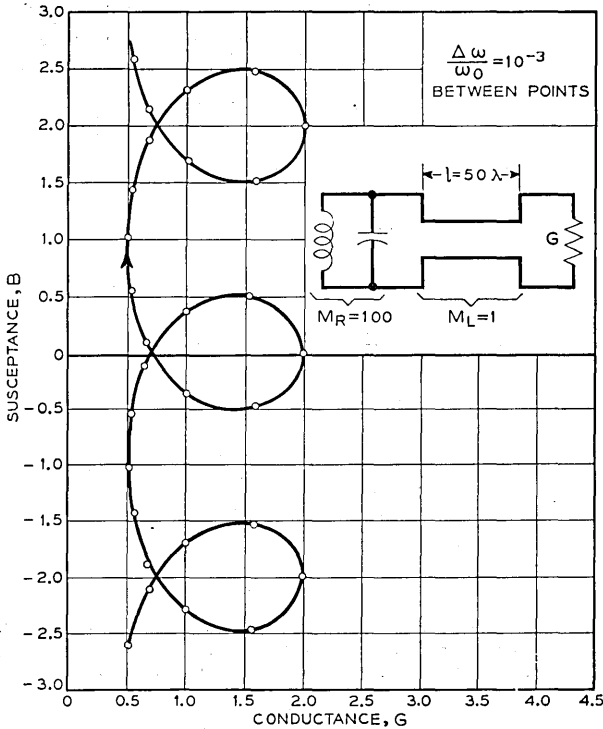


Fig. 41.—Susceptance vs conductance for a resonator coupled to a 50 wave length line terminated by a load having a standing wave ratio of 2. Characteristic admittance of the resonator is assumed to be equal to 100 in terms of a line characteristic admittance of unity. The circles mark off relative frequency increments

$$\frac{\Delta \omega}{\omega_0} = 10^{-3},$$

where  $\omega_0$  is the frequency of resonance.

(2) the length of the line called  $\theta$  when measured in radians or  $n$  when measured in wavelengths, (3) the standing wave ratio  $\sigma$ .

Figures 41 and 42 show admittance plots for two resonant circuits loaded by mismatched lines of different lengths. The feature to be observed is the loops, which are such that at certain points the same admittance is achieved at two different frequencies. It is obvious that a line representing  $-Y_e$

may cut such a curve at more than one point: thus, oscillation at more than one frequency is possible. Actually, there may be three intersections per loop. The two of these for which the susceptance  $B$  is increasing with frequency represent stable oscillation; the intersection at which  $B$  is decreasing with frequency represents an unstable condition.

The loops are of course due to reactance changes associated with variation of the electrical length of the line with frequency. Slight changes in tuning of the circuit or slight changes in the length of the line shift the loops up or down, parallel to the susceptance axis. Thus, whether the electronic admittance line actually cuts a loop, giving two possible oscillating frequencies, may depend on the exact length of the line as well as on the ex-

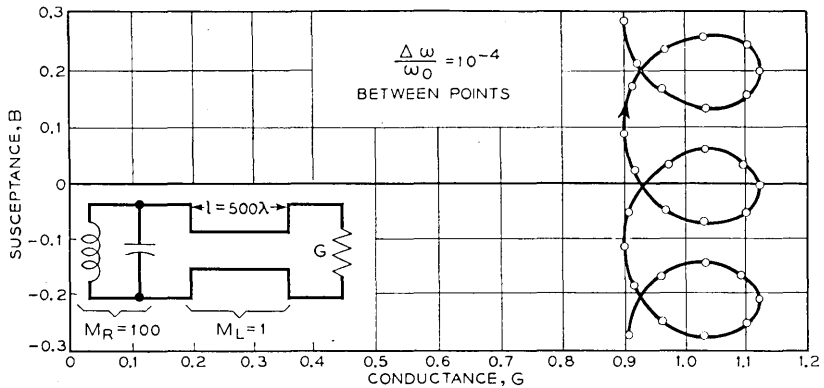


Fig. 42.—Susceptance vs conductance for line 500 wave lengths long terminated by a load having a standing wave ratio of 1.11. Circles mark off relative frequency increments of  $10^{-4}$ . Characteristic admittance to the resonator equals 100.

istence of loops. The frequency difference between loops is such as to change the electrical length of the line by one-half wavelength.

The existence or absence of loops and their size depend on all three parameters. Things which promote loops are:

Low ratio of  $M_R/M_L$  or  $Q_E$

Large  $n$  or  $\theta$

High  $\sigma$

As any parameter is changed so as to promote the existence of loops, the  $Y$  curve first has merely a slight periodic variation from the straight line for a resistively loaded circuit. Further change leads to a critical condition in which the curve has cusps at which the rate of change of admittance with frequency is zero. If the electronic admittance line passes through a cusp,

the frequency of oscillation changes infinitely rapidly with load. Still further change results in the formation of loops. Further change results in expansion of loops so that they overlap, giving more than three intersections with the electronic admittance line.

Loops may exist for very low standing wave ratios if the line is sufficiently long. Admittance plots for low standing wave ratio are very nearly cycloidal in shape; those for higher standing wave ratios are similar to cycloids in appearance but actually depart considerably from cycloids in exact form.

By combining the expression for the near resonance admittance of a tuned circuit with the transmission line equation for admittances, the expression for these admittance curves is obtained. Assuming the termination to be an admittance  $Y_T$  which at frequency  $\omega_0$  is  $\theta_0$  radians from the resonator,

$$Y = j2M_R\Delta\omega/\omega_0 + M_L \frac{(Y_T/M_L) + j \tan \theta_0(1 + \Delta\omega/\omega_0)}{1 + j(Y_T/M_L) \tan \theta_0(1 + \Delta\omega/\omega_0)}. \quad (9.25)$$

The critical relation of parameters for which a cusp is formed is important, for it divides conditions for which oscillation is possible at one frequency only and those for which oscillation is possible at two frequencies. This cusp corresponds to a condition in which the rate of change with frequency of admittance of the mismatched line is equal and opposite to that of the circuit. This may be obtained by letting  $Y_T$  be real.

$$Y_T/M_L > 1, \quad \theta_0 = n\pi \text{ where } n \text{ is an integer.}$$

The standing wave ratio is then

$$\sigma = Y_T/M_L. \quad (9.26)$$

The second term on the right of (9.25) is then

$$Y_2 = M_L \left( \frac{\sigma + j \tan \theta_0 \Delta\omega/\omega_0}{1 + j\sigma \tan \theta_0 \Delta\omega/\omega_0} \right). \quad (9.27)$$

For very small values of  $\Delta\omega$  we see that very nearly

$$Y_2 = M_L[\sigma - j(\sigma^2 - 1)\theta_0\Delta\omega/\omega_0]. \quad (9.28)$$

Thus for the rate of change of total admittance to be zero

$$\begin{aligned} 2M_R &= M_L(\sigma^2 - 1)\theta_0 \\ \theta_0 &= 2(M_R/M_L)(\sigma^2 - 1) \\ &= 2Q_E/(\sigma^2 - 1). \end{aligned} \quad (9.30)$$

Thus, the condition for no loops, and hence, for a single oscillating frequency, may be expressed

$$\theta_0 < 2Q_E/(\sigma^2 - 1) \quad (9.31)$$

or

$$\sigma < \sqrt{1 + 2Q_E/\theta_0}.$$

We will remember that  $\theta_0$  is the length of line in radians,  $\sigma$  is the standing wave ratio, measured as greater than unity, and  $Q_E$  is the external  $Q$  of the resonator for unity standing wave ratio.

Replacing a given length of line by the same length of wave guide, we find that the phase angle of the reflection changes more rapidly with frequency, and instead of (9.31) we have the condition for no loops as

$$\begin{aligned} \theta &< 2Q_E(1 - (\lambda/\lambda_0)^2)/(\sigma^2 - 1) \\ \sigma &< \sqrt{1 + 2Q_E(1 - (\lambda/\lambda_0)^2)/\theta_0}. \end{aligned} \quad (9.32)$$

Here  $\lambda$  is the free space wavelength and  $\lambda_0$  is the cutoff wavelength of the guide.

Equations (9.32) are for a particular phase of standing wave, that is, for relations of  $Y_T$  and  $\theta_0$  which produce a loop symmetrical above the  $G$  axis. Loops above the  $G$  axis are slightly more looped than loops below the  $G$  axis because of the increase of  $\theta_0$  with frequency. For reasonably long lines, (9.32) applies quite accurately for formation of loops in any position; for short lines loops are of no consequence unless they are near the  $G$  axis.

An important case is that in which the resonant load is coupled to the resonator by means of a line so short that it may be considered to have a constant electrical length for all frequencies of interest. The resonant load will be assumed to be shunted with a conductance equal to the characteristic admittance of the line. As the multiple resonance of a long mismatched line resulted in formation of many loops, so in this case we would rightly suspect the possibility of a single loop.

If the resonant load is  $\frac{1}{4}$ ,  $\frac{3}{4}$ , etc. wavelengths from the resonator, and both resonate at the same frequency, a loop is formed symmetrical about the  $G$  axis. Figure 43 is an admittance curve for resonator and load placed  $\frac{1}{4}$  wavelength apart. Tuning either resonator or load moves this loop up or down.

If the distance from resonator to resonant load is varied above or below a quarter wave distance, the loop moves up or down and expands. This is illustrated by an eighth wavelength diagram for the same resonator and load as of Fig. 43 shown in Fig. 44.

When the distance from the resonator to the resonant load, including the effective length of the coupling loop, is  $\frac{1}{2}$ ,  $1$ ,  $1\frac{1}{2}$ , etc. wavelengths, for frequencies near resonance the resonant load is essentially in shunt with the resonator, and its effect is to increase the loaded  $Q$  of the resonator. An admittance curve for the case is shown in Fig. 45. In this case the loops

have moved considerably away in frequency, and expanded tremendously. There are still recrossings of the axis near the origin, however, as indicated in this case by the dashed line which represents 2 crossings, in this case about 4% in frequency above and below the middle crossing if the length of the line  $l$  is  $\lambda/2$ .

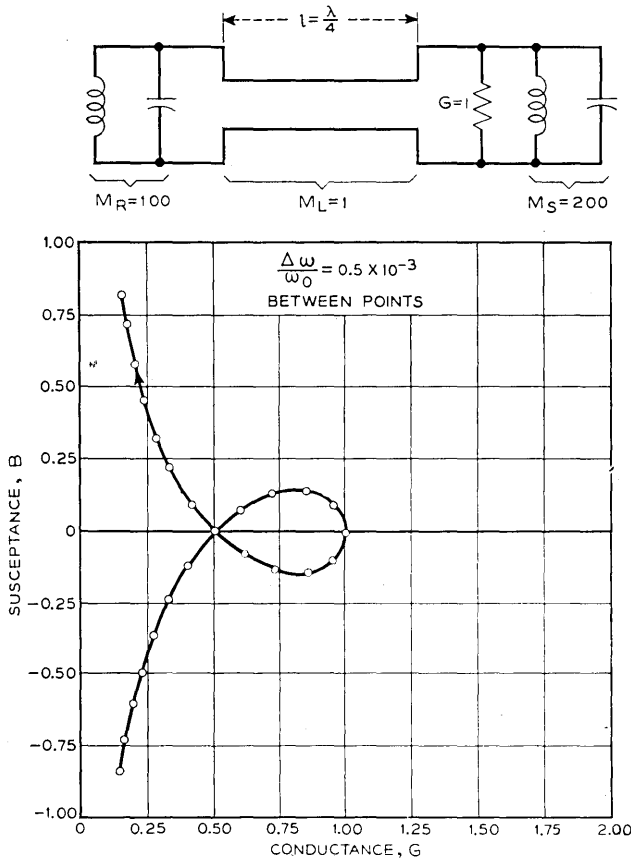


Fig. 43.—Susceptance vs conductance for two resonators coupled by a quarter wave line. The resonator at which the admittance is measured has a characteristic admittance of 100 in terms of a line characteristic admittance of unity. The other resonator has a characteristic admittance of 200 and a shunt conductance of unity. The circles mark off relative frequency increments of  $\frac{1}{2} \times 10^{-3}$  in terms of the resonant frequency.

As a sort of horrible example, an admittance curve for a high  $Q$  load 50 wavelengths from the resonator was computed and is shown in Fig. 46. Only a few of the loops are shown.

Admittance curves for more complicated circuits such as impedance transformers can be computed or obtained experimentally.

As has been stated, one of the most serious effects of such mismatched long line or resonant loads is that on the electronic tuning. For instance, consider the circuit admittance curve to be that shown in Fig. 47, and the minus electronic admittance curve to be a straight line extending from the origin. As the repeller voltage is varied and this is swung down from the  $+B$  axis its extreme will at some point touch the circuit admittance line

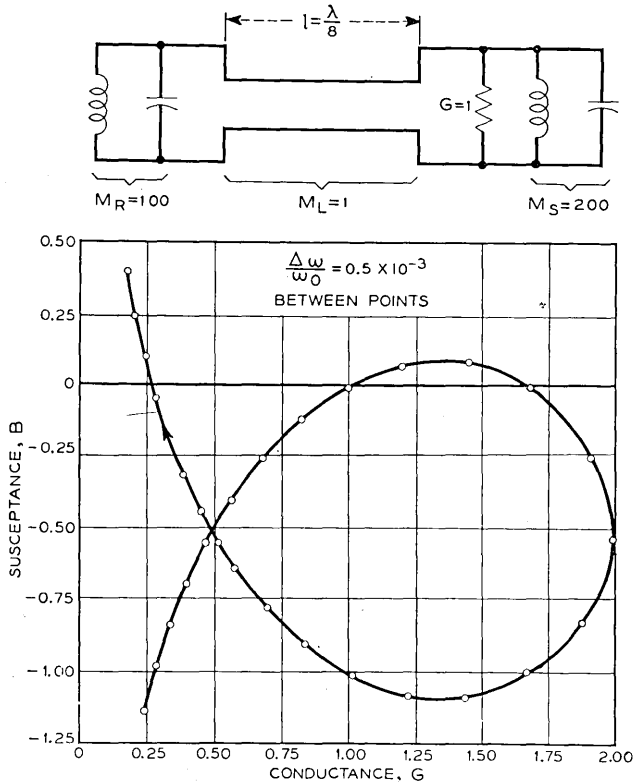


Fig. 44.—Susceptance vs. conductance for the same resonators as of Fig. 43 coupled by a one-eighth wave line.

and oscillation will commence. As the line is swung further down, the frequency will decrease. Oscillation will increase in amplitude until the  $-Y_e$  line is perpendicular to the  $Y$  line. From that point on oscillation will decrease in amplitude until the  $-Y_e$  line is parallel to the  $Y$  curve on the down side of the loop. Beyond this point the intersection cannot move out on the loop, and the frequency and amplitude will jump abruptly to correspond with the other intersection. As the  $-Y_e$  line rotates further,

amplitude will decrease and finally go to zero when the end of the  $-Y_e$  line touches the  $Y$  curve. If the  $-Y_e$  line is rotated back, a similar phenomenon is observed. This behavior and the resulting electronic tuning characteristic are illustrated in Figs. 47 and 48. Such electronic tuning

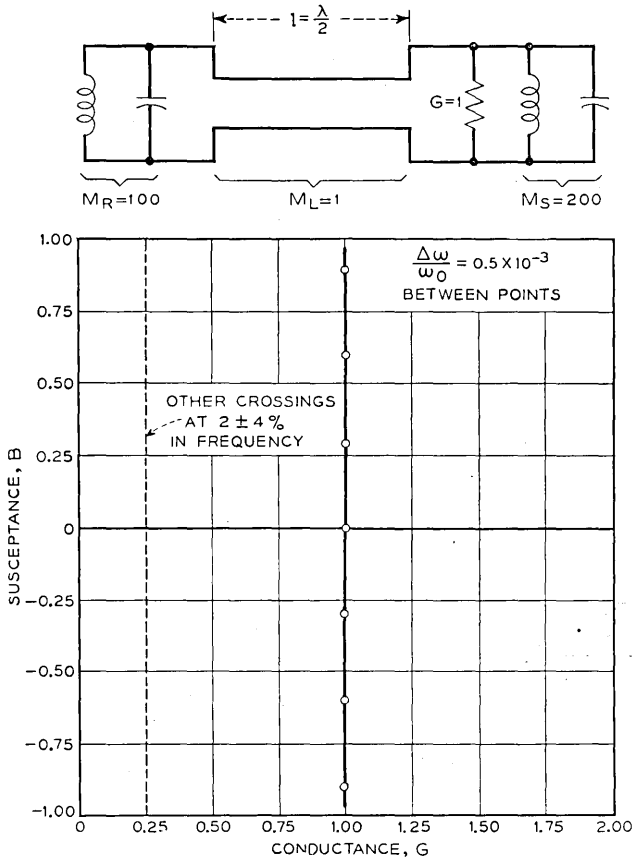


Fig. 45.—Susceptance vs conductance for the same resonators as of Fig. 43 coupled by a one-half wave line. The dash line indicates two other crossings of the 0 susceptance axis, at frequencies  $\pm 4\%$  from the resonant frequency of the resonators.

characteristics are frequently observed when a reflex oscillator is coupled tightly to a resonant load.

### C. Effect of Short Mismatched Lines on Electronic Tuning

In the foregoing, the effect of long mismatched lines in producing additional multiple resonant frequencies and possible modiness in operation has



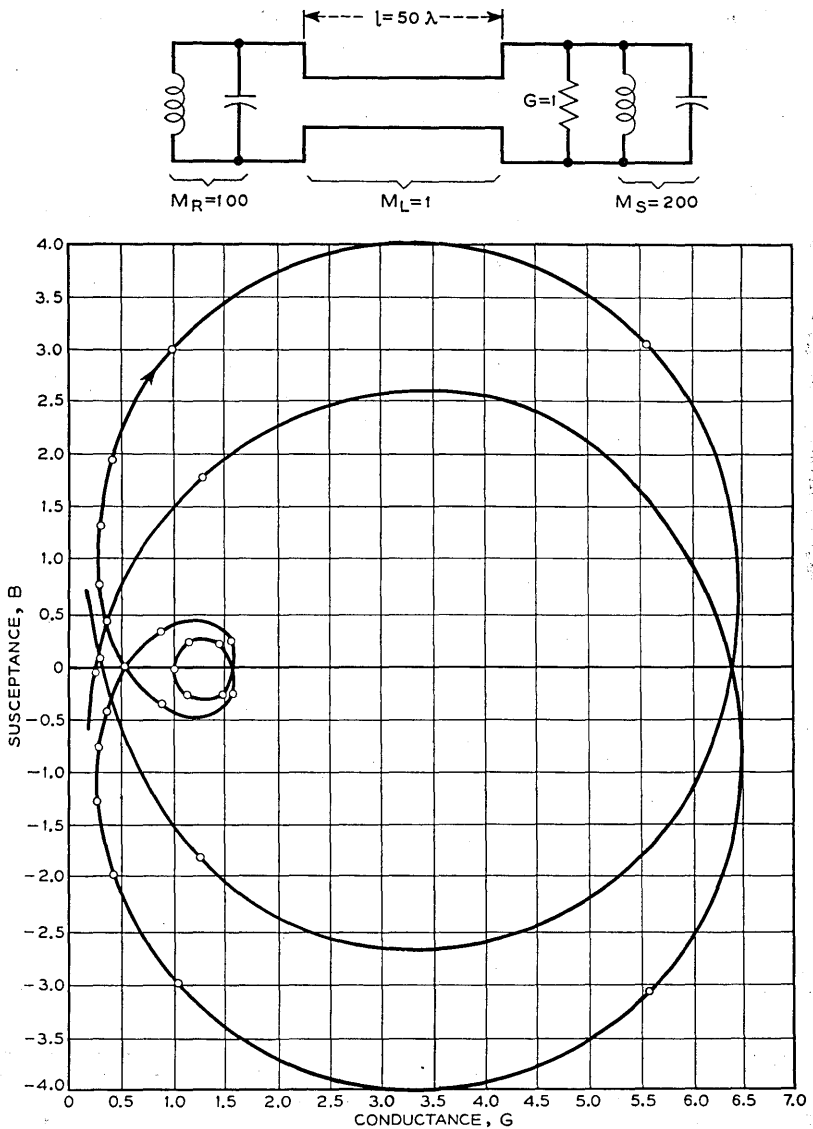


Fig. 46.—Susceptance vs conductance for the resonators of Fig. 43 coupled by a line 50 wave lengths long.

been explained. The effect of such multiple resonance on electronic tuning has been illustrated in Fig. 48.

If a short mismatched line is used as the load for a reflex oscillator, there

may be no additional modes, or such modes may be so far removed in frequency from the fundamental frequency of the resonator as to be of little

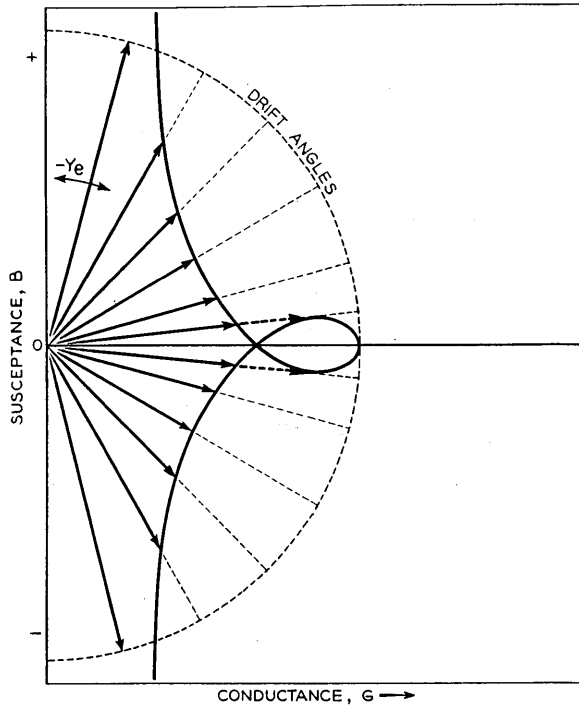


Fig. 47.—Behavior of the intersection between a circuit admittance line with a loop and the negative of the electronic admittance line of a reflex oscillator as the drift angle is varied (circuit hysteresis).

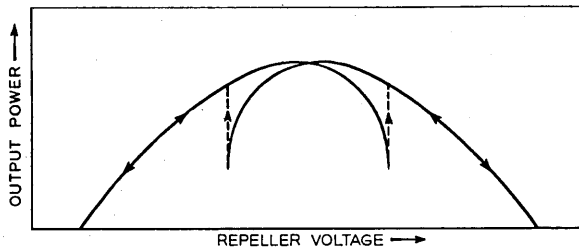


Fig. 48.—Output vs repeller voltage for the conditions obtaining in Fig. 47.

importance. Nonetheless, the short line will add a frequency-sensitive reactance in shunt with the resonant circuit, and hence will change the characteristic admittance of the resonator.

Imagine, for instance, that we represent the resonator and the mismatched line as in shunt with a section of line  $N$  wavelengths or  $\theta$  radians long mismatched in a frequency insensitive manner so as to give a standing wave ratio  $\sigma$ . If  $M_L$  is the characteristic admittance of the line, the admittance it produces at the resonator is

$$Y_L = M_L \frac{\sigma + j \tan \theta}{1 + j \sigma \tan \theta}. \quad (9.33)$$

Now, if the frequency is increased,  $\theta$  is made greater and  $Y$  is changed.

$$\partial Y_L / \partial \theta = M_L \frac{j(1 - \sigma^2) \sec^2 \theta}{(1 + j \sigma \tan \theta)^2}. \quad (9.34)$$

We are interested in the susceptive component of change. If

$$Y_L = G_L + jB_L \quad (9.35)$$

we find

$$\partial B_L / \partial \theta = M_L \frac{(1 - \sigma^2)(1 - \sigma^2 \tan^2 \theta) \sec^2 \theta}{(1 + \sigma^2 \tan^2 \theta)}. \quad (9.36)$$

Now, if frequency is changed by an amount  $df$ ,  $\theta$  will increase by an amount  $\theta(df/f)$  and  $B_L$  will change by an amount

$$dB_L = (\partial B_L / \partial \theta)(2\pi N)(df/f). \quad (9.37)$$

We now define a parameter  $M_M$  expressing the effect of the mismatch as follows

$$\pi(\partial B_L / \partial \theta) = M_M. \quad (9.38)$$

Then

$$dB_L = 2NM_M(df/f). \quad (9.39)$$

If the characteristic admittance of the resonator is  $M_R$ , then the characteristic admittance of the resonator plus the line is

$$M = M_R + NM_M. \quad (9.40)$$

If, instead of a coaxial line, a wave guide is used, and  $\lambda_0$  and  $\lambda$  are the cutoff and operating wavelengths, we have

$$dB_L = 2NM_M(df/f)(1 - (\lambda/\lambda_0)^2)^{-\frac{1}{2}} \quad (9.41)$$

and

$$M = M_R + NM_M(1 - (\lambda/\lambda_0)^2)^{-\frac{1}{2}} \quad (9.42)$$

In Fig. 49 contour lines for  $M_M$  constant are plotted on a Smith Chart (reflection coefficient plane). Over most of the plane  $M_M$  has a moderate

positive value tending to increase characteristic admittance and hence decrease electronic tuning. Over a very restricted range in the high admittance region  $M_M$  has large negative values and over a restricted range outside of this region  $M_M$  has large positive values.

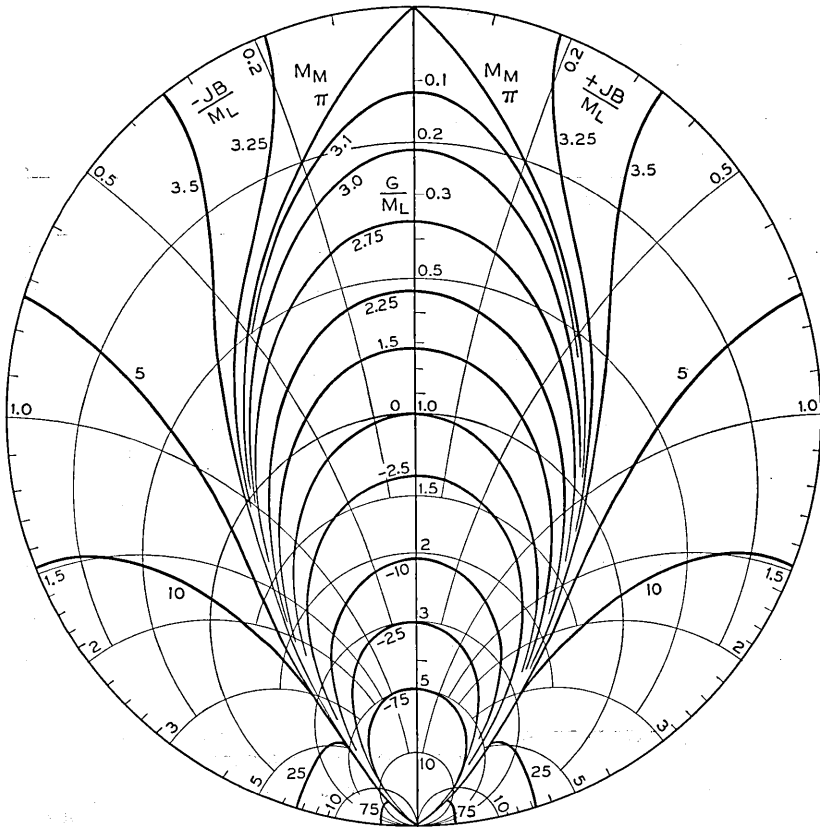


Fig. 49.—Lines of constant value of a parameter  $M_M$  shown on a chart giving the conductance and susceptance of the terminating admittance of a short line. The parameter plotted multiplied by the number of wave lengths in the line gives the additional characteristic admittance due to the resonant effects of the line. The parameter  $M_M$  is of course 0 for terminated lines (center of chart).

This is an appropriate point at which to settle the issue: what do we mean by a “short line” as opposed to a “long line.” For our present purposes, a short line is one short enough so that  $M_M$  does not change substantially over the frequency range involved. Thus whether a line is short or not depends on the phase of the standing wave at the resonator (the position

on the Smith Chart) as well as on the length of the line.  $M_M$  changes most rapidly with frequency in the very high admittance region.

As a simple example of the effect of a short mismatched line on electronic tuning between half power points, consider the case of a reflex oscillator with a lossless resonator so coupled to the line that the external  $Q$  is 100 and the electronic conductance is 3 in terms of the line admittance. Suppose we couple to this a coaxial line 5 wavelengths long with a standing wave ratio  $\sigma = 2$ , vary the phase, and compute the electronic tuning for various

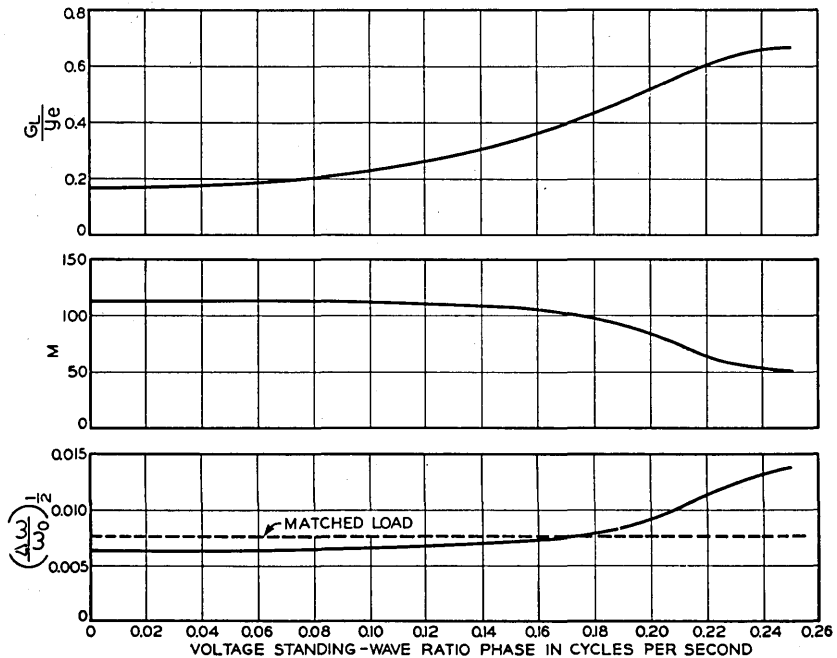


Fig. 50.—The normalized load conductance, the characteristic admittance of the resonator and the normalized electronic tuning range to half power plotted vs standing wave ratio phase for a particular case involving a short miterminated line. The electronic tuning for a matched line is shown as a heavy horizontal line in the plot of  $(\Delta\omega/\omega_0)_{1/2}$ .

phases. We can do this by obtaining the conductance and  $M_L$  from Fig. 49 and using Fig. 15 to obtain  $(\Delta\omega/\omega_0)_{1/2}$ . In Fig. 50, the parameters  $G_L/y_e$  (the total characteristic admittance including the effect of the line),  $N$ , and, finally,  $(\Delta\omega/\omega_0)_{1/2}$  have been plotted vs standing wave phase in cycles.  $(\Delta\omega/\omega_0)_{1/2}$  for a matched load is also shown. This example is of course not typical for all reflex oscillators: in some cases the electronic tuning might be reduced or oscillation might stop entirely for the standing wave phases which produce high conductance.

## X. VARIATION OF POWER AND ELECTRONIC TUNING WITH FREQUENCY

When a reflex oscillator is tuned through its tuning range, the load and repeller voltage being adjusted for optimum efficiency for a given drift angle, it is found that the power and efficiency and the electronic tuning vary, having optima at certain frequencies.

When we come to work out the variation of power and electronic tuning with frequency we at once notice two distinct cases: that of a fixed gap spacing and variable resonator (707A), and that of an essentially fixed resonator and a variable gap spacing (723A etc.); see Section XIII. Here we will treat as an example the latter case only.

The simplest approximation of the tuning mechanism which can be expected to accord reasonably with facts is that in which the resonator is represented as a fixed inductance, a constant shunt "stray" capacitance and a variable capacitance proportional to  $1/d$ , where  $d$  is the gap spacing. The validity of such a representation over the normal operating range has been verified experimentally for a variety of oscillator resonators. Let  $C_0$  be the fixed capacitance and  $C_1$  be the variable capacitance at some reference spacing  $d_1$ . Then, letting the inductance be  $L$ , we have for the frequency

$$\omega = (L(C_0 + C_1 d_1/d))^{1/2}. \quad (10.1)$$

Suppose we choose  $d_1$  such that

$$C_0 = C_1. \quad (10.2)$$

Then, letting

$$d/d_1 = D \quad (10.3)$$

$$\omega_1 = (2LC_0)^{1/2} = 2\pi f_1 \quad (10.4)$$

$$\omega/\omega_1 = W. \quad (10.5)$$

We find

$$W = 2^{1/2}(1 + 1/D)^{-1/2}. \quad (10.6)$$

This relation is shown in Fig. 51, where  $D$  is plotted vs  $W$ . It is perfectly general (within the validity of the assumptions) for a proper choice of reference spacing  $d_1$ . We have, then, in Fig. 51 a curve of spacing  $D$  vs reduced frequency  $W$ .

The parameter which governs the power and efficiency is  $G_R/y_e$ . We have

$$G_R/y_e = (G_R/\beta^2)(2V_0/I_0\theta). \quad (10.7)$$

As  $V_0$ ,  $I_0$  and  $\theta$  will not vary in tuning the oscillator, we must look for variation in  $G_R$  and  $\beta^2$ .

For parallel plane grids, we have

$$1/\beta^2 = (\theta_o/2)^2/\sin^2(\theta_o/2) \quad (10.8)$$

where  $\theta_o$  is the transit angle between grids. We see that in terms of  $W$  and  $D$  we can write

$$\theta_o = \theta_1 WD. \quad (10.9)$$

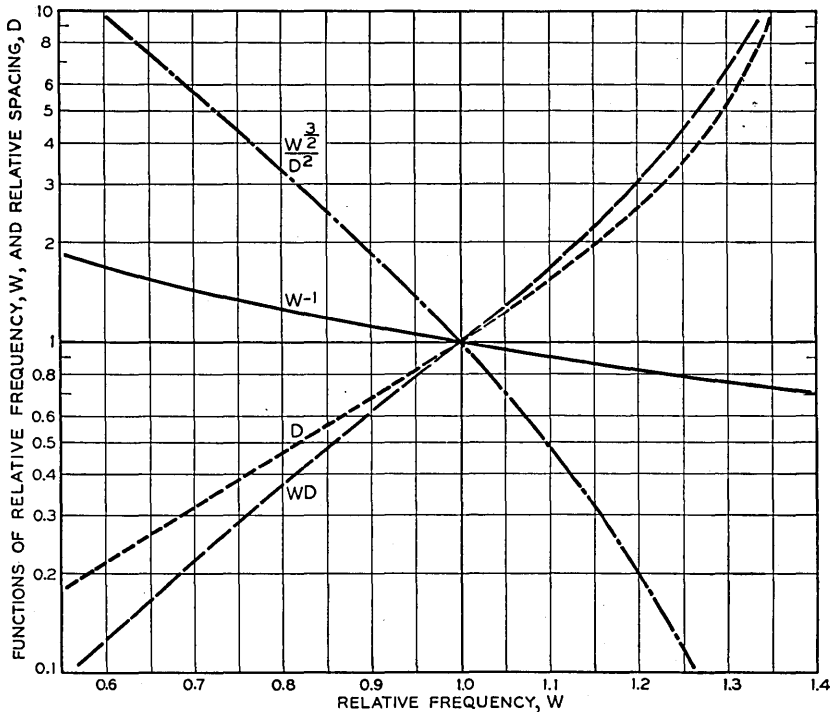


Fig. 51.—Various functions of relative frequency  $W$  and relative spacing  $D$  plotted vs relative frequency.

Here  $\theta_1$  is the gap transit angle at a spacing  $d_1$  and a frequency  $W_1$ . So that we may see the effect of tuning on  $1/\beta^2$ ,  $WD$  has been plotted vs  $W$  in Fig. 51 and  $1/\beta^2$  has been plotted vs  $\theta_o$  in Fig. 52.

We now have to consider losses. From (9.7) of Appendix IX we see that the grid loss conductance can be expressed in the form

$$G_o = G_{o1} W^3 / D^2. \quad (10.10)$$

Here  $G_{o1}$  is the grid loss conductance at  $d = d_1$  and  $\omega = \omega_1$ .

Finally, let us consider the resonator loss. If the resonator could be represented by an inductance  $L$  with a series resistance  $R$ , at high frequencies the conductance would be very nearly

$$G_L = R/(\omega L)^2. \quad (10.11)$$

If  $R$  varies as  $\omega^{\frac{3}{2}}$ , we see that we could then write

$$G_L = G_{L1}W^{-\frac{1}{2}}. \quad (10.12)$$

Here  $G_{L1}$  is the conductance at a frequency  $\omega_1$ .

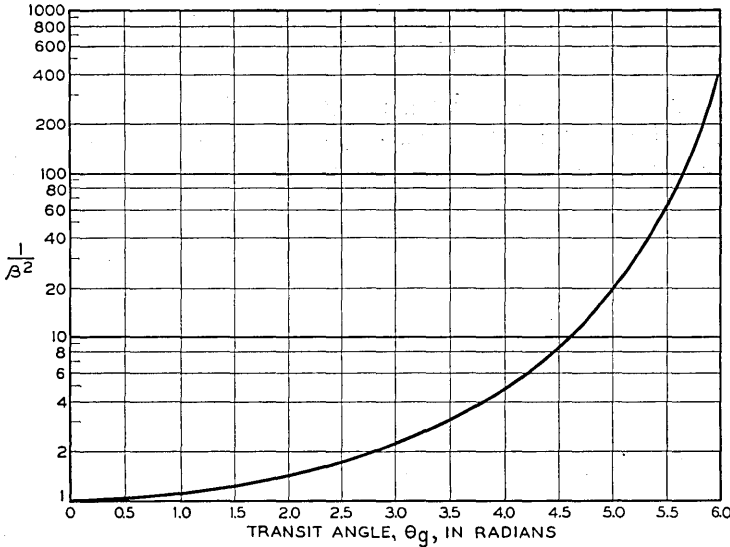


Fig. 52.—The reciprocal of the square of the modulation coefficient is a function of the gap transit angle in radians for the case of fine parallel grids.

As an opposite extreme let us consider the behaviour of the input conductance of a coaxial line. It can be shown that, allowing the resistance of such a line to vary as  $\omega^{\frac{3}{2}}$ , the input conductance is

$$G_l = A\omega^{\frac{3}{2}} \csc^2(\omega\ell/C). \quad (10.13)$$

Here  $\ell$  is the length of the line and  $C$  is the velocity of propagation. If  $G_L$  given by (10.12) and  $G_l$  of 10.13 give the same value of conductance at some angular frequency  $\omega_1$  then it will be found that for values of  $\ell$  typical of reflex oscillator resonators the variation of  $G_l$  with  $\omega$  will be significantly less than that of  $G_L$ . Although typical cavities are not uniform lines (10.13) indicates that a slower variation than (10.12) can be expected. It will be found moreover that the shape of the power output vs frequency curves are not very sensitive to the variation assumed. Hence as a reasonable compromise it will be assumed that the resonator wall loss varies as



$$G_s = G_{s1}W^{-1}. \quad (10.14)$$

In Fig. 51  $W^{-1}$  has been plotted vs  $W$ .

Now let us take an actual example. Suppose that at  $D = 1$ , i.e. ( $d = d_1, \omega = \omega_1$ )

$$\theta = 2$$

$$G_{o1} = .270/y_e$$

$$G_{s1} = .095/y_e$$

The information above has been used in connection with Figs. 51 and 52 and ratio of resonator loss to small signal electronic admittance,  $G_R/y_e$ , has been plotted vs  $W$  in Fig. 53. A 2K25 oscillator operated at a beam

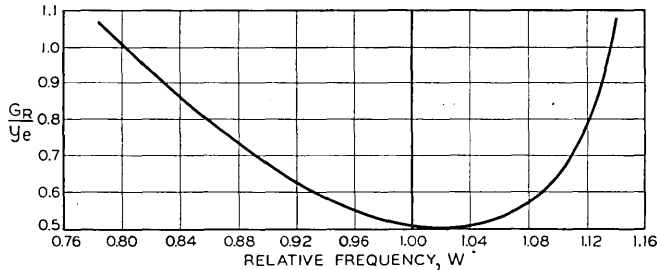


Fig. 53.—Computed variation of ratio of resonator loss to small signal electronic admittance vs relative frequency  $W$  for certain resonator parameters assumed to fit the characteristics of the 2K25.

voltage,  $V_0$ , of 300 volts had a total cathode current  $I_0$  of 26 ma. This current passed three grids on the first transit and back through the third grid on the return transit. On a geometrical basis, 53% of the cathode current should make this second transit across the gap. Thus the useful beam power was about

$$P_0 = (.53) (300) (.026) = 4.1.$$

If we assume a drift effectiveness factor  $F$  of unity, then for the  $7\frac{3}{4}$  cycle mode, the efficiency should be given by  $H_m$  divided by  $7\frac{3}{4}$ .  $H_m$  is plotted as a function of  $G_R/y_e$  in Fig. 7. Thus, we can obtain  $\eta$ , the efficiency, and hence the power output. This has been done and the calculated power output is plotted vs  $W$  in Fig. 54, where  $W = 1$  has been taken to correspond to 9,000 mc. It is seen that the theoretical variation of output with frequency is much the same as the measured variation.

Actually, of course, the parameters of the curve were chosen so that it corresponds fairly well to the experimental points. The upper value of  $W$  at which the tube goes out of oscillation is most strongly influenced by the value of  $\theta_1$  chosen. We see from Fig. 51 that as  $W$  is made greater than unity  $WD$  increases rapidly and hence, from Fig. 52,  $\beta^2$  decreases rapidly, increasing  $G_R/y_e$ . On the other hand, as  $W$  is made smaller than unity,  $\beta^2$  approaches unity but the grid loss term  $W^4/D^2$  increases rapidly, and this term is most effective in adjusting the lower value of  $W$  at which oscillation will cease. Finally, the resonator loss term, varying as  $W^{-1}$ , does not change rapidly and can be used to adjust the total loss and hence the optimum value of  $G_R/y_e$  and the optimum efficiency.

It is clear that the power goes down at low frequencies chiefly because in moving the grids very close together to tune to low frequencies with a fixed inductance the resonator losses and especially the grid losses are increased.

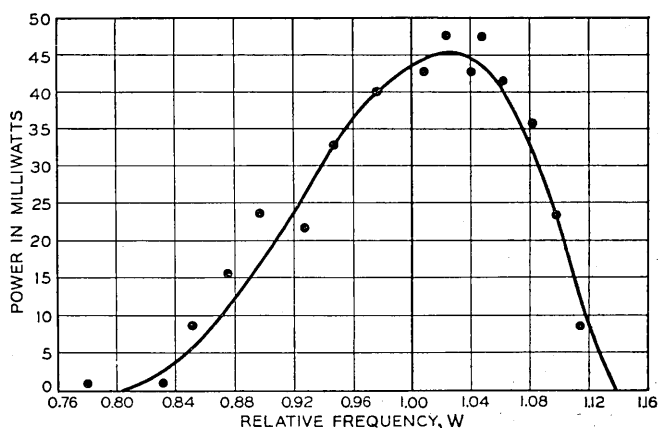


Fig. 54.—Computed curve of variation of power in milliwatts with relative frequency  $W$  for the parameters used in Fig. 53. The circles are experimental points. The curve has been fitted to the points by the choice of parameters.

In going to high frequencies the power decreases chiefly because moving the grids far apart to tune to high frequencies decreases  $\beta^2$ . Both of these effects are avoided if a fixed grid spacing is used and the tuning is accomplished by changing the inductance as in the case of the 707A. In such tubes there will be an upper frequency limit either because even with a fixed grid spacing  $\beta^2$  decreases as frequency increases, or else there will be a limit at the resonant frequency of the smallest allowable external resonator, and there will be a lower frequency limit at which the repeller voltage for a given mode approaches zero; however, the total tuning range may be 3 to 1 instead of around 30% between extinction points, as for the 2K25.

The total electronic tuning between half-power points at optimum loading,  $2(\Delta f)_{\frac{1}{2}}$ , can be expressed

$$2(\Delta f)_{\frac{1}{2}} = (fy_e/M)(2\Delta\omega/\omega_0)/(y_e/M). \quad (10.15)$$

We can obtain  $(2\Delta\omega/\omega_0)/(y_e/M)$  from Fig. 16.

If we assume a circuit consisting of a constant inductance  $L$  and a capacitance, the characteristic admittance of the resonator is

$$M = 1/\omega L = \frac{1}{2}\pi f_1 W \quad (10.16)$$

and

$$2(\Delta f)_{\frac{1}{2}} = 2\pi W^2 f_1^2 L y_e (2\Delta\omega/\omega_0)/(y_e/M) \quad (10.17)$$

and we have

$$y_e = \beta^2 I_0 (2\pi N) / 2V_0. \quad (10.18)$$

Here  $N$  is the total drift in cycles.

A rough calculation estimates the resonator inductance of the 2K25 as  $.30 \times 10^{-9}$  henries. Using the values previously assumed,  $I_0 = (.53)(.026)$ ,  $V_0 = 300$ ,  $N = 7\frac{3}{4}$ , and the values of  $G_R/y_e\beta^2$  and  $f_1$  previously assumed, we can obtain electronic tuning.

A curve for half power electronic tuning vs  $W$  has been computed and is shown in Fig. 55, together with experimental data for a 2K25. The experimental data fall mostly above the computed curve. This could mean that the inductance has been incorrectly computed or that the drift effectiveness is increased over that for a linear drift field, possibly by the effects of space charge. By choosing a value of the drift effectiveness factor other than unity we could no doubt achieve a better fit of the electronic tuning data and still, by readjusting  $G_{g1}$  and  $G_{s1}$ , fit the power data. This whole procedure is open to serious question. Further, it is very hard to measure such factors as  $G_{g1}$  for a tube *under operating conditions*, with the grids heated by bombardment. Indirect measurements involve many parameters at once, and are suspect. Thus, Figs. 54 and 55 are presented merely to show a qualitative correspondence between theory and experiment.

## XI. NOISE SIDEBANDS IN REFLEX OSCILLATIONS

In considering power production, the electron flow in reflex oscillators can be likened to a perfectly smooth flow of charge. However, the discrete nature of the electrons, the cause of the familiar "shot noise" in electron flow engenders the production of a small amount of  $r$ - $f$  power in the neighborhood of the oscillating frequency—"noise sidebands". Thus the energy spectrum of a reflex oscillator consists of a very tall central spike, the power output of the oscillator, and, superposed, a distribution of noise energy having its highest value near the central spike.

Such noise or noise "sidebands" can be produced by any mechanism which causes the parameters of the oscillator to fluctuate with time. As the mean speed, the mean direction, and the convection current of the electron flow all fluctuate with time, possible mechanisms of noise production are numerous. Some of these mechanisms are:

(1) Fluctuation in mean speed causes fluctuation in the drift angle and hence can give rise to noise sidebands in the output through frequency modulation of the oscillator.

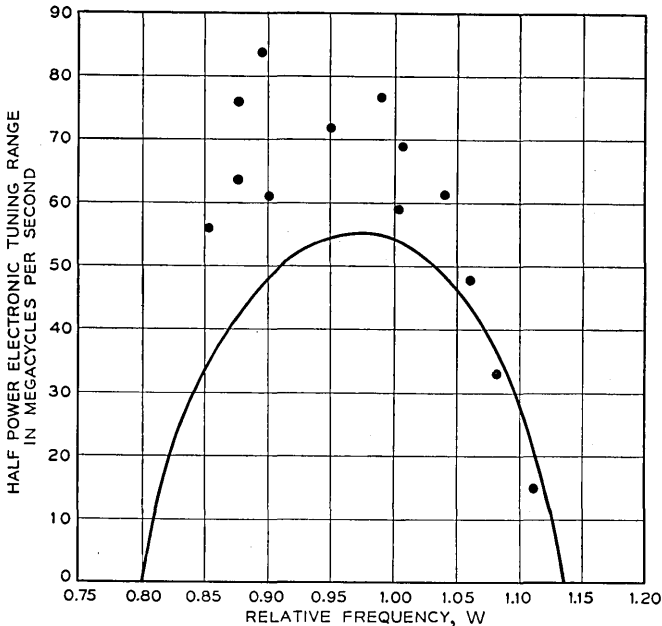


Fig. 55.—Computed variation of electronic tuning range in megacycles vs relative frequency  $W$ . The curve is calculated from the same data as that in Fig. 54 with no additional adjustment of parameters. Points represent experimental data.

(2) If the drift field acts differently on electrons differently directed, fluctuations in mean direction of the electron flow may cause noise sidebands through either amplitude or frequency modulation of the output.

(3) Low frequency fluctuations in the electron convection current may amplitude modulate the output, causing noise sidebands, and may frequency modulate the output when the oscillator is electronically tuned away from the optimum power point.

(4) High frequency fluctuations in the electron stream may induce high frequency noise currents in the resonator directly.

Mechanism (4) above, the direct induction of noise currents in the resonator by noise fluctuations in the electron stream, is probably most impor-

tant, although (3) may be appreciable. An analysis of the induction of noise in the resonator is surprisingly complicated, for the electron stream acts as a non-linear load impedance to the noise power giving rise to a complicated variation of noise with frequency and with amplitude of oscillation. On the basis of analysis and experience it is possible, however, to draw several general conclusions concerning reflex oscillator noise.

First, it is wise to decide just what shall be the measure of noise. The noise is important only when the oscillator is used as a beating oscillator, usually in connection with a crystal mixer. A power  $P$  is supplied to the mixer at the beating oscillator frequency. Also, the oscillator supplies at signal frequency, separated from the beating oscillator frequency by the intermediate frequency, a noise power  $P_n$  proportional, over a small frequency range, to the band-width  $B$ . An adequate measurement of the noisiness of the oscillator is the ratio of  $P_n$  to the Johnson noise power,  $kTB$ . The general facts which can be stated about this ratio and some explanation of them follow:

(1) Electrons which cross the gap only once contribute to noise but not to power. Likewise, if there is a large spread in drift angle among various electron paths, some electrons may contribute to noise but not to power.

(2) The greater the separation between signal frequency and beating oscillator frequency (i.e., the greater the intermediate frequency) the less the noise.

(3) The greater the electronic tuning range, the greater the noise for a given separation between signal frequency and beating oscillator frequency. This is natural; the electronic tuning range is a measure of the relative magnitudes of the electronic admittance and the characteristic admittance of the circuit.

(4) The degree of loading affects the noise through affecting the bunching parameter  $X$ . The noise seems to be least for light loading.

(5) Aside from controlling the degree of loading, resonator losses do not affect the noise; it does not matter whether the unused power is dissipated inside or outside of the tube.

(6) When the tube is tuned electronically, the noise usually increases at frequencies both above and below the optimum power frequency, but the tube is noisier when electronically tuned to lower frequencies. At the optimum frequency, the phase of the pulse induced in the circuit when an electron returns across the gap lags the pulse induced on the first crossing by  $270^\circ$ . When the drift time is shortened so as to tune to a higher frequency, the angle of lag is decreased and the two pulses tend to cancel; in tuning electronically to lower frequencies the pulses become more nearly in phase.

An approximate theoretical treatment leads to the conclusion that aside from avoiding loss of electrons in reflection, or very wide spreads in transit

time for various electrons, (see (1) above) and aside from narrowing the electronic tuning range, which may be inadmissible, the only way to reduce the noise is to decrease the cathode current. This is usually inadmissible. Thus, it appears that nothing much can be done about the noise in reflex oscillators without sacrificing electronic tuning range.

The seriousness of beating oscillator noise from a given tube depends, of course, on the noise figure of the receiver without beating oscillator noise and on the intermediate frequency. Usually, beating oscillator noise is worse at higher frequencies, partly because higher frequency oscillators have greater electronic tuning (see (3) above). At a wavelength of around 1.25 cm, with a 60 mc I.F. amplifier, the beating oscillator noise may be sufficient so that were there no other noise at all the noise figure of the receiver would be around 12 db.

Beating oscillator noise may be eliminated by use of a sharply tuned filter between the beating oscillator and the crystal. This precludes use of electronic tuning. Beating oscillator noise may also be eliminated by use of a balanced mixer in which, for example, the signal is fed to two crystals in the same phase and the beating oscillator in opposite phases. If the I.F. output is derived so that the signal components from the two crystals add, the output due to beating oscillator noise at signal frequencies will cancel out. There is an increasing tendency for a number of reasons to use balanced mixers and thus beating oscillator noise has become of less concern.

## XII. BUILD-UP OF OSCILLATION

In certain applications, reflex oscillators are pulsed. In many of these it is required that the *r-f* output appear quickly after the application of *d-c* power, and that the time of build-up be as nearly the same as possible for successive applications of power. In this connection it is important to study the mechanism of the build-up of oscillations.

In connection with build-up of oscillations; it is convenient to use complex frequencies. Impedances and admittances at complex frequencies are given by the same functions of frequency as those at real frequencies. Suppose, for instance, the radian frequency is

$$\omega = w - j\alpha \quad (12.1)$$

This means the oscillations are increasing in amplitude. The admittance of a conductance *G* at this frequency is

$$Y = G$$

The admittance of a capacitance *C* and the impedance of an inductance *L* are

$$Y = j\omega C = jwC + \alpha C \quad (12.2)$$

$$Z = j\omega L = jwL + \alpha L \quad (12.3)$$

In other words, to an increasing oscillation reactive elements have a "loss" component of admittance or impedance. This "loss" component corresponds not to dissipation but to the increasing storage of electric or magnetic energy in the reactive elements as the oscillation increases in amplitude.

The admittance curves plotted in Figs. 41-46 may be regarded as contours in the admittance plane for  $\alpha = 0$ . If such a contour is known either by calculation or experiment, and it is divided into equal frequency increments, a simple construction will give a neighboring curve for  $\omega = \omega - j\Delta\alpha$  where  $\Delta\alpha$  is a small constant. Suppose that the change in  $Y$  for a frequency  $\Delta\omega_1$  is  $\Delta Y_1$ . Then for a change  $-j\Delta\alpha$

$$\Delta Y = -j \frac{\Delta Y_1}{\Delta\omega_1} \Delta\alpha. \quad (12.4)$$

Thus, to construct from a constant amplitude admittance curve an admittance curve for an increasing oscillation, one takes a constant fraction of each admittance increment between constant frequency increment points (a constant fraction of each space between circles in Figs. 41-46), rotates it 90 degrees clockwise, and thus establishes a point on the new curve.

This construction holds equally well for any conformal representation of the admittance plane (for instance, for the reflection coefficient plane represented on the Smith chart).

The general appearance of these curves for increasing oscillations in terms of the curve for real frequency can be appreciated at once. The increasing amplitude curve will lie to the right of the real frequency curve where the latter is rising and to the left where the latter is falling. Thus the loops will be diminished or eliminated altogether for increasing amplitude oscillations, and the low conductance portions will move to the right, to regions of higher conductance. This is consistent with the idea that for an increasing oscillation a "loss" component is added to each reactance, thus degrading the "Q", increasing the conductance, and smoothing out the admittance curve.

The oscillation starts from a very small amplitude, presumably that due to shot noise of the electron stream. For an appreciable fraction of the build-up period the oscillation will remain so small that nonlinearities are unimportant. The exponential build-up during this period is determined by the electronic admittance for very small signals.

As an example, consider a case in which the electronic admittance for small signals is a pure conductance with a value of  $-y_e$ . Here the fact that that the quantity is negative is recognized by prefixing a minus sign.

Assume also that the circuit admittance including the load may be expressed as in (a-22) of Appendix I, which holds very nearly in case there is only one resonance in resonator and load. Then for a complex frequency  $\omega_0 - j\alpha_0$  the circuit admittance will be

$$Y_c = G_c + 2M\alpha_o/w_o \quad (12.5)$$

Thus in this special case we have for oscillation

$$y_{eo} = G_c + 2M\alpha_o/w_o \quad (12.6)$$

and

$$\alpha_o = \frac{w_o}{2M} (Y_{eo} - G_c). \quad (12.7)$$

The amplitude, then, builds up initially according to the law

$$V = V_o e^{\alpha_o t}. \quad (12.8)$$

If the amplitude does not change too rapidly, the build-up characteristic of an oscillator can be obtained step-by-step from a number of contours for constant  $\alpha$  and from a  $-Y_e$  curve marked with amplitude points. The  $-Y_e$  curve might, for instance, be obtained from a Rieke diagram and an admittance curve.

Consider the example shown in Fig. 56. Fig. 56a shows curves constructed for complex frequencies from the admittance curve for the resonant circuit for real frequency. In addition the negative of the electronic admittance is shown. Oscillation will start from some very small amplitude,  $V = V_o$ , and build-up at an average rate given by  $\alpha = 2.5 \times 10^{-6}$  until  $V = 1$ . Let  $V_o = .1$ . Then the interval to build-up from  $V = .1$  to  $V = 1$  is

$$\begin{aligned} \Delta t_1 &= \frac{\ln\left(\frac{1}{.1}\right)}{2.5 \times 10^{-6}} \\ &= .92 \times 10^{-6} \text{ seconds.} \end{aligned}$$

From amplitude 1 to amplitude 2 the average value of  $\alpha$  will be  $1.5 \times 10^{-6}$  and the time interval will be

$$\begin{aligned} \Delta t_2 &= \frac{\ln\left(\frac{2}{1}\right)}{1.5 \times 10^{-6}} \\ &= .46 \times 10^{-6} \text{ seconds.} \end{aligned}$$

Similarly, from 2 to 3

$$\begin{aligned} \Delta t_3 &= \frac{\ln\left(\frac{3}{2}\right)}{.5 \times 10^{-6}} \\ &= .80 \times 10^{-6} \text{ seconds.} \end{aligned}$$

The build-up curve is shown in Fig. 56b.

Similarly, from a family of admittance contours constructed from a cold impedance curve, and from a knowledge of frequency and amplitude vs time,



$Y_e$  can be obtained as a function of time. It may be that in many cases the real part of the frequency is nearly enough constant during build-up so that only the amplitude vs time need be known. As the input will commonly be a function of time for such experimental data,  $Y_e$  vs time will yield  $Y_e$  at vari-

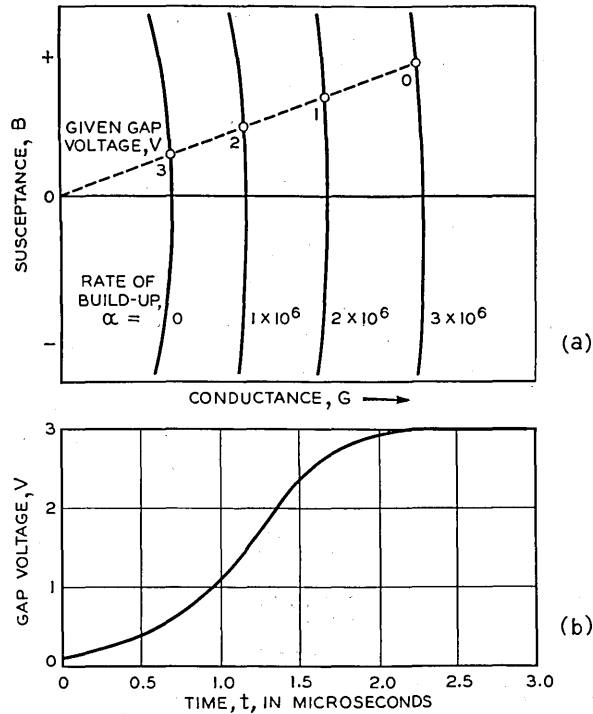


Fig. 56.—*a*. A plot of the circuit admittance (solid lines) for various rates of build-up specified by the parameters  $\alpha$ . The voltage builds up as  $e^{\alpha t}$ . The circuit conductance is greater for large values of  $\alpha$ . The negative of the electronic admittance is shown by the dashed lines. The circles mark off the admittance at which various amplitudes or voltages of oscillation occur. The intersections give the rates of build-up of oscillation at various voltages. By assuming exponential build up at a rate specified by  $\alpha$  between the voltages at these intersections, an approximate build-up can be constructed.

*b*. A build-up curve constructed from the data in Fig. 56a.

ous amplitudes and inputs. Curves for various rates of applying input will yield tables of  $Y_e$  as a function of both input and amplitude.

It will be noted that to obtain very fast build-up with a given electronic admittance, the conductance should vary slowly with  $\alpha$ . This is the same as saying that the susceptance should vary slowly with  $\omega$ , or with real frequency. For singly resonant circuits, this means that  $\omega_0/M$  should be large.

Suppose the admittance curve for real frequency, i.e.  $\alpha = 0$ , has a single

loop and is symmetrical about the  $G$  axis as shown in Fig. 57. Suppose the  $-Y_e$  curve lies directly on the  $G$  axis. The admittance contours for increasing values of  $\alpha$  will look somewhat as shown. Suppose build-up starts on Curve 2. When Curve 1 with the cusp is reached, the build-up can continue along either half as the loop is formed and expands, resulting either of the two possible frequencies of Curve 0. Presumably in this symmetrical

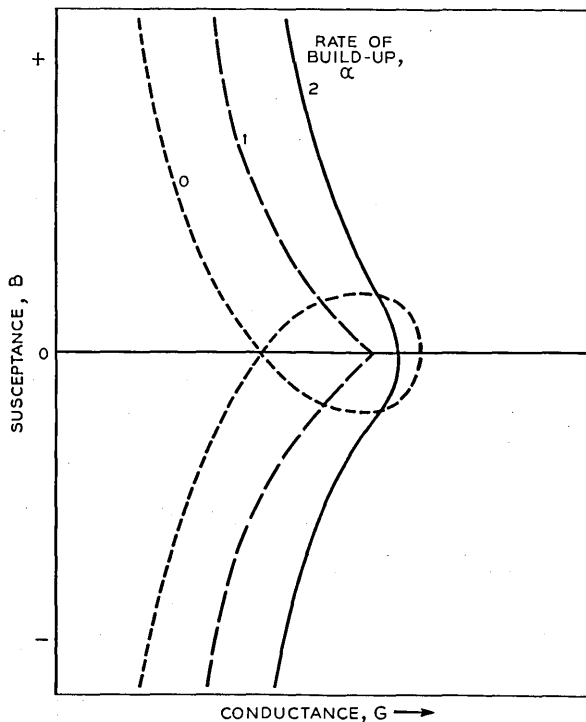


Fig. 57.—Circuit admittance vs circuit conductance in arbitrary units for different rates of build-up at turn-on. When the build-up is rapid ( $\alpha = 2$ ) the admittance curve has no loop. As the rate of build-up decreases the curve sharpens until it has a cusp  $\alpha = 1$ . As the rate of build-up further decreases the curve develops a loop ( $\alpha = 0$ ). There may be uncertainty as to which of the final intersections with the  $\alpha = 0$  line will represent oscillation.

case, nonsynchronous fluctuations would result in build-up to each frequency for half of the turn-ons. If one frequency were favored by a slight dissymmetry, the favored frequency would appear on the greater fraction of turn-ons. For a great dissymmetry, build-up may always be in one mode, although from the impedance diagram steady oscillation in another mode appears to be possible.

In the absence of hum or other disturbances the build-up of oscillations starts from a randomly fluctuating voltage caused by shot noise.<sup>11</sup> Thus, from turn-on to turn-on some sort of statistical distribution may be expected in the time  $\tau$  taken to reach a given fraction of the final amplitude. In unpublished work Dr. C. R. Shannon of these laboratories has shown that in terms of  $\alpha_0$ , the initial rate of build-up, the standard deviation  $\delta\tau$  and the root mean square deviation  $(\overline{\delta\tau^2})^{1/2}$  are given by

$$\delta\tau = .38/\alpha_0 \quad (12.9)$$

$$(\overline{\delta\tau^2})^{1/2} = .64/\alpha_0 \quad (12.10)$$

Thus the "jitter" in the successive positions of the r-f pulses associated with evenly spaced turn-ons is least when the initial rate of build-up, given by  $\alpha_0$ , is greatest.

Such conditions do not obtain on turn-off, and there is little jitter in the trailing edge of a series of r-f pulses. This is of considerable practical importance.

### XIII. REFLEX OSCILLATOR DEVELOPMENT AT THE BELL TELEPHONE LABORATORIES

For many years research and development directed towards the generation of power at higher and higher frequencies have been conducted at the Bell Telephone Laboratories. An effort has been made to extend the frequency range of the conventional grid controlled vacuum tube as well as to explore new principles, such as those embodied in velocity variation oscillators. The need for centimeter range oscillators for radar applications provided an added impetus to this program and even before the United States entry into the war, as well as throughout its duration, these laboratories, cooperating with government agencies, engaged in a major effort to provide such power sources. The part of this program which dealt with high power sources for transmitter uses has been described elsewhere. This paper deals with low power sources, which are used as beating oscillators in radar receivers. In the following sections some of the requirements on a beating oscillator for a radar receiver will be outlined in order to show how the reflex oscillator is particularly well suited for such an application.

#### A. *The Beating Oscillator Problem*

The need for a beating oscillator in a radar system arises from the necessity of amplifying the very weak signals reflected from the targets. Immediate rectification of these signals would entail a very large degradation in signal to noise ratio, although providing great simplicity of operation. It would also lead to a lack of selectivity. Amplification of the signals at the

<sup>11</sup> See Appendix 10.

signal frequency would require centimeter range amplifiers having good signal to noise properties. No such amplifiers existed for the centimeter range, and it was necessary to beat the signal frequency to an intermediate frequency for amplification before rectification. For a number of reasons, such intermediate frequency amplifiers operate in the range of a few tens of megacycles, so that the beating oscillator must generate very nearly the same frequency as the transmitter oscillator.

In radar receivers operating at frequencies up to several hundred megacycles, conversion is frequently achieved with vacuum tubes. For higher frequencies crystal converters have usually been employed. With few exceptions, the oscillators to be described were used with these crystal converters which require a small oscillator drive of the order of one milliwatt. In general it is desirable to introduce attenuation between the oscillator and the crystal to minimize effects due to variation of the load. Approximately 13 db is allowed for such padding so that a beating oscillator need supply about 20 milliwatts. Power in excess of this is useful in many applications but not absolutely necessary. Since the power output requirements are low, efficiency is not of prime importance and is usually, and frequently necessarily, sacrificed in the interest of more important characteristics.

The beating oscillator of a radar receiver operating in the centimeter range must fulfill a number of requirements which arise from the particular nature of the radar components and their manner of operation. The intermediate frequency amplifier must have a minimum pass band sufficient to amplify enough of the transmitter sideband frequencies so that the modulating pulse is reproduced satisfactorily. It is not desirable to provide much margin in band width above this minimum since the total noise increases with increasing band width. It is therefore necessary for best operation that the frequency of the beating oscillator should closely follow frequency variations of the transmitter, so that a constant difference frequency equal to the intermediate frequency is maintained.

This becomes more difficult at higher frequencies, inasmuch as all frequency instabilities, such as thermal drifts, frequency pulling, etc. occur as percentage variations. Some of the frequency variations occur at rapid rates. An example of this is the frequency variation which is caused by changes in the standing wave presented to the transmitter. Such variations may arise, for instance, from imperfections in rotating joints in the output line between the transmitter to the scanning antenna.

For correction of slow frequency drifts a manual adjustment of the frequency is frequently possible, but instances arise, notably in aircraft installations, in which it is not possible for an operator to monitor the frequency constantly. Rapid frequency changes, moreover, occur at rates in excess of the reaction speed of a normal man. Hence for obvious tactical reasons

it is imperative that the difference frequency between the transmitter and the beating oscillator should be maintained by automatic means. As an illustration of the problem one may expect to have to correct frequency shifts from all causes, in a 10,000 megacycle system, of the order of 20 megacycles. Such correction may be demanded at rates of the order of 100 megacycles per second per second.

Although the frequency range of triode oscillators has since been somewhat extended, at the time that beating oscillators in the 10 centimeter range were first required the triode oscillators available did not adequately fulfill all the requirements. In general the tuning and feedback adjustments were complicated and hence did not adapt themselves to automatic frequency control systems. Velocity variation tubes of the multiple gap type which gave more satisfactory performance than the triodes existed in this range. These, however, generally required operating voltages of the order of a thousand volts and frequently required magnetic fields for focusing the electron stream. The tuning range obtainable by electrical means was considerably less than needed and, just as in the case of the triode oscillator, the mechanical tuning mechanism did not adapt itself to automatic control. These difficulties focussed attention on the reflex oscillator, whose properties are ideally suited to automatic frequency control. The feature of a single resonant circuit is of considerable importance in a military application, in which simple adjustments are of primary concern. The repeller control of the phase of the negative electronic admittance which causes oscillation provides a highly desirable vernier adjustment of the frequency, and, since this control dissipates no power, it is particularly suited to automatic frequency control. Furthermore, since the upper limit on the rate of change of frequency is set by the time of transit of the electrons in the repeller field and the time constant of the resonant circuit, both of which are generally very small fractions of a micro-second, very rapid frequency correction is possible.

As the frequency is varied with the repeller voltage, the amplitude of oscillation also varies in a manner previously described. The signal to noise performance of a crystal mixer depends in part on the beating oscillator level and has an optimum value with respect to this parameter. In consequence, there are limitations on how much the beating oscillator power may depart from this optimum value. This has a bearing on the oscillator design in that the amount of amplitude variation permitted for a given frequency shift is limited. The usual criterion of performance adopted has been the electronic tuning, i.e. the frequency difference, between points for a given repeller mode at which the power has been reduced to half the maximum value.

Reception of the wrong sideband by the receiver causes trouble in con-

nection with automatic frequency control circuits in a manner too complicated for treatment here. In some cases this necessitates a restriction on the total frequency shift between extinction points for a given repeller mode. The relationship between half power and extinction electronic tuning has been discussed in Section VII.

In addition to the electrical requirements which have been outlined, military applications dictate two further major objectives. The first is the attainment of simple installation and replacement, which will determine, in part, the outward form of the oscillator. The second is low voltage operation, which fundamentally affects the internal design of the tubes. In some instances military requirements conflict with optimum electronic and circuit design, and best performance had to be sacrificed for simplicity of construction and operation. In particular, in some cases it was necessary to design for maximum flexibility of use and compromise to a certain extent the specific requirements of a particular need.

In the following section we will describe a number of reflex oscillators which were designed at the Bell Telephone Laboratories primarily to meet military requirements. These oscillators are described in approximate chronological order of development in order to indicate advances in design and the factors which led to these advances.

The reflex oscillators which will be described fall into two general classifications determined by the method employed in tuning the resonator. In one category are oscillators tuned by varying primarily the inductance of the resonator and in the other are those tuned by varying primarily the capacitance of the resonator. The second category includes two types in which the capacitance is varied in one case by external mechanical means and in the second case by an internal means using a thermal control.

#### B. *A Reflex Oscillator With An External Resonator—The 707*

The Western Electric 707A tube, which was the first reflex oscillator extensively used in radar applications, is characteristic of reflex oscillators using inductance tuning. It was intended specifically for service in radar systems operating at frequencies in a range around 3000 megacycles. Fig. 58 shows a photograph of the tube and Fig. 59 an x-ray view showing the internal construction. A removable external cavity is employed with the 707A as indicated by the sketch superimposed on the x-ray of Fig. 59. Such cavities are tuned by variation of the size of the resonant chamber. Such tuning can be considered to result from variation of the inductance of the circuit.

The form of this oscillator is essentially that of the idealized oscillator shown in Fig. 58. The electron gun is designed to produce a rectilinear cylindrical beam. The gun consists of a disc cathode, a beam forming elec-

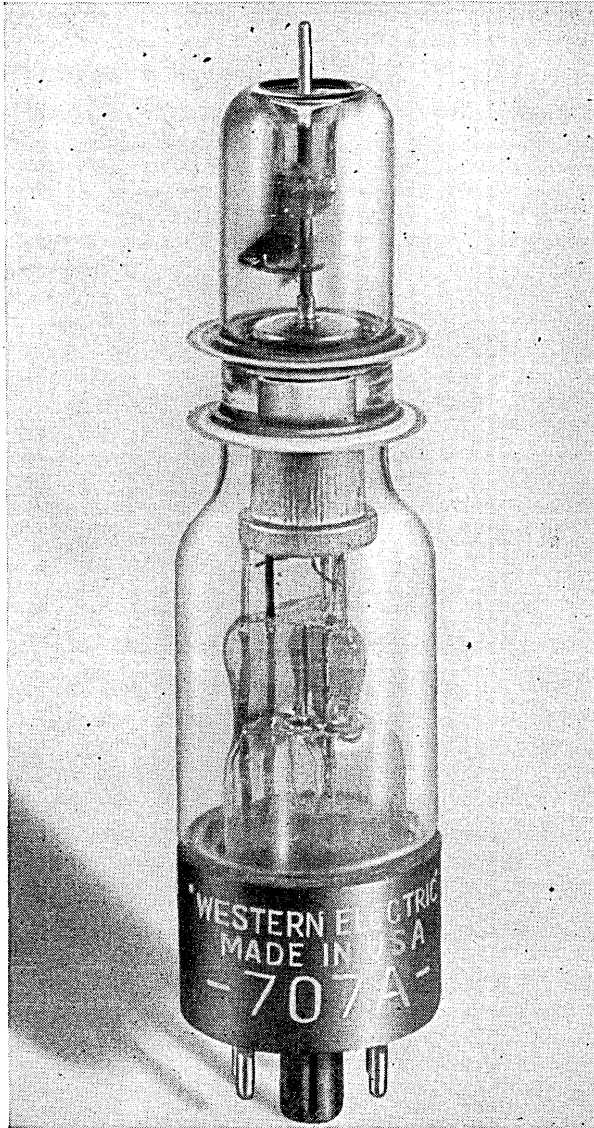


Fig. 58.—External view of the W.E. 707-A reflex oscillator tube. This tube is intended for use with an external cavity and was the first of a series of low voltage oscillators.

trode and an accelerating electrode  $G_1$  which is a mesh grid formed on a radius. The gun design is based on the principle of maintaining boundary conditions such that a rectilinear electron beam will flow through the resonator gap. The resonator grids  $G_2$  and  $G_3$  are mounted on copper discs.

One of these has a re-entrant shape to minimize stray capacitance in the resonant circuit. These discs are sealed to glass tubing which provides a

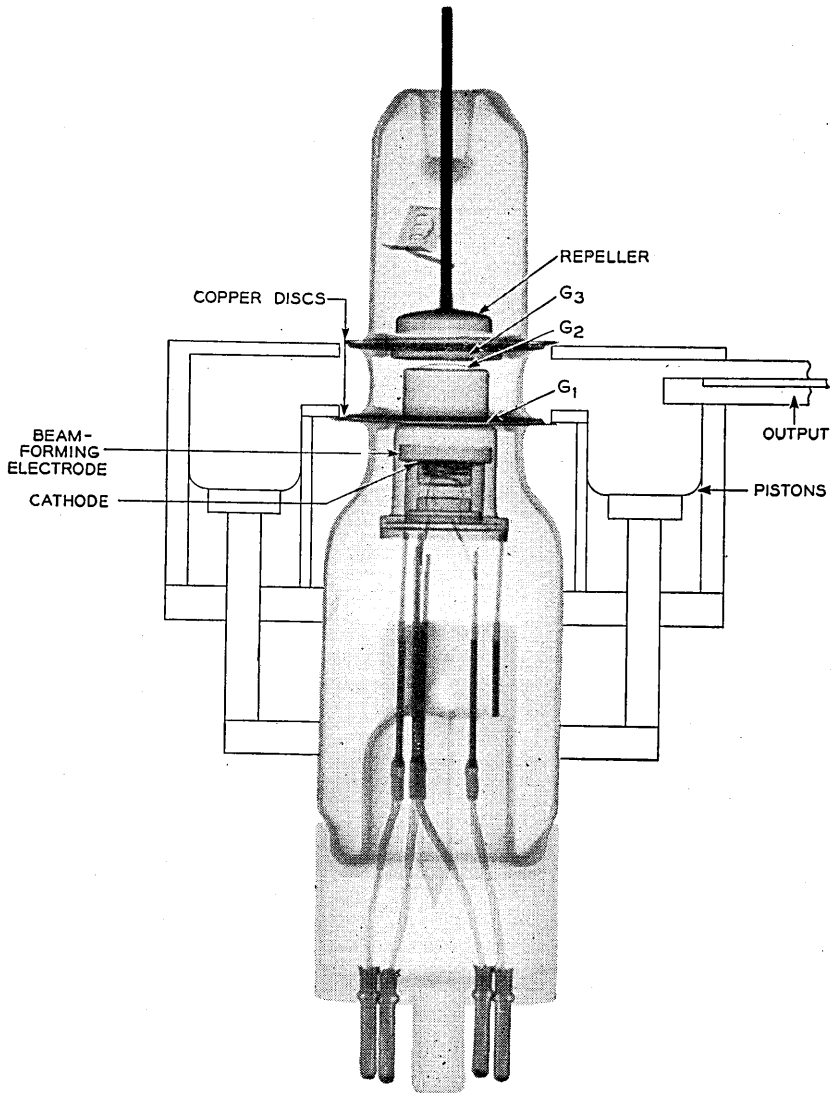


Fig. 59.—X-ray view of the W.E. 707-A shows the method of applying an external cavity tuned with a piston.

vacuum envelope. The discs extend beyond the glass to permit attachment to the external resonant chamber. The shape of the repeller is chosen



to provide as nearly as possible a uniform field in the region into which the beam penetrates.

A wide variety of cavity resonators has been designed for use with this oscillator. An oscillator of this construction is fundamentally capable of oscillating over a much wider frequency range than tubes tunable by means of capacitance variation. The advantage arises from the fact that the interaction gap where the electron stream is modulated by the radio frequency field is fixed. As discussed in more detail in Section X, this results in a slower variation of the modulation coefficient with frequency and also a slower variation of cavity losses and gap impedance than in an oscillator in which tuning is accomplished by changing the gap spacing. A cavity designed for wide range frequency coverage using the 707A tube is shown in Fig. 60. Using such a cavity it is possible to cover a frequency range from 1150 to 3750 megacycles. The inductance of the circuit is varied by moving the shorting piston in the coaxial line. For narrow frequency ranges,

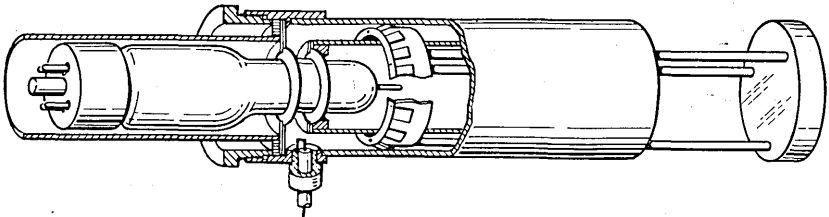


Fig. 60.—Sketch showing a piston tuned circuit for the W.E. 707-A which will permit operation from 1150 to 3750 mc.

cavities of the type shown in Fig. 61 are more suitable. In such cavities tuning is effected by means of plugs which screw into the cavity to change its effective inductance. Power may be extracted from the cavity by means of an adjustable coupling loop as shown in Fig. 61.

The 707A was the first reflex oscillator designed to operate at a low voltage i.e. 300 volts. This low operating voltage proved to be a considerable advantage in radar receivers because power supplies in this voltage range provided for the i.f. amplifiers could be used for the beating oscillator as well. Operation at this voltage was achieved by using an interaction gap with fine grids, which limits the penetration of high frequency fields. This results in a shorter effective transit angle across the gap for a given gap spacing and a given gap voltage than for a gap with coarse or no grids. Hence, for a given gap spacing a good modulation coefficient can be obtained at a lower voltage. Moreover, since drift action results in more efficient bunching at low voltages, a larger electronic admittance is obtained than with an open gap. This gain in admittance more than outweighs the

greater capacitance of a gap with fine grids, so that a larger electronic tuning range is obtained than with an open gap. The successful low voltage operation of the 707A established a precedent which was followed in all the succeeding reflex oscillators designed for radar purposes at the Bell Tele-

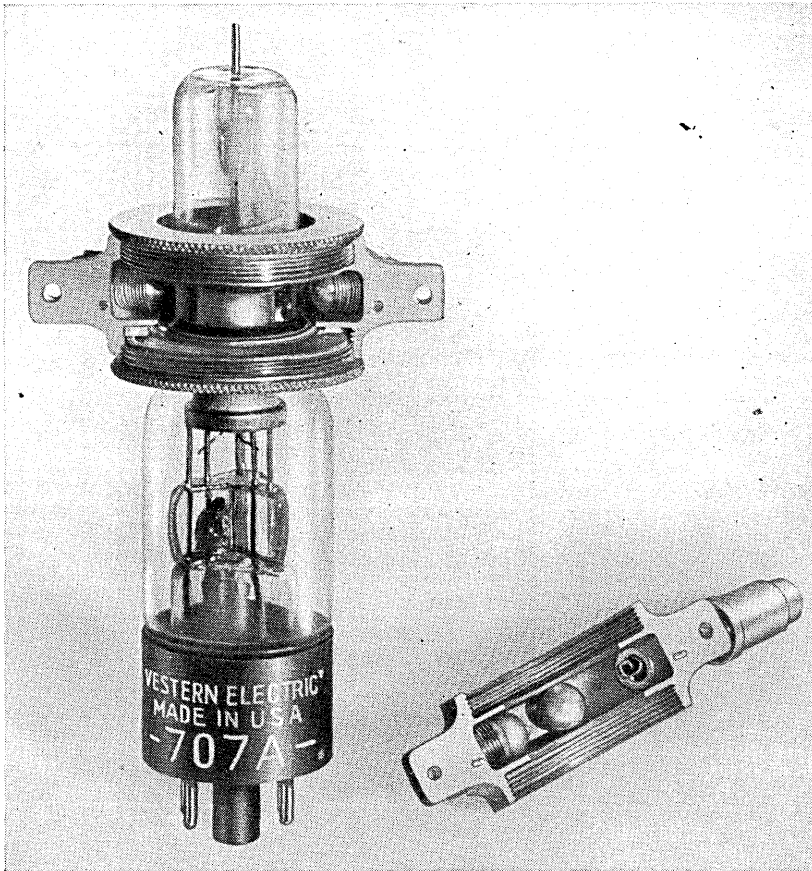


Fig. 61.—A narrow tuning range cavity for the W.E. 707-A of the type used in radar systems. The inductance of the cavity can be adjusted by moving screws into it. This view also shows the adjustable coupling loop.

phone Laboratories. The 707A is required to provide a minimum power output of 25 milliwatts and a half power electronic tuning of 20 megacycles near 3700 megacycles. The power output and the electronic tuning are in excess of this value over the range from 2500 megacycles to 3700 megacycles in a repeller mode having  $3\frac{3}{4}$  cycles of drift.

*C. A Reflex Oscillator With An Integral Cavity—The 723*

The need for higher definition in radar systems constantly urges operation at shorter wavelengths. Thus, while radar development proceeded at 3000 megacycles, a program of development in the neighborhood of 10,000 megacycles was undertaken. Although waveguide circuit techniques were employed to some extent at 3000 megacycles, the cumbersome size of the guide made its use impractical in the receiver and hence coaxial techniques were employed. The 1" by  $\frac{1}{2}$ " guide used at 10,000 megacycles is convenient in receiver design and also desirable because the loss in coaxial conductors becomes excessive at this frequency. Hence, one of the first requirements on an oscillator for frequencies in this range was the adaptability of the output circuit to waveguide coupling.

In considering possible designs for a 10,000 megacycle oscillator the simple scaling of the 707A was studied. This appeared impractical for a number of reasons. The most important limitation was the constructional difficulty of maintaining the spacing in the gap with sufficient accuracy with the glass sealing technique available. Also, variations in the capacitance caused by variations in the thickness of the seals caused serious difficulties in predetermining an external resonator. Contributing difficulties arose from the power losses in the glass within the resonant circuit and the problem of making the copper to glass seals close to the internal elements.

Consideration of these factors led to a new approach to the problem, in which the whole of the resonant circuit was enclosed within the vacuum envelope. This required a different mechanism for tuning the resonator, since variation of the inductance of a cavity requires relatively large displacements which are difficult to achieve through vacuum seals. The alternative is to vary the capacitance of the gap. Since the gap is small a relatively large change in capacitance can be achieved with a small displacement. This sort of tuning permits the use of metal tube constructional techniques, and these were applied.

As a matter of historical interest an attempt at this technique made at the Bell Telephone Laboratories is shown in Fig. 62. This device was held together by a sealing wax and string technique and was not tunable in the first version. It oscillated successfully on the pumps, however, and a second version was constructed which was tuned by means of an adjustable coaxial line shunting the cavity resonator. Adjustment of this auxiliary line gave a tuning range of 7.5%. Such a tuning method is fraught with the complications outlined in Section IX.

An early reflex oscillator tube of the integral cavity type designed at the Bell Telephone Laboratories was the Western Electric 723A/B.

This design was superseded later by the W.E. 2K25 which has a greater frequency range and a number of design refinements. From a constructional point of view the two types are closely similar, however, and to avoid duplication the later tube will be described to typify a construction which served as a basis for a whole series of oscillators in the range from 2500 to 10,000 Mc/s.

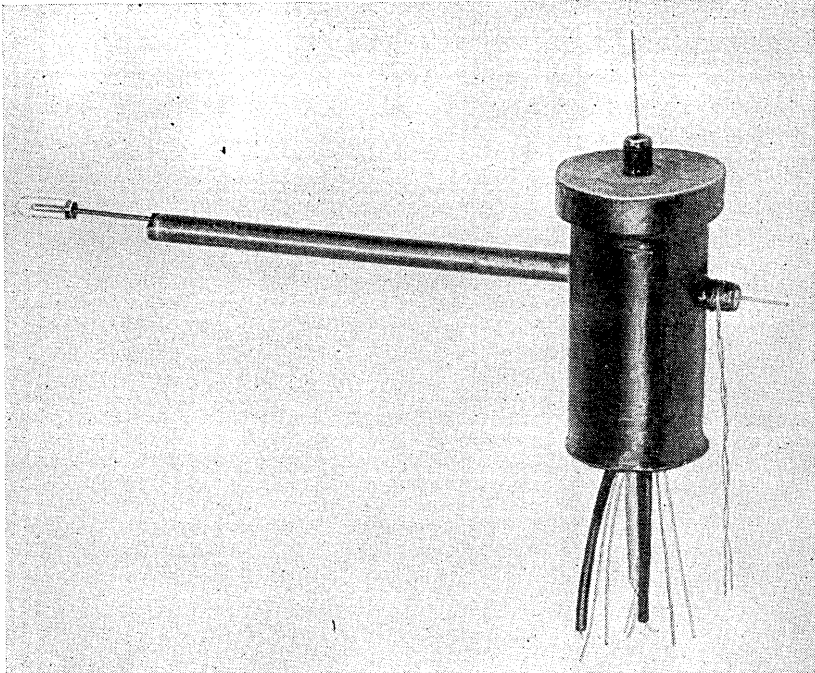


Fig. 62.—An early continuously pumped metal reflex oscillator tuned with an external line.

Before proceeding to a description of the 2K25 tube it seems desirable to recapitulate in more detail the design objectives from a mechanical point of view. These were:

1. To provide a design which would lend itself to large scale production and one sufficiently rugged as to be capable of withstanding the rough use inherent in military service.
2. To provide output means which permit coupling to a wave guide in such a manner that installation or replacement could be accomplished in the simplest possible manner.
3. To provide a tuning mechanism for the resonant circuit which, while simple, would give sufficiently fine tuning to permit setting and holding

a frequency within one or two parts in 10,000. In addition, in order to avoid field installation it was desired to have the tuning mechanism cheap enough to be factory installed and discarded with each tube.

4. The oscillator was required to be compact and light in weight to facilitate its use in airborne and pack systems.

Figure 63 shows a cross-section view of the final design of the 2K25 reflex oscillator. The resonant cavity is formed in part by the volume included between the frames which support the cavity grids and also by the volume between the flexible vacuum diaphragm and one of the frames. This diaphragm also supports a vacuum housing containing the repeller. The electron optical system consists of a disc cathode, a beam electrode and an accelerating grid. These are so designed as to produce a slightly convergent outgoing electron stream. The purpose of this initial convergence is to offset the divergence of the stream caused by space charge after the stream passes the accelerating grid and to minimize the fraction of the electron stream captured on the grid frame on the round trip. The repeller is designed to provide as nearly as possible a uniform retarding field through the stream cross-section.

Power is extracted from the resonant circuit by the coupling loop and is carried by the coaxial line to the external circuit. The center conductor of the coaxial line external to the vacuum is supported by a polystyrene insulator and extends beyond the outer conductor to form a probe. Coupling to a wave guide is accomplished by projecting this probe through a hole in that wall of the wave guide which is perpendicular to the E lines so that the full length of the probe extends into the guide. The outer conductor is connected to the wave guide either metalically or by means of an r.f. bypass or choke circuit. A more detailed section on such coupling methods will be given later.

The tube employed a standard octal base modified to pass the coaxial line. Thus if a standard octal socket is similarly modified and mounted on the wave guide it is possible to couple the oscillator to the wave guide and power supply circuits simply by plugging it into the socket, just as with any conventional vacuum tube.

The tuning means for this type of oscillator tube presented a serious problem. This will be appreciated when it is realized that the mechanism must permit setting frequencies correctly to within one megacycle in a device in which the frequency changes at the rate of approximately 200 megacycles per thousandth of an inch displacement of the grids. In other words, the tuner was required to make possible the adjustment of the grid spacing to an accuracy of five millionths of an inch. The design of the mechanism adopted was originated by Mr. R. L. Vance of these Laboratories. The operation of the tuner can be seen from an examination of the cross-section

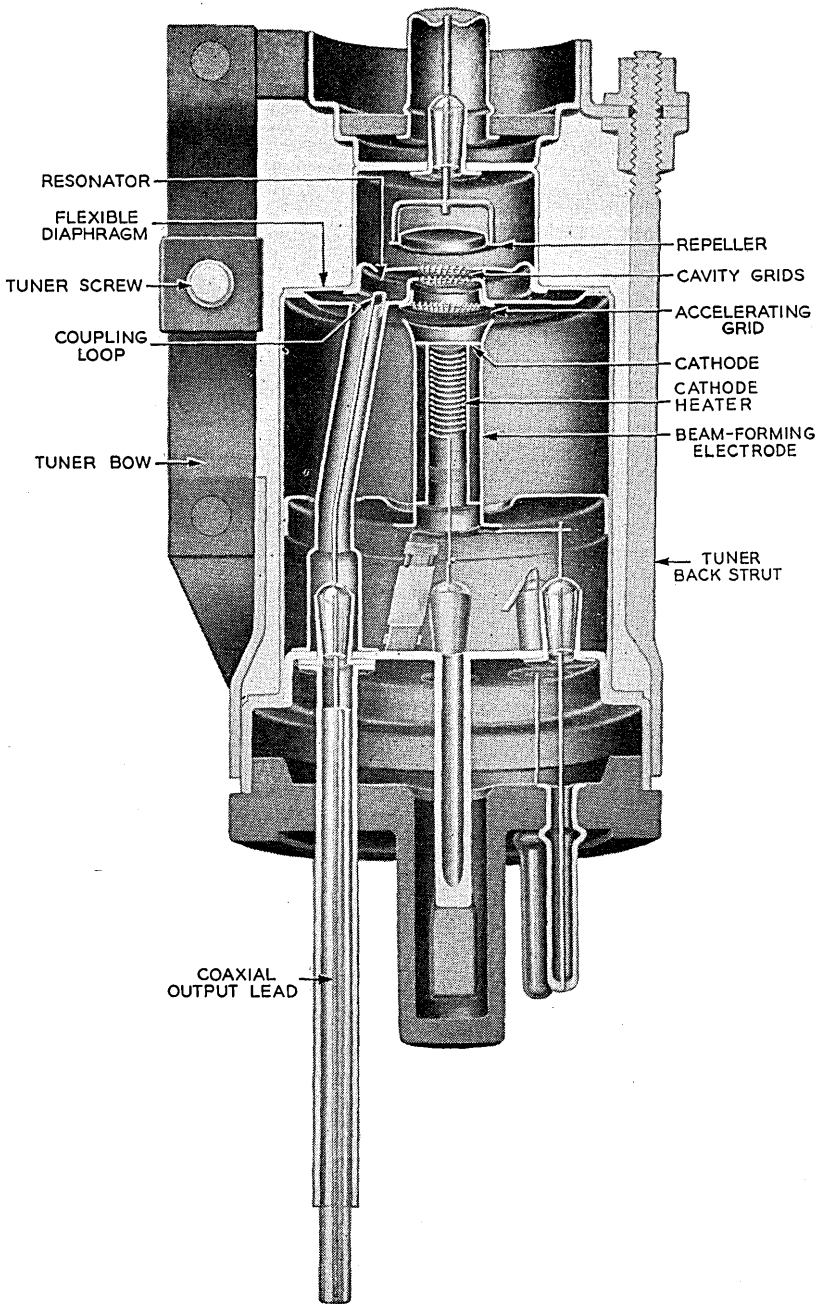


Fig. 63.—A 3 centimeter reflex oscillator with an internal resonator. This tube is a further development of the earliest internal resonator reflex oscillator designed at the Bell Telephone Laboratories.

and external views of Figs. 63 and 67. On one side of the tube a strut extending from the base is attached to the repeller housing. This strut acts as a rigid vertical support but provides a hinge for lateral motion. On the opposite side the support is provided by a pair of steel strips. These are clamped together where they are attached to the vacuum housing support and also where they are attached to a short fixed strut near the base. A nut is attached rigidly to the center of each strip. One nut has a right and the other a left handed thread. A screw threaded right handed on one half and left handed on the other half of its length turns in these nuts and drives them apart. The mechanism is thus a toggle which, through the linkage provided by the repeller housing, serves to move the grids relative to one another and thus to provide tuning action.

The 723A/B was originally designed for a relatively narrow band in the vicinity of 9375 megacycles. It operates at a resonator voltage of 300 volts and the beam current of a typical tube would be approximately 24 milliamperes. The design was based on the use of repeller voltage mode which with the manufacturing tolerances lay between 130 and 185 volts at 9375 megacycles. It is difficult to establish with certainty the number of cycles of drift for this mode. Experimental data can be fitted by values of either  $6\frac{3}{4}$  or  $7\frac{3}{4}$  cycles and various uncertainties make the value calculated from dimensions and observed voltages equally unreliable. This value is, however, of interest principally to the designer and of no particular moment in application. The performance was specified for the output line of the oscillator coupled to a  $\frac{5}{8}'' \times 1\frac{1}{4}''$  wave guide so that the probe projected full length into the guide through the wider wall and on the axis of the guide. With a matched load coupled in one direction and a shorting piston adjusted for an optimum in the other the oscillator was required to deliver a minimum of 20 milliwatts power output at a frequency of 9375 megacycles. Under the same conditions the electronic tuning was required to be at least 28 megacycles between half power points.

For reasons of continuity a more detailed description of the properties of the 3 centimeter oscillator will be given in a later section. The 723A/B oscillator served as the beating oscillator for all radar systems operating in the 3 centimeter range until late in the war when the 2K25 supplanted it. At the time that the 723A/B was developed the best techniques and equipment available were employed. In retrospect these were somewhat primitive and of course this resulted in a number of limitations of performance. Since the tubes designed as beating oscillators commonly served as signal generators in the development of ultra-high frequency techniques and equipment the wartime designer of such oscillators usually found himself in the position of lifting himself by his own bootstraps. In spite of these limitations the later modifications of the 723A/B which led to

the 2K25 did not fundamentally change the design but were rather in the direction of extending its performance to meet the expanding requirements of the radar art. The incorporation of the resonant cavity within the vacuum envelope resulted in a major revision of the scope of the designer's problems. He assumed a part of the burden of the circuit engineer in that it became necessary for him to design an appropriate cavity and predetermine the correct coupling of the oscillator to the load. The latter transferred to the laboratory a problem which in the case of separate cavity oscillators had been left as a field adjustment.

#### D. *A Reflex Oscillator Designed to Eliminate Hysteresis—The 2K29*

As service experience with the external cavity type of reflex oscillator was gained a number of limitations of such a design became apparent. The difficulties arose primarily from the conditions of military application. A typical difficulty was the corrosion of cavities and copper flanges under the severe tropical conditions met in some service applications. The difficulty of maintaining a moistureproof seal in a cavity tuned by variation of the inductance made it very difficult to alleviate this condition. The success of the all metal technique in the three centimeter range suggested the application of the same principles to the design of a 10 centimeter oscillator and this was undertaken.

Mechanically, the problem was straightforward, but an extrapolation of the electrical design of the 723A/B to 10 centimeters suffered from a fatal defect. The difficulty, previously described in Section VIII, was the discontinuous and multiple valued character of the output as a function of the repeller voltage. Reference to Fig. 19 will indicate the operational problems which would arise in an oscillator in which the hysteresis existed in marked degree. The a.f.c. systems were such that in starting the repeller voltage would start from a value more negative than required for oscillation and decrease. As the repeller voltage decreased through the range where oscillation would occur the frequency would of course cover a range of values. When the repeller voltage reached a value such that the frequency of the oscillator had a value differing from the transmitter by the intermediate frequency the steady shift of the repeller voltage would be stopped and would then hunt over a limited range about the value required to maintain the difference frequency. When adjusted for operation this condition would pertain with the repeller voltage at a value such that the oscillator would be delivering maximum power. If under operating conditions the frequency required of the oscillator by the system drifted to that corresponding to the amplitude jump at B, any further drift of frequency could not be corrected. Thus, one effect of the hysteresis is to limit the electronic tuning range. As a second possibility, let us assume that the



frequency has drifted so that the oscillator is operating in a range between A and B of Fig. 19. If now the operation of the system is momentarily interrupted the a.f.c. system will start hunting. This is done by returning to the non-oscillating repeller voltage just as when operation is initiated. When the hunting repeller voltage passes through the value between A and B from the non-oscillating state no oscillation occurs and hence the a.f.c. cannot lock in and the system becomes inoperative. Thus it is imperative that hysteresis be kept, as a minimum requirement, outside the useful electronic tuning range.

As indicated in Section VIII it was found that the electronic hysteresis occurred when the electron stream made more than two transits across the gap. Thus an added objective of the design of the 10 centimeter metal oscillator became the achievement of an electron optical system which would limit the number of transits to two while insuring that the maximum number of electrons leaving the cathode would make the two transits with a minimum spread in zero signal transit time.

Figure 64 shows a sectional view of the final design adopted. The electron optical structure differs from that of the 723A/B in a number of respects. The first grid of the 723A/B has been eliminated and one of the cavity grids now plays a dual role in simultaneously serving as an accelerating grid. The grids are curved towards the cathode, which has a central spike. This arrangement is intended to produce a hollow cylindrical electron stream. It will be observed that the second grid is larger in diameter than the first and that the repeller has a central spike. The design is such that the cylindrical beam entering the repeller region is caused to diverge radially, so that in re-traversing the gap after its reversal in direction it impinges on and is captured by the frame supporting the first grid.

The repeller design was determined by using an electrolytic trough to determine the potential plots for a number of trial configurations. Then by making point by point calculations of the electron paths the best configuration was chosen. A typical example of such path tracing is shown in Fig. 65. This figure shows the equipotential lines and the trajectories computed for electrons on the inner and outer boundaries of the outgoing stream. The method of calculating the trajectories has been described by Zworykin and Rajchman.<sup>12</sup> It assumes that space charge may be neglected. Fig. 65 shows that the repeller design is such that the cylindrical outgoing stream is focussed upon its return onto the frame supporting the first grid. The cathode spike prevents emission from the central portion of the cathode, since it would be difficult to prevent electrons from this portion from returning into the cathode space. A second requirement on

<sup>12</sup> V. K. Zworykin and J. A. Rajchman, *Proc. of I.R.E.*, Sept. 1939, Vol. 17, No. 9, pp. 558-566.

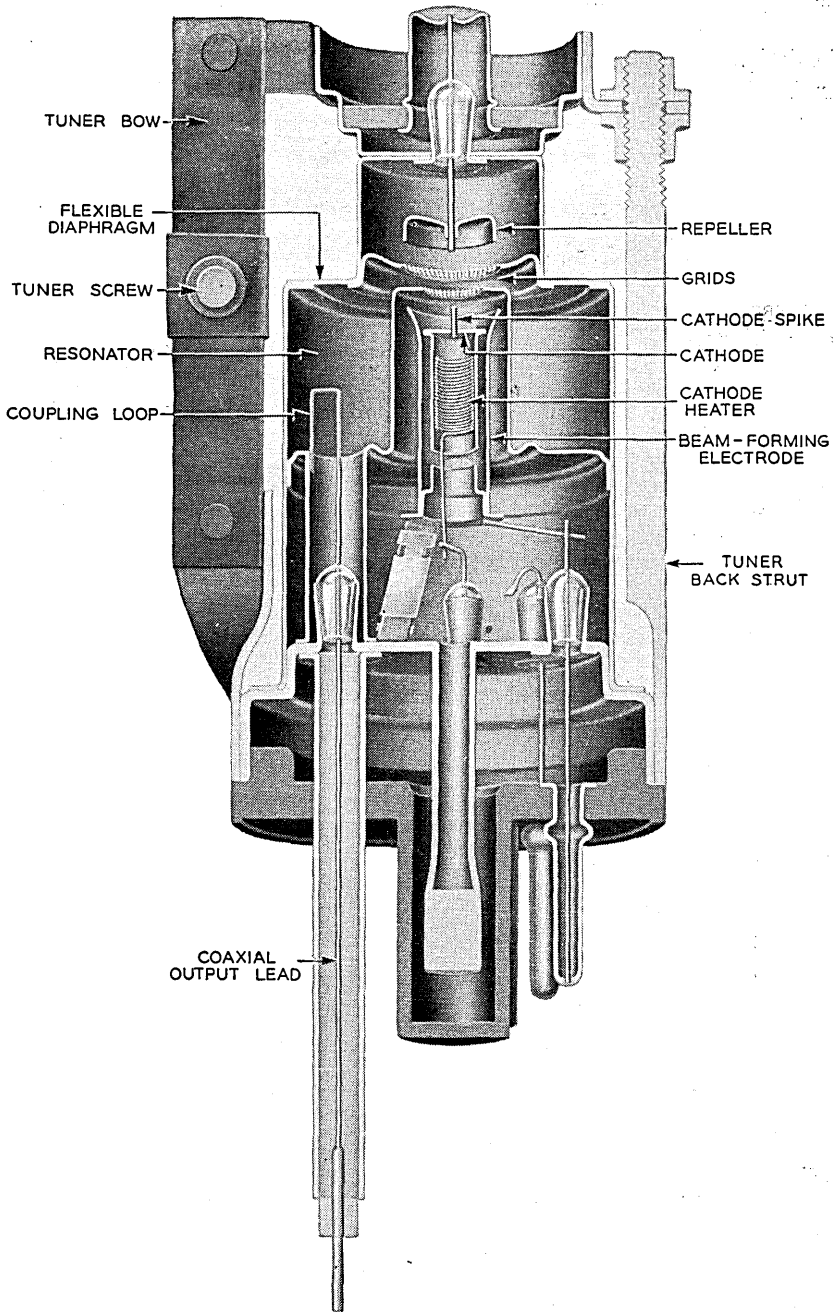


Fig. 64.—Section view of the W.E. 2K29 reflex oscillator shows the electron optical system used in eliminating hysteresis. (Fig. 65) This tube has an internal cavity and is designed for the frequency range from 3400 to 3960 mc/s.

the design was that the spread in the transit angle for zero signal should be small. This requirement is not as stringent as might be expected. The contribution to the electronic conductance by a current element whose

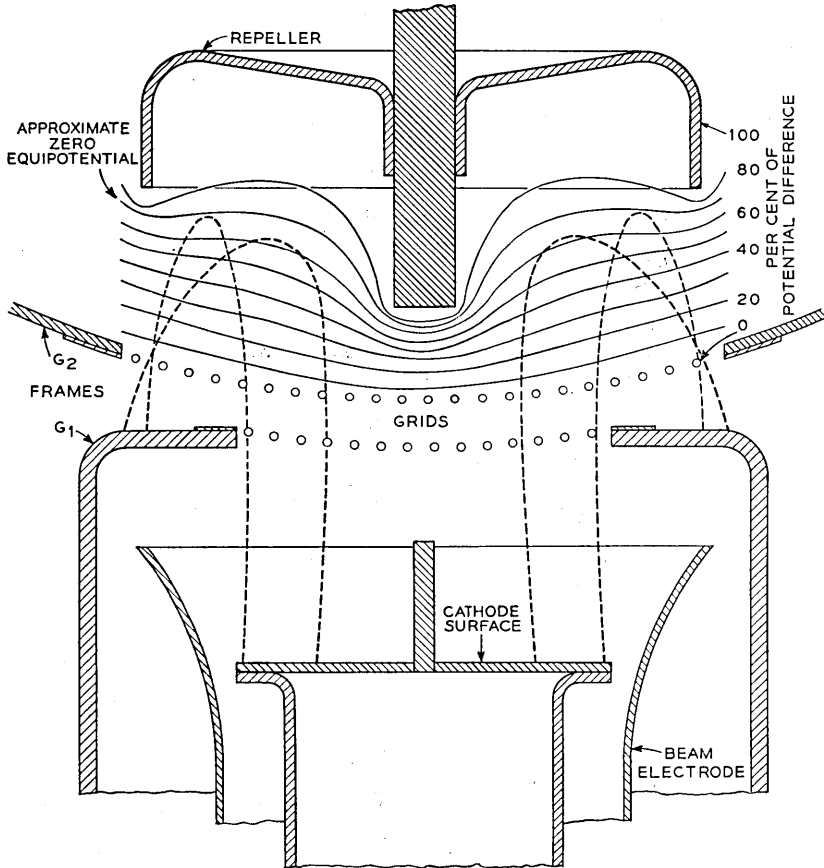


Fig. 65.—Repeller design for eliminating hysteresis in a reflex oscillator. The electrons make only two transits through the gap. The repeller does not return them to the cathode region but to the edge supporting one of the grids of the gap. Equipotentials determined from an electrolytic trough investigation are shown and the electron trajectories computed from these equipotentials.

transit angle deviates from the optimum by a small angle  $\Delta\theta$  varies as  $\cos \Delta\theta$ , so that even for spreads in angle as great as  $\pm 30^\circ$  the effect is not serious.

The design illustrated in Fig. 64 was strikingly effective in reducing hysteresis. Fig. 66 shows repeller characteristics for the original design which was extrapolated from the 723A/B and for the design of Fig. 64.

In addition to improving the electronic tuning characteristics the design was found to be more stable against variations in load, as would be expected from the discussion of Section VIII.

The arrangement adopted provided a prototype electron optical system which was used in a whole series of reflex oscillators designed for radar and communication systems. These tubes were the 726A, 726B and 726C, 2K29, 2K22, 2K23 and 2K56.

The output line of these tubes is intended to couple through an adapter to either a coaxial line or a wave guide. In the first case the adapter serves to couple the output line of the tube to the cable, in some instances through

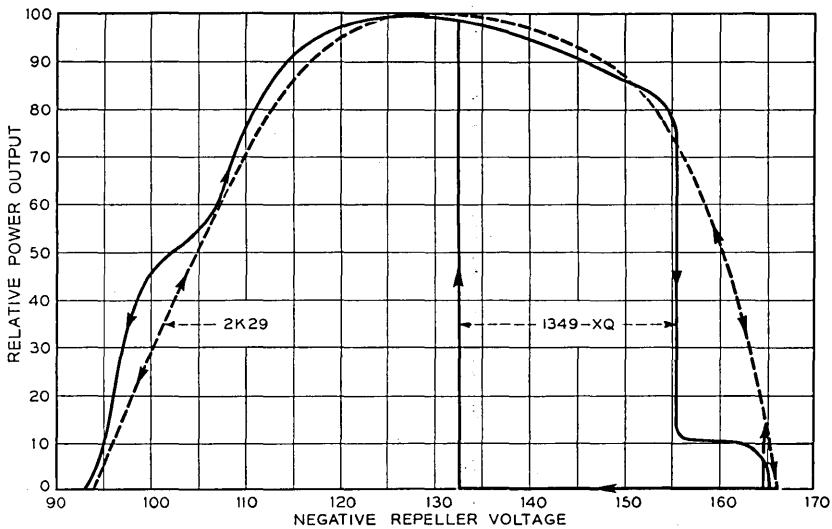


Fig. 66.—Use of the electron optical system shown in Fig. 65 eliminated the bad features of the repeller characteristics of the earlier 1349XQ in which the electrons were returned to the repeller region and gave the repeller characteristic of the final 2K29 (dashed line).

an impedance transformer and in some instances directly. As practice developed it became standard to design for optimum oscillator output characteristics with output line coupled to a 50 ohm resistive impedance. In the second case the adapter serves to couple the tube output line to the guide through a transducer.

A typical example of a reflex oscillator incorporating this construction is the 2K29. This tube is intended to cover the frequency range from 3400 to 3960 Mc/s. An external view of this tube is shown in Fig. 67. It will be observed that the center conductor of the output line extends beyond the polystyrene supporting bushing. Fig. 68 shows an adapting fitting which

permits the oscillator to be coupled to a fifty ohm coaxial cable. The center conductor of the tube output line projects into the split chuck, while contact is made to the outer conductor of the tube output line by the spring contact fingers *F*. The coupling unit can be mounted in a standard octal socket so that the tube can be coupled simultaneously to the power supplies and the high frequency circuit by a simple plug in operation. It is frequently desirable to insulate the outer conductor of the oscillator from

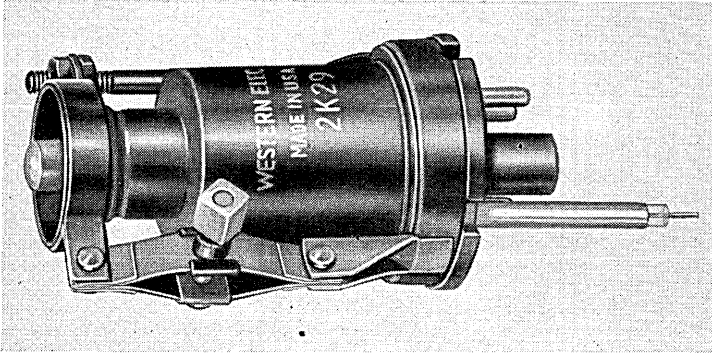


Fig. 67.—Metal reflex oscillator with enclosed resonator designed for operation from 3400 to 3960 mc/s.

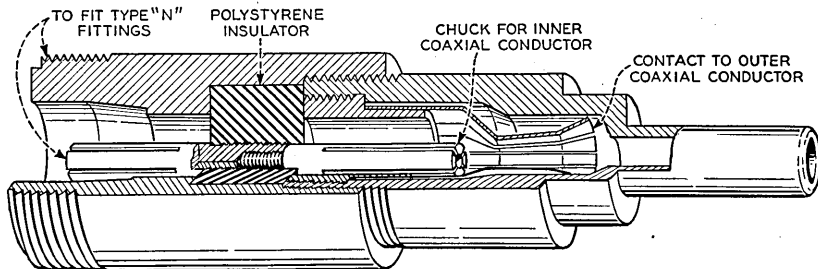


Fig. 68.—A transducer for connecting the output lead of the 2K29 to a 50 ohm cable.

the line for direct voltages while maintaining the high frequency contact. This can be accomplished with either an insulating sleeve of low capacitance or a modification of the design which incorporates a high frequency trap in the outer conductor. In some instances it is necessary to insulate the center conductor of the tube from the line for direct voltages. This can be done with a concentric condenser. The characteristic impedance of the section of the coupler may be made the same as that of the line by maintaining the proper ratio of the diameters of the condenser and the outer

conductor or may be arranged so that the condenser serves simultaneously as an impedance transformer to transform the impedance of the line to that required for best performance of the oscillator. A general discussion of the problems involved in such coupling designs will be given in a later section.

One of the primary considerations in the design of a reflex oscillator is the choice of resonator characteristics. The various controlling factors have been outlined in previous sections. In Section X it was shown that the power output and the electronic tuning optimize at different gap transit

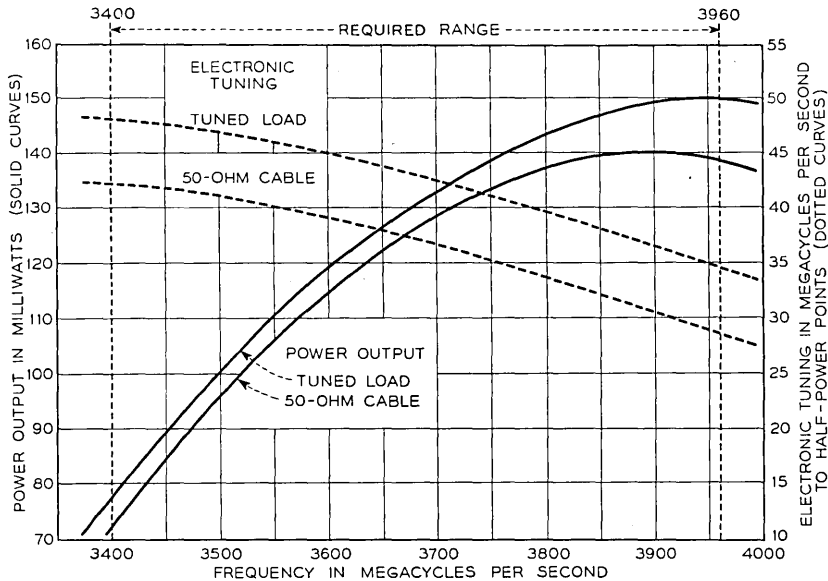


Fig. 69.—Power output and electronic tuning vs frequency for the 2K29 reflex oscillator. The solid lines give the performance into a load adjusted for optimum power output at each frequency. The dashed lines show the performance obtained when the tube is coupled to a 50 ohm load by means of the fitting of Fig. 68.

angles. It is therefore necessary to compromise with the ultimate use in mind. In a beating oscillator for a radar receiver, uniformity of the electronic tuning is of greater importance than uniformity of power output, since an adjustment of the coupling to the crystal permits some variation of the latter quantity. Hence, the resonator characteristics are chosen to provide as nearly uniform electronic tuning as possible. Fig. 69 shows the electronic tuning and power output characteristics for the Western Electric 2K29 tube. These are shown for two conditions. The solid lines show the power output and electronic tuning measured into an adjustable load which

made it possible to present to the oscillator at each frequency the admittance into which the oscillator delivered maximum power output. The solid lines show the power output and electronic tuning over the band with the oscillator connected to a load presenting a resistive 50 ohm impedance to the coupling unit of Fig. 68. The problems involved in obtaining such performance will be outlined in the next section.

#### *E. Broad-Band Reflex Oscillators—The 2K25*

As experience with the design of radar systems and components developed and as a better understanding of the operation and limitations of the individual components was achieved, a great deal of effort was directed toward simplifying and making more reliable the number of adjustments required to optimize the performance of a system. As an illustration of this problem as related to the beating oscillator, the development problem of the 2K25 will be described. As the number of radar systems in the three centimeter range increased it became apparent that to avoid self-jamming it would be desirable to assign frequencies to various sets operating, for example, in a fleet unit. Secondly, the over-all band of the three centimeter range was widened to cover from 8500 to 9660 Mc/s. Prior to this the 723A/B had been essentially a spot frequency oscillator and had been primarily tested as such. As was so frequently the case with tubes for military requirements, it was desired that the ultimate tube be interchangeable with an existing tube, in this case the 723A/B, and hence the improvements had to be effected within its framework.

Changes in the electronic design from that of the 723A/B produced an improved performance in the 2K25. These were a modification of the electron gun which increased the effectiveness of the electron stream and the elimination of a resonance of the region containing the electron gun which coupled with the resonant cavity and in some cases impaired the performance over the wide band. Beyond this the problem concerned the determination of an output coupling system which would provide the desired properties. This will be described in detail.

One of the most serious difficulties which occurred in early radar receivers arose from the general failure to appreciate the effect of the load impedance on the performance of an oscillator. This problem has been discussed in Section IX. In early radar receivers the method of coupling the beating oscillator to the crystal was dictated mainly by mechanical convenience rather than electrical considerations, and as a result most of the discontinuities of performance due to bad load conditions which are discussed in Section IX occurred at one time or another in most of the systems. For instance, users were much surprised to find that a beating oscillator which could be tuned to frequencies both above and below that required for

reception of the signal might yet fail to oscillate at the desired frequency. The convenience of simple replaceability of the local oscillator became in this instance a cross for its designer, since an exchange of tube would frequently eliminate the effect. This led to the obvious conclusion on the part of the user that the oscillator was defective, in spite of the fact that the presumably defective tube had passed the test specifications and would operate satisfactorily in some other receiver. The plain fact, in the light of later knowledge, was that the tubes were being improperly used, so that the usual range of manufacturing variations was not tolerable.

The appreciation of this fact led to a new approach to the problem of coupling the beating oscillator to a waveguide. In early designs the oscillator was decoupled from the load by withdrawing the probe from the waveguide. This presented the oscillator with an uncontrolled admittance with disastrous results in many cases. The new approach, proposed by the group working with Dr. H. T. Friis at the Bell Telephone Laboratories, was that of designing the receiver so that the beating oscillator could be operated into an essentially fixed impedance. The crystal was in this case loosely coupled to form a part of this load, so that variations in its impedance and the impedance looking toward the TR tube were largely masked. A great many further refinements in the design of the receiver have since been proposed, but this basic principle of defining the load into which the oscillator is required to operate is fundamental to all. In the interests of simplicity of use it appeared to be desirable to endeavor to pre-plumb the coupling of the oscillator to the wave guide. The tube designer in this instance found himself perforce, as so frequently occurs in dealing with micro-waves, a circuit designer—an instructive and illuminating experience which might happily be reversed.

The wave guide coupling was made separate from the tube, both to preserve the plug in feature of the tube and to maintain its interchangeability with the 723A/B. As a further simplification it was desired that the coupling should require no adjustments. A convenient fixed load admittance to present to this coupler is the characteristic admittance of the wave guide, since this can readily be maintained fixed over a wide band. The problem, then, is the apparently straightforward one of transforming the guide admittance to the admittance which the oscillator requires for optimum performance. Actually, the problem is complicated by the fact that the optimum admittance will vary throughout the band. The electronic admittance varies with frequency even for a fixed drift angle, because the modulation coefficient of the gap varies as the oscillator is tuned. The losses of the resonator also vary with frequency, both because of skin effect, the depth of penetration of the high frequency currents changing with frequency, and because the circulating currents in the resonator are a function



of the effective capacitance of the gap. As the capacitance increases in tuning to lower frequencies the  $I^2R$  losses therefore increase.

The objective of the coupling design may not be to obtain maximum power output at all points in the band but rather to obtain uniformity of electronic tuning and power output. An additional requirement in some cases is that a minimum sink margin as defined in section VIII should be maintained. This is equivalent to the problem arising in magnetron design of controlling the pulling figure.<sup>13</sup>

In designing an appropriate wave guide coupling a number of variables are at one's disposal. In the case of the W.E. 2K25 the variables available are, the length of the tube probe exposed within the guide, the offset of the probe from the axis of the guide, and the distance from the probe to the shorting piston in the guide. In addition, the characteristics of the output line of the tube are adjustable, and, finally, the coupling of the loop to the resonator can be adjusted. As one might expect, there is a large number of solutions with so many variables available. The most desirable solution is one which provides a low standing wave ratio in all parts of the coupling system. The method employed in the present case was to design a wave guide to coaxial transducer which would provide a smooth broad band transition from the wave guide characteristic admittance to the admittance of the coaxial line. In the ideal case, the characteristic admittance of the coaxial line to the loop should be maintained as uniform as possible. Structural considerations in the present case led to discontinuities which had to be appropriately balanced in the final transducer. Dr. W. E. Kock of the Bell Telephone Laboratories has given an expression which, for thin probes, relates the probe length, the offset and the distance of the backing piston when given the characteristic admittance of the coaxial line and the dimensions of the guide between which a match is required. Once such a transducer has been obtained, the admittances which must be presented to it in order to obtain maximum power from the oscillator are measured over the band. From such measurements it is then possible to determine the corrections in the loop size and in the transducer to obtain a given sink margin throughout the band. This last step actually involves a certain amount of cut and try in an effort to obtain satisfactory performance in all respects. Figure 70 illustrates the transducer developed for the W.E. 2K25 oscillator for use with 1" by  $\frac{1}{2}$ " wave guide. All tests made on this tube are specified in terms of operation in this coupler and with a load having the characteristic impedance of the 1" x  $\frac{1}{2}$ " guide presented to the coupler.

Figure 71 shows a performance diagram for a typical W.E. 2K25 oscillator operating in the coupler of Fig. 70. The reference plane for the diagram is

<sup>13</sup> J. B. Fisk, H. D. Hagstrum and P. L. Hartman, "The Magnetron as a Generator of Centimeter Waves", B. S. T. J. Vol. XXV No. 2, pp. 167-348 (April, 1946).

not the plane of the grids of the oscillator but is instead a more accessible reference plane external to the tube, in this instance the plane through the wave guide perpendicular to its axis which includes the tube probe. It will be observed that the sink margin in the case illustrated was equal to 5.5. At the frequency at which this diagram was obtained, the minimum sink margin permitted by the test specification is 2.5. The variation in this margin results from a variety of causes. As shown in Section III the sink margin is determined by the ratio of the total load conductance to the small signal electronic conductance. The total load conductance consists of the

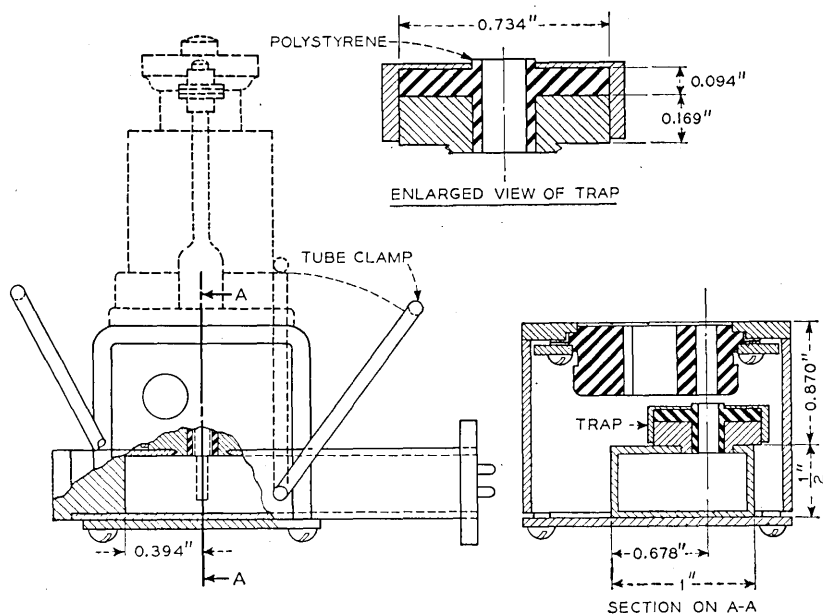


Fig. 70.—A broad band coupling designed to connect the 2K25 to a  $1" \times \frac{1}{2}"$  wave guide

conductance representing the resonator losses and the conductance arising from the wave guide load transformed through the coupling system. Hence, the coupled load will be subject to variations in the loop dimensions, the characteristics of the coupling line and the transducer. The resonator loss will differ from tube to tube because of the variation in the heating of the grids and resonator by the electron stream, and there will be variations arising from other causes. The electronic conductance varies from tube to tube primarily because of the spread in beam current and secondarily as a result of such factors as variations in the modulation coefficient of the gaps, non-uniformities in the drift space causing a spread in the transit time and

the like. The sum total of these variations necessitated the maintenance of an average sink margin of 6.7 times in order to insure a minimum of 2.5.

Figure 72 illustrates further characteristics of the 2K25 oscillator and coupling. These data are the results of standing wave measurements looking towards the coupler with the tube inoperative. From such "cold test"

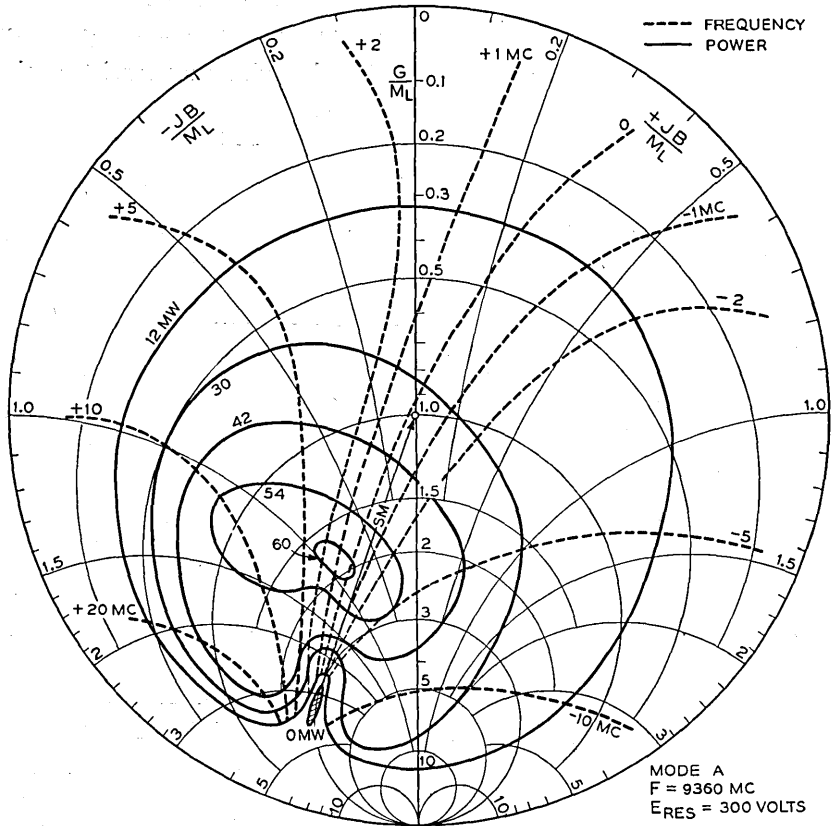


Fig. 71.—A Rieke diagram for the 2K25 connected to the load by the coupling of Fig. 70. This diagram was obtained for a repeller mode having a drift angle of  $15.5 \pi$  radians at a nominal frequency of 9360 mc/s.

measurements one may determine the intrinsic  $Q_0$  of the resonator and the external  $Q_E$ . The former is a measure of the resonator losses while the latter is a measure of the tightness of coupling of the oscillator to the load. The values of  $Q_0$  measured from a cold test have little significance in an oscillator in which heating of the resonator and especially of the grids is appreciable. This is particularly true of oscillators tuned by variation of

the capacitance of the interaction gap. It is possible to make hot tests in which the thermal conditions of operation are established without the interaction effects of the beam, but these measurements are not available for the 2K25. The external  $Q_E$  is not affected, at least to a first order, by thermal effects in the resonator. The third curve of Fig. 72 shows the ratio of the power delivered when a matched load is coupled to the coupler to the power delivered to a load which presents optimum impedance to the oscil-

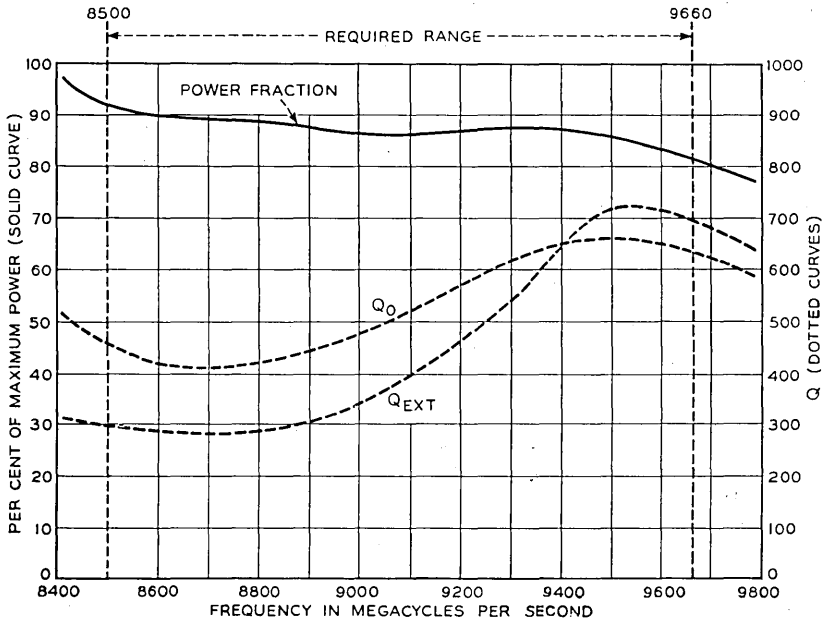


Fig. 72.—Variation of the percentage of maximum power output delivered, unloaded  $Q$ ,  $Q_0$ , and external  $Q$ ,  $Q_E$ , as functions of frequency for the 2K25 when coupled to the characteristic admittance of the  $1'' \times \frac{1}{2}''$  guide with the coupling of Fig. 70. The power variation is for a mode having  $15.5 \pi$  radians drift.

lator. These data are given for the normal operating repeller mode as discussed below.

It was pointed out early in this work that the available power output and electronic tuning have a contrary variation with respect to the number of cycles of drift in the repeller space. Consequently, this is one of the most important and exasperating parameters of the tube. Fig. 73 is a diagram illustrating the characteristics of a typical W.E. 2K25 oscillator. The abscissa is the repeller-cathode voltage which, for a fixed resonator voltage, determines the drift angle. Thus, as this voltage is made increasingly negative, successive modes of oscillation appear, corresponding to consecu-

tive decreasing values of  $n$ . Our best determination for the value of  $n$  for each mode is given. The base lines are displaced vertically on a uniform wavelength scale, so that the variation of repeller voltage with wavelength is indicated. The power output increases with decreasing values of  $n$  but the half power electronic tuning for each repeller mode has a contrary variation. The repeller mode chosen as providing the best compromise between power output and half power electronic tuning is the  $7\frac{3}{4}$  cycle mode. The design of the coupling unit and all the primary characteristics of the tube are based on the use of this mode. It will be observed that repeller

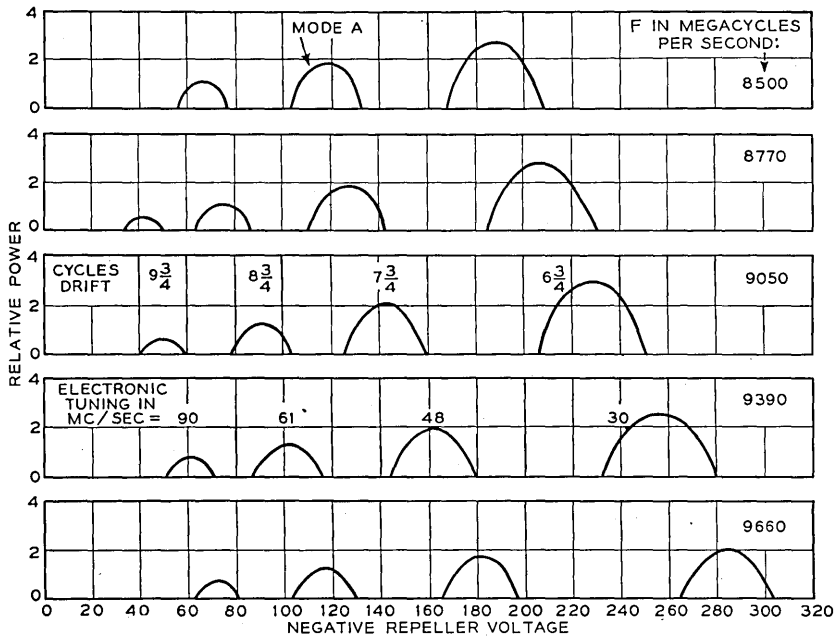


Fig. 73.—Operation of the 2K25 in various repeller modes and at various frequencies when connected to characteristic admittance of a  $1'' \times \frac{1}{2}''$  guide by the coupling of Fig. 70.

modes having  $n$  values less than 6 do not appear in Fig. 73. For values of  $n = 0, 1, 2$  and possibly 3, this is because the conductance representing the resonator losses is in excess of the electronic conductance. For the values of  $n = 4$  and 5 the coupled load conductance plus the resonator loss conductance in the specified transducer are in excess of the electronic conductance. Conversely for modes having  $n$  values in excess of 7 the coupling is weaker than desired.

Fig. 74 illustrates the broad band characteristics for a typical W.E. 2K25 tube operating in the coupling of Fig. 70 into a matched load. In Fig. 74

are shown the power output, half power electronic tuning, and sink margin as functions of frequency for the  $7\frac{3}{4}$  cycle mode.

#### F. Thermally Tuned Reflex Oscillators—The 2K45

The trend toward the simplification of radar systems to the fewest possible adjustments, coupled with the ever present possibility of enemy jamming, led to the attempt to produce a system which was described as a single knob system. The ultimate objective of such a system was ability to shift the frequency of the transmitter at will with a single control. This puts the chief burden on the receiver, which must automatically track with the

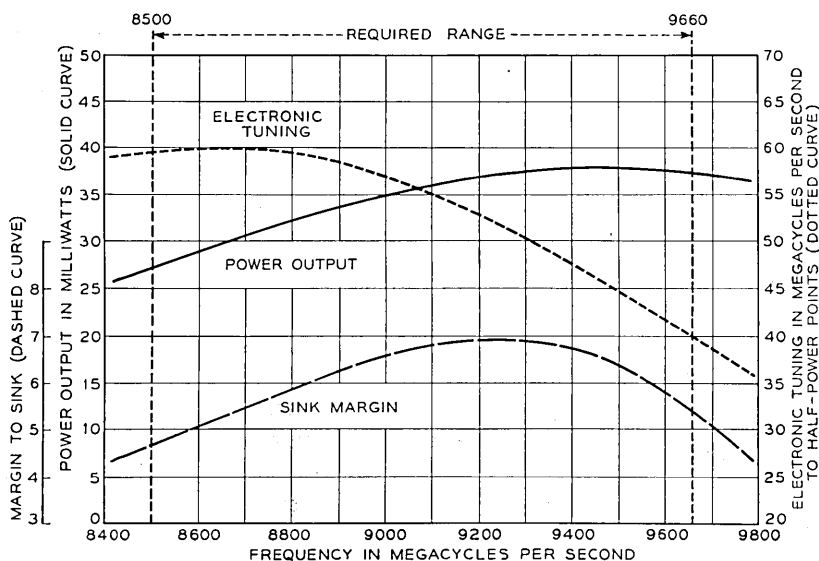


Fig. 74.—Variation of electronic tuning, power output and sink margin with frequency for the 2K25 in a repeller mode having  $15.5\pi$  radians drift. Characteristic admittance load and coupling of Fig. 70.

transmitter. The problem is much simplified by designing as many of the components as possible so that retuning is not required when the frequency is shifted within the requisite band. In the case of the beating oscillator it was necessary to devise a mechanism which would permit rapid automatic control over a frequency range of 1160 mc. This range was many times in excess of any immediately realizable electronic tuning range. It is of course apparent that such a method of tuning will also lend itself readily to use in many applications in which, although the transmitter frequency is nominally fixed, the system is required to operate under such extreme conditions that the sum total of the possible frequency deviations is in excess of the available

electronic tuning range. Examples of such systems are installations in high altitude air craft, in which wide variations in temperature and pressure may be expected.

It was highly desirable to have the frequency control electrical. One means of obtaining such a control is through motion of the resonator grids produced by the thermal expansion of an element heated electrically. A step in this direction was taken in the Sperry Gyroscope Company 2K21 oscillator in which the resonator was tuned by the thermal expansion of a strut heated by passing a considerable current through it.

At the Bell Telephone Laboratories the design for a thermally tuned beating oscillator was based on a method which permitted the control of a small current at a high voltage. In general, controlled high voltages are easily available both from power supplies and from control circuits. Further, it seemed desirable that the control of the heating should require no power. These considerations suggested that the heating of the thermal tuning element be accomplished by electron bombardment. Through the use of a negative grid to regulate the bombardment, the tuning control became a pure voltage adjustment. The bombardment method made it possible to utilize configurations in the tuner which would have been less practical if resistance heating had been employed.

An early reflex oscillator incorporating these ideas was the Western Electric 2K45 vacuum tube. Fig. 75 shows an external view of the tube which, except for the output coaxial line, looks like a forshortened 6L6 vacuum tube. The plug-in feature of the earlier mechanically tuned oscillators was maintained in this oscillator, which was designed to couple to the waveguide circuit through the same transducer developed for the 2K25.

Figures 76 and 77 are cross-sectional views of the 2K45 made at right angles to each other. The thermal tuning mechanism is contained in the upper part of the structure. It is a bimetallic combination consisting of a U shaped channel and a multi-leaf bow. The channel is formed of a material with a large coefficient of expansion and a high resistance to slow permanent deformation or creep at elevated temperatures. At the ends of this channel, tabs bent down at right angles to the channel axis, provide rigid vertical support for the channel without interfering with axial expansion. These tabs are connected to the resonator, which in turn is supported by the vacuum envelope as closely as possible in order to minimize the thermal impedance of the path. This connection also serves to cool the channel ends. The multi-leaf bow is welded to the channel at its end. The leaves are made of a material having a low coefficient of expansion and, as they are fastened to the channel at its ends, they remain cool and do not expand appreciably as the channel is heated. The purpose of the multi-leaf con-

struction of the bow is to reduce the internal stresses produced by bending during the tuning action.

A cathode, control grid and a pair of focussing wires are supported by micas in a position facing the open side of the U channel. The channel serves as an anode for the cathode current, which is controlled by the grid. The focussing wires beam the cathode current into the anode. The grid is proportioned so that under all operating conditions it remains negative, and the control system need supply no power to it.

The heating of the channel by the electron bombardment causes it to expand with a large differential with respect to the bow. As a result the bow flattens out and its center moves toward the channel. The purpose of this construction is to provide a magnification of the expansion of the

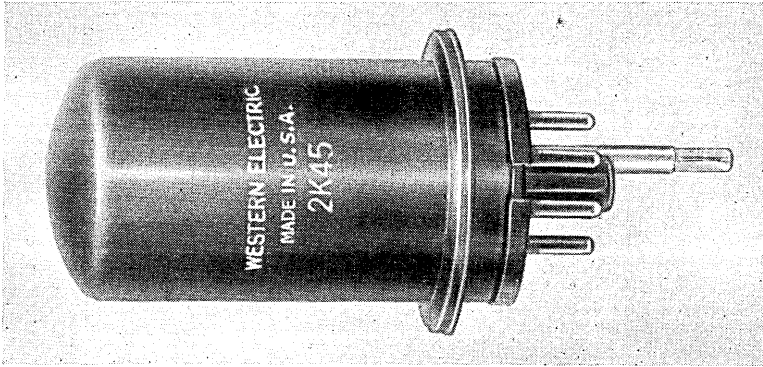


Fig. 75.—An external view of the W.E. 2K45—an early thermally tuned reflex oscillator designed by the Bell Telephone Laboratories.

channel which by itself would provide insufficient motion. The cross member welded to the center of the bow and the vertical struts transmit the motion of the bow to the diaphragm which supports one of the cavity grids. The action is illustrated in Fig. 78 which shows a series of X-ray views of an operating tube. Thus, the first view shows the conditions for no power applied to the tube, the second, for the tube operating but with the tuner grid biased to cut-off. The following views show the behavior with progressive increases in the power into the tuner channel.

The ramifications in the design of a thermal tuner are many and the possible configurations of the mechanism will depend greatly on the individual requirements of the application. It is possible, however, to lay down some basic principles. These are concerned with positiveness of action and speed of tuning. With regard to the first, it may seem anomalous to speak of



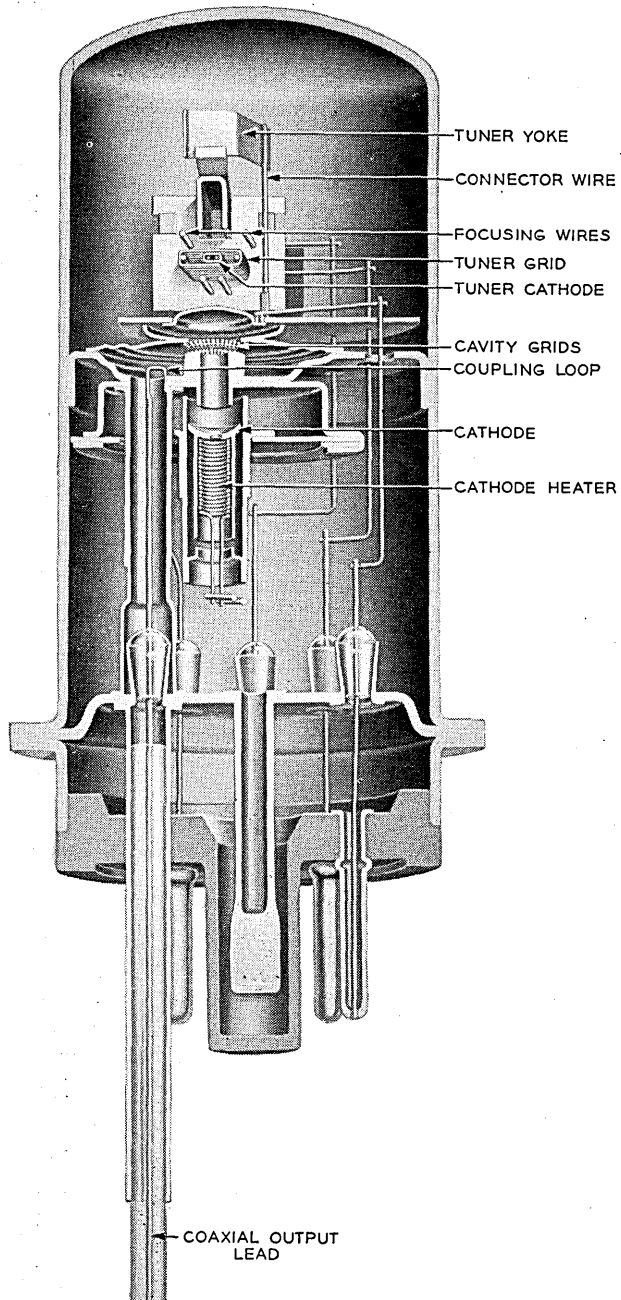


Fig. 76.—Internal features of the W.E. 2K45: section through the output lead and normal to the tuner cathode and strut.

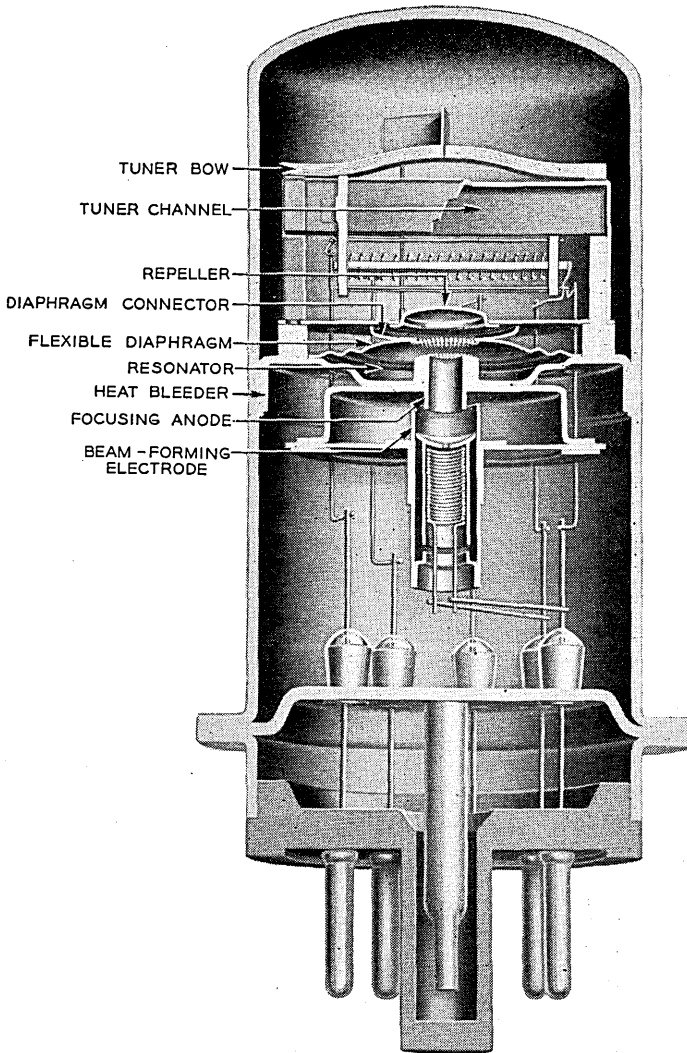


Fig. 77.—A section of the W.E. 2K45 cut parallel to the tuner cathode and strut.

positive action in a device which has thermal inertia. What is actually meant, however, may be best indicated by the following: Let us suppose that some power,  $P_a$ , must be dissipated in the tuner in order to hold the oscillator at a frequency,  $f_a$ . Now, suppose that the tube is operating with power less than  $P_a$  and that we are required to switch to frequency  $f_a$ . In order to switch rapidly, we apply power in excess of  $P_a$  to the tuner until the frequency has reached  $f_a$ , at which time we switch to the power  $P_a$  required

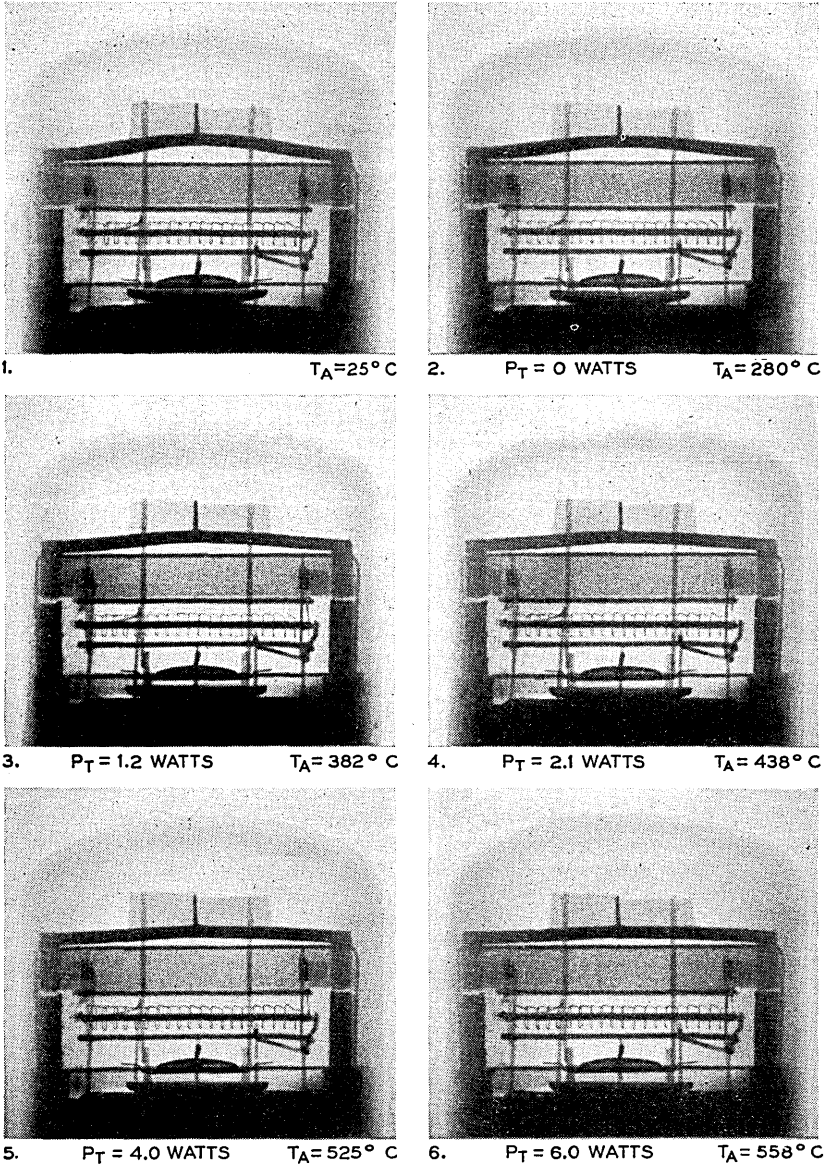


Fig. 78.—A series of x-ray photographs of the thermal tuning mechanism of an operating 2K45. These show the motion of the bows for successively increasing power inputs to the tuner channel.

to sustain  $f_a$ . We say that the control is positive if no overshoot occurs, i.e., if the frequency does not continue to change for a time and then return to

$f_a$ . We might equally well have illustrated this by an example in which the tuner was cooling. In order to avoid overshoot it is necessary that no thermal impedance exist between the heat source and the expanding element. Thus, as an example of a tuner in which overshoot will occur, one may cite an expanding strut in the form of a tube heated by a resistance heater internal to the tube. In order to transfer heat from the resistance heater to the tubing the former must of necessity operate at the higher temperature. Hence, in the example given above, when the power is switched to the sustaining value heat will continue to be transferred to the tubing until the heater and the tubing arrive at the same temperature. To minimize the thermal impedance the heat should be generated within the body of, or on the surface of, the expanding element. The resistance heating by current passing through the expanding element illustrates the first case and heating by electron bombardment the second.

The second principle is quite obvious when once stated. If a rapid shift in frequency is to be obtained at any point within the required tuning range, then the potential tuning range must be considerably in excess of that required. Thus, if the tube is operating near one of the required frequency limits and one demands that it go to the limit, the shift will progress very slowly in the absence of excess range. If, however, it is possible to overdrive the limit, the time required will be materially shortened. On the basis of actual tube design this requires that the safe maximum or full on power into the tuner must be considerably in excess of the power required to hold the tuner at the frequency band limit nearest the full on condition. The tuning mechanism must be capable of continuous operation under the full on condition in case this accidentally persists. Further, the power required to hold the tuner at the other end of its band must be considerably in excess of zero in order that rapid cooling may occur near this limit. It is not necessary that the tuner produce motion for power inputs outside the band limits; the essential condition is that the rates of heating and cooling near these limits should have values considerably greater than zero.

It is always possible to purchase heating speed by the expenditure of power in available over-drive. The cooling speed, on the other hand, is controlled by the temperature difference between the source and sink, the heat capacity of the tuner and the mechanism of cooling. Two methods of cooling are available, conduction and radiation. For small amounts of motion and in circumstances where large forces are not required, conduction cooling can provide a satisfactory answer. In cases in which a large amount of motion is required, as in the 2K45, conduction cooling imposes a number of serious restrictions. The expanding element must be made from a material having a large coefficient of expansion and necessarily must be long. Unfortunately, alloys having large expansion coefficients are very poor con-

ductors of heat. In the case of conduction the cooling rate will depend on the ratio of the length times the heat capacity divided by the cross-section. For radiation cooling the rate depends on the heat capacity divided by the radiating area and is independent of the length except as the heat capacity depends upon this factor. Radiation cooling has the advantage that it permits more freedom of structural shape and the material may be chosen on the basis of strength. In the operating range of the 2K45 the heat radiated is approximately four times that conducted away.

The automatic frequency control circuits which have been used with thermally tuned beating oscillators in radar receivers have been of a full on or off type so that they do not continuously hold the frequency at a fixed reference difference from the transmitter frequency. The reason for this in part is that a pulse transmitter gives the required reference information only during the pulse. Thus with an on-off control circuit if at a given pulse a correction of frequency is demanded the power into the tuner is turned full on or off, depending on the direction of the correction, and left in this condition until the occurrence of the next pulse which again determines the direction of the control. The result is that the frequency of the beating oscillator continually hunts about the transmitter frequency. The control system must be designed to hold the hunting deviation within tolerable limits. It is of course possible to work within narrower limits than full on or off tuner power. One advantage of full on or off control is that it results in the minimum tuning time between required frequencies since the tuning rate is at all times held to the maximum possible value.

Under certain conditions the performance of a thermal tuner may be completely described by a time constant. In general, however, this is not the case and the information required in designing a control system is concerned first with initiation of operation and second with the factors determining the magnitude of the hunting deviation. For initiation of operation, one is concerned with the time required for the oscillator to reach the operating frequency. The quantities known as the cycling times give upper limits for this quantity. The cycling times are to a certain extent arbitrarily defined as indicated in the following. There are two band limit frequencies,  $f_c$ , the limit requiring the lesser power input,  $P_c$ , and corresponding to a tuner temperature,  $T_c$ , and  $f_h$ , the limit for which the power input will be  $P_h$ , and the temperature,  $T_h$ . The cycling time for heating,  $\tau_h$ , is defined and measured in the following manner. The power input to the tuner is set to  $P_c$  and held at this value until equilibrium is established. The power input is then switched to the maximum allowed value,  $P_m$  and the time interval,  $\tau_h$ , between the instant of switching and the instant at which the frequency of operation has reached  $f_h$  is measured. Correspondingly, the cycling time  $\tau_c$  for cooling is measured by setting to  $P_h$  until equilibrium is

established and then switching the tuner power off and measuring the interval,  $\tau_c$ , until the operating frequency reaches  $f_c$ . These quantities are of importance in determining the "Out of Operation" time in case the frequency reference of the control system is momentarily lost, so that the control starts cycling in order to re-establish the reference.

While the cycling times can be taken to give an indication of the average speed of tuning, more detailed information is required to determine the hunting deviation. This demands a knowledge of the instantaneous tuning rates which will result at any point in the band when the power is switched full on or off. These rates vary through the band since the overdrive available, for example, on heating will decrease as the operating frequency approaches the limit nearest to the maximum drive.

In the following, an outline will be given of the factors which must be considered in designing a thermally tuned reflex oscillator. The 2K45 will be used as an illustration. Our first consideration concerns the time required for the tuner to heat and cool between given temperatures. In Appendix XI expressions are derived for the cycling times  $\tau_h$  and  $\tau_c$ . The expressions applicable to the 2K45 are:

$$\tau_h = \frac{CT_m}{2KT_m^4} [F_1(T_{rh}) - F_1(T_{rc})] \quad (13.1)$$

$$\tau_c = \frac{CT_0}{2KT_0^4} [F_2(T_{sc}) - F_2(T_{sh})] \quad (13.2)$$

where the symbols are defined in the appendix. The functions  $F_1$  and  $F_2$  are plotted in terms of the reduced temperatures,  $T_r$  and  $T_s$  in Figs. 79 and 80. In the analysis conduction cooling is neglected and it is assumed that the whole of the expanding element operates at the same temperature. Because of these limitations the theory is largely qualitative. It will be observed that the cycling time,  $\tau_h$ , is proportional to the ratio of the heat energy stored in the tuner at the maximum equilibrium temperature to the rate of loss of energy at this temperature. It is therefore apparent that this equilibrium temperature should have the maximum possible value, and also that the heat capacity of the tuner should be kept to a minimum. Assuming for simplicity that the frequency of oscillation is proportional to the temperature, so that a given temperature difference is proportional to the frequency, one sees by examining the function  $F_1$  that it is desirable to keep the reduced temperatures  $T_{rh}$  and  $T_{rc}$  small compared to 1. Under these circumstances, the cycling time  $\tau_h$  will have its minimum value and will be more or less independent of the reduced temperatures. If we examine the expression for the cycling time for cooling,  $\tau_c$ , we observe that this is proportional to the ratio of the heat stored in the tuner at the equilibrium

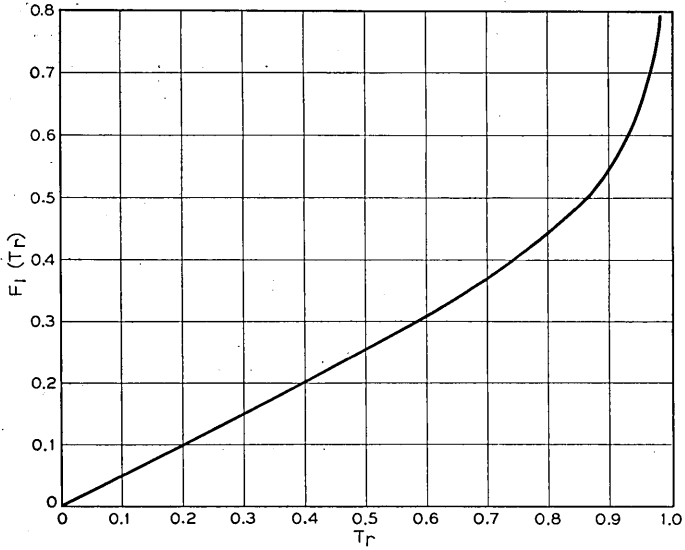


Fig. 79.—A plot of a function used in determining the time required for the temperature of a thermal tuner to rise between two given values when the tuner is cooled by radiation alone. The abscissae are given in terms of a reduced temperature.

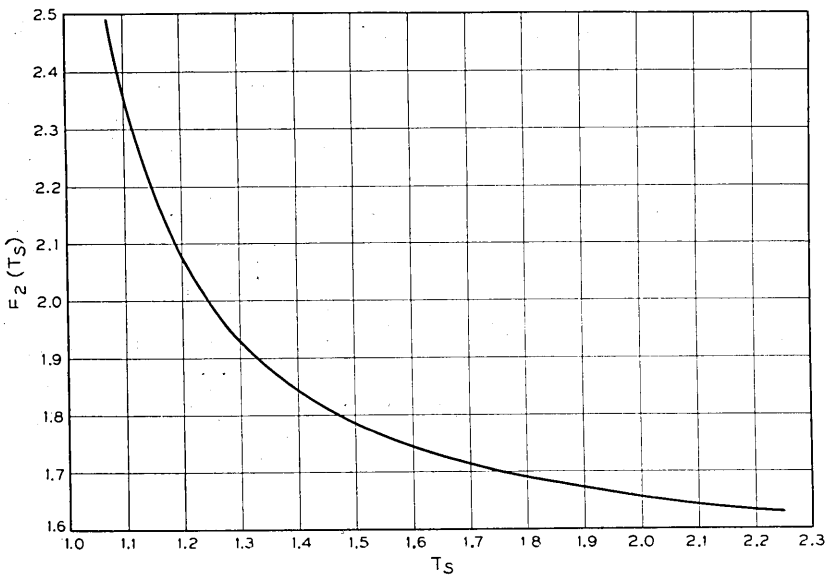


Fig. 80.—A plot of a function used in determining the time required for the temperature of a thermal tuner to fall between two given values when cooled by radiation alone. The abscissae are given in terms of a reduced temperature.

temperature  $T_0$  corresponding to zero bombardment power divided by the rate of heat loss at this temperature. This indicates a rather paradoxical result, that the temperature for zero bombardment power should be as high as possible. This arises from the dependence on radiation cooling. We are limited in setting the value of  $T_0$  by the form of the function  $F_2$ , which requires that the reduced temperatures  $T_{sc}$  and  $T_{st}$  should be very large compared to 1. Since the true temperatures corresponding to these reduced values must simultaneously be small compared to  $T_m$ , it is apparent that we are not completely free to make  $T_0$  large, and a compromise must be worked out.

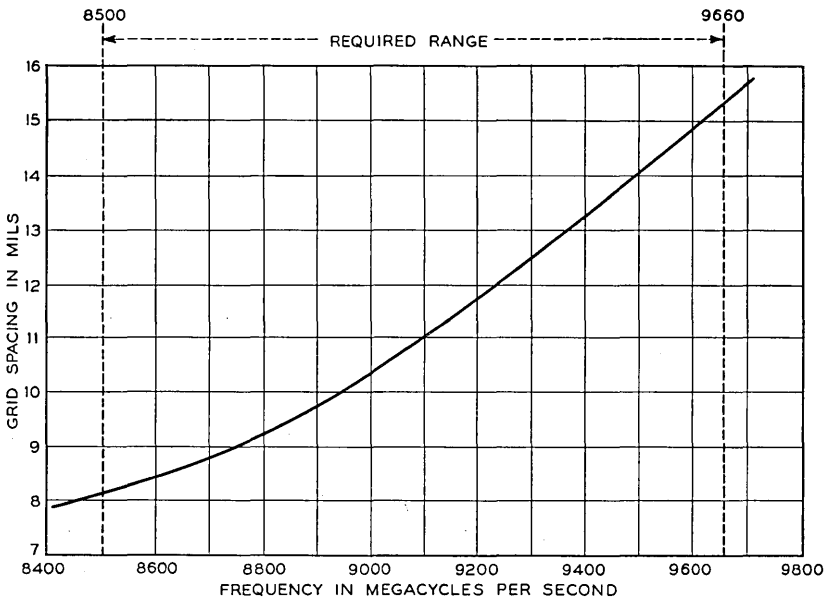


Fig. 81.—Variation of the frequency of resonance vs gap displacement for the W.E. 2K45 resonator. The vertical lines show the required tuning range.

In determining a practical design for a thermal tuner, the first characteristic which must be known is the variation of the resonant frequency of the oscillator cavity as a function of gap displacement. It is apparent that, for the highest speed of tuning, the rate of change of frequency with gap displacement should have the maximum possible value. However, this tuning characteristic is dictated by the performance requirements of the tube as an oscillator and hence is not available as a variable in the design. Fig. 81 shows the variation of frequency with gap displacement for the 2K45 resonator. The required range is indicated.

When the required motion is known a choice may be made of a mechanism



for a tuner. There is a certain amount of arbitrariness in choosing the limiting dimensions of the tuner. If the expanding element is to be short it is necessary either to operate over a very wide range of temperatures or else use some mechanical means of amplifying the motion obtained over a more limited range. Since the more limited is the required temperature range the greater is the tuning speed, it is obviously advantageous to use mechanical amplification. As previously pointed out the electron bombardment method of heating and radiation cooling are especially suitable to such a mechanism because of the freedom of design they permit. Previous dis-

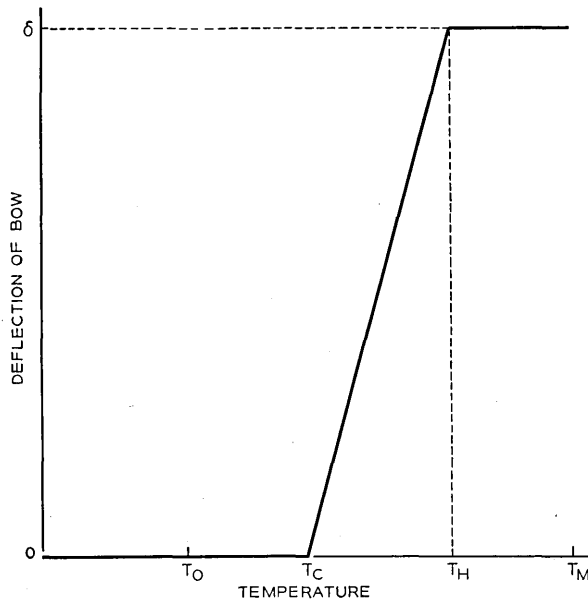


Fig. 82.—The ideal type of deflection vs temperature characteristic desired for a thermally tuned oscillator. The motion  $\delta$  is that required to shift the resonant frequency of the cavity through its required band.

cussion has shown that the temperatures corresponding to zero and maximum power input must be separated by wide margins from the temperatures corresponding to the limits of the tuning range. Any motion which occurs in these margins is unnecessary and in general undesirable. Ideally, the tuning mechanism should have a characteristic as shown in Fig. 82. The type of tuning mechanism chosen for the 2K45 is a first approximation to such a characteristic, as is shown in Fig. 83, which gives a family of characteristics corresponding to various initial offsets of the bow for a given length of bow. The bows are formed to a sinusoidal shape. This structure gives

a large mechanical amplification of the expansion of the tuner. The tuner is made as long as will fit conveniently into the tube envelope. Further arbitrary decisions are required with regard to the power which can be ex-

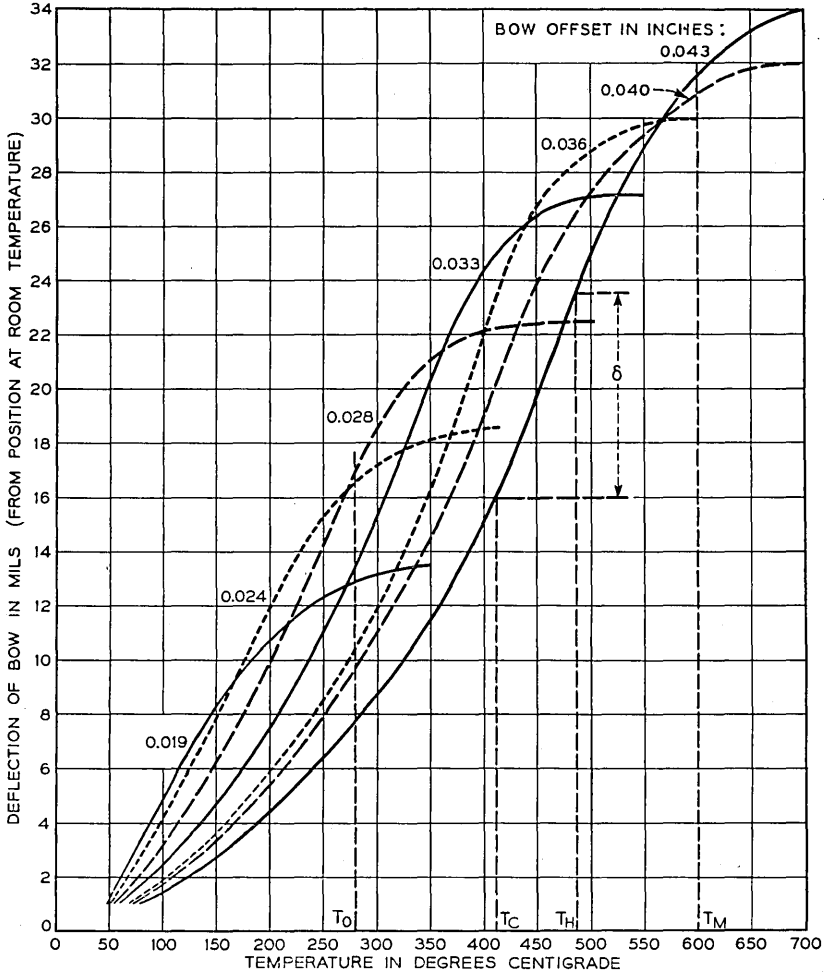


Fig. 83.—A family of deflection vs temperature characteristics for the type of tuning mechanism used in the W.E. 2K45. The parameter is the initial offset of the bows from the channel at room temperature.

pected in operating the tuner. With such decisions made, the tuner design can then be completed as a compromise of a great many variables. Limitations on the strength of the tuner materials at elevated temperatures deter-

mine a maximum safe operating temperature. The anode material is chosen to have a large coefficient of expansion and resistance to "creep" at elevated temperatures. In choosing the form of the tuner it is necessary to keep constantly in mind the necessity of maintaining the minimum ratio of heat capacity to radiating surface. A minimum operating temperature of the tuner is determined by heat flow to it from extraneous sources. Figure 84 shows the temperature as a function of bombardment power input for the 2K45 tuner. It will be observed that the heat from sources other than bombardment produces a considerable rise in temperature. One principal source of uncontrolled heating is radiation from the tuner cathode. This

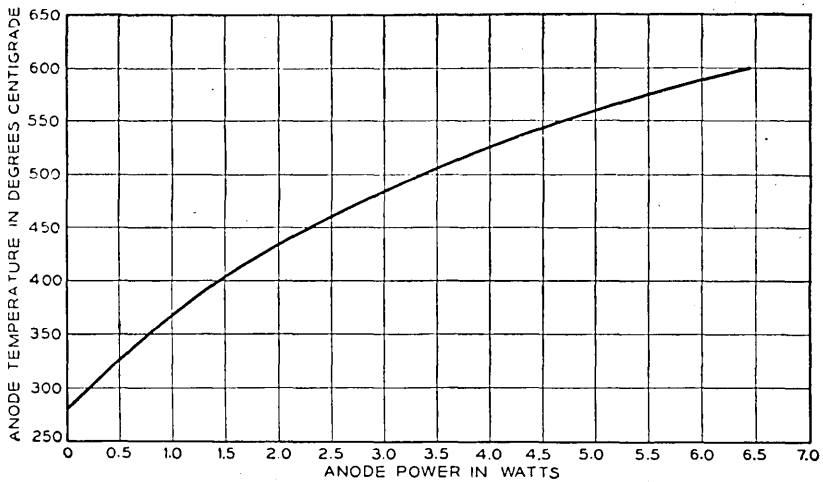


Fig. 84.—The tuner anode temperature as a function of the bombardment power. The temperature rise at zero bombardment power is caused by radiation from the thermal cathode and extraneous sources.

is minimized by keeping the cathode as remote from the anode as is consistent with the required electronic characteristics.

When the maximum and minimum operating temperatures and the length of the channel are determined the remaining problem is to determine and offset for the tuning bow which will provide the optimum tuning characteristics. We wish to obtain characteristics such that the heating time  $\tau_h$  and the cooling time  $\tau_c$  are approximately equal and of a minimum value. The choice of the bow offset also involves a choice of an initial gap spacing for the resonator. On Fig. 83 the boundary values for the limiting temperatures  $T_0$  and  $T_m$  are indicated by vertical lines. With any given bow offset which corresponds to a particular tuning characteristic a limit is set on the initial gap spacing by the requirement that the total motion of the bow between

room temperature and  $T_m$  shall not exceed the initial gap spacing. From our previous analysis we know that to provide maximum tuning speed we desire to make the temperature intervals  $T_c - T_0$  and  $T_m - T_h$  as large as possible. For any given tuning characteristic these intervals may be adjusted by a variation of the initial gap spacing subject to the limitation just

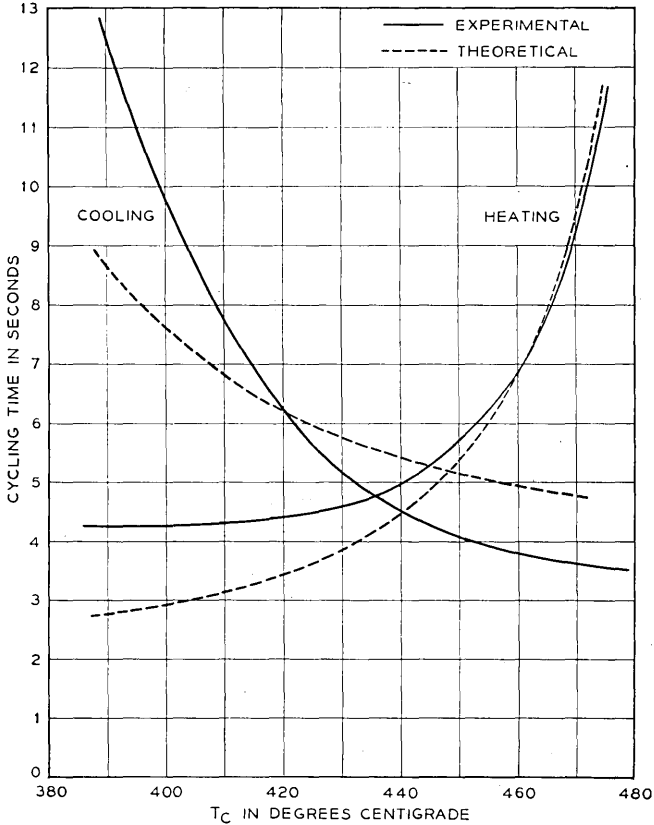


Fig. 85.—The cycling time of the W.E. 2K45 as a function of the temperature of the channel at the band frequency limit requiring the smaller tuner power. The solid lines are the experimental curves, the dashed lines are theoretical results. One point on the heating time is fitted in order to determine the heat capacity of the tuner.

imposed. Since  $T_c$  and  $T_h$  are interrelated for a given bow characteristic by the fact that they correspond to a specific increment of motion  $\delta$  determined by the cavity design, we may study the effect of shifting the interval  $\delta$  along the tuner characteristic by varying the initial gap offset. We may specify this in terms of value of  $T_c$ . The result of such a study is shown in Fig. 85. The optimum offset corresponds to the temperature at which the

curves for  $\tau_b$  and  $\tau_c$  cross over. The optimum bow offset is then the value which provides the minimum value at the crossover. From the theory given earlier it is possible to compute these curves. If we had analytical expressions for the motion of the tuner with temperature and for the variation of frequency with gap spacing it should be possible to obtain completely theoretical curves.

As a test of the theory of heating and cooling it is sufficient to use the experimental curves for the motion of the tuner with temperature and the variation of frequency with gap spacing in conjunction with the heating and cooling curves of Figs. 79 and 80 calculated from equations (13.1) and (13.2). The value of  $K$  which must be determined in order to obtain numerical values from the curves of Figs. 79 and 80 may be determined from Fig. 84 by using the relationship

$$K = \frac{P_a - P_b}{T_a^4 - T_b^4}$$

where  $P_a$  and  $P_b$  are the bombardment power inputs corresponding to anode temperatures  $T_a$  and  $T_b$ . There is no ready means for directly determining the heat capacity  $C$ . However, if one point on either the heating or cooling curves is fitted to the experimental data the value of  $C$  may be determined and the remainder of the points computed. The results of such a computation are shown by the dashed lines in Fig. 85. In view of the restrictive assumptions of a uniform anode temperature and the neglect of all conduction cooling the agreement in general form is reasonably good.

The W.E. 2K45 includes a number of advances in reflex oscillator technique over the 2K25. It will be observed in Figs. 76 and 77 that the electron optical system employed in the gun differs from that used in the 2K25. In the 2K25 a gun producing a rectilinear beam was employed. In the 2K45 the gun consists of a concave cathode surrounded by a cylindrical electrode and a focussing anode. The design of this type of gun was originated by Messrs. A. L. Samuel and A. E. Anderson at these laboratories. The design is such as to produce a radial focus beam which converges into the cylindrical section of the focussing anode. After the beam enters the focussing anode its convergence is decreased by its own space charge, and the beam passes through the grids at approximately the condition of minimum diameter. Between the second grid and the repeller the beam continues to diverge radially on the outbound and return trips. The intention of the design is that the beam shall have diverged sufficiently so that the maximum possible fraction will recross the gap within a ring having an inner diameter equal to the first grid and outer diameter equal to the second grid. Under these conditions only a small fraction of the beam will return into the cathode region, the remainder being captured on the support of the first grid after the

second transit of the gap. This tends to eliminate electronic tuning hysteresis and the repeller characteristic of the 2K45 is essentially free of this phenomenon. This gun design has the further advantage that it avoids the necessity for the first grid used in the 2K25. This eliminates the current interception on this grid with a resulting increase in the effective current crossing the gap. This type of gun also permits the design of a more efficient resonator by reducing the grid losses.

A second variation in design from the 2K25 is that in the 2K45 the second grid moves with reference to the repeller. This has the advantage of reducing the variation of the repeller voltage for optimum power with resonator tuning. The drift angle in a uniform repeller field is given by

$$\theta = \frac{k \sqrt{V_0}}{V_0 + V_R} \ell f \quad (13.3)$$

where  $\ell$  is the spacing between the repeller and the second grid of the resonator. If the same drift angle  $\theta$  is maintained at all frequencies in the band, then the repeller voltage must vary. If  $\ell$  is fixed as  $f$  increases  $V_R$  must also increase in order to maintain a fixed fraction. If  $\ell$  varies and increases as  $f$  decreases then a smaller variation in  $V_R$  is required and in the particular case that  $\ell$  varies inversely with  $f$  the repeller variation may be made zero. Usually other requirements determine the variation of  $\ell$  and it is not always possible to make the variation zero. In the case of the 2K45 the variation over the band is approximately half the amount which would occur if  $\ell$  were fixed.

The output coupling and line of the 2K45 were designed so that the oscillator would provide the desired characteristics in the same waveguide adapter as designed for the 2K25. The power output as a function of frequency for a typical tube is shown in Fig. 86a. Curves A, B and C of Fig. 86 show the variation of power output with cavity tuning when the repeller voltage is set for an optimum at the indicated frequency and held fixed as the cavity tuning is varied. The frequency shift between half power points in this case is very much wider than with repeller tuning. This is a consequence of the fact that whereas in repeller tuning both the frequency and the drift time change in a direction to shift the transit angle away from the value for maximum power, with cavity tuning only the frequency changes. Moreover, the fact that the repeller to second grid spacing in this design varies with frequency tends to reduce the variation of the drift angle with frequency. The envelope of the curves A, B and C gives the power output as a function of frequency when the repeller voltage is adjusted to an optimum at each frequency.

Fig. 86b gives the half power electronic tuning as a function of frequency measured statically and also dynamically with a 60 cycle repeller sweep. The difference arises from thermal effects.

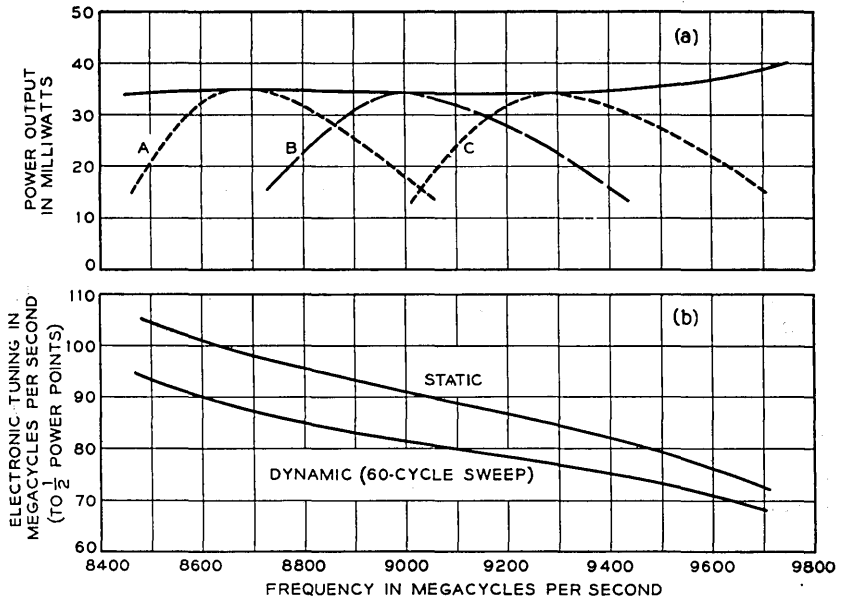


Fig. 86.—Characteristics of the W.E. 2K45 reflex oscillator. Fig. 86-a shows the variation of the power output as a function of frequency in two cases. The curves *A*, *B* and *C* illustrate the power variation with frequency when the repeller voltage is set for the optimum at the indicated frequency and held fixed as the cavity tuning is changed. The envelope of these curves shows the power variation with frequency when the repeller voltage is maintained at its optimum value for each frequency.

In Fig. 86b the electronic tuning is shown, in one case where the repeller voltage is shifted between half power points so slowly that thermal equilibrium exists at all times and in the dynamic case in which the repeller voltage is shifted at a 60 cycle rate.

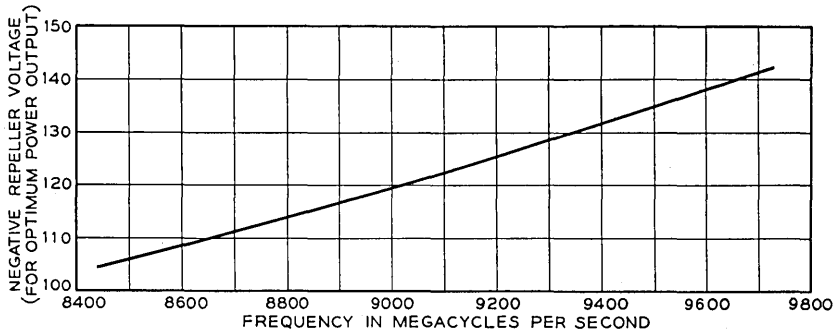


Fig. 87.—Repeller voltage for optimum power as a function of frequency for the W.E. 2K45 oscillator.

Fig. 87 shows the variation of repeller voltage for optimum power with frequency. This variation is so nearly linear that it has been proposed that

a potentiometer properly ganged with the transmitter in radar systems would provide optimum output throughout the band. This is an advantage over electronic tuning, since the signal to noise performance of the receiver depends in part on the beating oscillator power into the crystal.

In a thermally tuned tube it is necessary to provide safeguards against excessive power input to the tuning strut since this might produce a permanent deformation and impair tuner operation. A simple method for obtaining such protection is to use low-frequency cathode feedback produced by a cathode resistor. With a cathode biasing resistor of 725 ohms the grid may be held 15 volts positive with respect to the more positive end of the cathode biasing resistor indefinitely without damage to the tuner when the normal plate voltage of 300 volts is applied.

The grid control characteristics for a typical 2K45 shown in Fig. 88 were obtained while using the cathode biasing resistor. These characteristics may be given in two ways. In one case the repeller voltage is held fixed and the characteristics are given over a range between half power points. It will be observed in this case that the characteristics are discontinuous because of the electronic tuning resulting from the repeller voltage shifts between ranges. For the other case the repeller voltage is maintained at its optimum value at each frequency.

In either case, one striking feature is the essential linearity of the variation of frequency with grid voltage. This is of considerable importance in many frequency stabilizing systems and represents an advantage of thermal tuning over electronic tuning. In the case of electronic tuning, as shown in Section VII, the rate of change of frequency with repeller voltage varies rapidly as the repeller voltage shifts away from the optimum value. Since frequency stabilization is essentially a feedback amplifier problem in which the rate of change of the frequency with the control voltage enters as one of the factors determining the feedback, it is apparent that the frequency stabilization will vary as the repeller voltage is shifted. In contrast, for the case of thermal tuning, because of the linearity of frequency with grid voltage, the stabilization will be independent of the frequency. It should not be for-

2K45 Operating Conditions

	Normal	Maximum
Heater Voltage . . . . .	6.3	6.8 Volts
Resonator Voltage . . . . .	300	350 Volts
Klystron Current . . . . .	22	30 mA
Repeller Voltage Range . . . . .	-60 to -175	-350 Volts
Tuner Current . . . . .	0 to 25	mA
Tuner Power . . . . .		7.0 Watts
$\tau_h$ (9660-8500 Mc/s) . . . . .	6.0	9.0 Sec
$\tau_c$ (8500-9660 Mc/s) . . . . .	6.0	9.0 Sec



gotten, however, that thermal tuning is inherently slower in action than electronic tuning, since the latter is capable of frequency correction rates limited, for practical purposes, only by the control circuits, whereas in

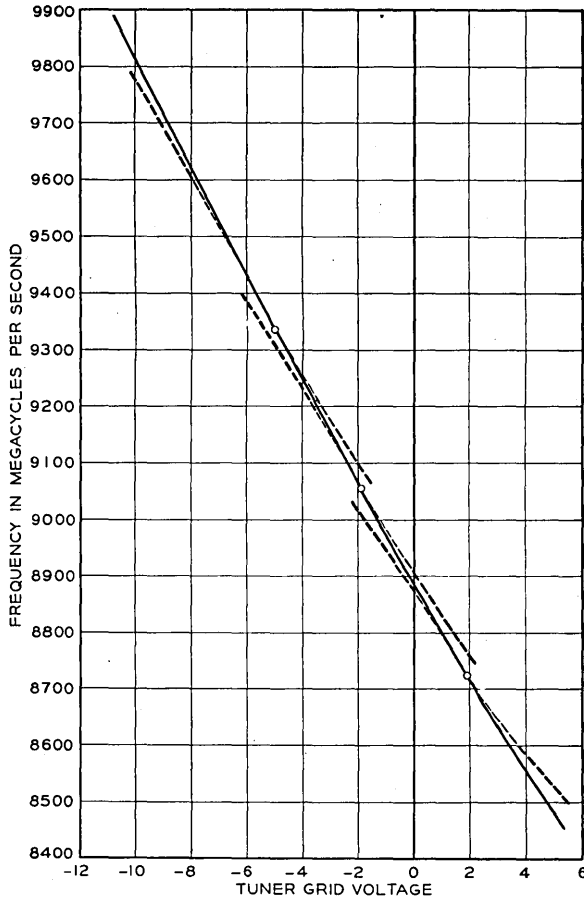


Fig. 88.—Frequency as a function of the grid voltage for the W.E. 2K45 oscillator. The dashed lines show the variation when the repeller voltage is held fixed for the mid-range value and the solid lines shows the variation with the repeller voltage maintained at its optimum value for each frequency. These characteristics apply when a 725 ohm biasing resistor is connected in series with the tuner cathode.

thermal tuning the thermal inertia of the tuning strut limits the tuning speed to rates of the order of  $100 \text{ mc/sec}^2$  for the 2K45.

The operating conditions for the 2K45 are given in the table at the bottom of page 595.

*G. An Oscillator With Waveguide Output—The 2K50*

Late in the war it became apparent that there was an urgent need for radar systems which would permit a very high degree of resolution. Such resolution requires the use of the shortest wavelengths possible, and as a practical step development work was undertaken in the neighborhood of 1 cm.

Work at these Laboratories led to a tube which produced over 20 milliwatts and was thermally tunable over the desired frequency range by means roughly similar to those employed in the 2K45. This tube had a wave guide output. It had no grids; a sharply focused beam passed through a .015" aperture in the resonator. The tube operated at a cavity voltage of 750 volts.

Work by Dr. H. V. Neher at the M.I.T. Radiation Laboratory resulted in a design for an oscillator using grids which operated at a resonator voltage of 300 volts. At the request of the Radiation Laboratory, the Bell Telephone Laboratories undertook such development and modification as was necessary to make the design conform to standard manufacturing techniques. This work was carried out with the close cooperation of Dr. Neher.

Figure 89 shows an external view of the tube and Fig. 90 a cross sectional view of the final structure. There are two striking departures in this tube from the designs previously described. One of these is that the axis of symmetry is no longer parallel to the axis of the envelope but instead is perpendicular to it. This construction makes possible in part the other striking feature of the tube, which is the wave guide output. A number of factors combine to make this type of output desirable and practical. The resonant cavity for a wavelength near 1.25 cm. becomes extremely small. Were loop coupling used this would necessitate a very small coupling loop and also a very small diameter output line. The small dimensions with loop coupling would require tolerances extremely difficult to maintain with conventional vacuum tube techniques. On the other hand, the wave guide used at 1.25 cm. is of dimensions (.170" x .420") such that a wave guide output with a choke coupling can readily be incorporated in a standard vacuum tube envelope.

The wave guide coupling is accomplished by means of a tapered wave guide which couples to the cavity through a non-resonant iris. The guide tapers in the narrow dimension only, from the iris to a circular output window. The tapered guide couples to the window by means of a circular half wave choke. The VSWR introduced by the window is 1.1 or less. External to the tube, there is an insulating fitting which permits the tube to be coupled directly to the guide by means of a second choke coupling. This makes it possible to operate the shell of the tube at a different potential

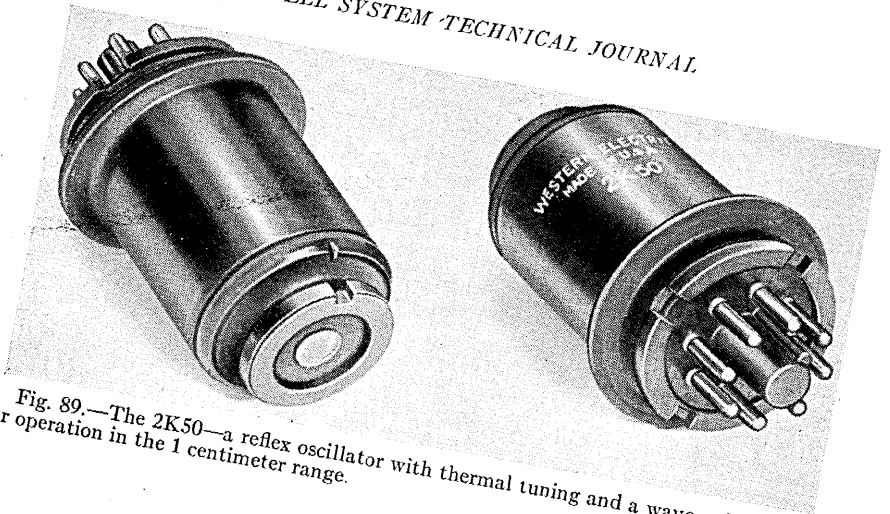


Fig. 89.—The 2K50—a reflex oscillator with thermal tuning and a wave guide output or operation in the 1 centimeter range.

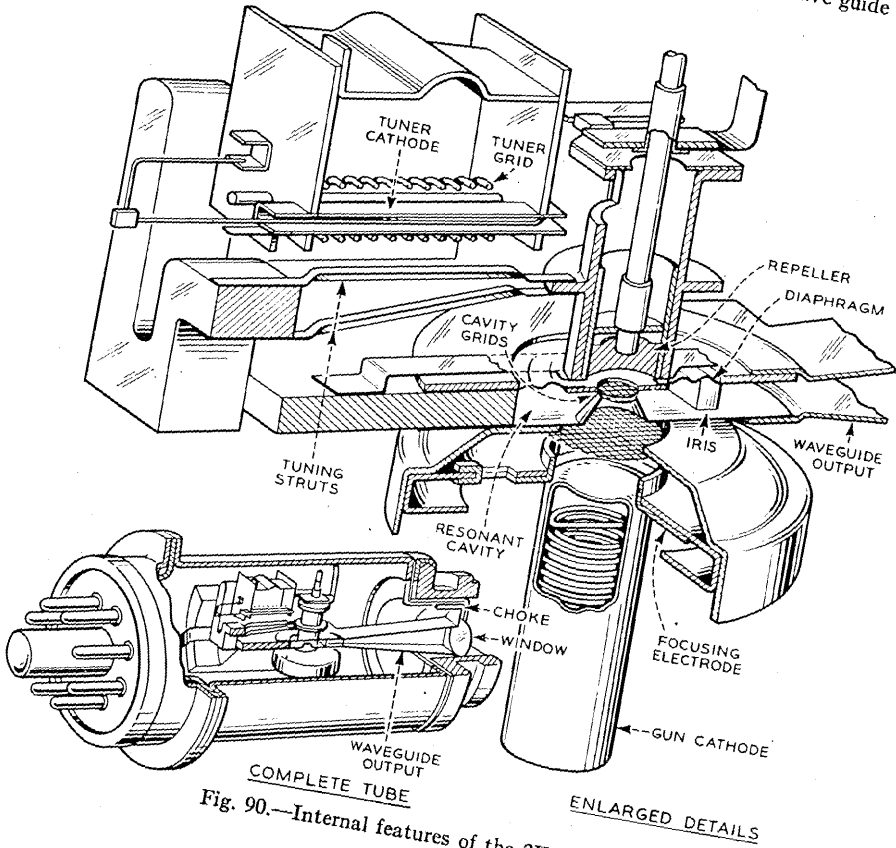


Fig. 90.—Internal features of the 2K50.

than the guide. This is desirable in a radar receiver for circuit reasons, which require that the cathode of the oscillator be at ground potential.

The iris size is a compromise chosen to provide sufficient sink margin throughout the band. An iris coupling inherently varies with frequency and provides a weaker coupling at lower frequencies. Hence, since a suffi-

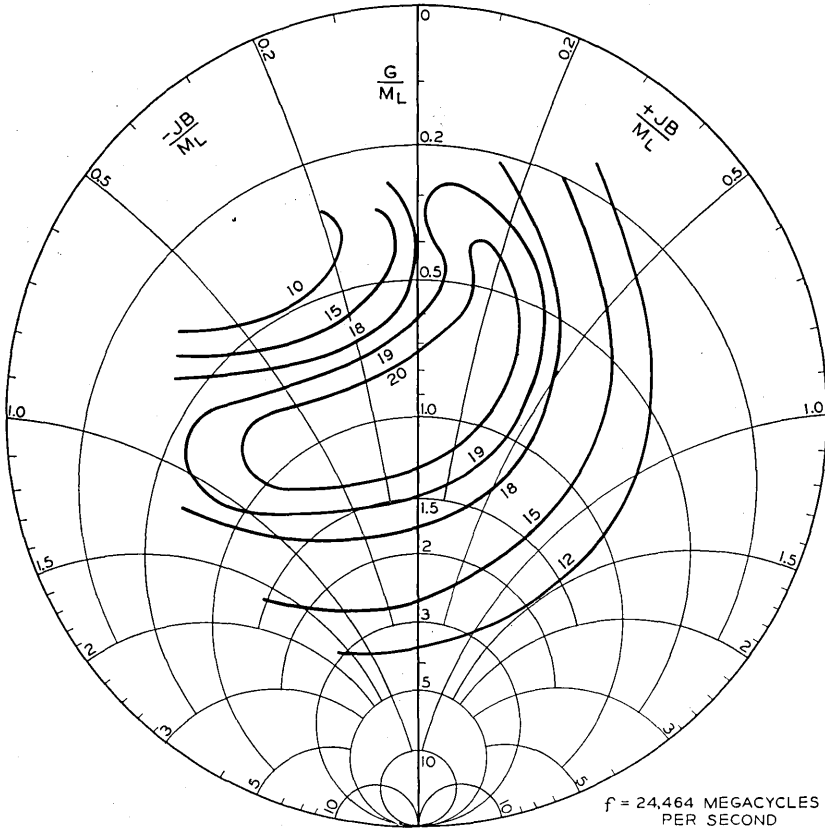


Fig. 91.—A performance diagram for the 2K50 at the high frequency band limit. This diagram shows loci of constant power as a function of the admittances presented at the plane of the tube window. Admittances are normalized in terms of the characteristic admittance of the wave guide.

cient sink margin must be provided at the wavelength where the coupling is a maximum, this means that an excess of sink margin exists at the low frequency end of the band. This is illustrated by the impedance performance diagrams of Figs. 91 to 93.

The 2K50 presented a difficult mechanical problem which will be appreciated when the minute dimensions of the resonant cavity are observed in

Fig. 90. The electron optical system consists of a concave cathode, a cylindrical beam electrode, and a grid concave towards the cathode. This produces an electron beam which converges into a conical nose and through the cavity grids to the repeller space. The repeller, which returns the beam across the gap, is rigidly held in a mica supported in a cylindrical housing connected to a diaphragm which serves as one wall of the resonator. The

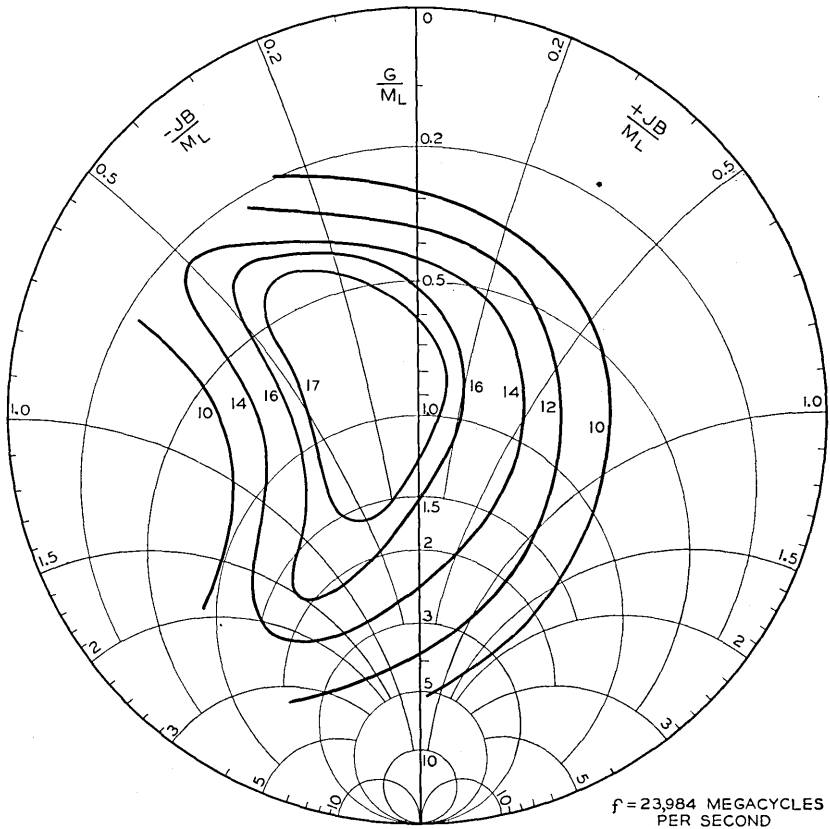


Fig. 92.—Performance diagram for the 2K50 at the mid-band frequency.

cylindrical housing is connected to a thermal tuning mechanism consisting of a simple framed structure in the shape of a right triangle. The base of the triangle is a heavy piece of metal brazed to the cavity block and a bleeder shoe which in turn is brazed to the bulb. One leg of the triangle can be heated by electron bombardment controlled, as in the 2K45, by a negative grid. The other leg is heated only by conduction. Since both legs are made from the same material, general heating of the structure will produce

only a second order effect. Because of the small motion required to tune the 2K50 through its range, the tuner dimensions permit reliance on conduction cooling.

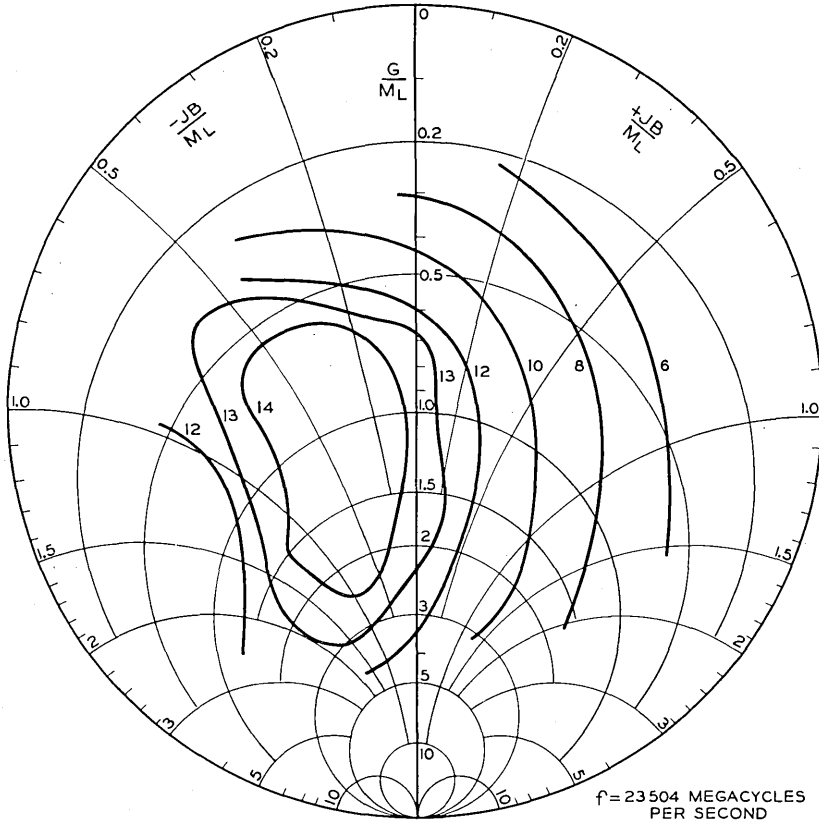


Fig. 93.—Performance diagram for the 2K50 at the low frequency band limit.

The characteristics of the thermal tuner of the 2K50 differ considerably from the 2K45. In Appendix XI expressions are given for the heating and cooling times as

$$\tau_h = \frac{c}{k} \log_e \frac{P_m - kT_c}{P_m - kT_h} \quad (13.4)$$

$$\tau_c = \frac{c}{k} \log_e \frac{T_h}{T_c} \quad (13.5)$$

It is desirable that the cycling times should be equal. Equating (13.4) and (13.5) one obtains

$$P_m = k(T_h + T_c). \quad (13.6)$$

This states that the maximum permitted temperature,  $T_m = P_m/k$ , shall exceed the temperature  $T_h$  by the same temperature difference as that by which  $T_c$  exceeds the sink temperature. From (13.4) and (13.5) it can be seen that to minimize the heating and cooling times the heat capacity should be small and the heat conductivity of the strut should be large. It is also evident that the ratio  $T_h/T_c$  should be as nearly unity as possible. This requires that the tuner should produce the required displacement in the smallest temperature interval possible. If a given temperature difference is required to produce the necessary motion, then from a speed standpoint it is desirable to make both  $T_h$  and  $T_c$  large in order that their ratio shall be nearly unity. The allowable temperature is usually limited by constructional considerations.

Over the normal tuning range of a reflex oscillator we have previously shown that the tuning characteristic may be represented by

$$\lambda = \alpha \sqrt{C_f + C(x)} \quad (13.7)$$

where  $\alpha$  is a constant

$C_f$  is a lumped fixed capacitance

$$C(x) = \frac{\beta}{x}$$

$\beta$  is a constant.

Hence one can show that for small changes  $\Delta x$  from  $x_0$

$$\Delta\lambda = -\frac{\frac{1}{2}\lambda_0\beta\Delta x}{x_0^2 C_0} \quad (13.8)$$

$$C_0 = C_f + C(x_0). \quad (13.9)$$

One may also show that for the type of tuner employed and the small motions involved in the 2K50 the displacement of the grids as a function of the temperature difference  $T - T_0$  will be

$$x = x_0 - H(T - T_0) \quad (13.10)$$

whence

$$\Delta\lambda = \frac{\frac{1}{2}\lambda_0\beta H(T - T_0)}{x_0^2 C_0}. \quad (13.11)$$

If at time  $t = 0$ ,  $x = x_0$ ,  $T = T_0$ ,  $\lambda = \lambda_0$ , we have for heating

$$\lambda' - \lambda_0 = \frac{\frac{1}{2}\lambda_0\beta H}{x_0^2 C_0} \left( \frac{P_i}{k} - T_0 \right) (1 - e^{-(kt/c)}). \quad (13.12)$$

If we give  $P_i$  its maximum value  $P_m$  then at  $t = \infty$  the temperature of the strut will be  $\frac{P_i}{k} = T_m$ ,  $\lambda = \lambda_m$

$$\text{and} \quad \Delta\lambda = \lambda_m - \lambda_0 = \frac{\frac{1}{2}\lambda_0\beta H}{x_0^2 C_0} (T_m - T_0) \quad (13.13)$$

$$\text{or} \quad \lambda - \lambda_0 = (\lambda_m - \lambda_0)(1 - e^{-(kt/c)}). \quad (13.14)$$

Thus the behavior of this type of tuner may be described by a time constant which is given by  $\tau = \frac{c}{k}$ . This has been verified experimentally for the 2K50, in which this constant has been found to have a typical value of 1.3 seconds.

The instantaneous tuning rates at a given wavelength based on full on-full off operation can be shown to be

$$\frac{df}{dt} = -\frac{1}{\tau} \frac{f}{f_m} (f - f_m) \quad \text{heating} \quad (13.15)$$

$$\frac{df}{dt} = \frac{1}{\tau} \frac{f}{f_0} (f_0 - f) \quad \text{cooling} \quad (13.16)$$

where  $f_0$  is the frequency at zero tuner power

$f_m$  is the frequency at maximum permitted drive.

Figure 94 shows the instantaneous tuning rate as a function of frequency on heating and cooling.

Typical power output versus frequency characteristics for the 2K50 are shown in Fig. 95. Curve A shows the power output with the repeller voltage optimized at each frequency while Curve B gives the variation when the repeller voltage is set for an optimum at the center of the band and held fixed as the frequency changes. For constructional reasons the spacing between the repeller and second cavity grid is fixed in the 2K50 so that on a proportional frequency basis the range between half power points with fixed repeller voltage is smaller for the 2K50 than for the 2K45.

Figure 96 shows the frequency vs. grid voltage characteristics for the 2K50. For normal operation with full on-full off operation the grid voltage is switched between zero and cutoff.

#### H. A Millimeter Range Oscillator

During the latter stages of work on the 2K50 development, work was started on an oscillator for a wavelength range around .625 cm. The design of this developmental tube known as the 1464XQ was undertaken.

There are several difficulties in going from 1.25 cm. to .625 cm. Greater accuracy of construction is required and the cathode must be operated at a higher current density. The greatest difficulty arises from the fact that the grids cannot be directly scaled in size from those used in tubes for longer wavelengths.



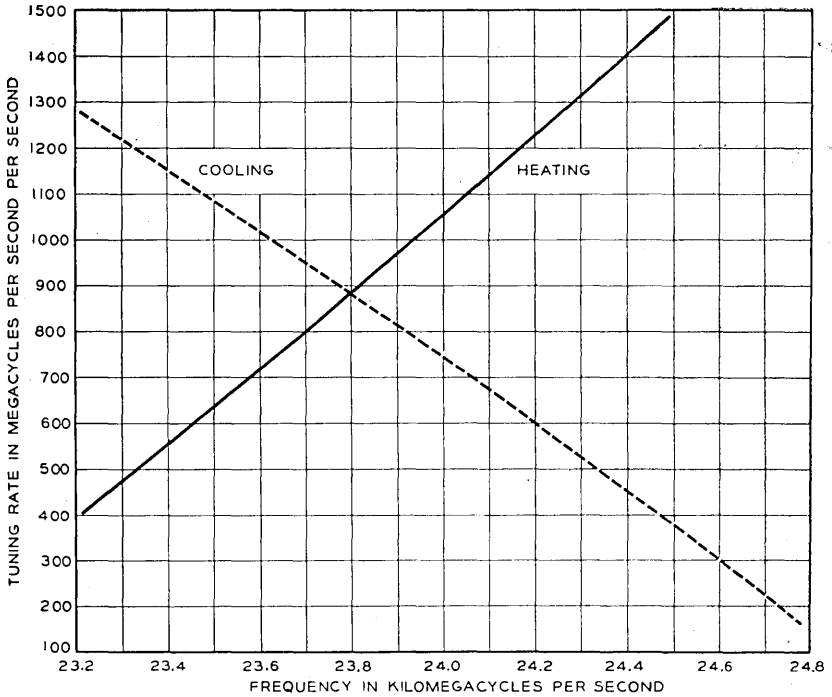


Fig. 94.—Computed instantaneous tuning rates on heating and cooling for the 2K50 oscillator. These results are based on a time constant of 1.3 seconds and on the assumption of "full on or off" operation.

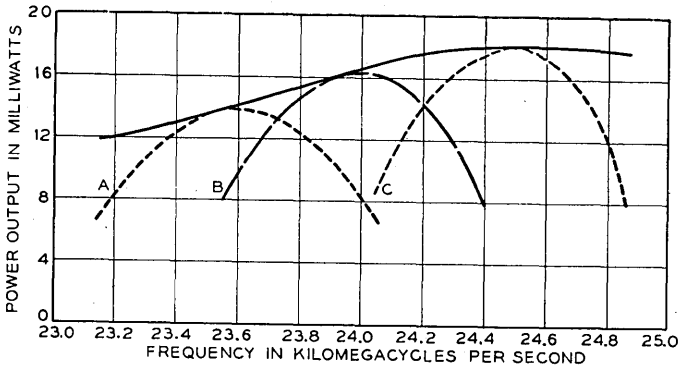


Fig. 95.—Power output characteristics of the 2K50 oscillator. Curves A, B and C illustrate the power variation with frequency when the repeller voltage is set for the optimum at the indicated frequency and held fixed as a cavity tuning is changed. The envelope of these curves shows the power variation with frequency when the repeller voltage is maintained at its optimum value for each frequency.

Let us consider the factors involved in scaling from a tube operating at a given frequency to a smaller tube operating at a higher frequency. If the cathode is operated space-charge-limited and the anode voltage is the same as for the larger tube, the total electron current will be the same and each grid wire will intercept as much current and hence receive the same power to dissipate as in the larger tube. Suppose the length of a grid wire in the larger tube is  $l_0$  and in the smaller tube the length of the corresponding wire is  $l_1$ . Suppose that all the other dimensions of the smaller tube, including

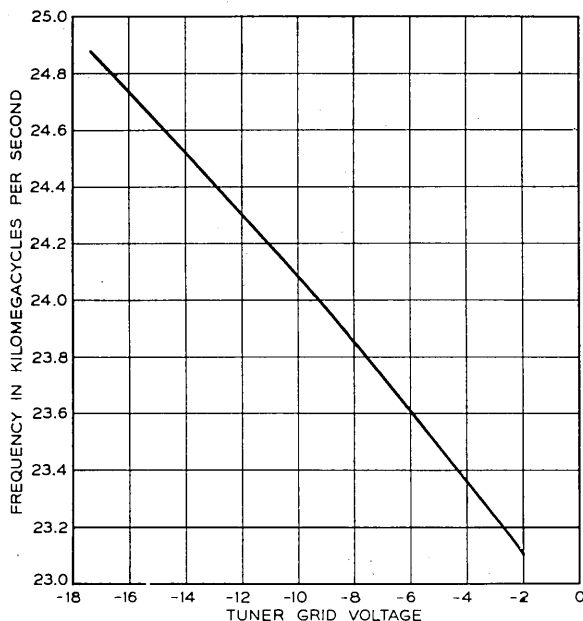


Fig. 96.—Frequency vs tuner grid voltage for the 2K50.

the diameter of the grid wire, are reduced in the ratio  $l_1/l_0$ . We do not know *a priori* whether or not the temperature distribution along the grid wires of the smaller tube will be the same as that for the larger tube; suppose, however, that it is. Then if  $T_0$  is the temperature at some typical point, say, the hottest, on the grid wire of the larger tube, and  $T_1$  is the temperature at the similar point on the smaller tube, the power the wire loses by radiation in the large tube,  $P_{r0}$  and in the small tube,  $P_{r1}$  are given by

$$P_{r0} = Al_0^2 T_0^4 \quad (13.17)$$

$$P_{r1} = Al_1^2 T_1^4. \quad (13.18)$$

Here  $A$  is nearly constant for given tube geometry and materials. In radiation the power lost varies as the area, which varies as  $l^2$ , and as the temperature to the fourth power.

The power lost by end cooling, for the large and the small tube,  $P_{e0}$  and  $P_{e1}$  will be given by

$$P_{e0} = Bl_0T_0 \quad (13.19)$$

$$P_{e1} = Bl_1T_1. \quad (13.20)$$

Here  $B$  is another constant. These relations express the fact that the power lost by end cooling (thermal conduction) varies as cross sectional area divided by length and hence as  $l$  and as temperature difference, taken as proportional to  $T$ .

Now, in scaling the tube the power to be dissipated has been kept constant. Further, in making the tube small, the hottest point of the grid cannot be run hotter than the melting point of the wire; in fact, it cannot be run nearly this hot without unreasonable evaporation of metal. Suppose we let the grid in the smaller tube attain the maximum allowable temperature  $T_m$  and let the power the wire must dissipate be  $P$ . Then for the large tube

$$P = P_{r0} + P_{e0} = (Al_0T_0^3 + B)l_0T_0 \quad (13.21)$$

and for the smaller tube

$$P = P_{r1} + P_{e1} = (Al_1T_m^3 + B)l_1T_m. \quad (13.22)$$

Hence, the smallest value  $l_1$  can have without running the grid too hot is given by the equation

$$l_1 = l_0 \frac{T_0}{T_m} \frac{(Al_0T_0^3 + B)}{(Al_1T_m^3 + B)}. \quad (13.23)$$

We see that if  $l_0$  is very small,

$$\begin{aligned} Al_0T_m^3 &\ll B \\ Al_1T_m^3 &\ll B \end{aligned} \quad (13.24)$$

Numerical examples show that this is so for a tube such as the 2K50. This means that nearly all of the power dissipated by the grid is lost through end cooling, not radiation.<sup>14</sup> Further, in the 2K50 the grid is already operating near the maximum allowable temperature. Hence, nearly,  $T_0 = T_m$  and the smallest ratio in which the tube can be scaled down without overheating the grids is approximately unity. This means that in making a tube for .625 cm. the grid wire cannot be made half the diameter of the wire used in

<sup>14</sup>The fact that one kind of dissipation predominates in both cases justifies the assumption of the same temperature distribution in both cases.

the 2K50. In fact, the diameter of the grid wire can be made but little smaller. Thus, in the 1464XQ the grid is relatively coarse compared with that in the 2K50. This results in a reduced modulation coefficient and hence in less efficiency.

In going to .625 cm., resonator losses are of course greater. The surface resistivity of the resonator material varies as the square root of the frequency. Surface roughness becomes increasingly important in increasing resistance at higher frequencies. Further, in order to provide means for moving the diaphragm in tuning, it was necessary in the 1464XQ to use a second mode resonator (described later) and this also increases losses over those encountered at lower frequencies.

Development of the 1464XQ was stopped short of completion with the cessation of hostilities. However, oscillation in the range .625-.660 cm. had been obtained. The power output varied from 2-5 milliwatts between the short wave and long wave extremes of the tuning range. The cathode current was around 20 ma, the resonator voltage 400 volts. The tube operated in several repeller modes in a repeller voltage range 0 to -180 volts.

Figures 97 and 98 illustrate features of the 1464XQ oscillator. Figure 98 is a scale drawing of the resonator and repeller structure. The electron beam is shot through two apertures covered with grids of .6 mil tungsten wire. These grids are 80% open and are lined up. The aperture in the grid nearest the gun is 23 mils in diameter and the second aperture is 34 mils in diameter. The repeller is scaled almost exactly from the 723A 3 cm. reflex oscillator. A second mode resonator is used. The inner part, a, of Fig. 98 is about the size of a first mode resonator. This is connected to an outer portion, c, by a quarter wave section of small height, b, which acts as a decoupling choke. The resonator is tuned by moving the upper disk with respect to the lower part, thus changing the separation of the grids. The repeller is held fixed. Power is derived from the outer part, c, of the resonator by means of an iris and a wave guide, which may be seen in the section photograph Fig. 97. There is an internal choke attached to the end of the part of the wave guide leading from the resonator. This is opposed to a short section of wave guide connected to the envelope, and in the outer end of this wave guide there is a steatite and glass window of a thickness to give least reflection of power.

#### I. *Oscillators for Pulsed Applications—The 2K23 and 2K54*

All the reflex oscillators described in the preceding sections have been low power oscillators intended for beating oscillator or signal oscillator applications. Some limitation on the power capability of these oscillators in the form previously described is set by the power handling capacity of the grids. If the tubes are pulsed with pulse durations which are short compared with

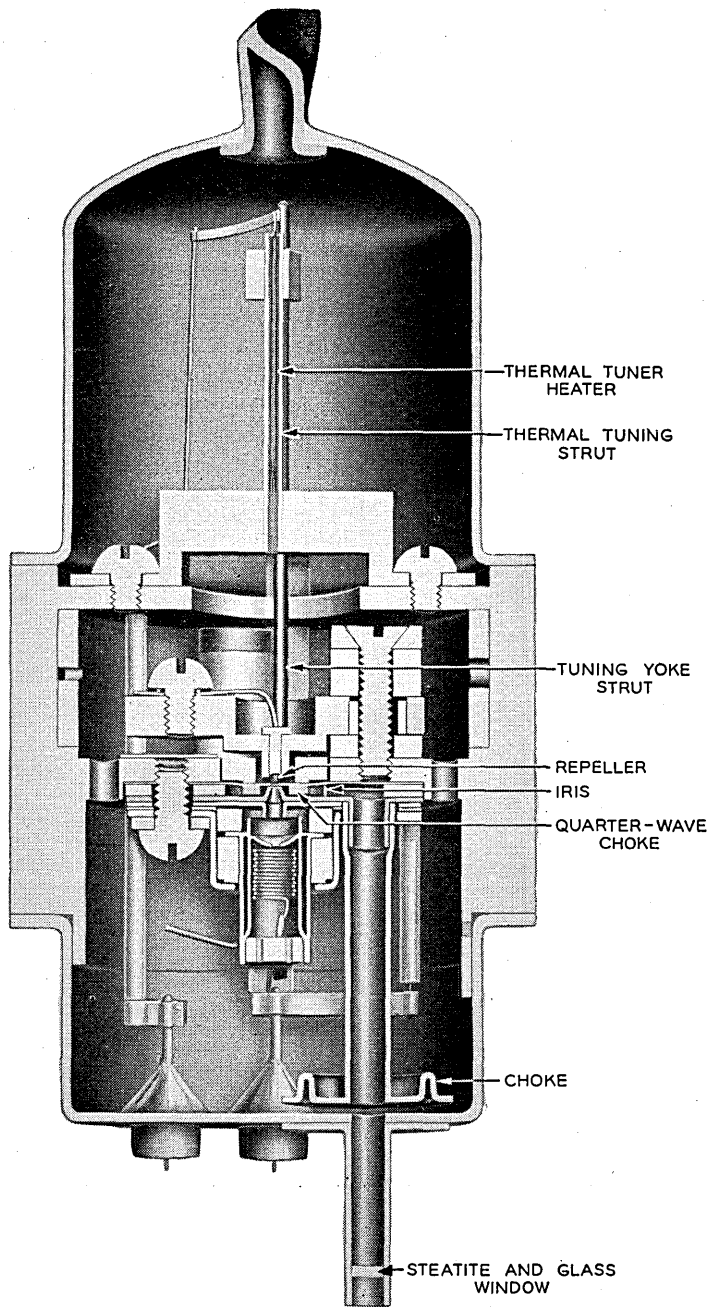


Fig. 97.—An experimental thermally tuned reflex oscillator, the 1464, designed for operation between the wave lengths of .6 and .7 cms.

the thermal time constant of the grids, then the peak power input to the oscillators may be increased over the continuous limit by the duty factor, provided that the voltages applied are consistent with the insulation limits of the tubes and that the peak currents drawn from the cathode are not in excess of its capacity.

An application for a pulsed oscillator arose in the AN/TRC-6 radio system.<sup>15</sup> This was an ultra-high frequency military communication system using pulse position modulation to convey intelligence. With the high gain which may be achieved with antennas in the centimeter range, the power necessary in the transmitter for transmission over paths limited by line of sight is of the order of a few watts peak. In beating oscillator applications the power output is of secondary importance to electronic tuning, so that the reflex oscillators previously described were designed to operate with a drift time in the repeller space such as to provide the desired tuning. In a

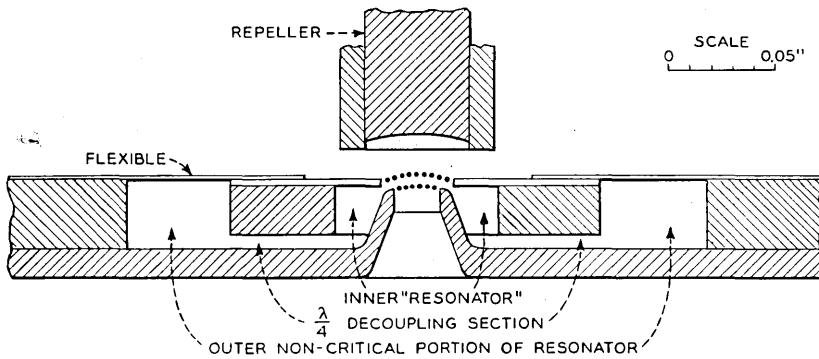


Fig. 98.—The resonator and repeller structures of the oscillator shown in Fig. 97.

pulsed transmitter electronic tuning is unnecessary and indeed undesirable, since it leads to frequency modulation on the rise and fall of the pulse. In section III it is shown that for maximum efficiency with a given resonator loss there will be an optimum value for the drift time. If there were no resonator loss this time would be  $\frac{3}{4}$  cycles, which is the minimum possible. By utilizing the optimum drift angle and taking advantage of the higher peak power inputs permitted by pulse oscillator it was possible to obtain peak power outputs of the order of several watts using the same structure as employed for the beating oscillators previously described without exceeding the power dissipating capability of such a structure. From the standpoint of military convenience this was a very desirable situation for reasons of simplicity of tuning and ease of installation.

<sup>15</sup> A Multi-channel Micro-wave Radio Relay System, H. S. Black, W. Beyer, T. J. Grieser, and F. A. Polkinghorn, *Electrical Engineering* Vol. 65, No. 12, pp. 798-806, Dec. 1946.

The first tube designed for this service was the 2K23. It was based on the design employed in the 2K29 and operated with a drift time of  $1\frac{3}{4}$  cycles in the repeller space. A severe limitation on the performance was set by the requirement that a single oscillator should cover the frequency range from 4275 to 4875 Mc/s. It is shown in Section X that in an oscillator tuned by changing the capacitance of the gap the efficiency will vary considerably

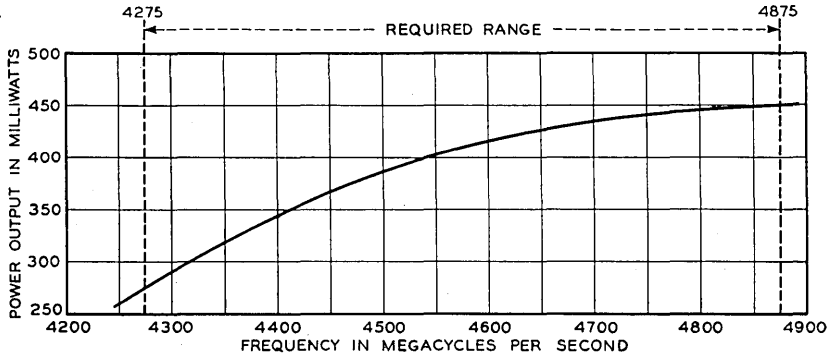


Fig. 99.—Variation of the peak power output vs frequency for the 2K23 reflex oscillator. This tube was designed for pulse operation with a duty factor of 10 in a repeller mode having  $3.5\pi$  radians drift.

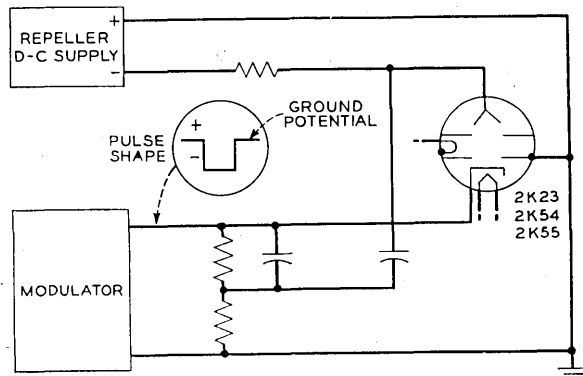


Fig. 100.—Modulator circuit for use in connection with reflex oscillators showing means for applying pulse voltage to the repeller to reduce frequency modulation during pulsing.

over such a tuning range. In the case of the 2K23 the variation of the peak power output with frequency is shown in Fig. 99. The duty factor at which the tube was used (the ratio of the time between pulses to the pulse length) was 10. In the AN/TRC-6 application the tube was operated on a fixed current basis; i.e., the pulse amplitude was adjusted to a value such that the average current drawn was 15 ma. The schematic of the circuit employed in pulsing oscillators in this way is shown in Fig. 100. The resonator

of the oscillator is operated at ground and the cathode of the oscillator is pulsed negative with respect to this ground. The repeller voltage is referenced from the cathode and this reference is maintained during the pulse. Some frequency modulation occurs during the rise and fall of the pulse because of the changing electron velocity. This can be reduced in part by applying a part of the pulse in the repeller circuit proportioned in such a way as to tend to maintain the drift time independent of the cathode to resonator voltage. Satisfactory performance is achieved in this way.

As mentioned previously, the intelligence is conveyed by pulse position modulation. The AN/TRC-6 system uses time division multiplex to provide eight communication channels. The multiplexing is achieved by transmitting a four micro-second marker pulse which provides a time reference followed by eight one micro-second pulses. The time of each of the latter pulses is independently varied in position with reference to the marker pulse.

The time interval from the marker to each pulse could be measured to either the leading or trailing edge of the pulse. In Section XII it is shown that the leading edge of the r.f. pulse will be subject to what is commonly called "jitter" because of the random time of rise which will result if oscillation starts from shot or Johnson noise. Conceivably oscillation might be started by shock excitation of the resonant circuit by the pulsed beam current. However, in Appendix X it is shown that the initial excitation produced by shot noise in the beam exceeds that induced by the current transient by a factor of approximately 100. The trailing edge of the pulse will not be subject to this form of jitter provided two conditions are met. First, the pulse duration must be long enough so that oscillation builds up to full amplitude during the pulse. Second, the receiver must have a sufficient bandwidth so that the transient which occurs on reception of the leading edge has fallen to a small value by the time the trailing edge is received. Since these conditions were met in the AN/TRC-6 system, the trailing edge of the pulse was used.

In the latter stages of the development of the AN/TRC-6 system it was decided to remove the restriction that the required tuning range should be covered with a single transmitter tube. This made possible the achievement of a design which would provide an improved performance throughout the band. In order to improve the circuit efficiency of the resonator, the new designs were based on the oscillator structure which was employed in the 2K45. It has been pointed out previously that this makes possible a considerably higher resonant impedance of the cavity, partly because of the reduced gap capacitance and also because the smaller first and second grids reduce the resonator losses. These effects were reflected in the higher efficiency obtained in the 2K54 and 2K55.



The three tubes, the 2K23, 2K54 and 2K55 were intended to couple to wave guide circuits. Although direct coupling to the guide through a wave guide output would have been desirable in some ways, it would have resulted in a very large and awkward structure. It seemed best, therefore, to retain the coaxial output feature of tubes designed for beating oscillator service. From a standpoint of convenience, it would have been desirable

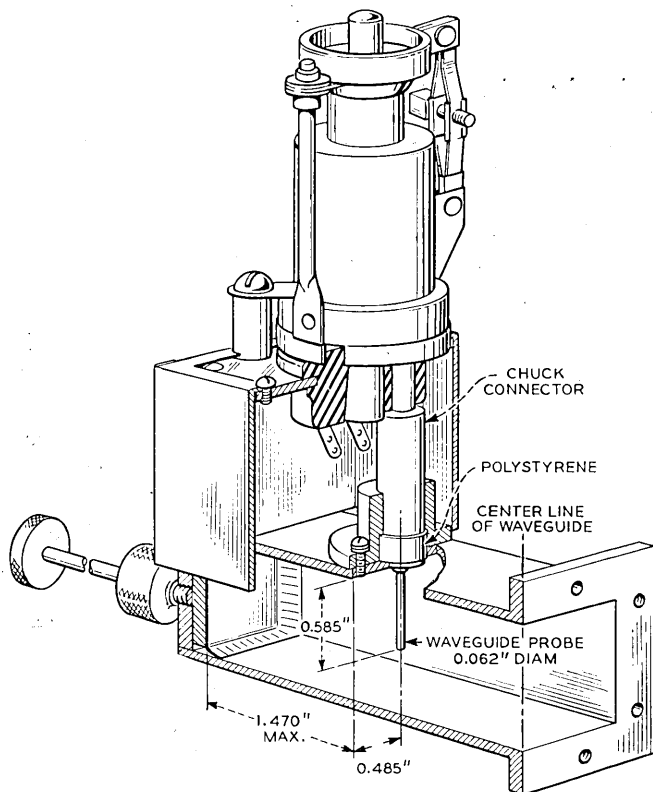


Fig. 101.—A transducer designed to adapt the 2K23, 2K54 and 2K55 oscillators to a terminated wave guide load. If the back piston of this coupling is set at a distance of 1.08" from the center of the probe the impedance presented to the oscillator line is 50 ohms with a 1 db variation over the required frequency range.

to have had the wave guide probe an integral part of the tube, as is the case in the 2K25. However, the length of a quarter wave probe at the operating wave lengths of the AN/TRC-6 system made such a design hazardous. Because of this a transducer was developed into which the tube could be plugged. This is shown in Fig. 101. The central chuck extends the center conductor of the output coaxial of the tube into the guide. It had been

originally intended to design this transducer so that all elements would be fixed. It was found, however, that an adjustable back piston setting permitted compensation for manufacturing tolerances in the tubes as well as permitting the presentation of a better impedance to the oscillator over the band than was attainable with a fixed transducer. This is illustrated in Fig. 102 which shows the power output versus frequency for a typical 2K54 and a typical 2K55 as a function of frequency for three cases. In one case, as shown by curve B, the power output is delivered at all frequencies into the optimum impedance, i.e. the impedance into which the oscillator will deliver maximum power. Curve A shows the power output delivered into

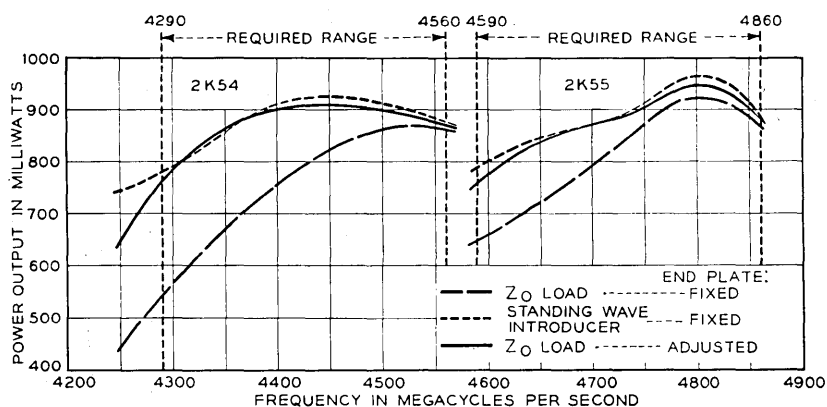


Fig. 102.—Peak power output vs frequency for the 2K54 and 2K55 oscillators for several load conditions. Curves A give the performance obtained when the tubes operate into a characteristic admittance load through the coupling of Fig. 101 with the end plate fixed so that the admittance presented to the tubes is constant to within 1 db over the frequency range. Curves B give the performance obtained when the optimum impedance is presented to the oscillators throughout the band. Curves C give the performance obtained when the tubes are coupled to a characteristic admittance load with the coupling unit of Fig. 101 and with a back piston adjusted to the best value at each frequency.

a transducer which has the back piston fixed at a distance from the probe, so chosen that the impedance seen by the oscillator is flat over the band to within 1 db. Curve C shows the power output when the back piston of the transducer is adjusted so that the tube delivers maximum power. It can be seen that the performance obtained under the latter circumstances is very nearly as good as that obtained when the optimum impedance is presented to the oscillator.

From Sections III and IX we would expect that, since the coupling system is such as to give maximum power throughout the band, the sink margin should be slightly greater than 2. Figures 103 to 106 give impedance performance diagrams for 2K54 and 2K55 at the four transmitting frequencies

of the AN/TRC-6 system. From this it can be seen that the sink margin is approximately 2 at all frequencies. In a transmitter tube another factor, which is of small importance in a beating oscillator, becomes of interest. This factor is the pulling figure, which is defined as the maximum frequency

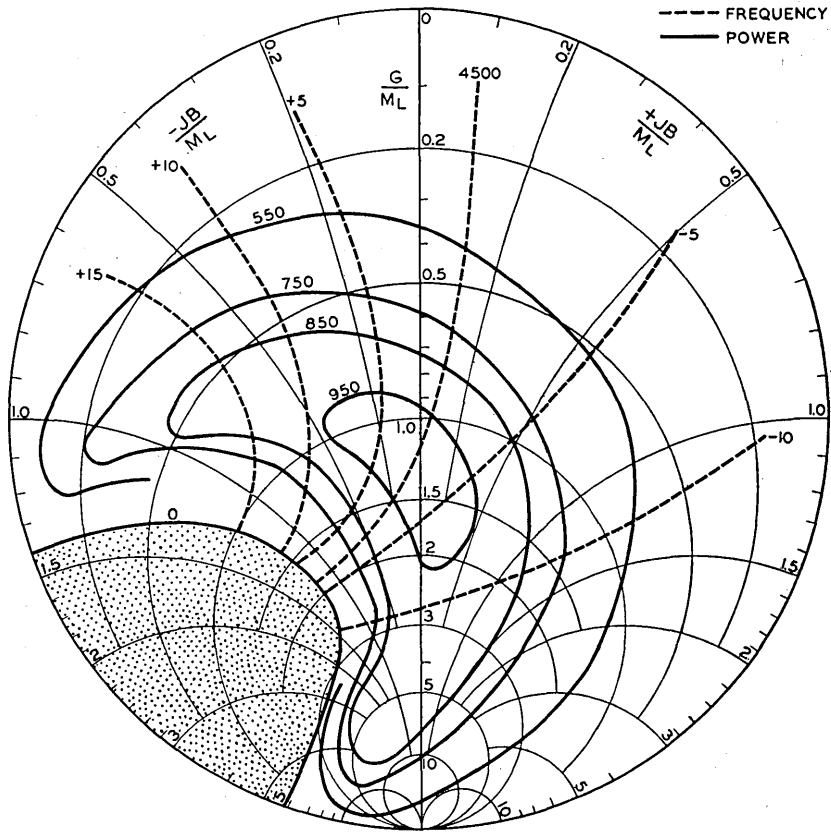


Fig. 103.—Rieke diagram for the 2K54 at a nominal frequency of 4500 megacycles. The point at the unity *vswr* condition is obtained by adjusting the repeller voltage and the back piston of the coupling of Fig. 101 to the values which gave maximum power. These conditions were then held fixed for the remainder of the chart.

excursion which will be produced when a VSWR of 3 db is presented to the transmitter and the phase is varied over 180°. Fig. 107 gives the pulling figure as a function of frequency for the 2K54 and 2K55. The requirements on the pulling figure for the 2K54 and 2K55 were not severe, since in the AN/TRC-6 system the tube is coupled to the antenna by a very short wave guide run and, furthermore, the antennas are fixed.

Investigation of the pulling figure of early models of the 2K55 led, however, to the disclosure of one unforeseen pitfall arising from the existence of electronic hysteresis. It had at first been considered that electronic hysteresis would not be of importance in the transmitter tube, where the feature of electronic tuning was of no importance. This might be true in a CW oscillation.

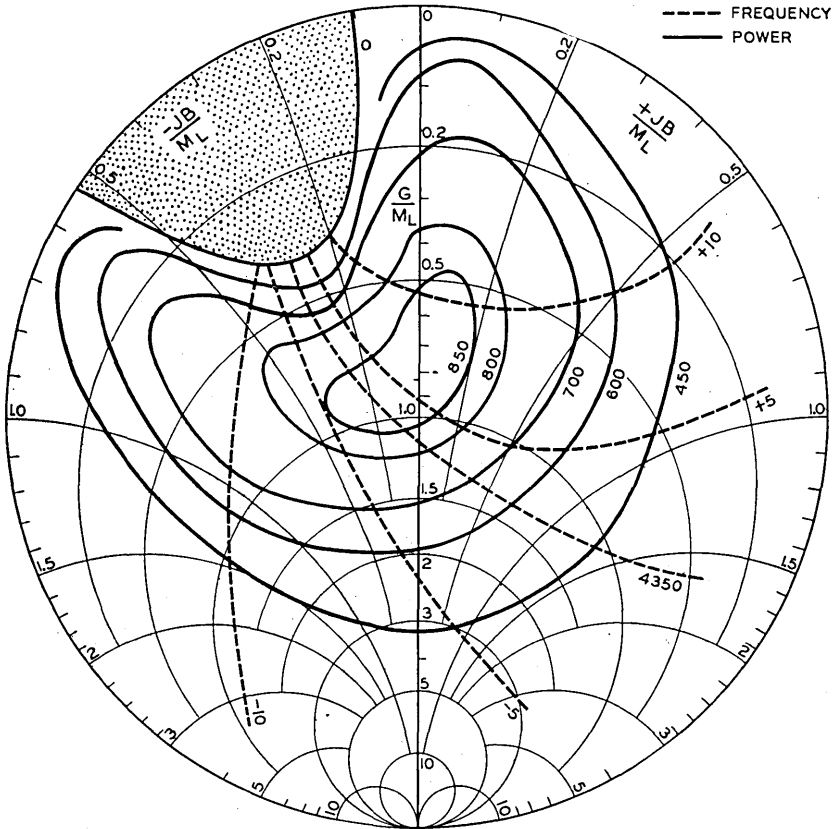


Fig. 104.—Rieke diagram for the 2K54 oscillator at a nominal frequency of 4350 megacycles. The unity  $\text{tswr}$  point was obtained as described in Fig. 103.

tor, but in a pulsed oscillator the existence of hysteresis resulted in an unforeseen reduction of the sink margin. Since the oscillator is being pulsed, for each pulse the oscillating conditions are being re-established. Although the cathode-repeller voltage need not vary during the pulsing, the fact that the cathode-resonator voltage is being changed means that for each pulse the drift angle in the repeller space varies on the rise and fall of the pulse. The effect during the rise of the pulse is the same as though the repeller

voltage were made less negative. In other words, on the rise of each pulse the situation is equivalent to that in a *CIW* oscillator when, for a fixed resonator voltage, one starts with a repeller voltage too negative to permit oscillation and then reduces the repeller voltage until oscillation occurs. Let us now suppose that the hysteresis is such that under these circumstances

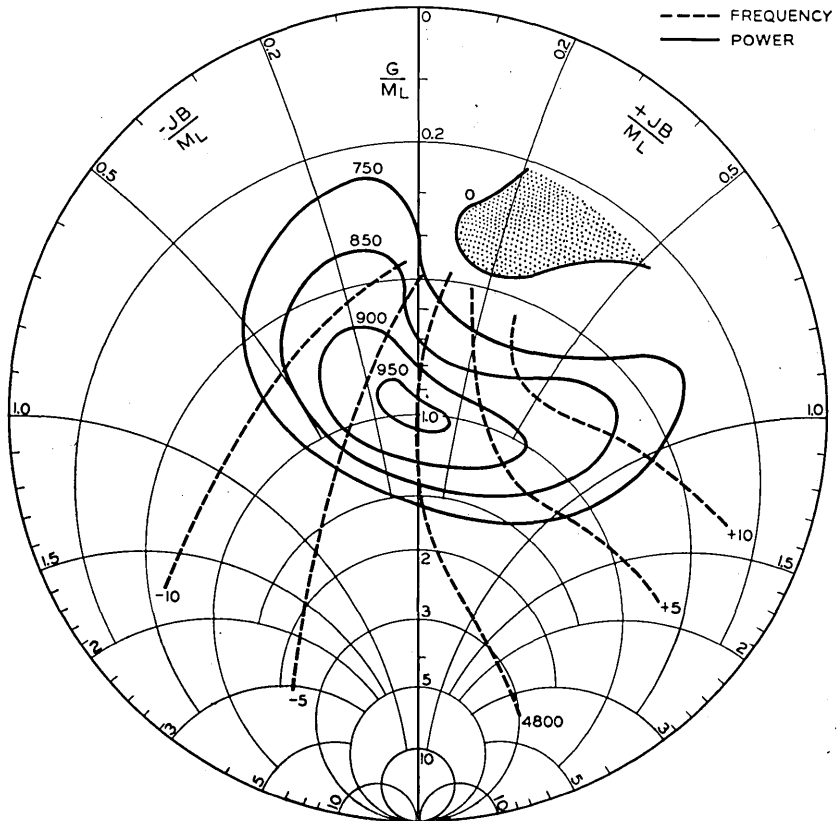


Fig. 105.—Rieke diagram for the 2K55 oscillator at a nominal frequency of 4800 megacycles. The unity *vsr* point was obtained as described in Fig. 103.

the amplitude of oscillation would suddenly jump to a large value. We would then obtain a variation of peak power output as a function of the repeller voltage shown in Fig. 108. Ordinarily, the repeller voltage would be adjusted so as to obtain maximum power output as, for example, with the repeller voltage  $V_{R1}$ . Next, let us suppose that a variable impedance is presented to the oscillator with the repeller voltage held fixed at value  $V_{R1}$ , as would be done, for example, in obtaining an impedance performance

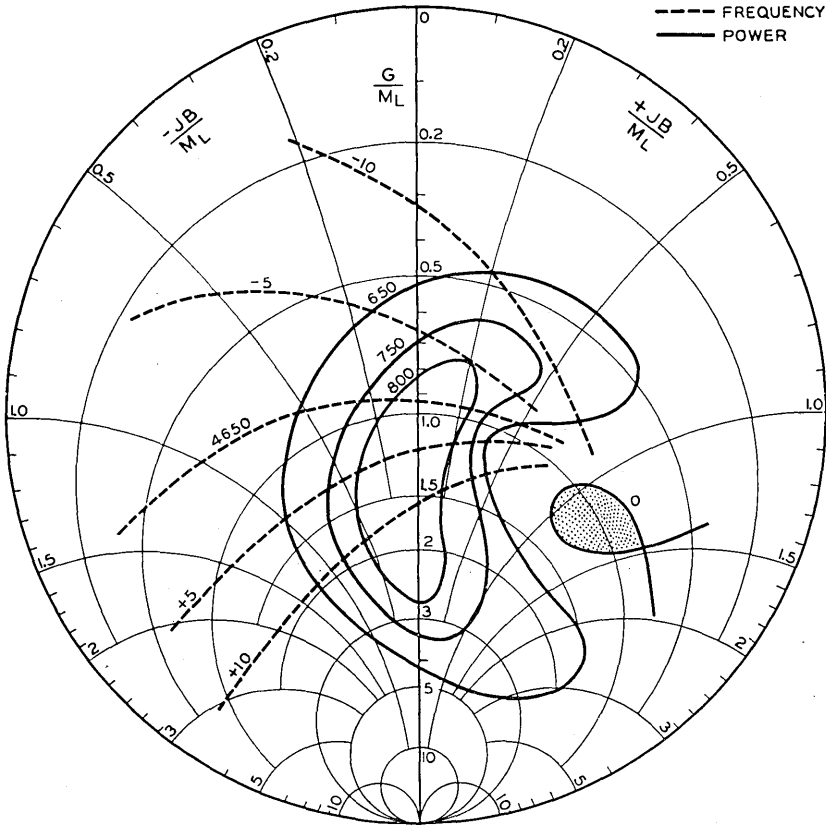


Fig. 106.—Rieke diagram for the 2K55 oscillator at a nominal frequency of 4650 megacycles. The unity *vsur* point was obtained as described in Fig. 103.

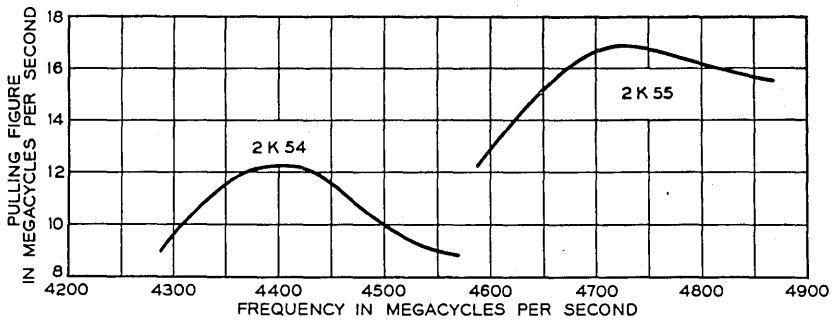


Fig. 107.—Pulling figures for the 2K54 and 2K55 reflex oscillators as functions of frequency. With a unity *vsur* load the repeller voltage and back piston of the coupling of Fig. 101 were adjusted for a maximum power and held fixed for the pulling figure measurements.

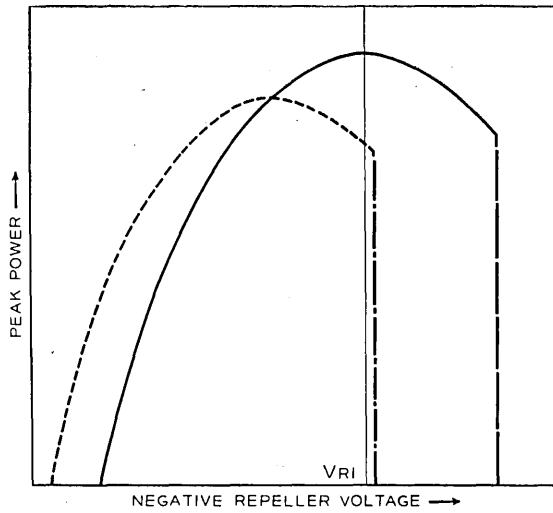


Fig. 108.—The variation of power output with repeller voltage for a pulsed reflex oscillator exhibiting hysteresis.

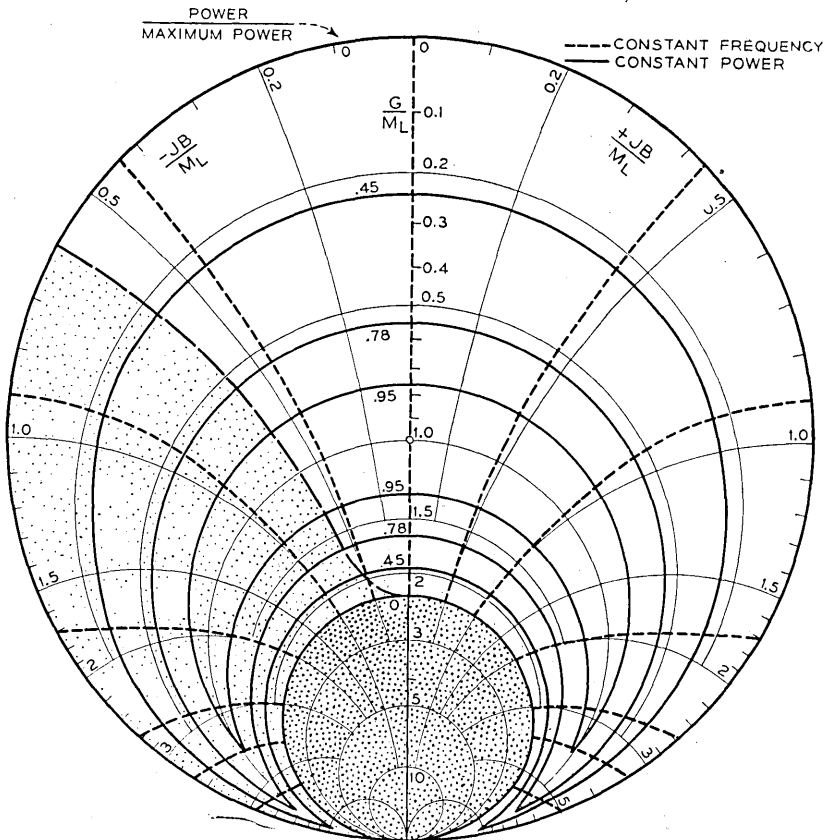


Fig. 109.—The effect of hysteresis on the Rieke diagram of a pulsed reflex oscillator. The hysteresis shown in Fig. 108 can result in failure of a pulsed oscillator to operate in the lightly shaded portion of the Rieke diagram as well as the heavily shaded portion corresponding to the normal sink.

diagram. The effect of varying the impedance on the repeller characteristic in Fig. 108 is to shift the whole characteristic to the right or left, depending upon the phase of the impedance, as well as to change its general form as shown by the dotted curve. It can be seen from this that if the hysteresis is sufficiently bad and if the pulling figure exceeds a particular value, one

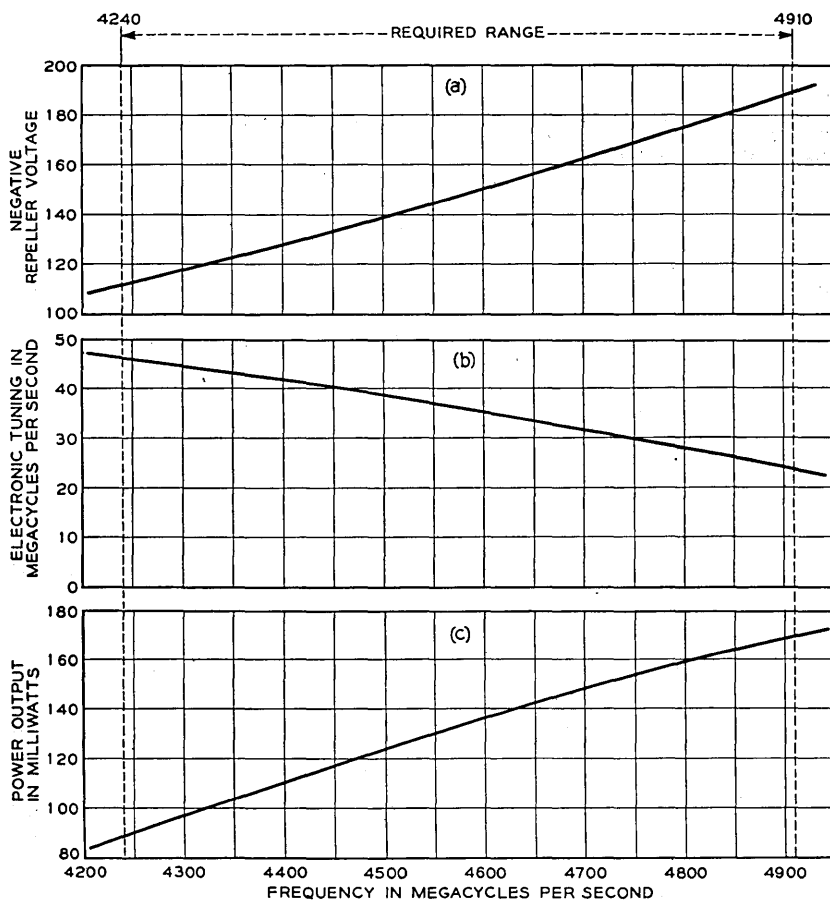


Fig. 110.—Performance characteristics of the 2K22 operated into a 50 ohm load.

effect of the hysteresis will be to reduce the sink margin, and this is found to be the case. Fig. 109 shows an impedance performance diagram obtained with pulsed operation for an early model of the 2K55 in which the hysteresis was excessive. From this it can be seen that the area of the sink on the diagram is very greatly increased and also that the sink margin is reduced from the theoretical value of somewhat in excess of 2 to a value of less than



1.1 although maximum power occurs at unity VSWR. A modification in the design reduced the hysteresis and eliminated this effect as shown by Figs. 103 to 106.

In addition to the transmitter tube for the AN/TRC-6 system, it was necessary to design a beating oscillator. This tube is known as the Western Electric 2K22. Its design was scaled from the 2K29, previously described. The tube was designed to operate into a 50 ohm impedance and can be coupled by a coaxial adapter to a 50 ohm line or by means of the transducer of Fig. 101 to a wave guide. When the back piston of the transducer is set at a distance of 1.080" from the probe center, the impedance presented to the oscillator is 50 ohms with approximately a 1 db variation over the frequency range. Fig. 110 gives the performance characteristics of the 2K22 operating into a 50 ohm load. The AN/TRC-6 system using these tubes provided a military communication system during the war. A description of this service has been given.<sup>12</sup> Also, models of the AN/TRC-6 system have been put into service to provide telephone communication between Cape Cod and Nantucket and also between San Francisco and Catalina Island.

#### *J. Scope of Oscillator Development at the Bell Telephone Laboratories*

The reflex oscillators discussed in the foregoing sections were developed primarily for beating oscillator service, and in one instance for a transmitter. Reflex oscillators also received wide application in test equipment. The best-known application of this type was in the spectrum analyzer, in which the electronic tuning characteristic of the oscillators made possible the display of output spectra, and especially of the spectra of magnetron oscillators, on an oscilloscope. This greatly facilitated the development of the magnetron. The reflex oscillator also was widely used as a signal generator, and the ease of frequency adjustment particularly suited it to this application. In some signal generators it was desired to pulse the reflex oscillator at low power levels. As an alternative to the method previously described, in which the voltage between the cathode and resonator was pulsed, it is possible to leave this voltage fixed and to pulse the voltage between the repeller and cathode. In this case the repeller-cathode voltage is set at a base value at which the tube will not oscillate and the pulse varies this voltage to the oscillating value.

The oscillators which have been described have been chosen to indicate various features of their development. In addition to these, a number of other oscillators were developed to meet various service needs. Figure 111 shows a chart giving the frequency ranges of these tubes. Of the eleven beating oscillators of the reflex oscillator type on the Army-Navy preferred

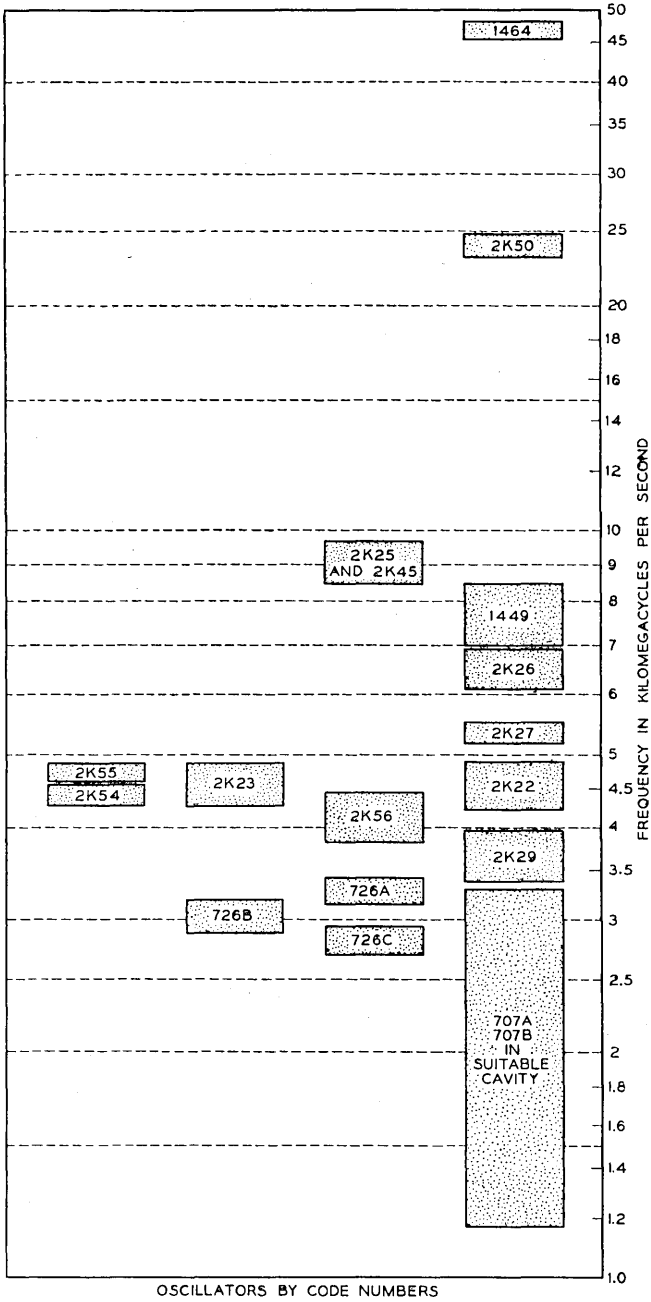


Fig. 111.—Reflex oscillators developed at the Bell Telephone Laboratories. The boxes around the tube numbers show the frequency range covered.

list of electron tubes for 1945, nine were developed at the Bell Telephone Laboratories.

## APPENDIX I

### RESONATORS

In thinking about resonators it is important in order to avoid confusion to keep a few fundamental ideas in mind. One of the most important is that we must not use the notion of scalar potential in connection with fluctuating magnetic fields. Electric fields produced by fluctuating magnetic fields cannot be derived from a scalar potential, and in the presence of such fields to speak about the potential at a point is hopelessly confusing.<sup>16</sup>

The idea of voltage as the line integral of electric field along a given path between two points is useful, but it must be remembered that the voltage depends on the path chosen. Consider, for instance, an ordinary 60-cycle transformer with the secondary wound of copper tubing. For a path from one secondary terminal to the other through the center of the tubing the voltage (integral of field times distance) is zero. For a path between terminals outside of core and coil, the voltage between terminals is  $d\psi/dt$ , where  $\psi$  is the magnetic flux linkage of the path and the coil, counting each line of force as many times as the path encircles it.

If resistance drop is neglected the work done in moving a charge through a conductor is zero. The line integral of an electric field around a closed path is  $d\psi/dt$ . If part of the path is through a conductor, or through a space where there is no electric field, the voltage along the rest of the path (as between portions of the conductor) is  $d\psi/dt$ . For paths linking different amounts of flux, the voltage will be different. In the case of low frequency transformers, all paths linking the terminals and lying outside of the core and coil link practically the same amount of flux, and there is little ambiguity about the voltage. In reflex oscillators the electrons travel from one field free region to another along a certain path and this determines the path along which the voltage should be evaluated.

To review: the voltage between two points is the integral of the field along the path times distance, and refers to a certain path. If the path begins and ends in a field free region, the voltage is  $d\psi/dt$ , where  $\psi$  is the magnetic flux linking the chosen path and a return path through the field free region.

To this should be added that high frequency currents and fields penetrate the surface of metals only a fraction of a thousandth of an inch in the centimeter range,<sup>17</sup> so that the interior of a conductor is field free, and fields inside of a metal enclosed space cannot produce fields outside of that space.

<sup>16</sup> The electric field can, of course, be derived from a scalar and a vector potential.

<sup>17</sup> As an example, for copper the field is reduced to (1/2.72) of its value at the surface

In considering resonators we should further note that the magnetic flux must be produced by a flow of current, either convection current or displacement current, around the lines of force. In a transformer this can be identified as the current flowing in the coils. In the resonators used in reflex oscillators it is the current flowing in the walls and, as displacement current, across the gap and from one face of the resonator to the other.

Two axially symmetrical resonators suitable for use in reflex oscillators are shown schematically in Figs. 112 and 113. The resonator in Fig. 112 has grids and might be used with a broad unfocused electron beam at a low d-c voltage; that shown in 113 has open apertures and might be used with a

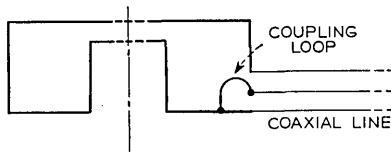


Fig. 112.—An oscillator cavity with grids and loop coupling to a coaxial line.

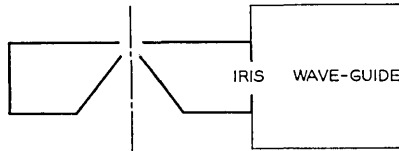


Fig. 113.—An oscillator cavity without grids and with iris coupling to a wave guide.

focused high voltage electron beam. In Fig. 112, the resonator is coupled to a coaxial line by means of a coupling loop or coil; in Fig. 113 the resonator is coupled to a wave guide by means of a small aperture or "iris."

Let us consider the resonator of Fig. 112 in the light of what we have just said. A magnetic field flows around the axis inside of the resonator. There is an electric field between the top and bottom inside surfaces of the resonator at a depth.

$$\delta = 3.82 \times 10^{-5} \sqrt{\lambda} \quad (a1)$$

Here  $\lambda$  is wavelength in centimeters. It may also be convenient to note that the surface resistivity of a centimeter square of resonator surface is, for copper,

$$R = .045/\sqrt{\lambda} \quad (a2)$$

This means that if a current of  $I$  amperes flows on a surface over a width  $W$  and a length  $l$ , the power dissipation is

$$P = I^2 R l / W \quad (a3)$$

For other non-magnetic metals, both  $\delta$  and  $R$  are proportional to the square root of the resistivity with respect to that of copper.

tor. There is no electric field outside of the resonator (except a very little that leaks out near the grids). To take a charge from one grid to another *outside* of the resonator requires no work. Thus the voltage across the gap is  $d\psi/dt$ , where  $\psi$  is the magnetic flux around the axis. Actually, there is a little magnetic flux between the grids, and hence the voltage near the edges of the grids is a little less than that at the center.

Current flows as a displacement current between the grids, and as convection current radially out around, and back along the inside of the resonator to the other grid. This current flow produces the magnetic field that links the axis.

Part of the magnetic flux links the coupling loop. If this part is  $\psi\ell$  and if the coupling loop is open-circuited, the voltage across the coupling loop will be  $d\psi\ell/dt$ .

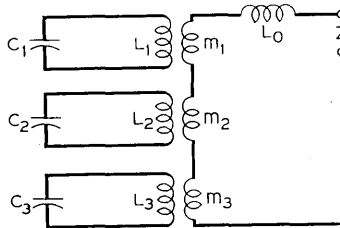


Fig. 114.—Equivalent circuit for a resonator having 3 modes of resonance.

In the resonator of Fig. 113, power leaks out through the iris into the wave guide. Part of the wall current in the resonator flows out through the hole into the guide; part of the magnetic flux in the resonator leaks out into the guide.

In dealing with resonators as resonant circuits of reflex oscillators, to which the electron stream and the load are coupled, we are interested in the gap and output impedances. For a clear and exact treatment, the reader is referred to a paper by Schelkunoff.<sup>18</sup> No exhaustive treatment of the problem will be given here, but a few important general results will be given.

If the resonator is lossless, the impedance looking into the loop may be represented exactly by an equivalent circuit indicated in Fig. 114. As coils used at low frequencies are really not simply ideal "inductances," (an idealized concept), but have many resonances (ascribed to distributed capacitance), so the resonator has many, in fact, an infinity of resonances. In the equivalent circuit shown in Fig. 114, only 3 of these are represented,

<sup>18</sup> S. A. Schelkunoff, Representation of Impedance Functions in Terms of Resonant Frequencies, *Proc. I.R.E.*, 32, 2, pp. 83-90, Feb., 1944.

by the inductances  $L_1, L_2, L_3$  and the capacitances  $C_1, C_2, C_3$ . These resonant circuits are coupled to the terminals by mutual inductances  $m_1, m_2, m_3$ . In series with these appears the inductance measured at very low frequencies  $L_0$ , the self inductance of the coupling loop. The circuit in Fig. 114 may be regarded as a symbolic representation to be used in evaluating  $Z$ , just as a mathematical expression may be a symbolic representation of the value of an impedance.

In practical cases, the resonances are usually considerably separated in frequency, and near a desired resonance the effect of others may be neglected. In addition, if the  $Q$  is high we may add a conductance  $G_R$  across the capacitance to represent resonator losses (Fig. 115). It would be equally legitimate to add a resistance in series with  $L$ . In Fig. 115 a load impedance  $Z_L$  has been added. Fig. 115 is a very accurate representation of a slightly lossy resonator, a low loss coupling loop, and a load impedance. The

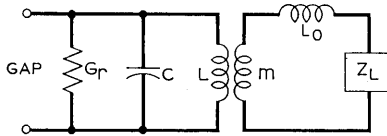


Fig. 115.—Equivalent circuit showing connection between the oscillator gap regarded as one pair of terminals and the oscillator load for an oscillator resonator having only one resonant frequency near the frequency of operation.

meaning of  $L$  and  $C$  will be made clearer a little later. We will now clarify the meaning of  $m$ . Suppose no current flows in the coupling loop ( $Z = \infty$ ). Let the peak gap voltage be  $V$ . The peak voltage across  $m$  will be

$$V_m = mV/L \quad (a4)$$

In a resonator, if a peak voltage  $V$  across the gap produces a peak flux  $\psi_m$  linking the coupling loop when no current flows in the coupling loop, then

$$V_m = d\psi_m/dt = mV/L \quad (a5)$$

This defines  $m$  in terms of magnetic field, and  $L$ .

Figure 115 is also a quite accurate representation of Fig. 113. In this case the "terminals" are taken as located at the end of the wave guide.  $L_0$  is the inductance of the iris, which will vary with frequency.

When we are interested in the impedance at the gap as a function of frequency, we may equally well use the equivalent circuit of Fig. 116. Here  $G_L$  represents conductance due to load;  $G_R$  represents conductance due to resonator loss. The total conductance, called  $G_C$ , is

$$G_C = G_R + G_L \quad (a6)$$

The circuit of Fig. 116 does not tell us how  $G_L$  varies with variation in load impedance  $Z_L$ . Further,  $L$  and  $C$  in this circuit are changed in changing  $Z_L$ , and include a contribution from the inductance of the coupling loop (which should not be very large).

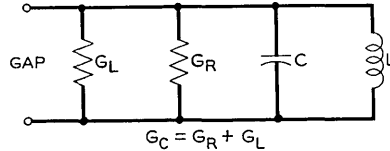


Fig. 116.—A simplified equivalent circuit of an oscillator resonator.

Several resonator parameters are vitally important in discussing reflex oscillators. These will be discussed referring to Fig. 116.  $G_L$  and  $G_R$  have already been defined. The resonant radian frequency  $\omega_0$  is of course

$$\omega_0 = (LC)^{-1/2} \quad (\text{a7})$$

A very important quantity will be called the characteristic admittance  $M$

$$M = (C/L)^{1/2} \quad (\text{a8})$$

This quantity is important because at a frequency  $\Delta\omega$  off resonance the admittance of the circuit is very nearly

$$Y = G + j2M\Delta\omega/\omega_0 \quad (\text{a9})$$

$$\Delta\omega = \omega - \omega_0$$

The “loaded”  $Q$  of the circuit will be referred to merely as  $Q$  and is

$$Q = M/G_C \quad (\text{a10})$$

The unloaded  $Q$  is

$$Q_0 = M/G_R \quad (\text{a11})$$

A quantity which may be called the “external  $Q$ ” is

$$Q_E = M/G_L \quad (\text{a12})$$

We see

$$1/Q_0 + 1/Q_E = 1/Q \quad (\text{a13})$$

The energy stored in the magnetic field at zero voltage across the resonator, and the energy stored in the electric field at the voltage maximum are both

$$W_s = (1/2)V^2C \quad (\text{a14})$$

$$= (1/2)V^2M/\omega_0 \quad (\text{a15})$$

Here  $V$  is the peak gap voltage. Expressions (a14) and (a15) are valuable in making resonator calculations from exact or approximate field distributions. They define  $C$ ,  $L$  and  $M$  in terms of electric and magnetic field. The energy dissipated per cycle is

$$W_L = \pi V^2 C / \omega_0 \quad (\text{a16})$$

Hence, we might have written  $Q$  as

$$Q = 2\pi W_s / W_L \quad (\text{a17})$$

This is one popular definition of  $Q$ .

In (a8)–(a17) we usually assume that there is no appreciable energy stored in the load or the field of the coupling loop, so that  $M$  is considered as unaffected by load. The effect of “high  $Q$ ” loads with considerable energy storage is considered in a somewhat different manner in Sec. IXB.

It must be emphasized that the expressions given above are valid for high  $Q$  circuits only (a  $Q$  of 50 is high in this sense). Expression (a17) is often used as a general definition of  $Q$ , but it is not complete without an additional definition of the meaning of resonance in a low  $Q$  circuit with many modes. Schelkunoff uses another definition of  $Q$ . Unforced oscillations in a damped circuit can be represented as a combination of several terms

$$V_1 e^{p_1 t} + V_2 e^{p_2 t} + \dots \quad (\text{a18})$$

$$p_1 = \alpha_1 + j\omega_1 \quad (\text{a19})$$

Schelkunoff takes the  $Q$  of the  $n$ th mode as

$$Q_n = \omega_n / \alpha_n \quad (\text{a20})$$

This is at least a consistent and complete definition. The reader can easily see that it accords with the definitions given for high  $Q$ 's in connection with the circuit of Fig. 116.

Sometimes there may be a complicated circuit between the gap and a coaxial line or wave guide. In this case, the circuits intervening between the gap and the line can be regarded as a 4 terminal transducer (Fig. 117). The constants of this transducer will vary with frequency. No further consideration of this generalized treatment will be given, as it is well covered in books on network theory. A particular representation of the transducer will be pointed out, however. If the impedance in the line is referred to a special point, one parameter can be eliminated, giving the equivalent circuit shown in Fig. 118. If the gap is short-circuited, the impedance is zero and the impedance at the special point to be chosen on the line is  $R$ ; the special point may be chosen as the potential minimum with the gap shorted.



$N$ , the voltage ratio of a perfect transformer, is usually complex. The impedance ratio  $NN^*$  is real. If we are not interested in the relation of output phase to gap phase, we may disregard the phase angle of  $N$ , and deal only with the impedance ratio, the absolute value of  $N$  squared, which we will call  $N^2$ . Thus, using this equivalent circuit and disregarding the phase of  $N$  we can for our purposes reduce the number of independent parameters from the usual 6 for a passive 4 terminal network to 4,  $Y (= G + jB)$ ,  $N^2$  and  $R$ . This reduction can greatly simplify the algebra and arithmetic of microwave problems. The circuit of Fig. 118 has an additional advantage; if we choose our impedance reference point on the output line or guide to be the suitable point nearest to the actual output

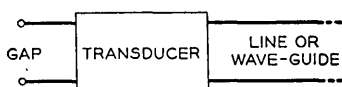


Fig. 117.—A 4-terminal transducer is the most general connection between the oscillator gap and a line or wave guide.

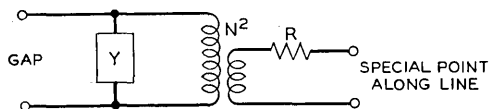


Fig. 118.—One circuit which will represent all the properties of a general 4-terminal transducer. This circuit consists of an admittance  $Y$  shunting the gap, a perfect transformer of complex ratio  $N$  and a series resistance  $R$ .

loop or iris, the circuit represents fairly accurately the frequency dependence of the output impedance if we merely take  $Y$  as

$$Y = G_R + j\omega(C - 1/\omega L) \quad (\text{a21})$$

Near resonance we may use the simpler form.

$$Y = G_R + j2M\Delta\omega/\omega_0 \quad (\text{a22})$$

Something has already been said in a general way about the evaluation of  $L$  and  $C$  in terms of the electric and magnetic field distribution in a resonator. It is completely outside of the scope of this paper to consider this subject at any length; the reader is referred to various books.<sup>19, 20, 21</sup> The discontinuity calculations of Whinnery and Jamieson<sup>22</sup> are also of great value in

<sup>19</sup> *Electromagnetic Waves*, S. A. Schelkunoff, Van Nostrand, 1943.

<sup>20</sup> *Fields & Waves in Modern Radio*, Ramo & Whinnery, Wiley, 1944.

<sup>21</sup> *Microwave Transmission Data*, Sperry Gyroscope Company, 1944.

<sup>22</sup> J. R. Whinnery and H. W. Jamieson, *Equivalent Circuits for Discontinuities in Transmission Lines*, *Proc. I.R.E.*, 32, 2, pp. 99-114.

making resonator calculations. These can be profitably combined with disk transmission line formulae.<sup>19, 20</sup>

The writers would like to point out that in the present state of the art the testing of resonator calculations by models is important. Models need not be made of the size finally desired. If all dimensions are made  $N$  times as large, the wavelength will be  $N$  times as great. The characteristic admittance  $M$  will be unchanged. If the material is the same, and the surface is smooth and homogeneous,  $Q$  and  $1/G_R$ , the shunt resonant resistance, will be  $\sqrt{N}$  times as great.

It is perhaps a needless caution to say that the accuracy of a method of resonator calculation cannot be judged by its mathematical complexity or the difficulty of using it. Methods of calculation which are simple and may seem to make unduly broad approximations are sometimes better founded than appears on the surface, and complicated methods, exact if carried far enough, may be so unsuited to the problem as to give very bad answers if used in obtaining approximate values.

## APPENDIX II

### MODULATION COEFFICIENT

In this appendix the effects of space charge are neglected.

The modulation coefficient  $\beta$  is defined as the peak energy in electron volts an electron can gain in passing through the field of a gap divided by the peak r-f voltage across the gap. If an electron were transported across the gap very quickly when the r-f voltage was at a maximum the energy in electron volts gained by the electron would be equal to the peak r-f voltage. Thus, the modulation coefficient can also be defined as the ratio of the peak energy actually gained to the energy which would be gained in a very quick transit at the time of maximum voltage.

In this appendix modulation coefficient will be considered only for r-f voltages small compared with the d-c accelerating voltage.

If an electron gains an energy  $\beta$  times the r-f voltage  $V$  across the gap, the work done on it is  $\beta eV$  electron volts. By the conservation of energy, an induced current must flow between the electrodes of the gap, transferring a charge  $\beta e$  against the voltage  $V$  and hence taking an amount of energy  $\beta eV$  from the circuit. Pursuing this argument we see that the modulation coefficient  $\beta$  times the electron convection current in the beam,  $q$ , gives the current induced in the gap by electron flow. In a circuit sense, there is fed into the gap, as from an infinite impedance source, an induced current  $\beta q$ .

We will assume that the gap involves a region in which the field along the electron path rises from zero and falls to zero again. This region is assumed

to be small compared with a wavelength and to have little a-c magnetic field in it, so that we can pretty accurately represent the field in this restricted region as the gradient of a potential. Along the path the potential is taken as the real part of

$$V(x)e^{j\omega t} \quad (b1)$$

For small gap voltages, to first order, the time that an electron reaches a given position may be taken as unaffected by the signal, so that

$$t = x/u_0 + t_0 \quad (b2)$$

Then the gradient along the path is

$$\frac{\partial V}{\partial x} = \text{Real } V'(x)e^{j(\omega x/u_0 + \omega t_0)}. \quad (b3)$$

The change in momentum in passing through the field may be obtained by integrating the force on an electron times the time through the field. Let points  $a$  and  $b$  be in the field-free region to the left and right of the gap. Then we have

$$\Delta(\dot{x}) = \text{Real } \frac{\eta}{u_0} \int_a^b V'(x)e^{j(\omega x/u_0 + \omega t_0)} dx \quad (b4)$$

$$\Delta(\dot{x}) = \text{Real } \frac{\eta e^{j\omega t_0}}{u_0} \int_a^b V'(x)e^{j\gamma x} dx \quad (b5)$$

$$\gamma = \omega/u_0. \quad (b6)$$

The integral will be a complex quantity. The exponential factor involving the starting time  $t_0$  will rotate this.  $\Delta(\dot{x})$  will have a maximum value when the rotation causes the vector to lie along the real axis, and this maximum value is thus the absolute value of the integral. Hence

$$\Delta(\dot{x})_{\max} = \frac{\eta}{u_0} \left| \int_a^b V'(x)e^{j\gamma x} dx \right|. \quad (b7)$$

For a-c voltages small compared with the voltage specifying the speed  $u_0$ , the energy change is proportional to the momentum change. For an electron transported instantly from one side of the gap to the other, the momentum change can be obtained by setting  $\gamma = 0$ .

$$\begin{aligned} \Delta(\dot{x})_0 &= \frac{\eta}{u_0} \int_a^b V'(x) dx \\ &= \frac{\eta}{u_0} V. \end{aligned} \quad (b8)$$

Here  $V$  is the voltage between  $a$  and  $b$ . Hence, the modulation coefficient  $\beta$  is given for small signals by

$$\beta = (1/V) \left| \int_a^b V'(x) e^{j\gamma x} dx \right| \quad (\text{b9})$$

$$V = V(b) - V(a) \quad (\text{b10})$$

$$\gamma = \omega/u_0 \quad (\text{b11})$$

$$u_0 = \sqrt{2\eta V_0} \quad (\text{b12})$$

Thus  $u_0$  is the electron velocity.

It is sometimes convenient to integrate by parts, giving the mathematical expression for  $\beta$  a different form

$$\beta = (1/V) \left| \frac{V'(x) e^{j\gamma x}}{j\gamma} \Big|_a^b - \frac{1}{j\gamma} \int_a^b V''(x) e^{j\gamma x} dx \right|$$

as  $V'(x)$  is zero at  $a$  and  $b$

$$\beta = (1/V) \left| \frac{1}{\gamma} \int_a^b V''(x) e^{j\gamma x} dx \right|. \quad (\text{b13})$$

An interesting and important case is that of a uniform field between grids. Let the first grid be at  $x = 0$  and the second at  $x = d$ . There is an abrupt transition to a gradient  $V/d$  at  $x = 0$ , and another abrupt transition to zero gradient at  $x = d$ . Thus, the integral (b13) is reduced to these two contributions, and we obtain

$$\beta = (1/V) \left| \frac{V}{\gamma d} \left( 1 - e^{j\gamma d} \right) \right|. \quad (\text{b14})$$

This is easily seen to be

$$\beta = \sin(\gamma d/2)/(\gamma d/2) \quad (\text{b14})$$

This function, the modulation coefficient for fine parallel grids, is plotted in Fig. 119.

Sometimes apertures, as, circular apertures, or long narrow slits are used without grids. There are important relations between the modulation coefficient for a path on the axis and one parallel to the axis for such systems.<sup>23</sup>

In a two-dimensional gap system with axial symmetry, if the modulation coefficient for a path along the axis is  $\beta_0$ , the modulation coefficient for a path  $y$  away from the axis is

$$\beta_y = \beta_0 \cosh \gamma y \quad (\text{b15})$$

<sup>23</sup> These relations first came to the attention of the writers through unpublished work of D. P. R. Petrie, C. Strachey and P. J. Wallis of Standard Telephones and Cables.

In an axially symmetrical electrode system, if the modulation coefficient on the axis is  $\beta_0$ , the modulation coefficient at a radius  $r$  is

$$\beta_r = \beta_0 I_0(\gamma r) \quad (\text{b16})$$

Here  $I_0$  is a modified Bessel function.

It is easy to see why (b15) and (b16) must be so. The field in the gap can be resolved by means of a Fourier integral into components which vary

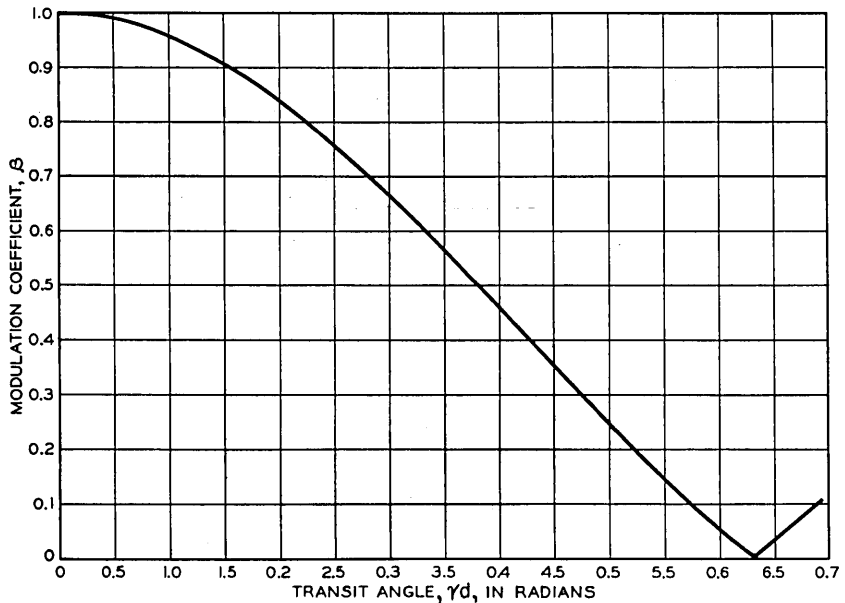


Fig. 119.—Modulation coefficient for fine parallel grids vs transit angle across the gap in radians.

$$\beta = |\sin(\gamma d/2)/(\gamma d/2)|, \quad \gamma = \omega/v_0 = 3170/\lambda\sqrt{V_0}.$$

sinusoidally along the axis and as the hyperbolic cosine (in the two-dimensional case) of the same argument normal to the axis or as the modified Bessel function (in the axially symmetrical case) of the same argument radially. When the integration of (b9) is carried out, only that portion of the Fourier integral representation for which the argument is  $\gamma x$  contributes to the result, and as that part contains as a factor  $\cosh \gamma x$  or  $I_0(\gamma x)$  (b15) and (b16) are established.

The simple theory of velocity modulation presented in Appendix III makes no provision for variation of modulation coefficient across the beam. If we confine ourselves to very small signals, we find that the factor which appears is  $\beta^2$ . We may distinguish two cases: If the distance from the axis

of symmetry were the same for both transits of the electron, we would do well to average  $\beta^2$ . If the electrons got thoroughly mixed up in position between their two transits, we would do well to average  $\beta$  and then square the average. We will present both average and r.m.s. values of  $\beta$ . The averaged value of  $\beta$  will be denoted as  $\beta_a$ , the r.m.s. value as  $\beta_s$ ; the value on the axis will be called  $\beta_0$ .

From (b15) and (b16) we obtain by simple averaging for the two dimensional case,

$$\beta_a = \beta_0 \frac{\sinh \gamma y}{\gamma y} \quad (\text{b17})$$

$$\beta_s = \beta_0 \left[ \frac{1}{2} \left( \frac{\sinh 2\gamma y}{2\gamma y} + 1 \right) \right]^{\frac{1}{2}} \quad (\text{b18})$$

and for an axially symmetrical case

$$\beta_a = \beta_0 2I_1(\gamma r) / (\gamma r) \quad (\text{b19})$$

$$\beta_s = \beta_0 [I_0^2(\gamma r) - I_1^2(\gamma r)]^{1/2} \quad (\text{b20})$$

It is convenient to rewrite these in a slightly different form, using (b15) and (b16).

$$\beta_a = \beta_y (\tanh \gamma y / \gamma y) \quad (\text{b21})$$

$$\beta_s = \beta_y \left[ \frac{\sinh 2\gamma y + 2\gamma y}{2\gamma y (\cosh 2\gamma y + 1)} \right]^{\frac{1}{2}} \quad (\text{b22})$$

$$\beta_a = \beta_r 2I_1(\gamma r) / (\gamma r) I_0(\gamma r) \quad (\text{b23})$$

$$\beta_s = \beta_r [1 - I_1^2(\gamma r) / I_0^2(\gamma r)]^{1/2} \quad (\text{b24})$$

Now consider two similar cases: two pairs of parallel semi-infinite plates with a very narrow gap between them, and two semi-infinite tubes of the same diameter, on the same axis and with a very narrow gap between them (see Fig. 120). For electrons traveling very near the conducting surface,  $V'$  is zero save over a very short range at the gap, and the modulation coefficient is unity. Thus, by putting  $\beta_y = \beta_r = 1$ , we can use expressions (b15)–(b24) directly to evaluate  $\beta_a$ ,  $\beta_s$  and  $\beta_0$  for the configurations described. These quantities are shown in Figs. 121 and 122.

Suppose, now, that the gap between the plates or tubes is not very small. In this case, we need to know the variation of potential with distance across the space  $d$  long which separates the edges of the gap in order to get the modulation coefficient at the very edge of the gap,  $\beta_y$  or  $\beta_r$ .

If the tubing or plates surrounding the gap are thick, we might reasonably

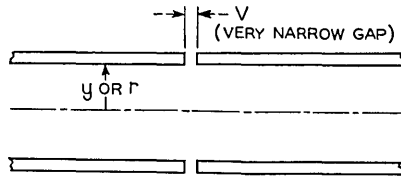


Fig. 120.—A gap consisting of pairs of semi-infinite planes or semi-infinite tubes.

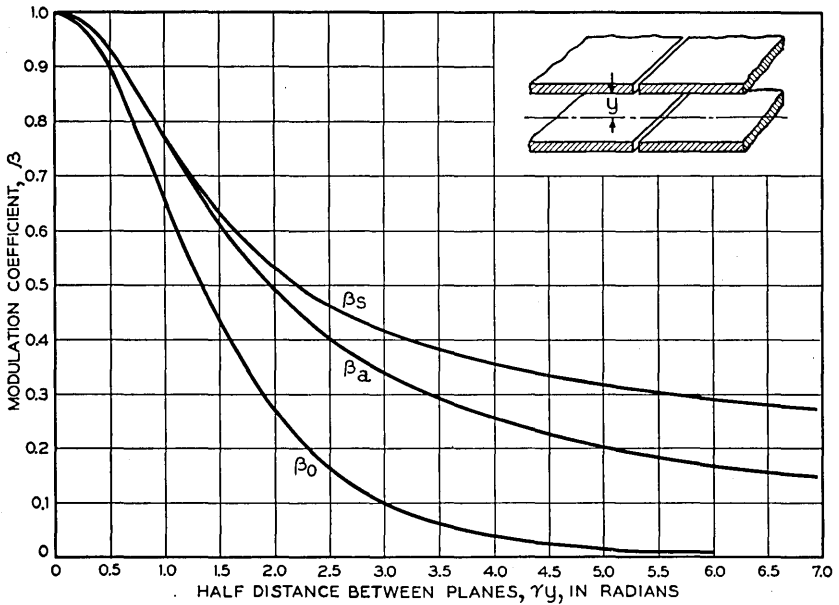


Fig. 121.—Modulation coefficient for two semi-infinite pairs of parallel planes with the edges very very close together, plotted vs the half distance between planes in radians.  $\beta_0$  is the modulation coefficient for electrons travelling along the axis.  $\beta_a$  is the average modulation coefficient and  $\beta_s$  is the r.m.s. modulation coefficient. The separation of the planes is  $2y$ ,  $\beta_0 = 1/\cosh \gamma y$ ,

$$\beta_0 = \tanh \gamma y / \gamma y, \quad \beta_s = \left[ \frac{\sinh 2\gamma y + 2\gamma y}{2\gamma y (\cosh 2\gamma y + 1)} \right]^{\frac{1}{2}}$$

assume a linear variation of potential with distance in the space between them. In this case, (b9) gives

$$\beta_y \text{ or } \beta_r = F_1(\gamma d) = \sin(\gamma d/2) / (\gamma d/2) \tag{b25}$$

This is the same function shown in Fig. 119.

If the tube wall or plates are very thin, one may, following Petrie, Strachey and Wallis<sup>23</sup> assume a potential variation between the edges of the gap of

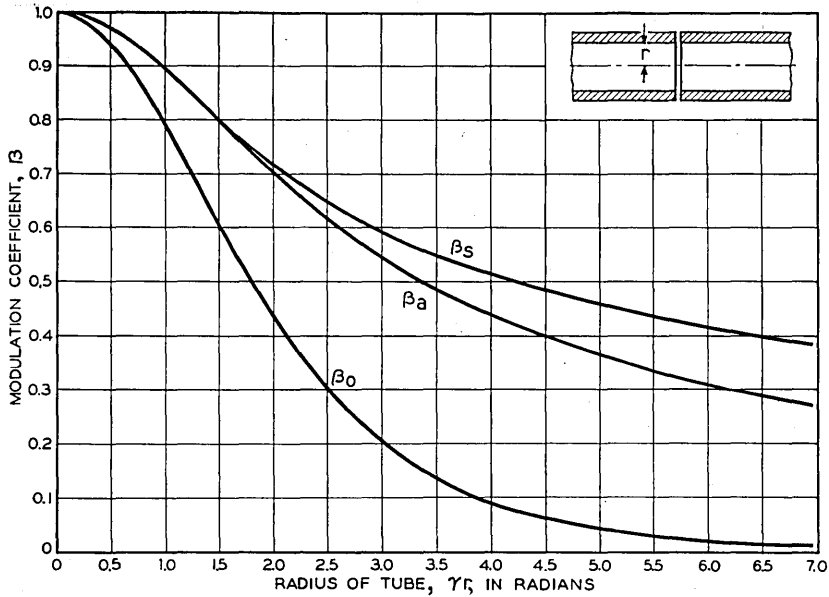


Fig. 122.—Modulation coefficient for two semi-infinite tubes separated by a very small distance, plotted vs the radius of the tube in radians.  $\beta_0$  is the modulation coefficient on the axis,  $\beta_a$  is the average modulation coefficient and  $\beta_s$  is the root mean square modulation coefficient.  $r$  is the radius of the cylinders.

$$\beta_0 = 1/I_0(\gamma r), \quad \beta_a = 2I_1(\gamma r)/\gamma r I_0(\gamma r),$$

$$\beta_s = [1 - I_1^2(\gamma r)/I_0^2(\gamma r)]^{1/2}$$

the form

$$V = \frac{1}{\pi} \sin^{-1} \frac{2x}{d} \quad (\text{b26})$$

In this case, (b9) gives

$$\beta_y \text{ or } B_r = F_2(\gamma d) = J_0(\gamma d/2) \quad (\text{b27})$$

Both  $F_1(\gamma d)$  and  $F_2(\gamma d)$  are plotted vs.  $\gamma d$  in Fig. 123.

Figures 121, 122 and 123 cover fairly completely the case of slits and holes. The same methods may be used to advantage in making an approximate calculation taking into account the effect of grid pitch and wire size on modulation coefficient.

Assume we have a pair of lined up grids, as shown in Fig. 124. Approximately, the potential near the left one is given as

$$V = V_1'x/2 + (aV_1'/4\pi) \ln \left[ 2 \left( \cosh \frac{2\pi x}{a} - \cos \frac{2\pi y}{a} \right) \right]. \quad (\text{b28})$$



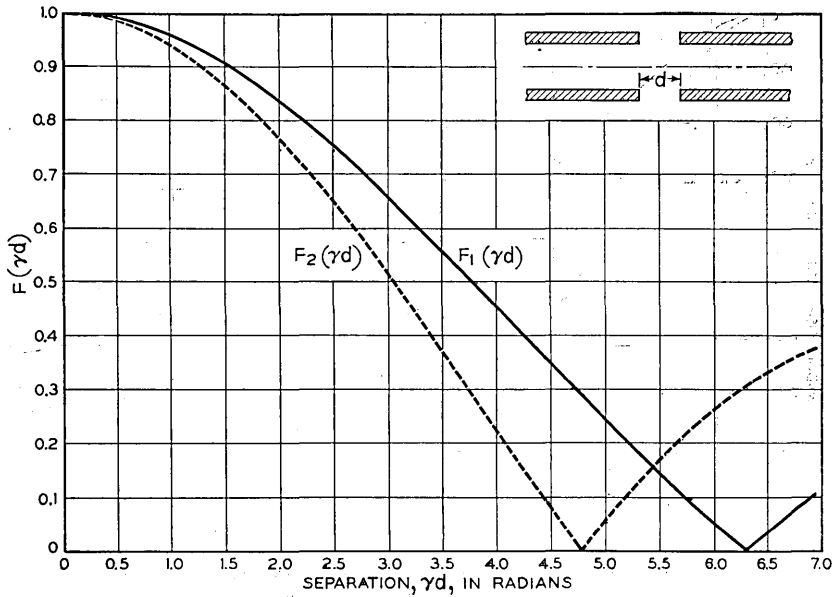


Fig. 123.—If the planes or tubes considered in Figs. 121 and 122 are separated by appreciable distance, the modulation coefficients given in those figures must be multiplied by a factor  $F(\gamma d)$ . In this figure, the multiplying factor is evaluated and plotted vs the separation in radians for two assumptions—that the gap has very blunt edges ( $F_1(\gamma d)$ ) and that the gap has very sharp edges ( $F_2(\gamma d)$ ).

This is zero far to the left and  $V'_1 x$  far to the right. This expression is useful only when the wire radius  $r$  is quite small compared with the separation  $a$ . Midway between wires,

$$V = V'_1 x/2 + (a V'_1/2\pi) \ln \left[ 2 \cosh \frac{\pi x}{a} \right] \tag{b29}$$

$$V'' = (V'_1 \pi/2a) \operatorname{sech}^2 \frac{\pi x}{a} \tag{b30}$$

If we use (b30) for each grid, the values of  $V''$  for the two grids will overlap somewhat. However, let us neglect this overlap, apply (b30) at each grid, and using (b13), integrate for each grid from  $-\infty$  to  $+\infty$ , giving

$$\begin{aligned} \beta_0 &= (1/V)(V'_1 \pi/\gamma a) \left| 1 - e^{j\gamma d} \right| \left| \int_{-\infty}^{\infty} \operatorname{sech}^2 \frac{\pi x}{a} e^{j\gamma x} dx \right| \tag{b31} \\ &= f \{ \sin (\gamma d/2)/(\gamma d/2) \} G_0(\gamma a) \end{aligned}$$

where

$$f = V'_1/(V/d) \tag{b32}$$

$$G_0(\gamma a) = \frac{1}{2} \left| \int_{-\infty}^{\infty} e^{(j\gamma a/\pi)u} \operatorname{sech}^2 u du \right| = (\gamma a/2)/\sinh (\gamma a/2) \tag{b33}$$

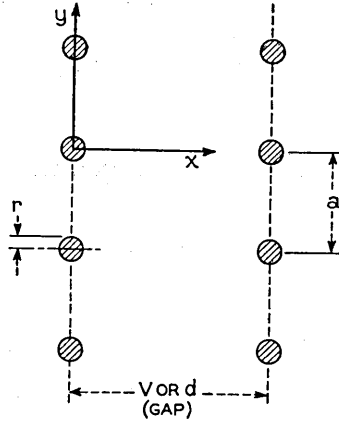


Fig. 124.—A gap consisting of lined up grids.

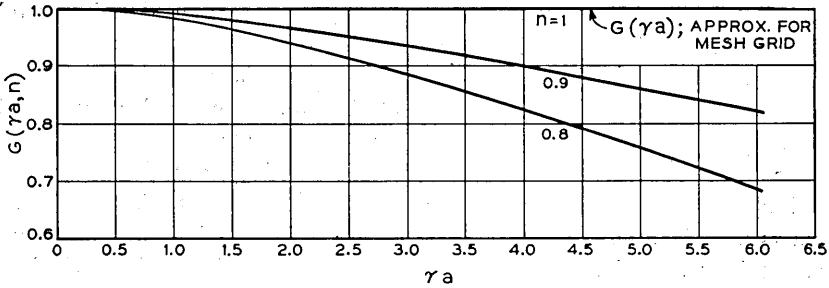


Fig. 125.—A factor used in obtaining the modulation coefficient of lined up grids vs the wire spacing in radians.  $n$  is the fraction open. The curve for  $n = 1$  also applies approximately for a mesh grid.

Suppose we average over the open space of the grid. If the grid is a fraction  $n$  open, from (b17) we see that the average over the open space will be obtained by substituting for  $G_0$  a quantity  $G(\gamma a, n)$  given by

$$G(\gamma a, n) = \{ \sinh (n\gamma a/2)/(n\gamma a/2) \} G_0(\gamma a) \tag{b34}$$

In Fig. 125,  $G(\gamma a, n)$  is plotted vs.  $\gamma a$  for  $n = 1, .9, .8$ . This about covers the useful range of values. It should be positively noted that the average is over the *open* area of the grid and applies to current getting through.

It remains to evaluate the factor  $f$ . Suppose  $x = 0$ . At the surface of the grid wire,  $y = r$ , the radius of the wire,

$$\delta V = (V_1' a/4\pi) \ln \left[ 2 \left( 1 - \cos \frac{2\pi r}{a} \right) \right] = (V_1' a/2\pi) \ln \left[ 2 \sin \frac{\pi r}{a} \right]$$

As we have already assumed  $r$  is small, we may as well write

$$\delta V = (V'_1 a / 2\pi) 2.3 \log_{10} \left( \frac{a}{2\pi r} \right) \quad (\text{b35})$$

This emphasizes the sign of  $\delta V$ .

According to (b28), the grid plane appears from a distance to be at zero potential. Thus,

$$V'_1 d - 2\delta V = V \quad (\text{b36})$$

and from (b32)

$$f = \{1 + (a/\pi d) 2.3 \log_{10} (a/2\pi r)\}^{-1} \quad (\text{b37})$$

If we go back over our results, we have for lined-up singly-wound grids, from (b31), (b34) and (b37), the average modulation coefficient

$$\beta_a = f \{ \sin(\gamma a/2) / (\gamma a/2) \} G(\gamma a, n) \quad (\text{b38})$$

The quantity  $\sin(\gamma a/2)$  can be obtained from Fig. 119,  $G(\gamma a, n)$  is plotted in Fig. 125, and  $f$  can be calculated from (b37) above.

It must be emphasized again that these expressions are good only for very fine wires ( $r \ll a$ ), and get worse the closer the spacing compared with the wire separation. It is also important to note that  $G(\gamma a, n)$  indicates little reduction of  $\beta_a$  even for quite wide wire separation. Now  $\gamma d$  will be less than  $2\pi$ , as  $\beta_a = 0$  at  $\gamma d = 2\pi$ . As  $a$  approaches  $d$  in magnitude, the assumptions underlying the analysis, in which the integration around each grid was carried from  $-\infty$  to  $\infty$ , become invalid and the analysis is not to be trusted.

It is very important to bear one point in mind. If we design a resonator assuming parallel conducting planes a distance  $L$  apart at the gap, and then desire to replace these planes with grids without altering the resonant frequency, we should space the grids not  $L$  apart but

$$d = fL \quad (\text{b39})$$

apart to get the same capacitance and hence the same resonant frequency.

Mesh grids are sometimes used. To get a rough idea of what is expected, we may assume the potential about a grid to be

$$V = V'_1 x/2 + (aV'_1/8\pi) \ln \left[ 2 \left( \cosh \frac{2\pi x}{a} - \cos \frac{2\pi y}{a} \right) \right] \\ + (aV'_1/8\pi) \ln \left[ 2 \left( \cosh \frac{2\pi y}{a} - \cos \frac{2\pi z}{a} \right) \right] \quad (\text{b40})$$

Here the grid is assumed to lie in the  $y, z$ , plane. This gives a mesh of wires about squares  $a$  on  $a$  side, the wires bulging at the intersections. We take  $r$  to be the wire radius midway between intersections.

We see that  $\beta_0$  will be the same in this case as in the case of a parallel wire grid. Thus the added wires, which intercept electrons, haven't helped us as far as this part of the expression goes.

As a further approximation, an averaging will be carried out as if the apertures had axial symmetry. Averaging will be carried out to a radius giving a circle of area  $a^2$ . The steps will not be indicated.

Further a factor analogous to  $f$  will be worked out. Again, the steps will not be indicated. The results are

$$\beta_a = g \{ \sin(\gamma d/2) / (\gamma d/2) \} G_1(\gamma a) \quad (\text{b41})$$

$$G_1(\gamma a) = 2I_1(\gamma a / \sqrt{\pi}) / (\gamma a / \sqrt{\pi}) G_0(\gamma a) \quad (\text{b42})$$

$$g = 1 + (.365 a/d) (\log_{10} (a/\pi r) - .69) \quad (\text{b43})$$

The quantity  $G_1(\gamma, a)$  is plotted in Fig. 125 for comparison with the parallel wire case. It should be emphasized that these expressions assume  $r \ll a$ , and that  $G_1(\gamma a)$  is really only an estimate based on a doubtful approximation. The indications are, however, that the only beneficial affect of going from a parallel wire grid to a mesh with the same wire spacing lies in a small decrease in  $\delta V$  (a small increase in the  $\mu$  of the grid), while by doubling the number of wires in the parallel wire grid,  $a$  can be halved, both raising  $\mu$  and increasing  $G(\gamma a, n)$ .

### APPENDIX III

#### APPROXIMATE TREATMENT OF BUNCHING

We assume<sup>24</sup> that the conditions are as shown in Fig. 126 where the electron energy on first entering the gap is specified by the potential  $V_0$ . Across the gap there exists a radio frequency voltage,  $V \sin \omega t$ . The ratio of the energy gained by the electron in crossing the gap to the energy which it would gain if the transit time across the gap were zero is called the modulation coefficient and is denoted by a factor,  $\beta$ . We assume that the modulation coefficient is the same for all electrons. We also neglect the effects of space charge throughout. After leaving the gap the electrons enter an electrostatic retarding field of strength  $E_0 = \frac{V_R + V_0}{l}$

<sup>24</sup> This analysis follows the method given by Webster, J. App. Phys. 10, July 1939, pp. 501-508.

such that the stream flow is reversed and caused to retrace the gap. The round trip transit time,  $\tau_a$ , in the retarding field when a signal exists across the gap is then given by

$$\tau_a = \frac{2 \sqrt{2\eta(V_0 + \beta V \sin \omega t_1)}}{\eta E_0} \quad (c1)$$

where  $\eta = \frac{e}{m} \times 10^7 = 1.77 \times 10^{15}$  in practical units and  $t_1$  is the time of first entry of the gap. The time of return to the gap will be

$$t_2 = t_1 + \tau_a \quad (c2)$$

More accurately  $t_1$  and  $t_2$  are measured from the central plane of the gap in which case a second term should be added to (c1) corresponding to motion at

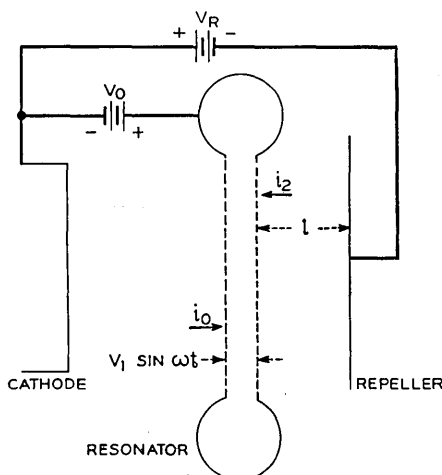


Fig. 126.—Diagram of a reflex oscillator showing quantities used in the treatment of bunching.

constant velocity. This term is, however, very small and will be neglected here. If  $i_2$  is the current returning to the gap and  $I_0$  the uniform current entering the gap on its first transit, then from conservation of charge one may write

$$I_0 dt_1 = i_2 dt_2 \quad (c3)$$

In what follows it will be first assumed that  $t_2$  and  $t_1$  are related by a single valued function. At the end of this appendix it will be shown that the analysis is also valid where the relating function is multiple valued.

We now make a Fourier series analysis of  $i_2$  in order to determine the

harmonic distribution. Thus

$$i_2 = a_0 + a_1 \cos(\omega t_2 + \varphi) + a_2 \cos 2(\omega t_2 + \varphi) + \dots \\ + b_1 \sin(\omega t_1 + \varphi) + b_2 \sin 2(\omega t_2 + \varphi) + \dots \quad (c4)$$

where

$$a_n = \frac{1}{\pi} \int_{-\pi}^{\pi} i_2 \cos n(\omega t_2 + \varphi) d\omega t_2 \\ b_n = \frac{1}{\pi} \int_{-\pi}^{\pi} i_2 \sin n(\omega t_2 + \varphi) d\omega t_2 \quad (c5)$$

Using (c1) to (c3) we change our variable to  $t_1$  obtaining

$$a_n = \frac{1}{\pi} \int_{-\pi}^{\pi} I_0 \cos n\omega \left( t_1 + \frac{2\sqrt{2\eta(V_0 + \beta V \sin \omega t_1)}}{E_0} + \varphi \right) d\omega t_1 \quad (c6)$$

$$\text{Let } \omega t_1 = \theta_1 \quad \omega \tau_0 = \frac{2\omega \sqrt{2\eta V_0}}{E_0} = \theta \quad X = \frac{\theta \beta V}{2V_0}$$

$$a_n = \frac{1}{\pi} \int_{-\pi}^{\pi} I_0 \cos n \left( \theta_1 + \varphi + \theta \left[ 1 + \frac{X}{\theta} \sin \theta_1 \right. \right. \\ \left. \left. - \frac{1}{2} \frac{X^2}{\theta^2} \sin^2 \theta_1 + \dots \right] \right) d\theta_1 \quad (c7)$$

(c7) cannot be evaluated in closed form without further restriction. The first order theory may be obtained by assuming that  $\frac{1}{2} \frac{nX^2}{\theta} \ll \frac{\pi}{2}$ . It is not sufficient to assume that  $\frac{X^2}{\theta} \ll X$ . The latter assumes that the third and higher terms of the expansion are small compared to the second. Let the integrand be denoted as  $i_0 \cos nx$ . The quantity to be evaluated is the argument of a trigonometric function where the total angle is of less importance than the difference  $nx - 2m\pi$  where  $m$  is the largest integer for which the difference is positive. The condition first expressed requires that the contribution of the third and higher terms to the difference phase shall be small. The restriction requires that

$$n \left( \frac{\beta V}{2V_0} \right)^2 \omega \tau_0 \ll \pi \quad (c8)$$

This is a more stringent requirement than

$$\frac{X}{\theta} = \frac{\beta V_1}{2V_0} \ll 1 \quad (c9)$$

(c9) requires only a small modulation depth while (c8) imposes a restriction on both the modulation depth and the drift time.

With the restriction (c8) imposed we obtain

$$a_n = \frac{1}{\pi} \int I_0 \cos n \left( \theta_1 + \varphi + \theta \left[ 1 + \frac{X}{\theta} \sin \theta_1 \right] \right) d\theta_1 \quad (\text{c10})$$

If we let  $\varphi = -\theta$  all coefficients  $b_n$  will be zero and

$$a_n = 2(-1)^n I_0 J_n(Xn), \quad a_0 = I_0 \quad (\text{c11})$$

Thus the first order expansion for the current returning through the gap is

$$i_2 = I_0 [(1 - 2J_1(X) \cos \omega(t_2 - \tau_0) + 2J_2(2X) \cos 2\omega(t_2 - \tau_0) \cdots)] \quad (\text{c12})$$

Our principal interest is in the fundamental component, which in complex notation is given by

$$(i_2)_f = -2I_0 J_1(X) e^{j\omega(t_2 - \tau_0)} \quad (\text{c13})$$

It is shown in Appendix II that the circuit current induced in the gap will be given, if account is taken of the phase reversal of  $\pi$  resulting from the reversal of direction of the beam, by

$$I_2 = -\beta(i_2)_f$$

The gap voltage at the time of return will be  $v = V \sin \omega t_2$  or in complex notation

$$v = V e^{j(\omega t_2 - (\pi/2))} \quad (\text{c14})$$

Hence the electronic admittance to the fundamental will be

$$Y_e = \frac{I_2}{v} = \frac{2I_0\beta}{V} J_1 \left( \frac{\omega\tau_0\beta V}{2V_0} \right) e^{-j(\omega\tau_0 - (\pi/2))} \quad (\text{c15})$$

In the foregoing it was assumed that  $t_2$  was a single valued function of  $t_1$ . We may generalize by writing (c3) as

$$\sum I_0 dt_1 = i_2 dt_2 \quad (\text{c16})$$

For sufficiently large signals there may be several intervals  $dt_1$  which contribute charge to a given interval  $dt_2$  and hence we write a summation for the left hand side of (c16). When the Fourier analysis is made and the change in variable from  $t_2$  to  $t_1$  is made the single integral breaks up into a sum of integrals. In Fig. 127 we plot time  $t_1$  on a vertical scale with the sine wave indicating the instantaneous gap voltage. Displaced to the right on a vertical scale we plot time  $t_2$ . The solid lines connect corresponding times in the absence of signal for increments of time  $dt_1$  and  $dt_2$ . When sufficiently

large signals are applied some of the electrons in the original interval  $dt_1$  will gain or lose sufficient energy to be thrown outside the original corresponding interval  $dt_2$  as for example as indicated by  $AB$ . If we consider a whole cycle of the gap voltage in time  $t_2$  it is apparent that, under steady state conditions, for every electron which is thrown outside the corresponding cycle in  $t_2$  another from a different cycle in  $t_1$  is thrown in whose phase differs by a multiple of  $2\pi$  as for example  $CD$ . In summing the effects of these charge increments the difference of  $2\pi$  in starting phase produces no physical effect. This is of course also true mathematically in the Fourier analysis of a periodic function since in integrating over an interval  $2\pi$  it is immaterial whether we integrate over a single interval or break it up into a

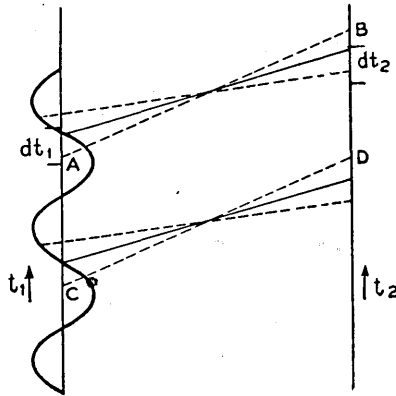


Fig. 127.—Diagram showing the relation between  $t_1$ , the time an electron crosses the gap for the first time, and  $t_2$ , the time the electron returns across the gap.

sum of integrals over intervals  $-\pi$  to  $a$ ,  $2\pi n_1 + a$  to  $2\pi n_1 + b$ ,  $2\pi n_2 + b$  to  $2\pi n_2 + c$ , etc. where the subintervals sum up to  $2\pi$ . Hence we conclude that the preceding analysis is also valid up to (c7) for signals sufficiently large so that  $t_2$  and  $t_1$  are related by a multiple valued function and is valid beyond that point provided that we do not violate (c8).

#### APPENDIX IV

##### DRIFT ANGLE AS A FUNCTION OF FREQUENCY AND VOLTAGE

Let  $\tau$  be the transit time in the drift space. Then the drift angle is

$$\theta = \omega\tau \quad (\text{d1})$$

For changes in voltage (resonator or repeller), both  $\tau$  and  $\omega$  will change.



Thus

$$\begin{aligned}\Delta\theta/\theta &= \Delta\omega/\omega + \Delta\tau/\tau \\ &= \Delta\omega/\omega + ((\partial\tau/\partial V)/\tau)\Delta V\end{aligned}\tag{d2}$$

As shown in Appendix VI, the derivative of  $\tau$  with respect to repeller voltage,  $\partial\tau/\partial V_R$ , is always negative, while the derivative of  $\tau$  with respect to resonator voltage,  $\partial\tau/\partial V_0$ , may be either negative or positive. For a linear variation of potential in the drift region,  $\partial\tau/\partial V_0$  is zero when  $V_R = V_0$  and negative for smaller values of  $V_R$ .

## APPENDIX V

### ELECTRONIC ADMITTANCE—NON-SIMPLE THEORY

A closer treatment of the drift action in the repeller space follows, in which are considered the changes which occur as the voltage on the cavity becomes large.

The additional terms to be considered come from an evaluation in series of the higher-order terms of (c7), which were neglected in Appendix III. Only the fundamental component of current will be considered, although other terms could be included if desired. The integrals of interest may be rewritten from (c7), using the relation  $\varphi = -\theta$ , as follows:

$$a_1 = \frac{I_0}{\pi} \int_{-\pi}^{\pi} \cos \left( \theta_1 + X \sin \theta_1 - \frac{1}{2} \frac{X^2}{\theta} \sin^2 \theta_1 + \frac{1}{2} \frac{X^3}{\theta^2} \sin^3 \theta_1 + \dots \right) d\theta_1\tag{e1}$$

$$b_1 = \frac{I_0}{\pi} \int_{-\pi}^{\pi} \sin \left( \theta_1 + X \sin \theta_1 - \frac{1}{2} \frac{X^2}{\theta} \sin^2 \theta_1 + \frac{1}{2} \frac{X^3}{\theta^2} \sin^3 \theta_1 + \dots \right) d\theta_1\tag{e2}$$

We shall hereinafter neglect terms of higher order in  $\frac{1}{\theta}$  than those explicitly shown here. With this neglect, we can expand the trigonometric functions, obtaining

$$\begin{aligned}a_1 &= \frac{I_0}{\pi} \int_{-\pi}^{\pi} \cos (\theta_1 + X \sin \theta_1) \left[ 1 - \frac{1}{8} \frac{X^4}{\theta^2} \sin^4 \theta_1 + \dots \right] d\theta_1 \\ &\quad - \frac{I_0}{\pi} \int_{-\pi}^{\pi} \sin (\theta_1 + X \sin \theta_1) \\ &\quad \cdot \left[ -\frac{1}{2} \frac{X^2}{\theta} \sin^2 \theta_1 + \frac{1}{2} \frac{X^3}{\theta^2} \sin^3 \theta_1 + \dots \right] d\theta_1\end{aligned}\tag{e3}$$

$$\begin{aligned}
 b_1 = & \frac{I_0}{\pi} \int_{-\pi}^{\pi} \sin(\theta_1 + X \sin \theta_1) \left[ 1 - \frac{1}{8} \frac{X^4}{\theta^2} \sin^4 \theta_1 + \dots \right] d\theta_1 \\
 & + \frac{I_0}{\pi} \int_{-\pi}^{\pi} \cos(\theta_1 + X \sin \theta_1) \\
 & \cdot \left[ -\frac{1}{2} \frac{X^2}{\theta} \sin^2 \theta_1 + \frac{1}{2} \frac{X^3}{\theta^2} \sin^3 \theta_1 + \dots \right] d\theta_1
 \end{aligned} \tag{e4}$$

Now of these terms, not all give contributions; some integrate to zero since the integrand is an odd function of  $\theta_1$ . Rewriting with those terms omitted,

$$\begin{aligned}
 a_1 = & \frac{I_0}{\pi} \int_{-\pi}^{\pi} \cos(\theta_1 + X \sin \theta_1) \left[ 1 - \frac{1}{8} \frac{X^4}{\theta^2} \sin^4 \theta_1 + \dots \right] d\theta_1 \\
 & - \frac{I_0}{\pi} \int_{-\pi}^{\pi} \sin(\theta_1 + X \sin \theta_1) \left[ \frac{1}{2} \frac{X^3}{\theta^2} \sin^3 \theta_1 + \dots \right] d\theta_1
 \end{aligned} \tag{e5}$$

$$b_1 = \frac{I_0}{\pi} \int_{-\pi}^{\pi} \cos(\theta_1 + X \sin \theta_1) \left[ -\frac{1}{2} \frac{X^2}{\theta} \sin^2 \theta_1 + \dots \right] d\theta_1. \tag{e6}$$

Evaluation of these terms is formally simplified by the following relationships, each obtained by differentiation of the previous one:

$$-2J_1(X) = \frac{1}{\pi} \int_{-\pi}^{\pi} \cos(\theta_1 + X \sin \theta_1) d\theta_1 \tag{e7}$$

$$-2J_1'(X) = -\frac{1}{\pi} \int_{-\pi}^{\pi} \sin(\theta_1 + X \sin \theta_1) \sin \theta_1 d\theta_1 \tag{e8}$$

$$-2J_1''(X) = -\frac{1}{\pi} \int_{-\pi}^{\pi} \cos(\theta_1 + X \sin \theta_1) \sin^2 \theta_1 d\theta_1. \tag{e9}$$

Continuation of this process gives all the terms of interest in (e5) and (e6). Hence

$$a_1 = I_0 \left( -2J_1 + \frac{1}{4} \frac{X^4}{\theta^2} J_1^{iv} + \frac{X^3}{\theta^2} J_1''' + \dots \right) \tag{e10}$$

$$b_1 = I_0 \frac{X^2}{\theta} (-J_1'' + \dots). \tag{e11}$$

Therefore the expression for the fundamental component of the beam current may be written as follows, passing to complex notation:

$$\begin{aligned}
 (i_2)_f & \sim a_1 \cos(\omega t_2 - \theta) + b_1 \sin(\omega t_2 - \theta) \\
 (i_2)_f & = (a_1 - j b_1) e^{j(\omega t_2 - \theta)} \\
 & = e^{j\omega t_2} e^{-j\theta} I_0 \left( -2J_1 + j \frac{X^2}{\theta} J_1'' + \frac{1}{\theta^2} (X^3 J_1''' + \frac{1}{4} X^4 J_1^{iv}) \right) + \dots
 \end{aligned} \tag{e12}$$

Following usual conventions, the real part of the complex expression represents the physical situation, and the exponential time function will usually be omitted in what follows.

Similarly to Appendix III, the induced current in the gap is

$$I_2 = -\beta(i_2)_f \\ = e^{j\omega t} \beta e^{-j\theta} I_0 \left( 2J_1 - j \frac{X^2}{\theta} J_1'' - \frac{1}{\theta^2} (X^3 J_1''' + \frac{1}{4} X^4 J_1^{iv}) \right). \quad (\text{e13})$$

The gap voltage is still the same, viz.

$$v \sim V \sin \omega t_2 \sim V e^{j(\omega t_2 - (\pi/2))} = + \frac{2V_0}{\beta} \frac{X}{\theta} e^{j(\omega t_2 - (\pi/2))}. \quad (\text{e14})$$

Accordingly, the electronic admittance to the fundamental will be

$$Y_e = \frac{I_2}{v} = \frac{I_0}{V_0} \beta^2 \frac{\theta}{X} e^{j((\pi/2) - \theta)} \left( J_1 - \frac{jX^2}{\theta^2} J_1'' - \frac{1}{\theta^2} \left( \frac{X^3}{2} J_1''' + \frac{X^4}{8} J_1^{iv} \right) \right) \quad (\text{e15})$$

The argument of  $J_1$  and its derivatives is understood to be  $X$ . The derivatives can be evaluated in terms of  $J_0$  and  $J_1$  by repeated use of the Bessel function recurrence relations (see Jahnke-Emde, Funktionentafeln, p. 144). The result is

$$Y_e = \frac{I_0}{V_0} \beta^2 \frac{\theta}{X} e^{j((\pi/2) - \theta)} \left( J_1 - \frac{j}{\theta} \left[ \left( 1 - \frac{X^2}{2} \right) J_1 - \frac{X}{2} J_0 \right] \right. \\ \left. - \frac{1}{\theta^2} \left[ \frac{1}{8} (X^2 + X^4) J_1 - \frac{1}{4} X^3 J_0 \right] + \dots \right). \quad (\text{e16})$$

The real part of this will be of interest; it is

$$G_e = + \frac{I_0}{V_0} \beta^2 \frac{\theta}{X} \sin \theta \left( J_1 + \frac{\cot \theta}{\theta} \left[ \left( 1 - \frac{X^2}{2} \right) J_1 - \frac{X}{2} J_0 \right] \right. \\ \left. - \frac{1}{\theta^2} \left[ \frac{1}{8} (X^2 + X^4) J_1 - \frac{1}{4} X^3 J_0 \right] \right). \quad (\text{e17})$$

The power generated by the electron stream is given by

$$P = -\frac{1}{2} G_e V^2 \\ = -I_0 V_0 \frac{2X}{\theta} \left( \sin \theta \left[ J_1 - \frac{1}{8\theta^2} ((X^2 + X^4) J_1 - 2X^3 J_0) \right] \right. \\ \left. + \frac{\cos \theta}{\theta} \left[ \left( 1 - \frac{X^2}{2} \right) J_1 - \frac{X}{2} J_0 \right] \right) + \dots \quad (\text{e18})$$

Of this power, only a part is usefully delivered to the load admittance  $G_L$ , the rest being dissipated because of the circuit loss conductance  $G_R$ . The power lost in the circuit is

$$P_R = \frac{1}{2}G_R V^2 = \frac{2V_0^2 G_R X^2}{\beta^2 \theta^2} \quad (\text{e19})$$

Accordingly, the useful power delivered to the load is

$$P_L = P - P_R \quad (\text{e20})$$

A quantity of interest is the maximum useful power which can be obtained from the reflex oscillator; this is given by

$$\frac{\partial P_L}{\partial X} = 0 = \frac{\partial P_L}{\partial \theta} \quad (\text{e21})$$

These two conditions are expressed by the next two equations.

$$2XJ_0 + \frac{1}{\theta} \cot \theta (-X^3 J_0 - X^2 J_1) + \frac{1}{\theta^2} \left( \left( \frac{7}{4}X^3 - \frac{1}{4}X^5 \right) J_0 + \left( -\frac{X^2}{2} - \frac{3}{2}X^4 \right) J_1 \right) + \frac{4V_0}{\beta^2 I_0} G_R \frac{X}{\theta \sin \theta} = 0 \quad (\text{e22})$$

$$XJ_0 + (-4 + X^2)J_1 + \theta \cot \theta \cdot 2J_1 - \frac{\cot \theta}{\theta} \left( \left( -\frac{1}{2}X^3 - 2X \right) J_0 + \left( 4 - \frac{7}{4}X^2 + \frac{1}{4}X^4 \right) J_1 \right) + \frac{1}{\theta^2} \left( -\frac{3}{2}X^3 J_0 + \frac{3}{4}(X^2 + X^4)J_1 \right) - \frac{4V_0}{\beta^2 I_0} G_R \frac{X}{\theta \sin \theta} = 0 \quad (\text{e23})$$

One may note that even if one sets  $G_R = 0$  and neglects terms in  $\frac{1}{\theta^2}$  the second of these equations is a little different from the corresponding one of Appendix III, so that a slightly different phase angle is predicted for maximum generated power. The result of Appendix III was

$$\theta \cot \theta = 1$$

predicting a phase angle  $\theta$  slightly less than  $\theta_n = (n + \frac{3}{4})2\pi$ . However, the zero order result here is

$$\theta \cot \theta = 2 - \frac{X^2}{2} = -.892 \quad (\text{e24})$$

predicting a phase angle a trifle larger than  $\theta_n$ , in the approximation of Appendix III.

The equations (e22) and (e23) may look as if drastic measures would now be needed, but a parametric solution is surprisingly easy; one need only solve (e22) for  $G_R$ , and substitute back into the power expression (e20). The results are

$$G_R = -\frac{I_0}{V_0} \frac{\beta^2}{4} \theta \sin \theta \left( 2J_0 + \frac{\cot \theta}{\theta} [-X^2 J_0 - X J_1] \right. \\ \left. + \frac{1}{\theta^2} \left[ \left( \frac{7}{4} X^2 - \frac{1}{4} X^4 \right) J_0 + \left( -\frac{X}{2} - \frac{3}{2} X^3 \right) J_1 \right] + \dots \right) \quad (\text{e25})$$

$$P_L = -I_0 V_0 \frac{X}{\theta} \sin \theta \left( 2J_1 - X J_0 + \frac{\cot \theta}{\theta} \left[ \left( -X + \frac{X^3}{2} \right) J_0 \right. \right. \\ \left. \left. + \left( 2 - \frac{X^2}{2} \right) J_1 \right] + \frac{1}{\theta^2} \left[ \frac{X^4}{2} J_1 + \left( -\frac{3}{8} X^3 + \frac{1}{8} X^5 \right) J_0 \right] \right) \quad (\text{e26})$$

$$G_L = -G_e - G_R = -\frac{I_0}{V_0} \beta^2 \frac{\theta}{X} \sin \theta \left( J_1 - \frac{1}{2} X J_0 + \frac{\cot \theta}{\theta} \right. \\ \left. \cdot \left[ \left( 1 - \frac{X^2}{4} \right) J_1 + \left( -\frac{X}{2} + \frac{X^3}{4} \right) J_0 \right] \right. \\ \left. + \frac{1}{\theta^2} \left[ \frac{1}{4} X^4 J_1 + \left( -\frac{3}{16} X^3 + \frac{1}{16} X^5 \right) J_0 \right] \right) \quad (\text{e27})$$

One further convolution is necessary, because the equations (e25) and (e26) are still subject to the optimum phase angle condition (e23). Since we are here carrying only terms as far as  $\frac{1}{\theta^2}$ , approximations are in order.

From (e24) we get the hint that  $\theta \cot \theta$  is of the order of unity, so that terms in  $\frac{\cot \theta}{\theta}$  are of the same order as those in  $\frac{1}{\theta^2}$ . Accordingly an approximate solution is obtainable by adding (e22) and (e23) and neglecting these small terms. The result is

$$\theta \cot \theta = 2 - \frac{X^2}{2} - \frac{3XJ_0}{2J_1} \equiv F(X) \quad (\text{e28})$$

Therefore the optimum phase angle is given by

$$\theta = \theta_n - \frac{F(X)}{\theta_n}, \quad \theta_n = (n + \frac{3}{4})2\pi \quad (\text{e29})$$

$$\sin \theta = -1 + \frac{[F(X)]^2}{2\theta_n^2} \quad (\text{e30})$$

$$\frac{\sin \theta}{\theta} = -\frac{1}{\theta_n} \left[ 1 + \frac{1}{\theta_n^2} (F - F^2/2) \right] \quad (\text{e31})$$

$$\frac{\cot \theta}{\theta} = \frac{1}{\theta_n^2} F(X) \quad (\text{e32})$$

From computation it turns out that in the range of interest, the quantity  $F(X)$  does not differ from  $(-1)$  by more than 20%.

The desired approximate solution comes now from substituting the explicit phase optimum (e29) to (e32) back into (e25)–(e27). The results are:

$$G_R = \frac{I_0}{V_0} \beta^2 \frac{\theta_n}{2} \left( J_0 + \frac{1}{\theta_n^2} S_1(X) \right) \quad (\text{e33})$$

$$P_L = I_0 V_0 \frac{X^2}{\theta_n} \left( \frac{2J_1}{X} - J_0 + \frac{1}{\theta_n^2} S_2(X) \right) \quad (\text{e34})$$

$$G_L = \frac{I_0}{V_0} \beta^2 \frac{\theta_n}{2} \left( \frac{2J_1}{X} - J_0 + \frac{1}{\theta_n^2} S_3(X) \right) \quad (\text{e35})$$

The S-functions are given by

$$S_1(X) = \left( -F - \frac{F^2}{2} - \frac{X^2 F}{2} + \frac{7}{8} X^2 - \frac{1}{8} X^4 \right) J_0 + \left( -\frac{X^2}{2} F - \frac{X^2}{4} - \frac{3}{4} X^4 \right) \frac{J_1}{X} \quad (\text{e36})$$

$$S_2(X) = \left( -F^2 - F \frac{X^2}{2} + 4F + \frac{1}{2} X^4 \right) \frac{J_1}{X} + \left( \frac{F^2}{2} + \frac{X^2 F}{2} - 2F - \frac{3}{8} X^2 + \frac{1}{8} X^4 \right) J_0 \quad (\text{e37})$$

$$S_3(X) = \left( \frac{F^2}{2} + \frac{FX^2}{2} - \frac{3}{8} X^2 + \frac{1}{8} X^4 \right) J_0 + \left( -F^2 - F \frac{X^2}{2} + \frac{1}{2} X^4 \right) \frac{J_1}{X} \quad (\text{e38})$$

The equations (e33)–(e35) have the following meaning: they presuppose that the load  $G_L$  has been adjusted for maximum useful power in the presence of circuit loss  $G_R$ , and that the drift angle is also optimum. Then the useful power is given parametrically in terms of the circuit conductance by equations (e33) and (e34), while (e35) gives the required optimum load conductance, also in terms of the parameter  $X$ .

The results may be expressed as a chart of useful power, plotted against the value of resonator loss conductance. This is done in Fig. 128.

One may also be interested in the maximum power which could be gen-

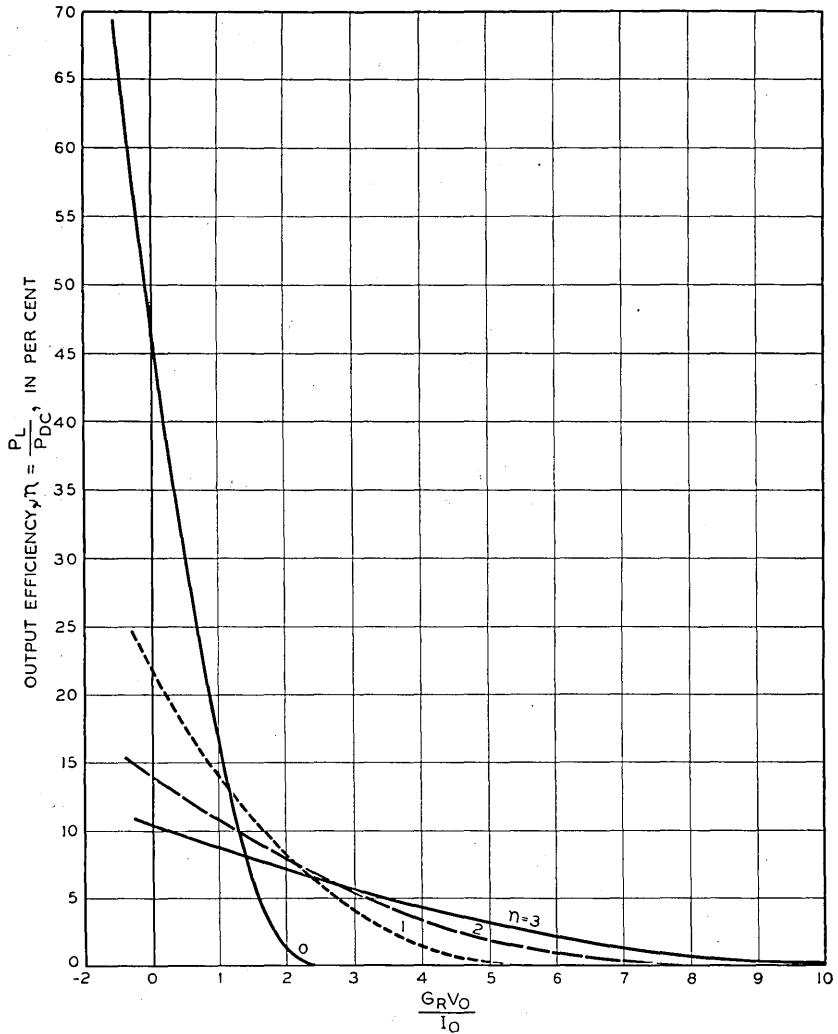


Fig. 128.—Plot of efficiency vs a parameter proportional to resonator loss for several repeller modes.

$\eta$	0	1	2	3
$\eta$	0.48	0.22	0.14	0.105

Fig. 129.—Maximum efficiency for several repeller modes.

erated if the resonator were perfect. This comes from setting  $G_R = 0$ , calculating the resulting value of useful power. The results are compared with the simpler theory in Fig. 129.

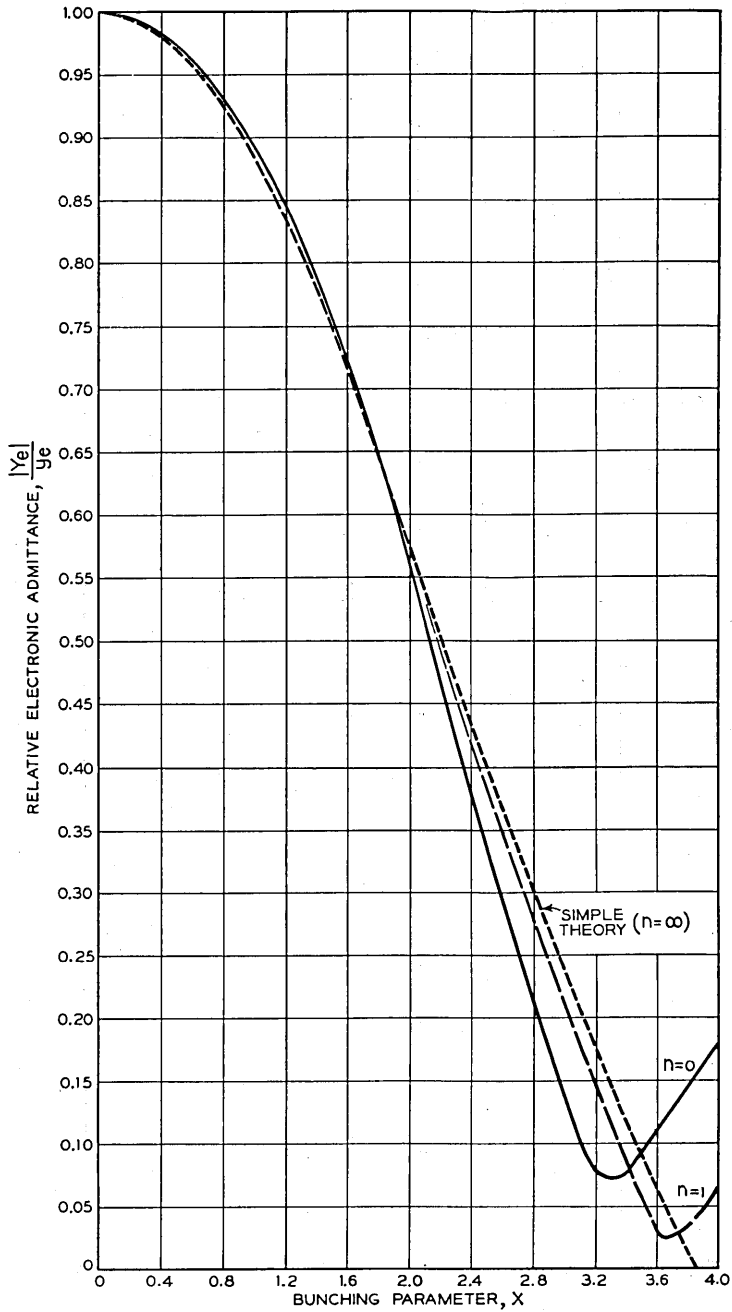


Fig. 130.—Relative electronic admittance vs bunching parameter for several repeller modes.



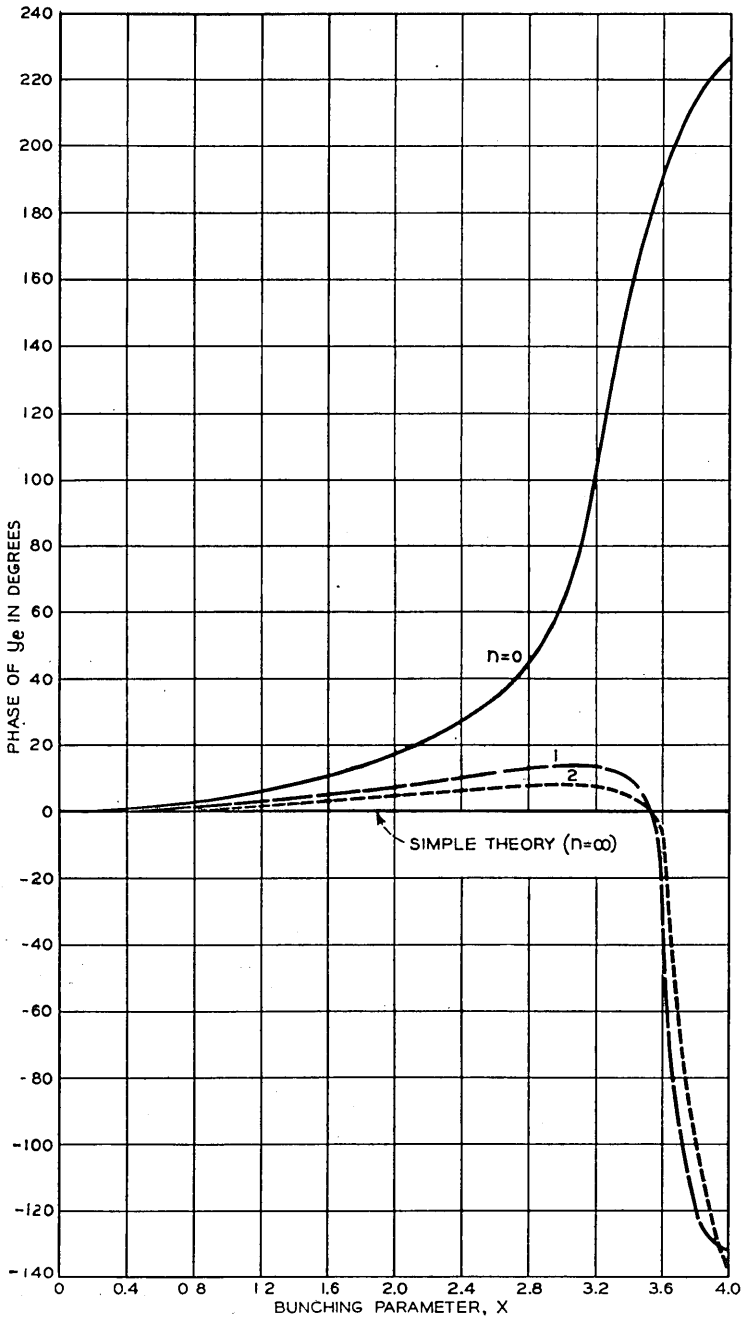


Fig. 131.—Phase of electronic admittance vs bunching parameter for several repeller modes.

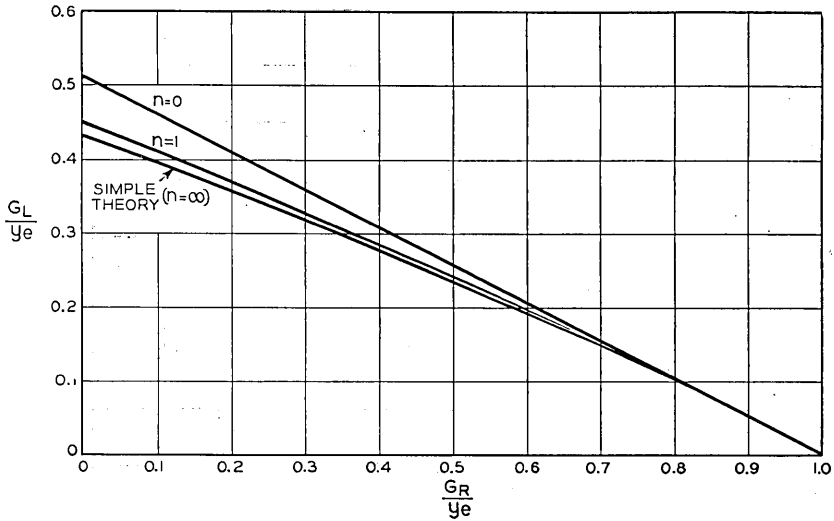


Fig. 132.—Optimum load conductance divided by small signal electronic admittance vs resonator loss conductance divided by small signal electronic admittance for several repeller modes.

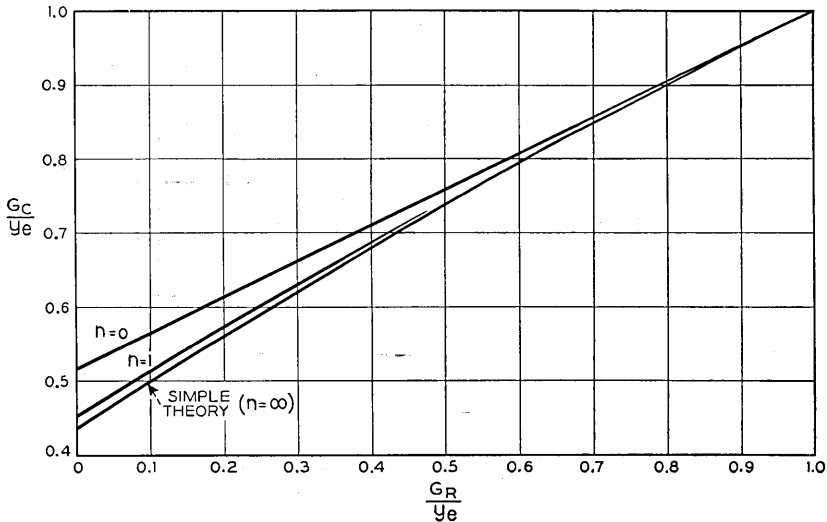


Fig. 133.—Optimum total circuit conductance divided by small signal electronic admittance vs resonator loss conductance divided by small signal electronic admittance for several repeller modes.

Further data which may be determined include the variation of the magnitude of the electronic admittance with gap voltage, in Fig. 130; also its phase, in Fig. 131. The optimum load conductance is plotted as a

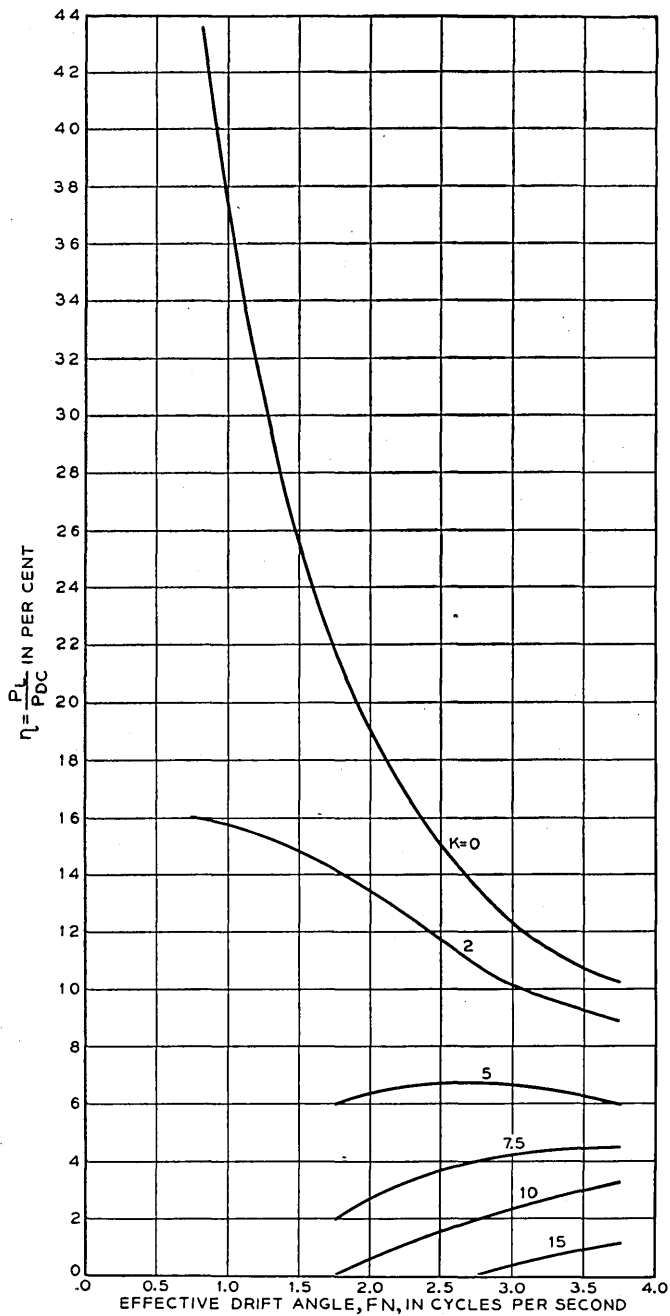


Fig. 134.—Efficiency vs effective drift angle for several degrees of resonator loss.

function of resonator loss in Fig. 132, and the total conductance, load plus loss, in Fig. 133. The next Fig. 134, plots efficiency versus mode number

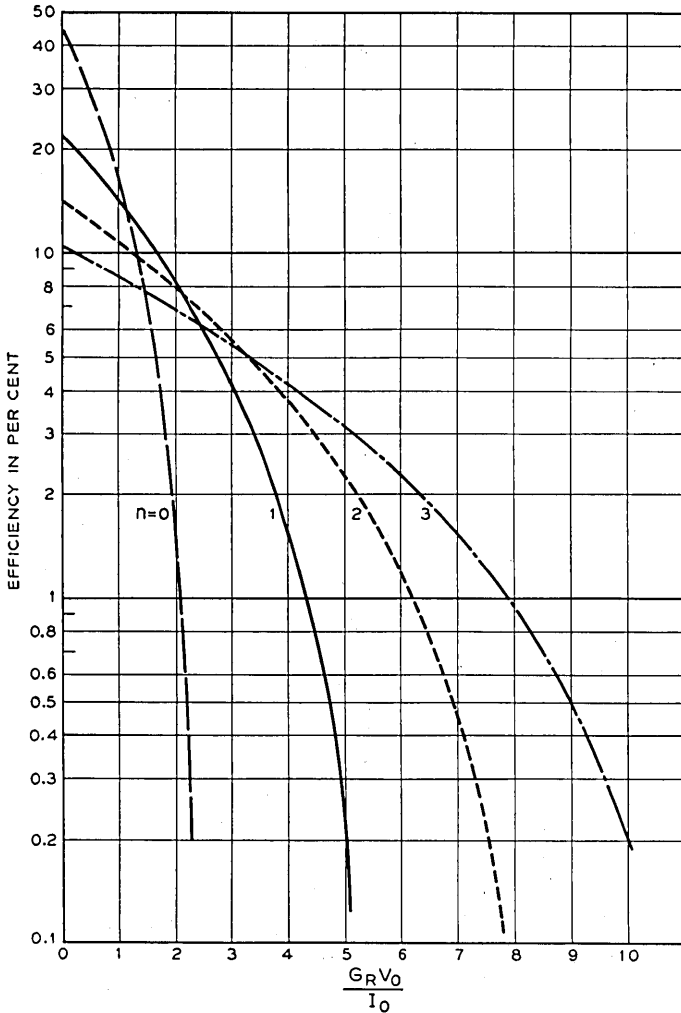


Fig. 135.—Efficiency vs a parameter proportional to resonator loss for several repeller modes.

with resonator loss as a parameter, while the next Fig. 135, plots efficiency versus resonator loss with mode number as a parameter.

Most of these graphs include for comparison the results of the simpler theory, and it can be seen that the deviations indicated by the second

order theory are ordinarily rather small even for the first two modes of operation, and are quite negligible for higher modes.

## APPENDIX VI

### GENERAL POTENTIAL VARIATION IN THE DRIFT SPACE

Suppose that the potential of the drift space is given by  $V(x)$ , where  $x = 0$  at zero potential and  $x = \ell$  at the gap. Then the transit time from the gap to zero potential and back again is

$$\tau_0 = (2/\sqrt{2\eta}) \int_0^\ell \frac{dx}{(V(X))^{3/2}} \quad (f1)$$

Imagine now that the entire drift space is raised by a very small amount  $\Delta V$ . The zero potential point will now occur at

$$x = -\Delta V/V'(0) \quad (f2)$$

where

$$V'(x) = dV/dx \quad (f3)$$

Hence the new transit time will be

$$\tau_0 + \Delta\tau = (2/\sqrt{2\eta}) \int_{-\Delta V/V'(0)}^\ell \frac{dx}{[V(x) + \Delta V]^{3/2}} \quad (f4)$$

Now let

$$z = x + \Delta V/V'(0) \quad (f5)$$

Then, including first order terms only, if  $V(x)$  can be expanded in a Taylor's series about 0,

$$\begin{aligned} \tau_0 + \Delta\tau &= (2/\sqrt{2\eta}) \int_0^{\ell + \Delta V/V'(0)} \frac{dz}{[V(z) - [V'(z)/V'(0)]\Delta V + \Delta V]^{3/2}} \\ &= (2/\sqrt{2\eta}) \left( \int_0^\ell \frac{dz}{[V(z)]^{3/2}} + \Delta V \int_0^\ell \frac{[(V'(z)/V'(0)) - 1] dz}{2[V(z)]^{5/2}} \right. \\ &\quad \left. + \frac{\Delta V}{V'(0)[V(\ell)]^{3/2}} \right) \end{aligned} \quad (f6)$$

Whence

$$\tau' = \frac{\Delta\tau}{\Delta V} = (2/\sqrt{2\eta}) \left( \frac{1}{V'(0)[V(\ell)]^{3/2}} + \int_0^\ell \frac{[(V'(z)/V'(0)) - 1] dz}{2[V(z)]^{5/2}} \right) \quad (f7)$$

In computing  $F$  it should be noted that by definition the gap voltage pre-

viously referred to as  $V_0$  is

$$V_0 = V(\ell) \quad (\text{f8})$$

In the notation as it has been modified, the transit time is

$$\tau_0 = (2/\sqrt{2\eta}) \int_0^\ell \frac{dz}{[V(z)]^{3/2}}. \quad (\text{f9})$$

For a constant retarding field in the drift space of magnitude  $E_0$ , we can write

$$\eta E_0(\tau_1/2) = v = \sqrt{2\eta V} \quad (\text{f10})$$

Here  $V$  is the total energy with which electrons are shot into the drift space. From (f10)

$$\tau_1 = \frac{2\sqrt{2\eta V}}{\eta E_0} \quad (\text{f11})$$

$$\tau_1' = d\tau/dV = \frac{2\sqrt{2\eta V}}{\eta E_0} \left( \frac{1}{2V} \right) = \frac{\tau_0}{2V}. \quad (\text{f12})$$

In the notation used earlier this is

$$\tau_1' = \frac{\tau_0}{2V(\ell)}. \quad (\text{f13})$$

Now we will compare  $\tau'$  from (f7) with  $\tau_1'$ , the rate of change of transit time for a linear field, taking  $\tau_1'$  for the same resonator voltage  $V(\ell)$  and the same transit time, given by (f1), as the nonlinear field. The factor  $F$  relating  $\tau'$  and  $\tau_1'$  will then be

$$\begin{aligned} F &= \tau'/\tau_1' \\ &= 2V(\ell) \left[ \left\{ \frac{1}{V'(0)[V(\ell)]^{3/2}} \right. \right. \\ &\quad \left. \left. + \int_0^\ell \frac{[V'(z)/V'(0) - 1] dz}{2[V(z)]^{3/2}} \right\} \int_0^\ell \frac{dz}{[V(z)]^{3/2}} \right]^{-1}. \end{aligned} \quad (\text{f14})$$

If an electron is shot into the drift space with more than average energy, its greater penetration causes it to take longer to return, but it covers any element of distance in less time. Consider a case in which the gradient of the potential is small near the zero potential (much change in penetration for a given change in energy) and larger near the gap. The first term in the brackets of (f14) will be large, and the second is in this case positive. This means that in this type of field the increased penetration per unit energy and the effect of covering a given distance in less time with increased energy work together to give more drift action than in a constant field. However,

we might have the gradient near the gap less than that at the zero potential. In that case the second term in the brackets would be negative. This means a diminution in drift action because the penetration changes little with energy while the electron travels faster over the distance it has to cover.

To show how large this effect of weakening the field near the zero potential point may be, we will consider a specific potential variation, one which approximates the field in a long hollow tubular repeller. The field considered will be that in which

$$V(z) = (e^z - 1)/e^\ell \quad (f15)$$

We obtain

$$F = (e^\ell - 1) + \frac{(e^\ell - 1)^{\frac{1}{2}}}{\tan^{-1}(e^\ell - 1)^{\frac{1}{2}}}. \quad (f16)$$

Now

$$V'(0) = e^{-\ell} \quad (f17)$$

$$V'(z) = 1 \quad (f18)$$

Hence

$$F = \left( \frac{1}{V'(0)} - 1 \right) + \frac{\left( \frac{1}{V'(0)} - 1 \right)^{\frac{1}{2}}}{\tan^{-1} \left( \frac{1}{V'(0)} - 1 \right)^{\frac{1}{2}}}. \quad (f19)$$

This shows clearly how the effective drift angle is increased as the field at the zero potential point is weakened. For instance, if  $V'(0) = \frac{1}{2}$ , so that the field at the zero potential point is  $\frac{1}{2}$  that at the gap, the drift effectiveness for a given number of cycles drift is more than doubled ( $F = 2.27$ ).

There is another approach which is important in that it relates the variations of drift time obtained by varying various voltages. Suppose the gap voltage with respect to the cathode is  $V_0$  and the repeller voltage with respect to the cathode is  $-V_R$ . Now suppose  $V_0$  and  $V_R$  are increased by a factor  $\alpha$ , so that the resonator and repeller voltages become  $\alpha V_0$  and  $-\alpha V_R$ . The zero voltage point at which the electrons are turned back will be at the same position and so the electrons will travel the same distance, but at each point the electrons will go  $\alpha^{-\frac{1}{2}}$  times as fast. If, instead of introducing the factor  $\alpha$ , we merely consider the voltages  $V_R$  and  $V_0$  to be the variables, we see that the transit time can be written in the form

$$\tau = V_0^{-\frac{1}{2}} F(V_R/V_0) \quad (f20)$$

The function  $F(V_R/V_0)$  expresses the effect on  $\tau$  of different penetrations of the electron into the drift field and the factor  $V_0^{-3/2}$  tell us that if  $V_R$  and  $V_0$  are changed in the same ratio, the drift time changes as one over the square root of either voltage.

We can differentiate, obtaining

$$\partial\tau/\partial V_R = V_0^{-3/2}F'(V_R/V_0) \quad (f21)$$

$$\partial\tau/\partial V_0 = -V_0^{-3/2}((V_R/V_0)F'(V_R/V_0) + (1/2)F(V_R/V_0)) \quad (f22)$$

If the electron gains an energy  $\beta V$  in crossing the gap, the effect on  $\tau$  is the same as if  $V_0$  were increased by  $\beta V$  and  $V_R$  were changed by an amount  $-\beta V$ , because in an acceleration of an electron in crossing the gap the electron gains energy with respect to both the resonator (where the energy is specified by  $V_0$  for an unaccelerated electron) and with respect to the repeller ( $-V_R$  for an unaccelerated electron). We may thus write

$$\begin{aligned} \partial\tau/\partial(\beta V) &= \partial\tau/\partial V_0 - \partial\tau/\partial V_R \\ &= -V_0^{-3/2}[(1 + V_R/V_0)F'(V_R/V_0) + \frac{1}{2}F(V_R/V_0)] \quad (f23) \end{aligned}$$

This expression (f23) is for the same quantity as (f7).  $V_0$  of (f23) is  $V(t)$  of (f7). Expressions (f21), (f22) and (f23) compare the effects on drift time of changing the repeller voltage alone, as in electronic tuning, the resonator voltage alone, and of accelerating the electrons in crossing the gap. As making the repeller more negative always decreases the drift time, we see that the two terms of (f22) subtract, and usually  $|\partial\tau/\partial V_0|$  will be less than  $|\partial\tau/\partial V_R|$ . In fact, for a linear variation potential in the drift space and for  $V_0 = V_R$ ,  $\partial\tau/\partial V_0 = 0$ . Weak fields at the zero potential point make the absolute value of  $F'(V_R/V_0)$  larger and hence tend to make both  $|\partial\tau/\partial V_R|$  and  $|\partial\tau/\partial(\beta V)|$  larger. However, these quantities are not changed in quite the same way.

The reader should be warned that (f14) and (f20)-(f23) apply only for fields not affected by the space charge of the electron beam. For instance, suppose we had a gap with a flat grid and a parallel plane repeller a long way off at zero potential. If edge effects and thermal velocities were neglected, we would have a Child's law discharge. The potential would be zero beyond a certain distance from the repeller, and we would have

$$V(z) = Az^{3/2}$$

According to (f14),  $F$  should be infinite. There is no reason to expect infinite drift action, however, for the drift field, which is affected by the fluctuating electron density in the beam, is a function of time, and (f14) does not apply.



## APPENDIX VII

## IDEAL DRIFT FIELD

The behavior of reflex oscillators has been analyzed on the basis of a uniform field in the drift space. It can be shown that this is not the drift field which gives maximum efficiency. The field which does give maximum efficiency under certain assumptions is described in this appendix.

Consider a reflex oscillator in which a voltage  $V$  appears across the gap. This voltage causes an energy change of  $\beta V \cos \theta_1$  for the electron crossing the gap. Here  $\theta_1$  is the phase at which a given electron crosses the gap for the first time. The effect of the drift space is to cause the electron to return after an interval  $\tau_a$  where  $\tau_a$  is a function of this energy.

$$\tau_a = f(\beta V \cos \theta_1) \quad (\text{g1})$$

Thus, each value of  $\tau_a$  will occur twice every cycle ( $2\pi$  variation of  $\theta_1$ ). We will have

$$\theta_1 = \omega t_1 \quad (\text{g2})$$

$$\theta_a = \omega(t_1 + \tau_a) \quad (\text{g3})$$

$$= \theta_1 + \varphi(\theta_1)$$

$$\varphi(\theta_1) = \omega \tau_a \quad (\text{g4})$$

Here  $t_1$  is the time at which an electron first crosses the gap and  $(t_1 + \tau_a)$  is the time of return to the gap.  $\theta_1$  and  $\theta_a$  are the phase angles of the voltage at first crossing and return.

The net work done by an electron in the two crossings is

$$W = \beta V e [-\cos \theta_1 + \cos (\theta_1 + \varphi(\theta_1))] \quad (\text{g5})$$

If the beam current has a steady value  $I_0$ , the power produced will be

$$P = (\beta V I_0 / 2\pi) \int_{-\pi}^{\pi} [-\cos \theta_1 + \cos (\theta_1 + \varphi(\theta_1))] d\theta_1. \quad (\text{g6})$$

The integral of  $\cos \theta_1$  is of course zero. Further, from (g4) we see that

$$\varphi(\theta_1) = \varphi(-\theta_1)$$

Hence

$$\begin{aligned} P &= (\beta V I_0 / 2\pi) \int_0^{\pi} [\cos (-\theta_1 + \varphi(\theta_1)) + \cos (\theta_1 + \varphi(\theta_1))] d\theta_1 \\ &= (\beta V I_0 / 2\pi) \int_0^{\pi} \cos \varphi(\theta_1) \cos \theta_1 d\theta_1. \end{aligned} \quad (\text{g7})$$

As  $\cos \varphi(\theta_1)$  cannot be greater than unity, it is obvious that this will have its greatest value if the following holds

$$0 < \theta_1 < \pi/2, \quad \varphi(\theta_1) = 2n\pi, \quad \cos \varphi(\theta_1) = +1 \quad (g8)$$

$$\pi/2 < \theta_1 < \pi, \quad \varphi(\theta_1) = (2m + 1)\pi, \quad \cos \varphi(\theta_1) = -1 \quad (g9)$$

These conditions are such that for a positive value of  $\cos \varphi$  the gap voltage is accelerating giving a longer drift time than obtains for a negative value of  $\cos \varphi(\theta_1)$  for which a retarding gap voltage is required. Thus, physically we must have

$$2n > 2m + 1 \quad (g10)$$

The simplest case is that for  $n = 1$  and  $m = 0$ , so that in terms of the gap voltage

$$v < 0, \quad \varphi(\theta_1) = \pi \quad (g11)$$

$$v > 0, \quad \varphi(\theta_1) = 2\pi$$

This sort of drift action is illustrated by the curve shown in Fig. 136.

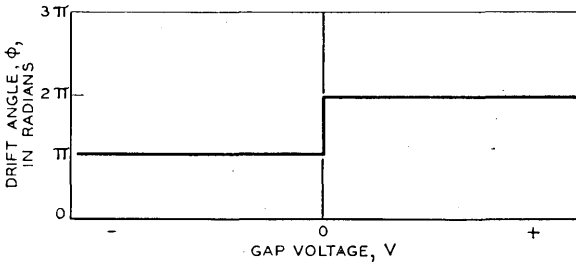


Fig. 136.—Ideal variation of drift time in the repeller region with resonator gap voltage.

The problem of finding the variation with distance which would give this result was referred to Dr. L. A. MacColl who gave the following solution:

Suppose  $V_0$  is the voltage of the gap with respect to the cathode and  $\Phi$  is the potential in the drift space. Let

$$x_0 = \sqrt{2\eta V_0}/\omega \quad (g12)$$

Here  $\omega$  is the operating radian frequency. Let  $x$  be a measure of distance in the drift field.

$$\Phi = V_0[1 - (x/x_0)^2], \quad 0 < x < x_0 \quad (g13)$$

$$\Phi = V_0\{1 - [(x/x_0)^2 + 1]^2/4(x/x_0)^2\}, \quad x > x_0$$

This potential distribution is plotted in Fig. 137.

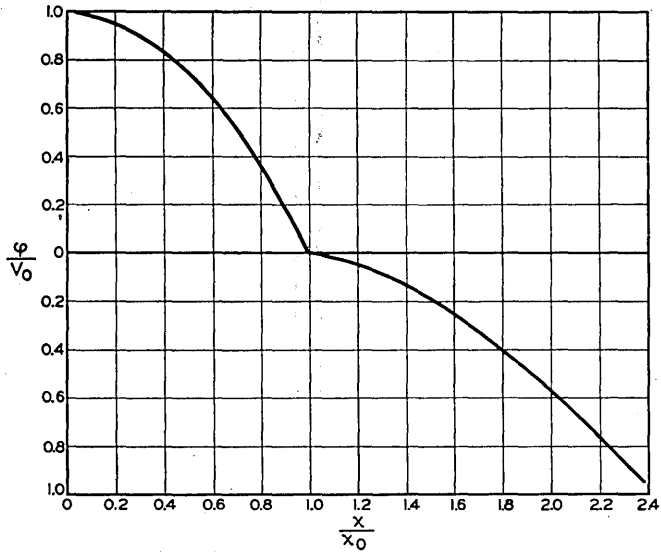


Fig. 137.—Variation of potential in the repeller region vs distance to give the characteristics shown in Fig. 7.1.

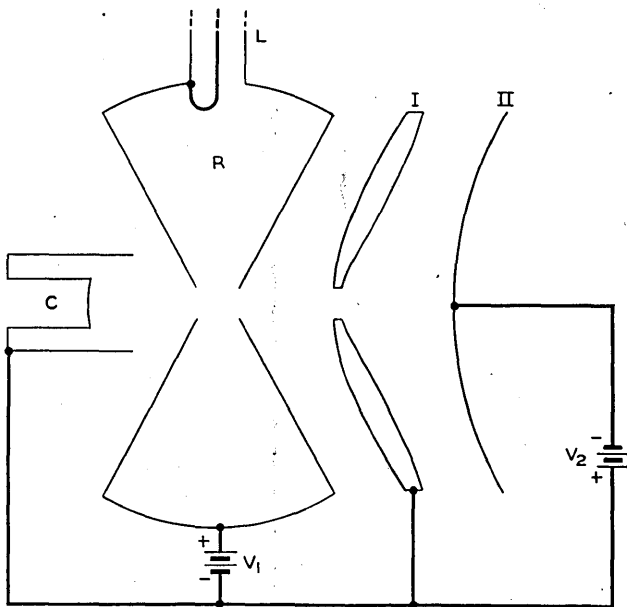


Fig. 138.—Electrodes to achieve approximately the potential variation in the drift region shown in Fig. 7.2.

The shapes for electrodes to realize this field may be obtained analytically by known means or experimentally by measurements in a water tank. The general appearance of such electrodes and their embodiment in a reflex oscillator are shown in Fig. 138. Here  $C$  is the thermionic cathode forming part of an electron gun which shoots an electron beam through the apertures or gap in a resonator  $R$ . The beam is then reflected in the drift field formed by the resonator wall, zero potential electrode I and negative electrode II, which give substantially the axial potential distribution shown in Fig. 137. Small apertures in the resonator wall and in electrode I allow passage of the electron beam without seriously distorting the drift field. Voltage sources  $V_1$  and  $V_2$  maintain the electrodes at proper potentials. Either suitable convergence of the electron beam passing through the resonator from the gun or axial magnetic focusing will assure return of reflected electrons through the resonator aperture. In addition, the aperture in electrode I forms a converging lens which tends to offset the diverging action of the fields existing between the resonator wall and I, and between I and II. R-f power is derived from resonator  $R$  by a coupling loop and line  $L$ .

## APPENDIX VIII

### ELECTRONIC GAP LOADING

If a measurement is made of gap admittance in the presence and in the absence of the electron beam passing across it once, it will be found that the electron stream gives rise to an admittance component  $Y$ . The susceptance is unimportant, but the conductance  $G$  can have a noticeable effect on the efficiency of an oscillator.

Petrie, Strachey and Wallis have provided an important expression for this gap conductance due to longitudinal fields when the r-f voltage is small compared with the beam voltage  $V_0$ .<sup>25</sup> In this analysis it is presumed that the fields in the beam are due to the voltages on the electrodes only and not to the space charge in the beam.<sup>26</sup> This analysis is of such importance that it is of interest to reproduce it in a slightly modified form. We will first consider the general cases of interaction with longitudinal fields and will then consider transverse fields also.

#### A. Longitudinal Field

Assume a stream of electrons flowing in the positive  $x$  direction, constituting a current  $-I_0$ , bunched to have an a-c convection current component

<sup>25</sup> These expressions were communicated to the writers through unpublished but widely circulated material by D. P. R. Petrie, C. Strachey and P. J. Wallis of Standard Telephones and Cables Valve Laboratory.

<sup>26</sup> The expressions are valid in the presence of space charge, but as the field is not known, they cannot be evaluated.

$i_1$ . Now if  $t_1$  is the time a particle passes  $x_1$  and  $t_2$  the time the particle passes  $x_2$ , the convection current at  $x_2$  will be

$$i_2 = (-I_0 + i_1) \frac{dt_1}{dt_2} + I_0. \quad (\text{h1})$$

This merely states that the charge which passes  $x_1$  in the time interval  $dt_1$  will pass  $x_2$  in the time interval  $dt_2$ . Suppose the electrons are accelerated at  $x_1$  by a voltage

$$V e^{j\omega t_1}$$

If  $V_0$  is the voltage specifying the average speed of the electrons, the velocity will be

$$v = (2\eta V_0)^{\frac{1}{2}} (1 + (V/V_0) e^{j\omega t_1})^{\frac{1}{2}} \quad (\text{h2})$$

We then have

$$t_2 = t_1 + \tau (1 + (V/V_0) e^{j\omega t_1})^{-\frac{1}{2}} \quad (\text{h3})$$

$$\tau = x (2\eta V_0)^{-\frac{1}{2}}$$

$$\frac{dt_2}{dt_1} = 1 - \frac{j\omega\tau(V/V_0)e^{j\omega t_1}}{2(1 + (V/V_0)e^{j\omega t_1})}. \quad (\text{h4})$$

Now assume  $(V/V_0) \ll 1$ . If we neglect higher powers than the first we can replace  $t_1$  by

$$t_1 = t_2 - \tau$$

and obtain

$$\frac{dt_1}{dt_2} = 1 + \frac{j\tau V e^{j\omega(t_1-\tau)}}{2V_0} \quad (\text{h5})$$

and from (h1), neglecting products of two a-c quantities

$$i_2 = i_1 - \frac{j\omega\tau I_0}{2V_0} V e^{j\omega(t_1-\tau)}. \quad (\text{h6})$$

Suppose we consider an electron stream travelling through a longitudinal field of potential fluctuating as  $e^{j\omega t}$  and of magnitude  $V(x)$ , where  $V(x)$  may be complex. Then the current at  $x_2$  due to the action of the field at  $x_1$  is, omitting for convenience the factor  $e^{j\omega t}$ ,

$$di_2 = \frac{jI_0 V'(x_1)}{2V_0} \gamma(x_2 - x_1) e^{-j\gamma(x_2-x_1)} dx_1 \quad (\text{h7})$$

$$\gamma = \omega/u_0 \quad (\text{h8})$$

$$u_0 = (2\eta V_0)^{\frac{1}{2}}. \quad (\text{h9})$$

Hence, the convection current at  $x_2$  is

$$i_2 = \frac{-jI_0}{2V_0} \int_{-\infty}^{x_2} V'(x_1) \gamma(x_2 - x_1) e^{-j\gamma(x_2 - x_1)} dx_1. \quad (\text{h10})$$

The power flow from the electron stream to the circuit is

$$P = \frac{1}{2} \int_{-\infty}^{\infty} V'(x_2) i_2^* dx_2 \quad (\text{h11})$$

$$P = \frac{jI_0}{4V_0} \int_{-\infty}^{\infty} \int_{-\infty}^{x_2} V'(x_2) V'^*(x_1) \gamma(x_2 - x_1) e^{j\gamma(x_2 - x_1)} dx_1 dx_2. \quad (\text{h12})$$

We have in (h12) an expression, based on the physics of the picture, for power flow from the electron stream to the circuit. This expression is a product of the electron convection current, due to bunching, and the electric field, and the product is integrated from  $x = -\infty$  to  $x = +\infty$ , which is merely a way of including all the a-c fields present. We could as well have integrated between two points  $a$  and  $b$  between which all a-c fields lie.

We will now go through some strictly mathematical manipulations of (h12), designed to transform it to a more handy form. In the following steps we may regard  $x_1$  and  $x_2$  as merely two different variables of integration, disregarding completely their physical significance.

Suppose in the  $x_1 x_2$  plane,  $x_1$  is measured  $+$  to the right and  $x_2$ ,  $+$  upwards. Then the plane is divided into two portions by the line  $x_2 = x_1$ , and we are integrating over the upper left portion. If we reverse the order of integration we obtain

$$P = \frac{jI_0}{4V_0} \int_{-\infty}^{\infty} \int_{x_1}^{\infty} V'(x_2) V'^*(x_1) \gamma(x_2 - x_1) e^{j\gamma(x_2 - x_1)} dx_2 dx_1. \quad (\text{h13})$$

Let us (a) interchange the variables of integration  $x_2$  and  $x_1$  and (b) take the conjugate of  $P$ . We obtain

$$P^* = \frac{jI_0}{4V_0} \int_{-\infty}^{\infty} \int_{x_2}^{\infty} V'(x_2) V'^*(x_1) \gamma(x_2 - x_1) e^{j\gamma(x_2 - x_1)} dx_1 dx_2. \quad (\text{h14})$$

The real part of  $P$  is  $\frac{1}{2} (P + P^*)$ ; hence

$$\text{Real} = \frac{jI_0}{8V_0} \int_{-\infty}^{\infty} \int_{-\infty}^{\infty} V'(x_2) V'^*(x_1) \gamma(x_2 - x_1) e^{j\gamma(x_2 - x_1)} dx_1 dx_2. \quad (\text{h15})$$

Let us consider the quantity

$$A = \int_{-\infty}^{\infty} V'(x) e^{j\gamma x} dx \quad (\text{h16})$$

$$\begin{aligned}
 |A|^2 &= AA^* = \left( \int_{-\infty}^{\infty} V'(x_2) e^{j\gamma x_2} dx_2 \right) \left( \int_{-\infty}^{\infty} V'^*(x_1) e^{-j\gamma x_1} dx_1 \right) \\
 &= \int_{-\infty}^{\infty} \int_{-\infty}^{\infty} V'(x_2) V'^*(x_1) e^{j\gamma(x_2-x_1)} dx_1 dx_2
 \end{aligned} \tag{h17}$$

$$\frac{\partial |A|^2}{\partial \gamma} = \frac{j}{\beta} \int_{-\infty}^{\infty} \int_{-\infty}^{\infty} V'(x_2) V'^*(x_1) \gamma(x_2 - x_1) e^{j\gamma(x_2-x_1)} dx_1 dx_2. \tag{h18}$$

Hence, we see

$$\text{Real} = \frac{I_0}{8V_0} \gamma \frac{\partial |A|^2}{\partial \gamma}. \tag{h19}$$

### B. Transverse Field

Suppose we consider the additional power transfer because of deflections. There will be two sources of energy transfer. First, imagine a fluctuating  $y$  component of velocity,  $\dot{y}$ . Let  $u_0$  be the  $x$  component of velocity and  $-I_0$  the convection current to the right. In a distance  $dx$  this will flow against the potential gradient in the  $y$  direction a distance

$$dy = (\dot{y}/u_0) dx \tag{h20}$$

and the power flowing to the field from the beam will be

$$dP = -\frac{I_0}{2} \frac{\partial V}{\partial y} (\dot{y}^*/u_0) dx. \tag{h21}$$

This is not the total power transfer, however. The beam will also suffer a displacement  $y$  in the  $y$  direction. Now the  $x$  component of field varies with displacement; hence the beam will encounter a varying field. We can write the instantaneous power transferred from the beam to the field. Let  $(V)_i$  be the instantaneous value of  $V$  and  $(y)_i$  be the instantaneous value of  $y$ . The instantaneous power will be

$$dp = -\left( \frac{d(V)_i}{dx} + \frac{\partial^2 (V)_i}{\partial x \partial y} (y)_i \right) dx. \tag{h22}$$

Let us compare this with the instantaneous power transferred from the beam to the field by a fluctuating convection current  $(i)_i$ :

$$dp = \frac{\partial (V)_i}{\partial x} (i)_i. \tag{h23}$$

We see that according to our convention that

$$P = VI^* \tag{h24}$$

we may write, from (h22)

$$P = -\frac{I_0}{2} \frac{\partial^2 V}{\partial x \partial y} y^* dx. \quad (\text{h25})$$

The  $y$  gradient of the potential at  $x_1$  produces a velocity at  $x_2$

$$\dot{y}_2 = \frac{\eta}{u_0} \int_{-\infty}^{x_2} \left( \frac{\partial V}{\partial y} \right)_1 e^{-j\gamma(x_2-x_1)} dx_1. \quad (\text{h26})$$

It produces a displacement at  $x_2$

$$y_2 = \frac{\eta}{u_0^2} \int_{-\infty}^{x_2} \left( \frac{\partial V}{\partial y} \right)_1 (x_2 - x_1) e^{-j\gamma(x_2-x_1)} dx_1. \quad (\text{h27})$$

Writing the total power as

$$P = P_1 + P_2. \quad (\text{h28})$$

We have the two contributions from (h22) and (h23) using (h9)

$$P_1 = \frac{-I_0}{4V_0} \int_{-\infty}^{\infty} \int_{-\infty}^{x_2} \left( \frac{\partial V}{\partial y} \right)_2 \left( \frac{\partial V}{\partial y} \right)_1^* e^{j\gamma(x_2-x_1)} dx_1 dx_2 \quad (\text{h29})$$

and

$$P_2 = \frac{-I_0}{4V_0} \int_{-\infty}^{\infty} \int_{-\infty}^{x_2} \left( \frac{\partial^2 V}{\partial x \partial y} \right)_2 \left( \frac{\partial V}{\partial y} \right)_1^* (x_2 - x_1) e^{j\gamma(x_2-x_1)} dx_1 dx_2. \quad (\text{h30})$$

Again, we will turn to mathematical manipulation disregarding the physical significance of the variables. If we change the order of integration, (h30) becomes

$$P_2 = \frac{-I_0}{4V_0} \int_{-\infty}^{\infty} \int_{x_1}^{\infty} \left( \frac{\partial^2 V}{\partial x \partial y} \right)_2 \left( \frac{\partial V}{\partial y} \right)_1^* (x_2 - x_1) e^{j\gamma(x_2-x_1)} dx_2 dx_1. \quad (\text{h31})$$

Integrating with respect to  $x_2$  by parts we obtain

$$\begin{aligned} P_2 = & -\frac{I_0}{4V_0} \left( \int_{-\infty}^{\infty} \left( \frac{\partial V}{\partial y} \right)_2 \left( \frac{\partial V}{\partial y} \right)_1^* (x_2 - x_1) e^{j\gamma(x_2-x_1)} dx_1 \right) \Big|_{x_1}^{\infty} \\ & - j \int_{-\infty}^{\infty} \int_{x_1}^{\infty} \left( \frac{\partial V}{\partial y} \right)_2 \left( \frac{\partial V}{\partial y} \right)_1^* \gamma (x_2 - x_1) e^{j\gamma(x_2-x_1)} dx_2 dx_1 \\ & - \int_{-\infty}^{\infty} \int_{x_1}^{\infty} \left( \frac{\partial V}{\partial y} \right)_2 \left( \frac{\partial V}{\partial y} \right)_1^* e^{j\gamma(x_2-x_1)} dx_2 dx_1. \end{aligned} \quad (\text{h32})$$

The first term is zero because  $\left( \frac{\partial V}{\partial y} \right)_1^*$  is zero at  $x_1 = -\infty$  and  $(x_2 - x_1)$  is



zero at  $x_2 = x_1$ . Changing the order of integration, we obtain

$$P_2 = +j \frac{I_0}{4V_0} \int_{-\infty}^{\infty} \int_{-\infty}^{x_2} \left( \frac{\partial V}{\partial y} \right)_2 \left( \frac{\partial V}{\partial y} \right)_1^* \gamma (x_2 - x_1) e^{j\gamma(x_2 - x_1)} dx_1 dx_2 \\ + \frac{I_0}{4V_0} \int_{-\infty}^{\infty} \int_{-\infty}^{x_2} \left( \frac{\partial V}{\partial y} \right)_2 \left( \frac{\partial V}{\partial y} \right)_1^* e^{j\gamma(x_2 - x_1)} dx_1 dx_2. \quad (\text{h33})$$

From (h29) and (h30) we see that the total power is

$$P = j \frac{I_0}{4V_0} \int_{-\infty}^{\infty} \int_{-\infty}^{x_2} \left( \frac{\partial V}{\partial y} \right)_2 \left( \frac{\partial V}{\partial y} \right)_1^* \gamma (x_2 - x_1) e^{j\gamma(x_2 - x_1)} dx_1 dx_2. \quad (\text{h34})$$

By the same means resorted to in connection with (h12) we find

$$\text{Real} = \frac{I_0}{8V_0} \gamma \frac{\partial |B|^2}{\partial \gamma} \quad (\text{h35})$$

$$B = \int_{-\infty}^{\infty} \frac{\partial V}{\partial y} e^{j\gamma x} dx. \quad (\text{h36})$$

We can go a step further. We have

$$A = \int_{-\infty}^{\infty} \frac{\partial V}{\partial x} e^{j\gamma x} dx. \quad (\text{h37})$$

Now

$$\frac{\partial A}{\partial y} = \int_{-\infty}^{\infty} \frac{\partial^2 V}{\partial x \partial y} e^{j\gamma x} dx. \quad (\text{h38})$$

Integrating by parts

$$\frac{\partial A}{\partial y} = \frac{\partial V}{\partial y} e^{j\gamma x} \Big|_{-\infty}^{\infty} - j\gamma \int_{-\infty}^{\infty} \frac{\partial V}{\partial y} e^{j\gamma x} dx. \quad (\text{h39})$$

The first term is zero, and we see that

$$|B|^2 = (|\partial A / \partial y|^2 / \gamma^2) \quad (\text{h40})$$

$$\text{Real} = \frac{I_0}{8V_0} \gamma \frac{\partial (|\partial A / \partial y|^2 / \gamma^2)}{\partial \gamma}. \quad (\text{h41})$$

### C. Electronic Gap Loading

In (h19) and (h41) we have expressed the power flow from the electron stream to the circuit in rather general terms. What we want immediately is the quantity (conductance) giving the power flow from the circuit to the stream for a single gap. Assume we have a single gap with unit peak r-f voltage across it. The power absorbed by the electron stream can be

attributed to a shunt conductance such that

$$\begin{aligned} P_R &= GV^2/2 = G/2 \\ G &= 2P_R. \end{aligned} \quad (\text{h42})$$

Also, in this case  $|A|$  is simply  $\beta$ , the modulation coefficient. Hence, the conductance due to action of the longitudinal fields is, from (h18), simply

$$G_1 = \frac{-I_0\gamma}{4V_0} \frac{\partial\beta^2}{\partial\gamma}. \quad (\text{h43})$$

And, due to the action of transverse fields there is another conductance, from (h41)

$$G_2 = \frac{I_0\gamma}{4V_0} \frac{\partial}{\partial\gamma} \left( \frac{1}{\gamma^2} \left( \frac{\partial\beta}{\partial y} \right)^2 \right) \quad (\text{h44})$$

$$G = G_1 + G_2. \quad (\text{h45})$$

These are surprisingly simple and very useful relations.

It is interesting to take an example which will indicate both effects. We have from (b24) for tubes of radius  $r_0$  with a narrow gap between them

$$\beta_s^2 = \beta_r^2 [1 - I_1^2(\gamma r_0)/I_0^2(\gamma r_0)]. \quad (\text{h46})$$

Accordingly, the part of the conductance due to the longitudinal field is

$$G_L = F_L(\gamma r_0) I_0 / 4V_0 \quad (\text{h47})$$

$$\begin{aligned} F_L(\gamma r_0) &= -\gamma \partial\beta_s^2 / \partial\gamma \\ &= -2 \left[ \left( \frac{I_1(\gamma r_0)}{I_0(\gamma r_0)} \right)^2 - \gamma r_0 \left( \frac{I_1(\gamma r_0)}{I_0(\gamma r_0)} \right) - \left( \frac{I_1(\gamma r_0)}{I_0(\gamma r_0)} \right)^3 \right]. \end{aligned} \quad (\text{h48})$$

Similarly, the part of the conductance due to the transverse field is

$$G_T = F_T(\gamma r_0) I_0 / 4V_0 \quad (\text{h49})$$

$$F_T(\gamma r_0) = -\gamma \frac{\partial}{\partial\gamma} \frac{1}{r_0^2} \int_0^{r_0} \left[ \left( \frac{1}{\gamma} \frac{\partial}{\partial r} \beta_r \right)^2 2r dr \right]. \quad (\text{h50})$$

From (b16) we obtain

$$\beta_r = I_0(\gamma r) / I_0(\gamma r_0) \quad (\text{h51})$$

$$\begin{aligned} \frac{1}{\gamma} \frac{\partial\beta_r}{\partial r} &= I_1(\gamma r) / I_0(\gamma r_0) \frac{1}{r_0^2} \int_0^{r_0} \left( \frac{1}{\gamma} \frac{\partial}{\partial r} \beta_r \right)^2 2r dr \\ &= \left[ \frac{I_2(\gamma r_0)}{I_0(\gamma r_0)} - \frac{I_1^2(\gamma r_0)}{I_0^2(\gamma r_0)} \right]. \end{aligned} \quad (\text{h52})$$

And from this we obtain

$$F(\gamma r_0) = -2 \left[ 1 - \frac{2I_1(\gamma r_0)}{\gamma r_0 I_0(\gamma r_0)} + \gamma r_0 \left( \frac{I_1(\gamma r_0)}{I_0(\gamma r_0)} \right) - \left( \frac{I_1(\gamma r_0)}{I_0(\gamma r_0)} \right)^3 - 2 \left( \frac{I_1(\gamma r_0)}{I_0(\gamma r_0)} \right)^2 \right]. \quad (\text{h53})$$

The total conductance is

$$G = G_1 + G_2 = (F_L(\gamma r_0) + F_T(\gamma r_0))I_0/4V_0. \quad (\text{h54})$$

In Fig. 139,  $(G_1V_0/I_0)$ ,  $(G_2V_0/I_0)$  and  $(GV_0/I_0)$  are plotted vs  $\gamma r_0$ . It may be seen that while the conductance due to transverse fields may be negative, the total conductance is always positive.

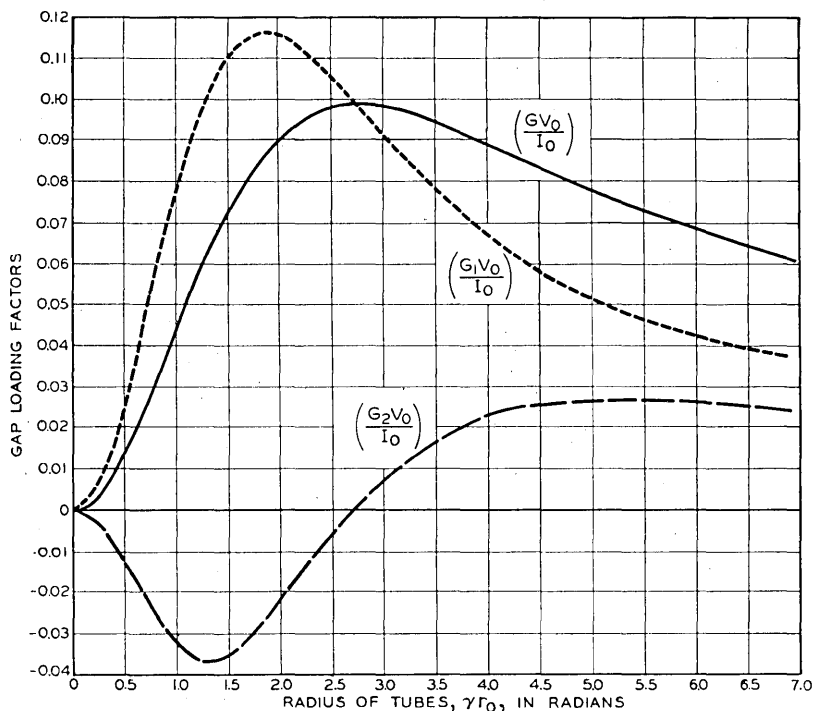


Fig. 139.—Gap loading factor vs radius of tubes forming gap measured in radians. The tubes are supposed to be filled with uniform electron flow. The curve involving  $G_1$  is that for longitudinal effects, that involving  $G_2$  is for transverse effects, and that involving  $G$  is for both combined.

This example tends to exaggerate the effects of transverse fields because the beam is assumed to fill the whole tube. In an actual case the beam

would probably not fill the whole tube, and the effect of transverse fields would be less.

Perhaps a more useful expression is one involving longitudinal fields only; that for infinitely fine parallel grids. In this case, if the separation is  $\ell$

$$\beta^2 = \sin^2 (\gamma\ell/2) / (\gamma\ell/2)^2 \quad (\text{h55})$$

and, from (h43)

$$G = \frac{I_0 \sin (\gamma\ell/2)}{2V_0 (\gamma\ell/2)} \left[ \frac{\sin (\gamma\ell/2)}{(\gamma\ell/2)} - \cos (\gamma\ell/2) \right]. \quad (\text{h56})$$

In Fig. 140,  $(GV_0/I_0)$  is plotted vs  $(\gamma\ell/2)$ . The negative conductance region beyond  $\gamma\ell = 2\pi$ , familiar through Llewellyn's work with diode oscillators, is of less interest in connection with reflex oscillators.

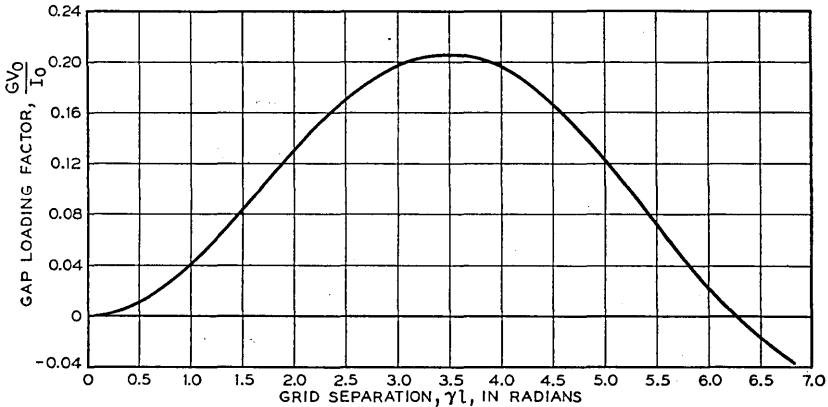


Fig. 140.—Gap loading factor for fine parallel grids vs grid separation in radians.

It is of some interest to compare the electronic gap loading with the small signal electronic conductance due to drift action. Assume, for instance, we have fine parallel plane grids for which  $\gamma\ell = \pi$ . From (h2) we get

$$(GV_0/I_0) = .202.$$

As the current crosses the gap twice we should count the current involved as twice the d-c beam current  $I_b$

$$G = .404 I_b/V_0.$$

From (2.1)

$$\beta = .633$$

$$\beta^2 = .400.$$

If we assume 3.75 cycles of drift, then from (2.4) the magnitude of the small signal electronic admittance is

$$\begin{aligned} y_e &= \beta^2 I_0 \theta / 2V_0 \\ &= 4.71 I_0 / V_0. \end{aligned} \quad (\text{h57})$$

Thus, in this example, the gap loading is about 1/10 of the small signal electronic admittance.

#### D. Bunching in the Gap

An unbunched stream will become bunched due to a single transit across an excited gap. Expression (h10) gives us a means for calculating the extent of this bunching. As an example, we will consider the case of fine parallel grids separated by a distance  $\ell$ . Then the gradient is given by

$$V'(x_1) = V/\ell \quad (\text{h58})$$

from  $x_1 = 0$  to  $x_1 = x_2 = \ell$ , and by zero elsewhere. Thus

$$\begin{aligned} i_2 &= \frac{jI_0 V}{2V_0 \ell} \int_0^\ell \gamma(\ell - x_1) e^{-j\gamma(\ell - x_1)} dx_1 \\ i_2/V &= (I_0/V_0)(1/2)[1 - (j/\gamma\ell)(1 - e^{j\gamma\ell})]e^{-j\gamma\ell}. \end{aligned} \quad (\text{h59})$$

It should be noted that for large values of  $\gamma\ell$

$$i_2/V = (1/2)(I_0/V_0)e^{-j\gamma\ell}. \quad (\text{h60})$$

For our previous example, if  $\gamma\ell = \pi$ ,

$$i_2/V = .592 (I_0/V_0) e^{-j\pi.53}. \quad (\text{h61})$$

If the current is referred to the center of the gap instead of the second grid, we obtain a current  $i$  such that

$$i/V = .592 (I_0/V_0) e^{-j1.96}. \quad (\text{h62})$$

Now, the electrons constituting current  $i$  will drift 3.75 cycles and will return across the gap in the opposite direction. To get the induced circuit current  $I$  we take this into account and multiply by  $\beta$

$$\begin{aligned} I/V &= -\beta(i/V) e^{-j\pi(3.75)} \\ &= -.375(I_0/V_0) e^{-j19\pi}. \end{aligned} \quad (\text{h63})$$

This is very nearly of the same size as the electronic gap loading.

The general conclusion seems to be that for typical conditions encountered in reflex oscillators, gap loading and bunching in the gap are small and probably less important than various errors in the theory.

## APPENDIX IX

## LOSSES IN GRIDS

Although the general problem of resonator loss calculation is not treated in this paper, grids seem peculiar to vacuum tubes and losses in grids will be discussed briefly.

Assume that we have a pair of grids of some mesh or network material, parallel, circular, and of a diameter compared with the wavelength small enough so that variation of voltage over the grids may be neglected. The capacitance inside of a radius  $r$  is

$$C = \epsilon \pi r^2 / d$$

$$\epsilon = 8.85 \times 10^{-14} \text{ farads/cm.} \quad (i1)$$

Here  $d$  is the separation between the grids. For unit r.m.s. voltage across the grids, the power dissipated in the part of both grids lying in the range  $dr$  at  $r$  is

$$dP = 2(\omega C)^2 (R dr / 2\pi r)$$

$$= \omega^2 \epsilon^2 \pi R r^3 dr / d^2. \quad (i2)$$

Here  $R$  is the surface resistivity. The total power is equal to  $V^2 G$ , where  $G$  is the conductance measured at the edge of the grids, and is

$$G = P = \frac{\omega^2 \epsilon^2 \pi R}{d^2} \int_0^{D/2} r^3 dr$$

$$= \omega^2 \epsilon^2 \pi R D^4 / 64 d^2. \quad (i3)$$

It is interesting to express  $\omega$  in terms of  $\lambda$ , the wavelength,  $c$  the velocity of light, and then to put in numerical values

$$G = (1/16) \pi^3 c^2 \epsilon^2 R D^4 / \lambda^2 d^2 \quad (i4)$$

$$G = 1.39 \times 10^{-5} R D^4 / \lambda^2 d^2. \quad (i5)$$

Now for the copper, the surface resistivity is

$$R_c = .045 / \sqrt{\lambda} \quad (i6)$$

where  $\lambda$  is measured in cm. Suppose the grid material is non-magnetic and has  $N$  times the low frequency resistivity of copper. Then for it, the surface resistivity will be  $N^{\frac{1}{2}}$  times that given by (i6). Suppose that the diameter of the grid wires is  $2r$  and the distance center to center is  $a$ . If current flowed on one half of the wire surface only, the surface resistivity parallel to the wires would be

$$R = N^{\frac{1}{2}} R_c (a / \pi r). \quad (i7)$$

If we use this as the surface resistivity in (i5) we obtain

$$G = 1.99 \times 10^{-7} \left( \frac{a}{r} \right) \sqrt{N/\lambda} / D^4 \lambda^2 d^2. \quad (\text{i8})$$

It is a somewhat remarkable fact that if we work out the loss for a pair of grids with surface resistivity  $R$  in one direction and infinite resistivity in the other direction (parallel wire grids) we get just twice the conductance given by (i5). Thus, it appears to be roughly true that if we have a given parallel wire grid, adding wires between the original wires and adding wires perpendicular to the original wires should have about the same effect in reducing circuit loss.

## APPENDIX X

### STARTING OF PULSED REFLEX OSCILLATOR

If a reflex oscillator is turned on gradually, the voltage from which the oscillations build up is certainly that due to shot noise in the electron stream. However, if the current is turned on as a pulse of short time of rise, it might be that the microwave voltage produced by the high frequency components of the pulse would be larger than the voltage produced by shot noise, and hence that oscillations would build up from the transient produced by the pulse and not from shot noise. This would be important because presumably the voltages produced by the pulse are always the same and related in the same manner to the time of application of the pulse; thus, in buildup from the transient of the pulse there would be no jitter.

In an effort to decide from which voltage the oscillations build up, we will consider Johnson noise and shot noise voltages.

Associated with a mode of oscillation of the resonator there is a mean stored energy  $kT$ . If  $L$  and  $C$  are the effective inductance and capacitance of the mode and  $\bar{I}^2$  and  $\bar{V}^2$  are the mean square current and voltage

$$kT = \bar{I}^2 L / 2 + \bar{V}^2 C / 2. \quad (\text{j1})$$

On the average, half of the energy is in the capacitance and half in the inductance; thus

$$\begin{aligned} \bar{V}^2 &= kT / C \\ &= kT \omega_0 / M. \end{aligned} \quad (\text{j2})$$

Here  $M$  is the characteristic admittance of the mode and  $\omega_0$  is the resonant radian frequency.

As an equivalent circuit for the mode we may use conductance  $G$  in shunt with an inductance  $L$  and a capacitance  $C$ . The impressed Johnson noise

current for a bandwidth  $B$  is

$$\overline{I_i^2} = 4kTGB. \quad (j3)$$

Suppose the current crossing the gap is  $2I_0$  (a current  $I_0$  with two transits). If the current has full shot noise (no space charge reduction of noise) the impressed shot noise current per unit bandwidth will be

$$\begin{aligned} \overline{I_s^2} &= 2e(2I_0)B \\ &= 4eI_0B. \end{aligned} \quad (j4)$$

Thus, we see that the shot noise voltage will be the Johnson noise voltage times the factor

$$\begin{aligned} \overline{I_s^2} &= \frac{e}{kT} \frac{I_0}{G} \\ &= \frac{11,600}{T} \frac{I_0}{G}. \end{aligned} \quad (j5)$$

The conductance  $G$  is given by

$$G = M/Q.$$

Let us take reasonable values,

$$T = 293^\circ \text{ K } (20^\circ \text{ C})$$

$$I_0 = .2 \text{ amperes}$$

$$M = .06 \text{ mhos}$$

$$Q = 400 \text{ (loaded } Q\text{)}.$$

The values of  $M$  and  $Q$  are about right for the 2K23 pulsed reflex oscillator. We obtain

$$\frac{\overline{I_s^2}}{\overline{I_i^2}} = 5.3 \times 10^4. \quad (j6)$$

Thus, shot noise is very much more important than Johnson noise.

From (j2) and (j5) we see that the shot noise voltage squared may be expressed as

$$\overline{V_s^2} = \frac{e\omega_0 I_0 Q}{M^2}. \quad (j7)$$

In pulsing a reflex oscillator, the voltage and current will be raised simultaneously; however for the sake of simplicity in calculation, we will assume that the voltage is constant and the injected current is zero at  $t = 0$ , rises



linearly with time to a value  $I_0$  at a time  $\Delta t$ , and remains constant thereafter. There will be a return current across the gap, the negative of the injected current and delayed by the drift time  $\tau$  with respect to the injected current.

In calculating the response to this applied current, loaded  $Q$  will be assumed to be infinite; actually, the shunt resistance will be positive when the current is small and negative when the current becomes large enough so that the electronic conductance is larger in magnitude than the circuit conductance. The assumption of zero conductance should, however, give us an idea of the transient which would be effective in starting the oscillator.

If a charge  $dq$  is put onto a capacitance  $C = M/\omega_0$  forming part of a resonant circuit of frequency  $\omega_0$ , the subsequent voltage across the circuit will be

$$dV = \frac{\omega_0}{M} e^{j\omega_0 t} dq. \quad (j8)$$

We see that for times late enough so that the injected and returned current are both constant, the voltage due to our assumed current will be

$$V = \frac{\omega_0}{M} I_0 \left( \int_0^{\Delta t} \frac{t_0}{\Delta t} e^{j\omega(t-t_0)} dt_0 + \int_{\Delta t}^t e^{j\omega(t-t_0)} dt_0 - \int_{\tau}^{\tau+\Delta t} \frac{t_0 - \tau}{\Delta t} e^{j\omega(t-t_0)} dt_0 - \int_{\tau+\Delta t}^t e^{j\omega(t-t_0)} dt_0 \right). \quad (j9)$$

Integrating, we find

$$V = \left( \frac{I_0}{M\Delta t\omega_0} \right) (1 - e^{-j\omega_0\tau})(e^{-j\omega_0\Delta t} - 1). \quad (j10)$$

If we have  $n + 3/4$  cycle drift,

$$e^{-j\omega_0\tau} = -j. \quad (j11)$$

The extreme value of  $(e^{-j\omega_0\Delta t} - 1)$  is  $-2$ . For this value we would obtain

$$|V|^2 = \frac{2I_0^2}{M^2\Delta t^2\omega_0^2}. \quad (j12)$$

From this and (j7) we obtain

$$\frac{\overline{V_s^2}}{|V|^2} = \frac{eQ\Delta t^2\omega_0^3}{2I_0}. \quad (j13)$$

Taking the values

$$e = 1.59 \times 10^{-19} \text{ coulombs}$$

$$I_0 = .2 \text{ amperes}$$

$$Q = 400 \text{ (loaded } Q)$$

$$\Delta t = .2 \times 10^{-6} \text{ seconds}$$

$$\omega_0 = 25 \times 10^9 \text{ radians/second.}$$

We obtain

$$\frac{\overline{V_s^2}}{|V|^2} = 99.2. \quad (j14)$$

The indications are that oscillations will built up from shot noise rather than from the high frequency transients induced by the pulse.

The preceding analysis assumes that the full shot noise voltage will appear across the resonator soon enough to override the pulse. The shot noise voltage will reach full amplitude in a time after application of the current of the order of  $Q/f_0 = 2\pi Q/\omega_0$ . For the values given above

$$2\pi Q/\omega_0 = .05 \times 10^{-6}$$

as this is a considerably smaller time than the .2 microseconds allotted for the buildup of the pulse, the assumption of full shot noise voltage is presumably fairly accurate.

## APPENDIX XI

### THERMAL TUNING

Two extreme conditions may exist

- (1) Cooling is by radiation alone
- (2) Cooling is by conduction alone.

#### (1) Radiation Cooling

The rate of change of temperature on heating will be given by

$$\frac{dT}{dt} = \frac{1}{C} [P_i - KT^4]. \quad (k1)$$

Where

$T$  is the absolute temperature of the expanding element.

$C$  is the heat capacity of the element.

$K$  is the radiation loss in watts/(degree Kelvin)<sup>4</sup>.

$P_i$  is the power input to the tuner in watts.

It is assumed that the temperature of the surroundings is constant and the power radiated to the expanding element is included in  $P_i$ . Let

$$P_i = KT_e^4 \quad \text{and} \quad T_r = \frac{T}{T_e}. \quad (k2)$$

$T_r$  is then a reduced temperature since  $T_e$  is the temperature which the expanding element would reach at equilibrium for a given power input, i.e.

$$T_e = \left(\frac{P_i}{K}\right)^{1/4}. \quad T_r \text{ is then always less than 1.}$$

Upon substitution of (k2) in (k1)

$$\frac{dT_r}{dt} = \frac{K}{C} T_e^3 [1 - T_r^4] \quad (k3)$$

which may be integrated to

$$\frac{C}{2KT_e^3} [\tan^{-1} T_r + \tanh^{-1} T_r] = t + t_0 \quad (k4)$$

where  $t_0$  is a constant of integration. Let

$$F_1(T_r) = [\tan^{-1} T_r + \tanh^{-1} T_r]. \quad (k5)$$

This function is plotted in Fig. 79. In order to determine the cycling time for heating  $\tau_h$  assume

$$\begin{array}{lll} \text{At } t = 0, & T_r = T_{rc} & \text{i.e. } T_{rc} = T_c/T_m \\ & & \\ & t = \tau_h, & T_r = T_{rh} \quad T_{rh} = T_h/T_m \end{array}$$

where

$T_m$  is the value of the temperature  $T_e$  corresponding to the maximum power input  $P_m$ .

$T_h$  is the temperature corresponding to one band limit.

$T_c$  is the temperature corresponding to the other band limit.

$T_h > T_c$ .

The cycling time for heating  $\tau_h$  is then

$$\tau_h = \frac{C}{2KT_m^3} [\tan^{-1} T_{rh} - \tan^{-1} T_{rc} + \tanh^{-1} T_{rh} - \tanh^{-1} T_{rc}] \quad (k6)$$

$$= \frac{C}{2KT_m^3} [F_1(T_{rh}) - F_1(T_{rc})] \quad (k7)$$

which gives the time required for the expanding element to rise in temperature from  $T_{rc}$  to  $T_{rh}$ , i.e. from  $T_c$  to  $T_h$ .

If we reduce the power input and wish to determine the cooling time the analysis is similar. If the power input from electron bombardment is reduced to zero there will still be power input to the tuner. The residual power which is kept to the minimum possible level comes from such sources, as heat radiated from the cathode and general heating of the envelope by the oscillator section.

Let  $P_0$  be the value of the reduced power input.

$$\text{Then} \quad -\frac{dT}{dt} = \frac{1}{C} (KT^4 - P_0) \quad (\text{k8})$$

$$\text{or} \quad \frac{dT_s}{dt} = -\frac{K}{C} T_0^3 (T_s^4 - 1). \quad (\text{k9})$$

$$\text{Here} \quad T_s = \frac{T}{T_0} \quad \text{and} \quad P_0 = KT_0^4 \quad (\text{k10})$$

where  $P_0$  is the power from other sources than direct bombardment. In this case  $T_s$  is always greater than 1.

Integration yields

$$\frac{C}{2KT_0^3} [\tan^{-1} T_s + \text{ctnh}^{-1} T_s] = t + t_0. \quad (\text{k11})$$

$$\text{Let} \quad F_2(T_s) = [\tan^{-1} T_s + \text{ctnh}^{-1} T_s]. \quad (\text{k12})$$

This function is plotted in Fig. 80. To determine the cycling time for cooling assume

$$\begin{array}{lll} \text{At time} & t = 0, & T_s = T_{sh} & \text{i.e. } T_{sh} = T_h/T_0 \\ & t = \tau_c, & T_s = T_{sc} & T_{sc} = T_c/T_0. \end{array}$$

$$\text{Then} \quad \tau_c = \frac{C}{2KT_0^3} [F_2(T_{sc}) - F_2(T_{sh})] \quad (\text{k13})$$

giving the time for the contracting element to cool from temperature  $T_{sh}$  to  $T_{sc}$ ; i.e. from  $T_h$  to  $T_c$ .

## (2) Conduction Cooling

The rate of change of temperature on heating will be given by

$$\frac{dT}{dt} = \frac{1}{C} (P_i - kT) \quad (\text{k14})$$

where

$T$  is the temperature difference between the tuning strut and the heat sink.

$C$  is the heat capacity of the strut.

$k$  is the conduction loss in watts/ $^{\circ}\text{C}$ .

$P_i$  is the power into the tuner.

The solution of (k14) is then,

$$\frac{P_i}{k} - T = \left( \frac{P_i}{k} - T_0 \right) e^{-(k/C)t} \quad (\text{k15})$$

where  $T_0$  is the temperature difference at  $t = 0$ .

If

the temperature difference from the sink is  $T_0 = T_c$  at the cooler limit of the band.

$T_h$  is the temperature difference from the sink at the hotter limit of the band.

$P_m$  is the maximum permitted input, then the cycling time for heating

$$\tau_h = \frac{C}{k} \log_e \frac{P_m - kT_c}{P_m - kT_h} \quad (\text{k16})$$

On cooling

$$\frac{dT}{dt} = -\frac{k}{C} t \quad (\text{k17})$$

from which

$$T = T_0 e^{-(k/C)t} \quad (\text{k18})$$

$$\tau_c = \frac{C}{k} \log_e \frac{T_h}{T_c} \quad (\text{k19})$$

#### ACKNOWLEDGMENTS

A large number of people have contributed to the work described in this paper. The program was carried on under the general direction of J. R. Wilson whose support and advice are gratefully acknowledged. J. O. McNally gave more specific direction to these efforts and is responsible for many of the design features. We are greatly indebted to him for his close support and encouragement.

Members of the Bell Laboratories technical staff concerned with various portions of the developments were E. M. Boone, K. Cadmus, R. Hanson, C. A. Hedberg, P. Kusch, C. G. Matland, H. E. Mendenhall, R. M. Ryder and R. C. Winans. R. S. Gormley of the Western Electric Company made considerable contributions to the work on the 2K25.

The mechanical design, construction and specifications for manufacture were carried out by a group of engineers under the direction of V. L. Ronci. This group included D. P. Barry, F. H. Best, S. O. Ekstrand, G. B. Gucker, C. Maggs, W. D. Stratton, R. L. Vance and E. J. Walsh. L. A. Wooten and his associates cooperated in numerous chemical problems throughout this work.

The authors wish to make particular acknowledgement of the work of two technical assistants, Miss Z. Marblestone and F. P. Dreschler, whose

diligent and painstaking efforts were a direct contribution to the successful completion of most of the designs described herein.

The NDRC Radiation Laboratories at the Massachusetts Institute of Technology extended very close cooperation both on problems of design and applications of the tubes. A. G. Hill and J. B. H. Kuper were particularly helpful with technical advice and support. H. V. Neher was responsible for the initial design of the 2K50 and assisted on its final development at the Bell Laboratories. G. Hobart assisted on the 2K50 at M.I.T. and also on the final development as a resident at Bell Laboratories.

Professor R. D. Mindlin on leave from Columbia University served as a consultant on vibration and stress analysis problems particularly on the design of diaphragms and mechanical and thermal tuning mechanisms.

In the preparation of the manuscript the authors are particularly indebted to R. M. Ryder for his extension of the simple bunching theory which is included as a part of this paper. L. A. MacColl provided the solution for several mathematical problems.

## Abstracts of Technical Articles by Bell System Authors

*Investigation of Oxidation of Copper by Use of Radioactive Cu Tracer.*<sup>1</sup> J. BARDEEN, W. H. BRATTAIN, and W. SHOCKLEY. A very thin layer of radioactive copper was electrolytically deposited on a copper blank. The surface was then oxidized in air at 1000°C for 18 minutes, giving an oxide layer with a thickness of  $1.25 \times 10^{-2}$  cm. After quenching, successive layers of the oxide were removed chemically, and the copper activity in each layer was measured. The observed self-diffusion of radioactive copper in the oxide agrees quantitatively with a theory based on the following assumptions: (a) The oxide grows by diffusion of vacant  $\text{Cu}^+$  sites from the outer surface of the oxide inward to the metal. (b) The concentration of vacant sites at the oxygen-oxide interface is independent of the oxide thickness, and drops linearly from this constant value to zero at the metal boundary. (c) Accompanying the inward flow of vacant sites, there is a flow of positive electron holes such as to maintain electrical neutrality. (d) Self-diffusion of copper ions takes place only by motion into vacant sites. The results give a fairly direct confirmation of the theory of oxidation first suggested by Wagner.

*A New Magnetic Material of High Permeability.*<sup>2</sup> O. L. BOOTHBY and R. M. BOZORTH. This paper describes the preparation, heat treatment, and properties of *supermalloy*, a magnetic alloy of iron, nickel, and molybdenum. In the form of 0.014 in. sheet it has an initial permeability of 50,000 to 150,000, a maximum permeability of 600,000 to 1,200,000, coercive force of 0.002 to 0.005 oersted, and a hysteresis loss of less than 5 ergs/cm<sup>3</sup>/cycle at  $B = 5000$ . Transformer cores made of insulated 0.001 in. tape, spirally wound, have about the same initial permeability and a maximum permeability of 200,000 to 400,000. The alloy has a Curie point of 400°C and appears to have an order-disorder transformation temperature somewhat above 500°C.

*Magnetoresistance and Domain Theory of Iron-Nickel Alloys.*<sup>3</sup> R. M. BOZORTH. Measurements of change of electrical resistivity with magnetization and with tension are reported for iron-nickel alloys containing 40 to 100 per cent nickel. When the magnetostriction is negative (81 to 100 per

<sup>1</sup> *Jour. of Chemical Physics*, December 1946.

<sup>2</sup> *Jour. Applied Physics*, February 1947.

<sup>3</sup> *Phys. Rev.*, Dec. 1 and 15, 1946.

cent nickel), tension ( $\sigma$ ) decreases resistivity, and magnetic field (H) increases it. Domain theory predicts the ratio  $\sigma/H$  at which the resistivity is equal to that of the unmagnetized specimen, and the theory is accurately confirmed. Measurements are made in transverse as well as longitudinal magnetic fields, and the difference between the resistances so measured is shown to be independent of the distribution of domains in the unmagnetized state; the erratic results reported in the literature are thus explained and avoided. When magnetostriction is positive, the limiting changes of resistivity with field and tension are sometimes found to be different; this is shown to be caused by the variation of magnetostriction with crystallographic direction.

*A Wide-Tuning-Range Microwave Oscillator Tube.*<sup>4</sup> JOHN W. CLARK and ARTHUR L. SAMUEL. This paper describes a reflex-type velocity-variation oscillator tube with a wide tuning range in the microwave band. The tube will oscillate from 2000 to 13,000 megacycles, but practical tuning considerations limit the band in any one circuit to a two-to-one frequency range. The problems involved in the design and a description of the various elements are given.

*Accelerated Ozone Weathering Test for Rubber.*<sup>5</sup> JAMES CRABTREE and A. R. KEMP. Light-energized oxidation and cracking by atmospheric ozone are the agencies chiefly responsible for the deterioration of rubber outdoors. Since these processes are separate and distinct, it is proposed to distinguish between them in the evaluation of rubber for resistance to weathering. An accelerated test for susceptibility to atmospheric ozone cracking is discussed. Apparatus for conducting the test and for measurement of ozone in minute concentration is described in detail.

*Measurements in Communications.*<sup>6</sup> N. B. FOWLER. For convenient reference, some of the more common measurement units and scales used in communication engineering are presented in tabular form together with supplementary explanatory text. Included in the table, which also indicates the limitations involved, are quantities used in measuring power, volume, circuit noise, sound, light, radio fields, crosstalk coupling, and certain other transmission concepts.

*An Improved 200-Mil Push-Pull Density Modulator.*<sup>7</sup> J. G. FRAYNE, T. B. CUNNINGHAM and V. PAGLIARULO. A completely new variable-

<sup>4</sup> *Proc. I.R.E. and Waves and Electrons*, January 1947.

<sup>5</sup> *Indus. & Engg. Chemistry, Analytical Edition*, December 1946.

<sup>6</sup> *Electrical Engineering*, February 1947.

<sup>7</sup> *Jour. S.M.P.E.*, December 1946.



density modulator utilizing a three ribbon push-pull valve is described. The entire valve is sealed by the force of the Alnico V permanent magnet on the Permendur pole pieces. Signal is applied to the center ribbon and noise-reduction currents are applied to the outer ribbons. True class A push-pull operation is obtained from the two component single ribbon valves by the use of an inverter prism which aligns the modulating and noise-reduction edges of each aperture.

An anamorphote condenser lens is used to eliminate lamp filament striations at the valve ribbon plane. An anamorphote objective lens gives a 4:1 reduction of the valve aperture in the vertical plane at the film and a 2:1 reduction along the length of the sound track. A meter is supplied to measure exposure as well as setting up "bias." A photocell monitor is supplied and a "blooming" light for indicating synchronous start marks.

Mathematical analysis of the exposure produced by the modulating ribbon is appended as well as a similar analysis of the four ribbon push-pull valve which the new valve supersedes.

*Factors Governing the Intelligibility of Speech Sounds.*<sup>8</sup> N. R. FRENCH and J. C. STEINBERG. The characteristics of speech, hearing, and noise are discussed in relation to the recognition of speech sounds by the ear. It is shown that the intelligibility of these sounds is related to a quantity called articulation index which can be computed from the intensities of speech and unwanted sounds received by the ear, both as a function of frequency. Relationships developed for this purpose are presented. Results calculated from these relations are compared with the results of tests of the subjective effects on intelligibility of varying the intensity of the received speech, altering its normal intensity-frequency relations and adding noise.

*Short Duration Auditory Fatigue as a Method of Classifying Hearing Impairment.*<sup>9</sup> MARK B. GARDNER. Earlier studies have classified deafness cases into two general groups, those having functional disorders of the middle ear and those having impairments resulting from atrophy of the nerve fibers terminating along the basilar membrane (conductive and nerve deafness types, respectively). Such classifications have been made using bone conduction threshold measurements and unilateral loudness balance results as the basis for differentiation. Bone conduction results, however, are often subject to considerable error while the unilateral loudness balance technique can only be applied to individuals having one normal and one impaired ear. These limitations introduce a need for a completely independent monaural method of classifying deafness types. This is particularly true for the selec-

<sup>8</sup> *Jour. Acous. Soc. Amer.*, January 1947.

<sup>9</sup> *Jour. Acous. Soc. Amer.*, January 1947.

tion of candidates suitable for the fenestration operation for the restoration of hearing in otosclerosis (immobilized stapes). The present paper is concerned with an investigation of short time auditory fatigue as a method of obtaining an impairment analysis. In this study, it was found that the fatigue of the conductively deafened observer was similar to the normal observer except the onset of fatigue was shifted by the amount of the threshold loss. For the nerve deafened observer, on the other hand, the onset of fatigue was found to occur at normal intensity levels. The occurrence of excessive fatigue in one of the nerve type impairment cases investigated appears to offer additional information on the nature of the lesion.

*A Sampling Procedure for Design Tests of Electron Tubes (Sponsored by Joint Electron Tube Engineering Council).*<sup>10</sup> S. W. HORROCKS, P. M. DICKERSON, H. F. DODGE,\* E. R. OTT, H. G. ROMIG,\* W. B. RUPP, J. R. STEEN, R. E. WAREHAM, AND A. K. WRIGHT. The Committee on Sampling Procedure was established on July 21, 1943 as part of the Electron Tube Section of the Radio Manufacturers Association (RMA). The purpose of the Committee is to develop sampling methods and to act in an advisory capacity towards standardization of Sampling Procedures throughout the Electron Tube industry. This Committee was later embodied as a main Committee of the Joint Electron Tube Engineering Council of the RMA and NEMA. This Council was established in 1945 to handle all engineering matters for the Electron Tube industry for both trade associations, Radio Manufacturers Association and National Electrical Manufacturers Association.

One of the earliest projects handled by the Committee was the development of a statistically sound sampling inspection procedure for so-called "design tests" of electron tubes. In general, design tests relate to characteristics that are normally quite stable and are relatively less important to the consumer. The nature of these tests is such that only relatively small samples are practicable. The Joint Army-Navy Specification JAN-1A incorporated a sampling plan for design tests allowing (1) not more than 10% of the sample tubes to contain design test defects of any one kind and (2) not more than 20% of the sample tubes to contain design test defects of any kind. Because of the extremely wide range in lot sizes for different classes of electron tubes, such a simplified sampling plan was in effect too strict for small lot sizes and too liberal for large lot sizes. Moreover, no distinction was made in the relative seriousness of different kinds of design test defects. The Committee accordingly set about to prepare a sampling inspection plan that would be relatively free of these faults. The new procedure covers all

<sup>10</sup> *Industrial Quality Control*, November 1946.

\* *Of Bell Tel. Labs.*

aspects of the acceptance problem and provides an operationally definite criterion for reducing inspection for a product whose quality is regularly well controlled within the intent of the specification.

The procedure developed by the Committee was approved by J.E.T.E.C. (Joint Electron Tube Engineering Council), was approved by the JAN Committee in September 1945, and is reproduced in full in this article. It will be noted that the procedure provides for two Acceptable Quality Levels (AQL), namely 6% defective and 3% defective for individual design test characteristics. Each design test of a particular type of electron tube is classified as either a Standard Design Test with an AQL = 6% or a Special Design Test with an AQL = 3%. For any design test, if product submitted for inspection has quality equal to the AQL, the chances of acceptance are of the order of 94 to 98 out of 100. If quality runs consistently better than the AQL, reduced inspection is permitted, thus serving as an incentive for the manufacturer to strive for better quality. The operating characteristics of the sampling plans involved are appended to this article and show the degree to which the plans will discriminate for various levels for submitted quality.

*Resonant Circuit Modulator for Broad Band Acoustic Measurements.*<sup>11</sup> GORDON FERRIE HULL, JR.\* A modulation method is described whereby a broad band frequency response is obtained for recording of sound. In particular low frequency sound approaching zero c.p.s. can be recorded. The theory of the resonant circuit modulating principle is first discussed followed by a description of the apparatus which was constructed for this purpose.

*Quality Reporting—Putting Inspection Results to Work.*<sup>12</sup> HAROLD R. KELLOGG. Quality reporting is an integral part of the general inspection problem. It cannot be divorced from the logic and aims of an overall inspection program. A discussion of quality reporting should therefore include consideration of (1) inspection procedures, including the collection of data; (2) appraisal of the data; (3) reporting and publicizing results. This outlines the program as it is discussed in this paper.

*Properties of Monoclinic Crystals.*<sup>13</sup> W. P. MASON. Two crystals of the monoclinic sphenoidal class have been found which have modes of vibration with zero temperature coefficients of frequency, and this property together

<sup>11</sup> *Jour. Applied Physics*, December 1946.

\* This research was carried out while the author was a member of the Technical Staff of the Bell Telephone Laboratories, Inc., Murray Hill, New Jersey.

<sup>12</sup> *Industrial Quality Control*, November 1946.

<sup>13</sup> *Phys. Rev.*, Nov. 1 and 15, 1946.

with the high electromechanical coupling and the high  $Q$ 's make it appear probable that these crystals may have considerable use as a substitute for quartz which is difficult to obtain in large sizes. These crystals are ethylene diamine tartrate ( $C_6H_{14}N_2O_6$ ) and dipotassium tartrate ( $K_2C_4H_4O_6, \frac{1}{2}H_2O$ ). Complete measurements of the elastic, piezoelectric, and dielectric constants of the dipotassium tartrate (DKT) crystal are given in this paper. The crystal has 4 dielectric constants, 8 piezoelectric constants, and 13 elastic constants. A discussion is given in the appendix of the method of measuring these constants by the use of 18 properly oriented crystals.

*An Acoustic Constant of Enclosed Spaces Correlatable with Their Apparent Liveness.*<sup>14</sup> J. P. MAXFIELD and W. J. ALBERSHEIM. An acoustic constant called liveness is derived, which constant is correlatable with the acoustic properties of the enclosed space and with the distance between the sound source and the listener. This constant represents the ratio of a time integral of the energy density of the reverberant sound to the unintegrated energy density of the direct sound. The validity of this constant is substantiated by empirical data. Certain subjective effects of monaurally reproduced sounds as a function of the liveness of its pick-up conditions are briefly discussed.

*Directional Couplers.*<sup>15</sup> W. W. MUMFORD. The directional coupler is a device which samples separately the direct and the reflected waves in a transmission line. A simple theory of its operation is derived. Design data and operating characteristics for a typical unit are presented. Several applications which utilize the directional coupler are discussed.

*Theory of the Beam-Type Traveling-Wave Tube.*<sup>16</sup> J. R. PIERCE. The small-signal theory of the beam traveling-wave tube has been worked out. The equations predict three forward waves, one increasing and two attenuated, and one backward wave which is little affected by the electron stream. The waves are partly electromagnetic and partly disturbance in the electron stream. The dependence of the wave propagation coefficients on voltage, current, circuit loss, and the other properties of the transmission mode which propagates energy and the cut-off transmission modes is given. Expressions for gain and noise figure and an estimate of power output are given. Appendix A gives an expression for the field in a uniform transmission system due to impressed current (as, of an electron stream) in terms of the parameters of the transmission modes. Appendix B calculates the propagation

<sup>14</sup> *Jour. Acous. Soc. Amer.*, January, 1947.

<sup>15</sup> *Proc. I.R.E.*, February 1947.

<sup>16</sup> *Proc. I.R.E.*, February 1947.

constant and the field for unit power flow for the gravest mode of helical transmission system.

*Traveling-Wave Tubes.*<sup>17</sup> J. R. PIERCE and L. M. FIELD. Very-broad-band amplification can be achieved by use of a traveling-wave type of circuit rather than the resonant circuit commonly employed in amplifiers. An amplifier has been built in which an electron beam traveling with about  $1/13$  the speed of light is shot through a helical transmission line with about the same velocity of propagation. Amplification was obtained over a bandwidth 800 megacycles between 3-decibel points. The gain was 23 decibels at a center-band frequency of 3600 megacycles.

*Attenuation of Forced Drainage Effects on Long Uniform Structures.*<sup>18</sup> ROBERT POPE. When forced drainage is applied to an underground metallic structure to provide cathodic protection, the greatest effects on the structure and earth potentials occur in the vicinity of the drainage point and anode. These effects taper off as the distance from the drainage point increases and even in the relatively simple case of a long, uniform structure, the manner in which these effects taper off or attenuate is quite complex. However, by making a few justifiable assumptions, relatively simple equations are developed which provide sufficiently accurate results in most practical cases. Furthermore, the simple equations bring out more clearly the relative importance of the various factors involved than do the more rigorous equations. The approximate equations have been used with fair success in predicting the effects of drainage on underground telephone cables in conduit and on buried coated cables. They should apply quite accurately to coated pipes, and there are examples of reasonably good application on some bare pipes.

The soil and structure characteristics which enter into the equations are discussed, and the units used established.

*Alkaline Earth Porcelains Possessing Low Dielectric Loss.*<sup>19</sup> M. D. RIGTERINK and R. O. GRISDALE. Alkaline earth porcelains have been prepared from mixtures of clay, flint, and synthetic fluxes consisting of clay calcined with at least three alkaline earth oxides. These porcelains possess excellent dielectric properties, have low coefficients of thermal expansion, are white, and are especially valuable as bases for deposited carbon resistors for which they were developed. Their characteristics make it probable that other uses will be found for materials of this type.

An illustrative composition is 50.0% Florida kaolin, 15.0% flint (325

<sup>17</sup> *Proc. I.R.E.*, February 1947.

<sup>18</sup> *Corrosion*, December 1946.

<sup>19</sup> *Jour. Amer. Ceramic Soc.*, March 1, 1947.

mesh), 35.0% calcine (200 mesh). The composition of the calcine is 40.0% Florida kaolin, 15.0%  $MgCO_3$ , 15.0%  $CaCO_3$ , 15.0%  $SrCO_3$ , 15.0%  $BaCO_3$ , calcined at  $1200^\circ C$ . The electrical properties of this body at 1 mc. are Q at  $25^\circ C$ , 2160; Q at  $250^\circ C$ , 280; Q at  $350^\circ C$ , 90; specific resistance at  $150^\circ C$ ,  $10^{13.5}$  ohm-cm. and at  $300^\circ C$ ,  $10^{10.7}$  ohm-cm.

*A Coaxial-Type Water Load and Associated Power-Measuring Apparatus.*<sup>20</sup> R. C. SHAW and R. J. KIRCHER. This paper presents a description of a coaxial-type water load and associated equipment suitable for measuring peak pulse powers of the order of a megawatt. Water-cell loads have been designed to operate at wavelengths of from 10 to 40 centimeters, where the average dissipation is of the order of 300 watts. Ordinary tap water is used in the load to dissipate the radio-frequency power.

*The Ammonia Spectrum and Line Shapes Near 1.25-cm Wave-Length.*<sup>21</sup> CHARLES HARD TOWNES. The ammonia "inversion" lines near 1.25-cm wave-length are resolved, their widths being decreased at low pressures to 200 kilocycles. Line shapes, intensities, and frequencies are measured and correlated with theory. Calculated intensities and Lorentz-type broadening theory fit experimental results if frequency of collision is fifteen times greater than that measured by viscosity methods. Splitting due to rotation is in fair agreement with a recalculation of theoretical values. A saturation effect is observed with increase of power absorbed per molecule and an interpretation made.

*Non-Uniform Transmission Lines and Reflection Coefficients.*<sup>22</sup> L. R. WALKER and N. WAX. A first-order differential equation for the voltage reflection coefficient of a non-uniform line is obtained and it is shown how this equation may be used to calculate the resonant wave-lengths of tapered lines.

*Temperature Coefficient of Ultrasonic Velocity in Solutions.*<sup>23</sup> G. W. WILLARD. Extensive measurements have been made, at ten megacycles, of the temperature dependence of ultrasonic velocity in liquids and liquid mixtures. All single liquids tested, except water, were found to have large negative temperature-coefficients in the temperature range of zero to  $80^\circ C$ . Water has a large positive coefficient at room temperature, decreasing to zero at  $74^\circ C$  and then becoming negative (with a peak velocity of 1557

<sup>20</sup> *Proc. I.R.E. and Waves and Electrons*, January 1947.

<sup>21</sup> *Phys. Rev.*, Nov. 1 and 15, 1946.

<sup>22</sup> *Jour. Applied Physics*, December 1946.

<sup>23</sup> *Jour. Acous. Soc. Amer.*, January 1947.

meters/sec). Solutions in water of various other liquids (and of some solids) give parabolic velocity vs. temperature curves like that for water but with the peak velocity and peak temperature values shifting with the concentration of the solution. In general increasing the concentration raises the peak velocity slightly and lowers the peak temperature markedly from the values for water alone. It has also been found possible by compounding three-component solutions to adjust the values of the peak velocity and peak temperature independently within a narrow range of velocities and a wide range of temperatures.

*Measurements of Ultrasonic Absorption and Velocity in Liquid Mixtures.*<sup>24</sup> F. H. WILLIS. The absorption ( $\alpha$ ) and velocity (V) of sound in liquid mixtures were measured at four frequencies ( $\nu$ ) in the range 3.8 to 19.2 mc, using the Debye-Sears-Lucas-Biquard optical technique improved by the addition of a differential photoelectric cell indicator. This improvement permitted the use of lower sound intensities together with a wider sound beam than in the visual extinction method, thus improving conditions with respect to cavitation and beam distortion. In the mixtures investigated,  $\alpha/\nu^2$  was found to be independent of frequency within the accuracy of the method, and there was no measurable dispersion of acoustic velocity. An absorption peak at intermediate concentrations not shifting with frequency was found in mixtures of acetone and water, and of ethyl alcohol and water, but was not in evidence in mixtures of acetone and ethyl alcohol, and of glycerol and water. The absorption peaks await theoretical explanation.

*Measuring Inter-Electrode Capacitances.*<sup>25</sup> C. H. YOUNG. New bridge, developed for measurement of extremely small values in high frequency tubes, useful to two-billionths of a microfarad.

<sup>24</sup> *Jour. Acous. Soc. Amer.*, January 1947.

<sup>25</sup> *Tele-Tech*, February 1947.

## Contributors to this Issue

WILLIAM M. GOODALL, B.S., California Institute of Technology, 1928; Bell Telephone Laboratories, 1928—. Mr. Goodall has worked on research problems in connection with the ionosphere, radio transmission and early radio relay studies, radar modulators, and more recently microwave radio relay systems.

J. P. KINZER, M.E., Stevens Institute of Technology, 1925. B.C.E., Brooklyn Polytechnic Institute, 1933. Bell Telephone Laboratories, 1925—. Mr. Kinzer's work has been in the development of carrier telephone repeaters; during the war his attention was directed to investigation of the mathematical problems involved in cavity resonators.

J. R. PIERCE, B.S. in Electrical Engineering, California Institute of Technology, 1933; Ph.D., 1936. Bell Telephone Laboratories, 1936—. Engaged in study of vacuum tubes.

ALLEN F. POMEROY, B.S. in E.E., Brown University, 1929. Public Service Electric and Gas Company, Electrical Testing Laboratory, 1923-1925, 1926; Weston Electrical Instrument Corporation, 1927; Bell Telephone Laboratories, 1929—. Since 1936 Mr. Pomeroy has been principally occupied in developing equipments to measure attenuations, phase shifts, envelope delays, and reflection coefficients for systems suitable for television transmission, and during the war in the development of radar testing equipment.

W. G. SHEPHERD, B. S. in Electrical Engineering, University of Minnesota, 1933; Ph.D. in Physics, University of Minnesota, 1937. Bell Telephone Laboratories, Inc., 1937—. From 1937 to 1939 Dr. Shepherd was engaged in non-linear circuit research. Since 1939 he has been engaged in the design of electron tubes.

I. G. WILSON, B.S. AND M.E., University of Kentucky, 1921. Western Electric Co., Engineering Department, 1921-25. Bell Telephone Laboratories, 1925—. Mr. Wilson has been engaged in the development of amplifiers for broad-band systems. During the war he was project engineer in charge of the design of resonant cavities for radar testing.



